Development and Characterization of Isogenic Cardiac Organoids Derived from Human Pluripotent Stem Cells

by

Alejandra Patino-Guerrero

A Dissertation Presented in Partial Fulfillment
of the Requirements for the Degree
Doctor of Philosophy

Approved April 2023 by the
Graduate Supervisory Committee:

Mehdi Nikkhah, Chair
Jennifer Blain-Christen
Vikram Kodibagkar
Brent Vernon
Wuqiang Zhu

ARIZONA STATE UNIVERSITY

May 2023

ABSTRACT

Cardiovascular diseases (CVDs) are the leading cause of mortality worldwide, causing nearly 25% of deaths in the United States. Despite the efforts to create in vitro models for the study and treatment of CVDs, these are still limited in their recapitulation of the heart tissue. Thus, the engineering of accurate cardiac models is imperative to gain more understanding and improve the outcome of CVDs. This Ph.D. dissertation focuses on the development and characterization of isogenic cardiac organoids derived from human induced pluripotent stem cells (hiPSCs). Additionally, the integration of chemical and biological cues for enriching their microenvironment and promoting their maturation state and function were studied. First, hiPSC-derived cardiac cells were utilized for the fabrication of multicellular spherical microtissues, namely isogenic cardiac organoids. The cellular composition and culture time of the engineered tissues were optimized to induce cellular aggregation and the formation of cell-cell interactions. Also, ribbon-like gold nanoparticles, namely gold nanoribbons (AuNRs), were synthesized, characterized, and biofunctionalized for their integration into the isogenic cardiac organoids. In-depth biological evaluation of the organoids showed enhanced cardiac maturation markers. Furthermore, a supplement-free cell culture regime was designed and evaluated for fabricating isogenic cardiac organoids. Mechanistic, cellular, and molecular-level studies demonstrated that the presence of hiPSC-derived cardiac fibroblasts (hiPSC-CFs) significantly improves the morphology and gene expression profile of the organoids. Electrophysiological-relevant features of the organoids, such as conduction velocity (CV), were further investigated utilizing a microelectrode array (MEA) platform. It was shown that MEA offers a simple, yet powerful approach to assessing electrophysiological

responses of the tissues, where a trend in decreased CV was found due to the presence of hiPSC-CFs. Overall, this dissertation has a broad impact casting light on the development strategy and biological mechanisms that govern the formation and function of isogenic cardiac organoids. Moreover, this study presents two unique approaches to promote maturation of stem cell-derived cardiac organoids: 1) through the integration of novel biofunctionalized nanomaterials, and 2) through a cell culture regime, leading to enhanced function of the organoids. The proposed micro-engineered organoids have broad applications as physiologically relevant tissues for drug discovery, CVDs modeling, and regenerative medicine.

ACKNOWLEDGEMENTS

I would like to start this section by acknowledging my Ph.D. mentor, Dr. Mehdi Nikkhah, for providing the continuous guidance and support that have allowed the completion of this dissertation. Additionally, I would like to thank Dr. Nikkhah for accepting me into the amazing Nikkhah Lab research group, and for always having an open door and an honest communication with me. Through his mentoring I have become a more mature researcher and a better human. I will be forever grateful for his compassion and patience through many challenges during my journey.

I also want to acknowledge the support of my Ph.D. committee: Dr. Jennifer Blain-Christen, Dr. Vikram Kodibagkar, Dr. Brent Vernon, and Dr. Wuqiang Zhu. Their generous guidance and advice have provided invaluable insight towards my research project.

The completion of this dissertation would not have been possible without the expertise of our collaborators, who have contributed with their technical knowledge and kind advice. Thanks to Dr. Oliver Graudejus and Dr. Ruben Ponce Wong, for providing all the technical support necessary for performing the MEA electrophysiology. Thanks to Dr. Ray Q. Migrino for his advice and guidance for the publication of our research. And last but not least, thanks to Dr. Barbara Smith for graciously providing access to the equipment in her lab. I would also like to acknowledge the Regenerative Medicine core facilities for providing the technical support and access to their equipment.

A big debt of gratitude is owed to all former and current members of the Nikkhah Lab research group. Their friendship and solidarity got me through the most difficult times. Thanks for being role models, their example motivates me every day to become a better

researcher. Thanks for all their feedback and support, all the scientific conversations, and all the fun; I thoroughly enjoyed their companionship. Likewise, to my friends and fellow graduate students from adjacent research groups, thanks for their kind words, advice and support.

I would like to acknowledge the funding agencies that made possible the work presented in this dissertation. First, to the Department of State and COMEXUS for funding and administering the Fulbright-Garcia Robles Scholarship. I am immensely grateful for this scholarship that allowed me to come to the United States to start my graduate program and start my career as a researcher. I would also like to thank to the Arizona Biomedical Research Commission (New Investigator Award #AWD32676), and the National Science Foundation (CAREER Award #1653193 and NANOSCALE Award #2016501), for providing the funding sources for this project.

Finally, I want to express my gratitude to the ASU Graduate College and the School of Biological and Health Systems Engineering for all the support they have provided during my Ph.D. journey.

TABLE OF CONTENTS

Page

CHAPTER Page

CHAPTER Page

CHAPTER Page

CHAPTER Page

CHAPTER Page

LIST OF TABLES

Table Page

LIST OF FIGURES

PREFACE

This dissertation presents the original work of the primary author, which has been published in the form of review and research articles. Chapter 2 details the state-of-the art for scaffold-free cardiac tissue engineering and explores the integration of nanomaterials (A. Patino-Guerrero, Veldhuizen, Zhu, Migrino, & Nikkhah, 2020). Chapter 3 discusses the synthesis, biofunctionalization, and characterization of gold nanoribbons, and their integration with isogenic cardiac organoids. Chapter 4 describes the development and characterization of isogenic cardiac organoids fabricated under a supplement starvation regimen (Alejandra Patino-Guerrero et al., 2023). Lastly, Chapter 5 expands the discussion regarding the electrophysiological analysis of the cardiac organoids.

CHAPTER 1

INTRODUCTION

1.1 OVERVIEW

Cardiovascular diseases (CVDs) are source of a great financial and public-health burden worldwide; it is estimated that 23% of the annual deaths in the United States are caused by heart diseases, and it is expected that cardiovascular risk factors rise globally in the near future (Gori, Lelieveld, & Münzel, 2020; Gregory A. Roth et al., 2020). This has led to the search for novel and efficient tools that help elucidating the mechanisms of CVDs. Recently, cardiac tissue engineering has emerged as a solution, providing more complex models that mimic some of the functions of the human heart. These models deliver alternatives for disease modeling, drug screening, and cardiac regeneration. However, the heart muscle, specifically the myocardium, is a complex tissue at a cellular and electromechanical level, and these models are still limited in their representation of the properties of the cardiac structures. For example, current engineered cardiac tissues lack representation of the cellular composition, spatial organization, and electrical features of the myocardium. Thus, the creation of more accurate cardiac tissue models, and a better understanding of their biological, and electromechanical features results imperative.

To address this critical need, throughout my doctoral studies, isogenic scaffold-free cardiac organoids derived from human induced pluripotent stem cells (hiPSCs) have been developed and characterized under varying culture regimes. First, we stablished the state-of-the-art in the field of scaffold-free cardiac tissue engineering and we discuss the integration of different nanoparticles for the enhancement of cardiac spheroids and organoids (A. Patino-Guerrero et al., 2020). We then generated isogenic hiPSC-CMs and

hiPSC-CFs through a directed differentiation protocol. We utilized the hiPSC-derived cardiac cells for the fabrication of multicellular cardiac spherical microtissues, namely isogenic cardiac organoids. We have optimized the cellular composition and culture time of the engineered tissues for inducing cellular aggregation and the formation of cell-to-cell interactions. Additionally, for their unique properties, such as electrical conductivity, and biocompatibility, gold nanoparticles have been of interest for their inclusion within the cardiac organoids. Specifically, we have produced gold nanoparticles with a ribbon-like morphology that have been embedded within the cardiac organoids. In order to have a better understanding of the metabolic characteristics of the hiPSC-CMs, we designed a supplement-free cell culture regime and evaluated its effects over the formation of isogenic cardiac organoids (Alejandra Patino-Guerrero et al., 2023). Finally, we assessed electrophysiological-relevant features of the microtissues, such as conduction velocity (CV), through a microelectrode array (MEA) platform. We aim that the development and in-depth characterization of isogenic scaffold-free cardiac organoids can help addressing current challenges in CTE; additionally, the performance of the cardiac organoids can be enhanced through novel cell culture methods and microenvironment modifications.

1.2 SPECIFIC AIMS

1.2.1 Specific Aim 1

***Nanoengineering of gold nanoribbons (AuNRs) and development of hiPSCs-derived isogenic scaffold-free cardiac organoids*.** In order to improve the performance of engineered cardiac tissues, we proposed the use of isogenic hiPSC-CMs and hiPSC-CFs for fabricating scaffold-free cardiac organoids. In addition, we hypothesized that the inclusion of AuNRs will enhance the microenvironment within the cardiac organoids,

helping with the maturation of the hiPSC-CMs and overall function of the tissues. Therefore, we first synthesized and characterized AuNRs. We also performed surface chemistry modification in to render the AuNRs biocompatible for the hiPSC-derived cardiac cells. Additionally, we optimized a differentiation protocol for the obtention of the two different lineages of cardiac cells utilized in this project. Finally, we performed toxicological, and structural evaluation of cardiac organoids embedded with AuNRs, along with gene expression analysis to assess the effect of the AuNRs in the engineered tissues.

1.2.2 Specific Aim 2

Development and characterization of scaffold-free isogenic cardiac organoids derived from hiPSCs under supplement starvation regime.

To enhance the formation of cardiac organoids, we introduced a 24-hour hiPSC-CM cell culture supplement starvation regime prior the formation of the microtissues. Morphological, structural, and molecular evaluation of the microtissues were performed in order to assess the maturation state of the hiPSC-CMs, and overall performance of the cardiac organoids.

1.2.3 Specific Aim 3

Electrophysiological characterization of scaffold-free cardiac organoids using MEA platform.

This aim involves the utilization of a 60-microelectrode platform for the thorough characterization of the electrophysiological features of isogenic cardiac organoids generated under a supplement starvation regime. First, the organoids were seeded in a MEA device and the signal from the spontaneous beating was acquired. Then, the obtained signals were processed in order to calculate the beating rate and CV of the tissues.

Additionally, heatmaps and videos were generated from the analyzed signals in order to produce a spatial representation of the localization of the organoids on the MEAs. These heatmaps were utilized to detect regions of interest (ROIs) with high spontaneous beating activity.

1.3 REFERENCES

Gori, T., Lelieveld, J., & Münzel, T. (2020). Perspective: cardiovascular disease and the Covid-19 pandemic. *Basic Research in Cardiology, 115*(3), 32. doi:10.1007/s00395-020-0792-4

Patino-Guerrero, A., Ponce Wong, R. D., Kodibagkar, V. D., Zhu, W., Migrino, R. Q., Graudejus, O., & Nikkhah, M. (2023). Development and Characterization of Isogenic Cardiac Organoids from Human-Induced Pluripotent Stem Cells Under Supplement Starvation Regimen. *ACS Biomaterials Science & Engineering*, *9*(2), 944-958. doi:10.1021/acsbiomaterials.2c01290

Patino-Guerrero, A., Veldhuizen, J., Zhu, W., Migrino, R. Q., & Nikkhah, M. (2020). Three-dimensional scaffold-free microtissues engineered for cardiac repair. *J Mater Chem B, 8*(34), 7571-7590. doi:10.1039/d0tb01528h

Roth, G. A., Mensah, G. A., Johnson, C. O., Addolorato, G., Ammirati, E., Baddour, L. M., . . . Fuster, V. (2020). Global Burden of Cardiovascular Diseases and Risk Factors, 1990–2019: Update From the GBD 2019 Study. *Journal of the American College of Cardiology, 76*(25), 2982-3021. doi:https://doi.org/10.1016/j.jacc.2020.11.010

CHAPTER 2

ENGINEERING THREE-DIMENSIONAL SCAFFOLD-FREE MICROTISSUES FOR CARDIAC REPAIR

2.1 ABSTRACT

Cardiovascular diseases, including myocardial infarction (MI), persist as the leading cause of mortality and morbidity worldwide. The limited regenerative capacity of the myocardium presents significant challenges specifically for the treatment of MI and, subsequently, heart failure (HF). Traditional therapeutic approaches mainly rely on limiting the induced damage or the stress of the remaining viable myocardium through pharmacological regulation of remodeling mechanisms, rather than replacement or regeneration of the injured tissue. The emerging alternative regenerative medicine-based approaches have focused on restoring the damaged myocardial tissue with newly engineered functional and bioinspired tissue units. Cardiac regenerative medicine approaches can be broadly categorized into three groups: cell-based therapies, scaffold-based cardiac tissue engineering, and scaffold-free cardiac tissue engineering. Despite significant advancements, however, the clinical translation of these approaches has been critically hindered by two key obstacles for successful structural and functional replacement of the damaged myocardium, namely: poor engraftment of engineered tissue into the damaged cardiac muscle and weak electromechanical coupling of transplanted cells with the native tissue. To that end, the integration of micro- and nanoscale technologies along with recent advancements in stem cell technologies have opened new avenues for engineering of structurally mature and highly functional scaffold-based (SB-CMTs) and scaffold-free cardiac microtissues (SF-CMTs) with enhanced cellular organization and

electromechanical coupling for the treatment of MI and HF. In this review article, we will present the state-of-the-art approaches and recent advancements in the engineering of SF-CMTs for myocardial repair.

2.2 INTRODUCTION

Around 6.5 million persons in the United States presented heart failure (HF) on 2016, with several thousand patients on a waiting list to receive a heart transplant (Virani et al., 2020). It is estimated that by 2030 more than 8 million will present with this condition (Savarese & Lund, 2017). Cardiovascular diseases (CVD), including myocardial infarction (MI), remain a leading cause of mortality and morbidity worldwide, accounting for over 30% of all human deaths(Benjamin et al., 2017). MI leads to loss of cardiomyocytes (CMs), which have limited regenerative capacity, as well as decreased contractility, adverse remodeling of the myocardium, and ultimately HF (Michael A. Laflamme & Murry, 2011). While age-adjusted CVD-related deaths have declined by about two-thirds in industrialized nations (Nabel & Braunwald, 2012) and the rate of acute hospitalization for HF in the US has declined from 2006 to 2014, the burden of HF remains considerable with 84,000 deaths primarily due to HF and total estimated cost of $11 billion in 2014 (Jackson et al., 2018).

Cardiac damage can result from various insults such as ischemic (i.e., MI), infectious (myocarditis), toxic (post-chemotherapy), infiltrative (amyloidosis), valvular (regurgitant or stenotic lesions) or other causes (Inamdar & Inamdar, 2016; Ziaeian & Fonarow, 2016). Despite the variety of underlying causes, significant loss of viable myocardium leads to shared pathogenetic mechanisms involving neurohormonal dysregulation, hemodynamic overload, cardiac remodeling, abnormal calcium cycling, and extracellular matrix (ECM)

dysfunction (Braunwald, 2013; De Angelis, Pecoraro, Rusciano, Ciccarelli, & Popolo, 2019). The healthy myocardium presents aligned fibers (**Figure 2.1 A(i), B(i)**); however, after MI, the heart undergoes an inflammatory stage, characterized by the presence of immune cell infiltration and the formation of granulation tissue (**Figure 2.1 A(ii), B(ii)**). Later, the resolution of the inflammatory stage leads to collagen deposition by myofibroblasts, resulting in thin hypocellular fibrotic tissue (**Figure 2.1 A(iii), B(iii)**) (Prabhu & Frangogiannis, 2016; Virag & Murry, 2003). The loss of viable CMs, in addition to the subsequent formation of fibrotic/scar tissue, leads to critical complications after MI (Thygesen, Alpert, & White, 2007), such as loss of mechanical contraction, which is often measured through the left ventricle (LV) EF (LVEF) (H. Z. Zhang, Kim, Lim, & Bae, 2013). Due to the extremely low renewal rate of CMs in the heart (Bergmann et al., 2009), CMs are not able to repopulate the damaged tissue in a timely manner to restore the normal function, leading to persistence and expansion of the non-compliant damaged tissue (Cleutjens & Creemers, 2002). A small population of multipotent stem cells, referred to as cardiac progenitor cells (CPCs), has been recently discovered to reside in the heart. However, the role of CPCs in the functional regeneration of the myocardium is still not clear and remains a controversial subject. It is believed that the primary function of CPCs lies in paracrine signaling rather than proliferation and repopulation of damaged cardiac tissue (Belostotskaya, Hendrikx, Galagudza, & Suchkov, 2020; Maxeiner et al., 2010; Torella, Ellison, Méndez-Ferrer, Ibanez, & Nadal-Ginard, 2006).

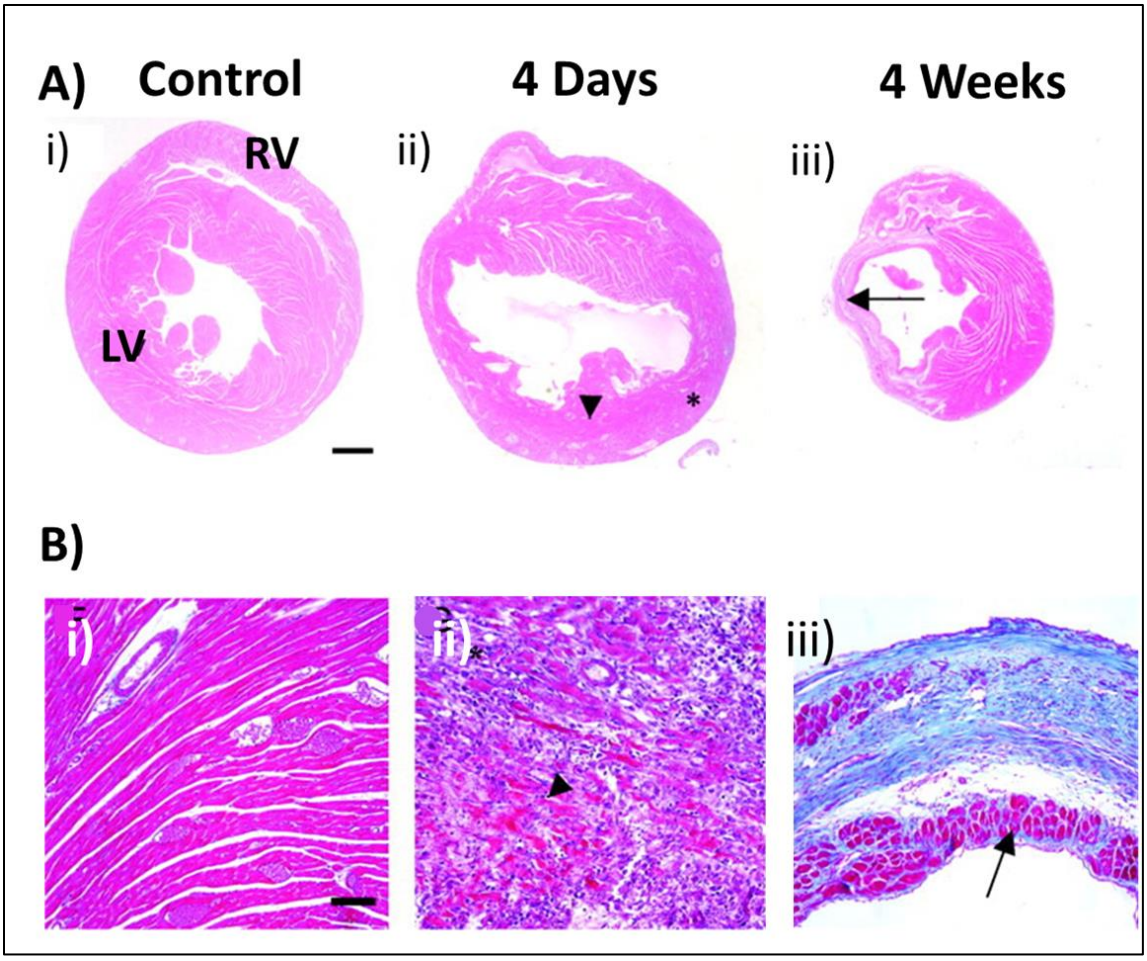

Figure 2.1. Stages of remodeling of the heart post-MI (murine). A) Hematoxylin and eosin (H&E) staining of i) healthy myocardium, ii) 4-day infarcted heart showing necrosis encapsulation (arrow head) and granulation tissue (*), and iii) 4-week infarcted heart showing thinning of the ventricular wall. (Scale bar 0.5mm) B) Masson trichrome staining of i) healthy myocardium, ii) 4-day infarcted heart (arrow head: necrosis), and iii) 4-week infarcted heart showing collagen deposition (blue). (Scale bar: 100µm). *Adapted with permission American Society for Investigative Pathology. (Virag & Murry, 2003) Copyright © (2003).*

Current pharmacologic therapy approaches rely on relieving the hemodynamic burden (afterload and preload reduction) to reduce stress on the remaining functional myocardium and modulating neurohormonal pathways that are triggered to compensate for reduced myocardial function (Bhatt, Ambrosy, & Velazquez, 2017). Three classes of drugs, including angiotensin-converting enzyme inhibitors/angiotensin II receptor

blockers, aldosterone antagonists, and β-adrenergic blockers, as well as the implantation of internal cardioverter defibrillation and cardiac resynchronization therapy, have been shown to improve survival in patients with HF with reduced ejection fraction (Braunwald, 2013). However, these approaches, while improving the function of the remaining viable myocardium and slowing adverse myocardial remodeling, do not replace the damaged myocardium. If pharmacologic therapy fails, heart transplantation or implantation of mechanical left ventricular assist device (LVAD) are treatment options of last resort. However, these approaches are still limited by an inadequate number of organ donors and potential complications derived from surgical procedures (Tonsho, Michel, Ahmed, Alessandrini, & Madsen, 2014). For instance, it has been demonstrated that LVAD promotes pathophysiological changes in the ECM of the myocardium by increasing collagen cross-linking and tissue stiffness (i.e., fibrosis), leading to inadequate contractility (Klotz et al., 2005). Additionally, the introduction of allograft organs elicits an immunologic response that can lead to acute rejection of the transplanted heart. To reduce this response, heart-transplanted patients undergo immunosuppression therapies; however, these therapies often lead to chronic side-effects (Mueller, 2004).

The field of cardiac regenerative medicine has surged in the past decade as a potentially powerful alternative approach, to the current pharmacological and surgical interventions, for treatment of MI and HF. The focus of cardiac regenerative medicine, and the strategies derived from it, is the repair and regeneration of the damaged myocardium upon MI to regain heart function and avoid the side effects and complications of traditional therapies. Despite significant advancements, there are still numerous challenges facing cardiac regenerative medicine such as notable loss of implanted cell, poor cellular survival

and coupling, and lack of integration/engraftment of the engineered tissues with the host myocardium. To that end, innovative regenerative medicine approaches are still emerging based on the advancements of stem cell bioengineering, and micro- and nanoscale technologies, to address these critical shortcomings (**Figure 2.2**). In this review article, we broadly highlight different approaches in cardiac regenerative medicine, discuss their advantages and shortcomings, and present how the challenges of traditional and conventional therapies could be overcome. We will then specifically explore different methods and materials used for the development of scaffold-free cardiac microtissues (SF-CMTs) and discuss their promising potential for myocardial repair and regeneration. We will further review the integration of nanomaterials with SF-CMTs, present commonly used materials, and evaluate specific study cases. Lastly, we will address the remaining challenges of SF-CMTs application and provide our prospective for future advancements in this field.

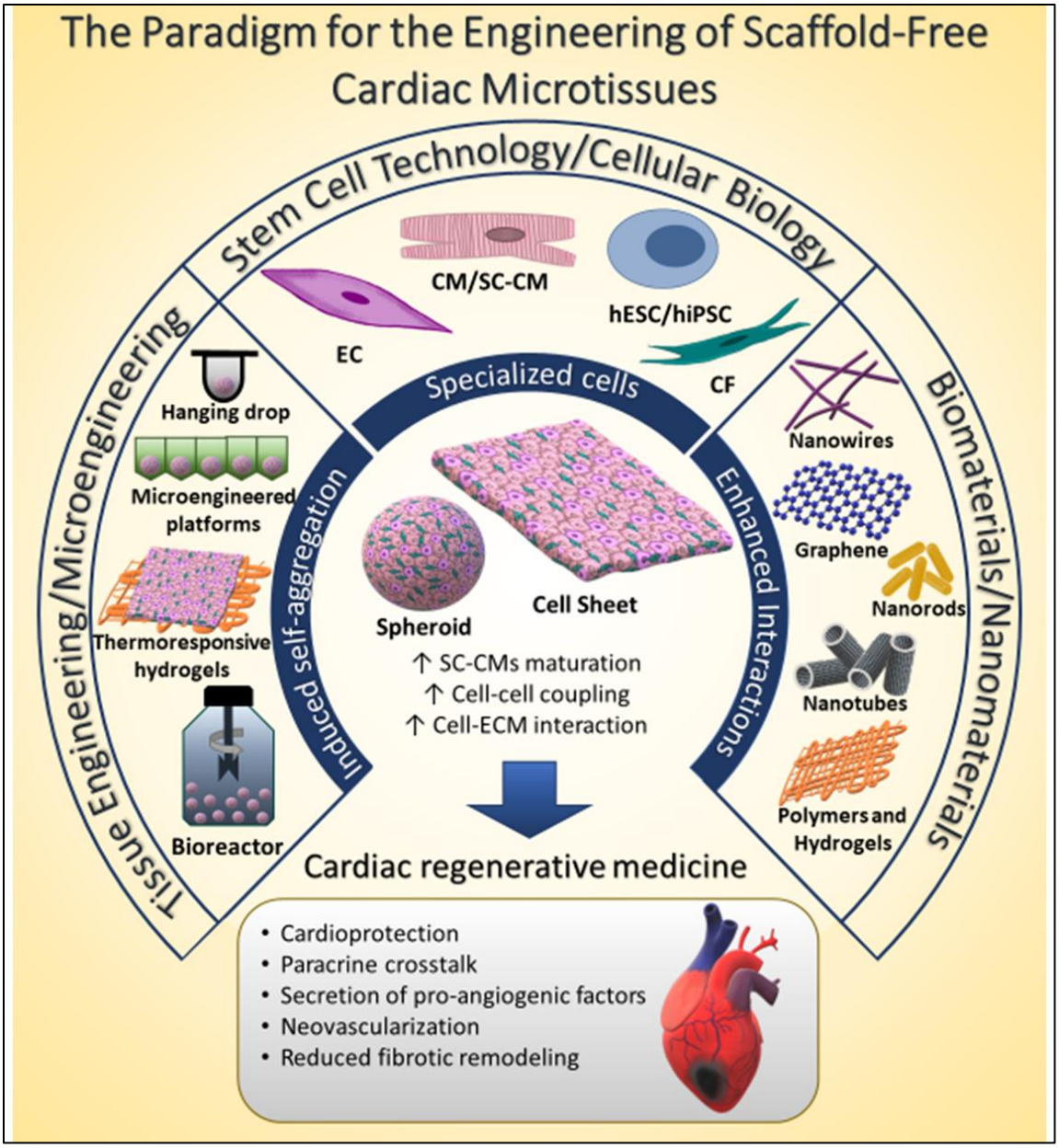

Figure 2.2. The paradigm for engineering of scaffold-free cardiac microtissues. The development and fabrication of SF-CMT based on a multidisciplinary approach, benefited from advancements in differentiation and characterization of stem cells as well as technological advancement in tissue engineering, microscale fabrication techniques, use of the nanomaterials, etc. The use of SF-CMT have demonstrated to be a promising approach for treatment of MI by providing cardioprotective effects, such as the induction of neovascularization and paracrine crosstalk. ↑ indicates increase or enhancement. Abbreviations: hESC: human embryonic stem cells, hiPSC: human induced pluripotent stem cells, CM: cardiomyocytes, SC-CM: stem cell-derived cardiomyocytes, CF: cardiac fibroblasts, EC: endothelial cells.

2.3 CELL-BASED CARDIAC THERAPY

Recent therapeutic approaches for the treatment of MI and chronic HF are based on recellularizing of the myocardium and eliciting the repairment and regeneration of the injured tissue (Shafei et al., 2017). The most straightforward techniques are based on bolus injection of either dissociated stem/progenitor or terminally differentiated cells through various delivery routes such as intracoronary and intramyocardial injections (Perin & López, 2006). Cell-based cardiac therapy aims to elicit the self-regeneration of the heart by introducing paracrine signaling cues and repopulating the damaged tissue with new healthy cells in order to improve the overall function and structural integrity of the myocardium (Golpanian, Wolf, Hatzistergos, & Hare, 2016). The selection of target cells from different sources is based on two main parameters: first, the potential for the cells to recellularize the damaged myocardium based on their proliferative and differentiation capacity; and second, their availability and abundance for harvesting and expansion *in vitro* (Segers & Lee, 2008). To date, stem and progenitor cells have been widely utilized for cell-based cardiac therapies due to their self-renewal capabilities and their potential to differentiate into cardiac lineages. Different sources have been used to obtain these cells with varying degrees of success (Behfar, Crespo-Diaz, Terzic, & Gersh, 2014). Some of the most widely utilized cells for cardiac regeneration are mesenchymal stem cells (MSCs), CPCs, embryonic stem cells (ESCs), and more recently, induced pluripotent stem cells (iPSCs). A comprehensive review of stem cell-based cardiac therapy for the treatment of MI and HF has been completed elsewhere (Ghiroldi et al., 2018). Herein, we briefly present representative studies of relevance for the field.

Adipose tissue has been identified as a viable source of MSCs due to its accessibility and ease of harvesting (R. H. Lee et al., 2004; Rodriguez, Elabd, Amri, Ailhaud, & Dani, 2005). Additionally, bone marrow (BM) has also been proposed as a suitable source of autograft MSCs for cell-based cardiac therapy. For instance, the therapeutic effect of these cells was evaluated in a study involving sixty-nine randomized patients with acute MI who received autologous intracoronary transplantation of BM-MSCs or saline solution (S. L. Chen et al., 2004). The investigators demonstrated that, three months after injection, the implanted BM-MSCs were viable and engrafted with the host myocardium. Cardiac function was improved in the group that received the BM-MSCs, measured by increased ejection fraction (EF) and decreased perfusion defects. However, the final differentiation stage and the detailed mechanism in the improvement of cardiac function by the implanted BM-MSCs were not elucidated in this study. Therefore, more in-depth mechanistic studies are necessary to understand better the role of these cells in improved clinical outcomes.

Cardiac tissue has also been proposed as a source for resident cardiac stem cells. For instance, CADUCEUS was a phase 1 clinical trial involving the delivery of autologous CPCs through intracoronary infusion after MI (Makkar et al., 2012). CPCs were extracted from an endomyocardial biopsy and injected into the myocardium 1.5-3 months after MI. The patients were observed for six months post-procedure, and no functional improvements were noted upon treatment. However, a significant reduction in scar mass, as well as a significant increase in viable heart tissue, were observed in comparison to the control group. Despite the significance of these studies, sourcing of stem cells from primary adult tissues presents technical challenges (Q. Sun, Zhang, & Sun, 2014), such as the harvesting of the sufficient cells and preparation of the cells prior to their implantation.

Pluripotent stem cells have also been proposed as an alternative and powerful source of cells for cardiac therapy, with extensive studies demonstrating the great potential of these cells for organ regeneration in clinical trials (Bretzner, Gilbert, Baylis, & Brownstone, 2011; Schwartz et al., 2012). Protocols for *in vitro* differentiation of ESCs towards CMs have been developed (Kehat et al., 2001) and optimized (Michael A Laflamme et al., 2007), and have enabled the use of human ESCs-derived CMs (hESC-CMs) for myocardial replacement therapy. For instance, in a recent work, the feasibility for using hESC-CMs in cardiac therapy was tested in non-human primate models of MI (Chong et al., 2014). hESC-CMs were delivered intramyocardially in the infarct and border zones. The explanted hearts that received the cell treatment showed extensive remuscularization, denoted by the presence of human cells in the infarct zone. Moreover, there was evidence of the formation of nascent intercalated disks, suggesting host-graft electromechanical coupling. However, the specimens that received cellular transplantation showed arrhythmias, most likely due to the immature state of the hESC-CMs. A similar study from a different group found that, due to the remuscularization of the myocardium injected by hESC-CMs, the mechanical function of the heart was improved (increased LVEF) (Y.-W. Liu et al., 2018). Overall, hESC-CMs are a promising alternative for cardiac cell-based therapies; however, more understanding of the mechanisms leading to arrhythmia is needed. In addition, ethical issues associated with the use of hESCs have limited the potential of these cells for cardiac therapy.

The successful reprogramming of human somatic cells into induced pluripotent stem cells (hiPSCs) in 2007 (Takahashi et al., 2007; J. Yu et al., 2007) opened a unique window of opportunity for cell-based regenerative therapies. The possibility of obtaining hiPSCs

without the ethical and technical challenges of sourcing them has led to extensive investigations of their potential, specifically for heart regeneration. There have been several advancements in directed differentiation protocols of hiPSC-CMs *in vitro* since the establishment of the first protocol in 2009 (Jianhua Zhang et al., 2009). Since then, several methods have been tested and optimized to increase the production yield of CMs and other cardiac-associated cells without the technical and ethical issues as well as accessibility limitations associated with the use of primary ESC-CMs. Differentiation of hiPSC toward cardiac lineage often requires a purification stage to increase the yield of produced CMs. This purification step has been particularly critical, as it is well accepted that differentiation protocols could also produce other cell types such as fibroblasts or endothelial cells (ECs) (Ban, Bae, & Yoon, 2017). The potential of hiPSC-CMs for cardiac repairment has started to be explored in a recent reported clinical trial. This study involved direct injection of allogenic hiPSC-CMs in the myocardium of patients with severe LV disfunction and MI history, at the same time of a coronary artery bypass grafting surgery (ClinicalTrials.gov Identifier: NCT03763136: Treating Heart Failure With hPSCc-CMs (HEAL-CHF)) (Mallapaty, 2020). Despite promising efforts, the study is still ongoing, and no peer-reviewed results have been published to the date. To that end, more studies are needed in order to evaluate the efficacy of hiPSC-CM in cardiac therapy.

2.3.1 Challenges of cell-based cardiac therapy

As discussed earlier, injection of dissociated cells in preclinical studies and clinical trials has demonstrated modest improvement in overall cardiac function, attributed mainly to the paracrine communication of the implanted cells with the native host tissue. For

instance, the secretion of angiogenic factors and extracellular vesicles within the native tissue have shown to induce neovascularization within the implanted zones (Kholia et al., 2016). To that end, despite significant advancements, there are still several setbacks regarding cell-based cardiac therapy approaches. First, there is no consensus over the optimal cell type or delivery method to be used since the outcome could be widely influenced by the cell type, the stage of the MI, etc. (Pagano et al., 2019). Additionally, there is a lack of control over the differentiation fate of the stem/progenitor cells upon implantation, as the harsh microenvironment within the infarcted myocardium appears not to favor CM fate (Segers & Lee, 2008) (e.g., endothelial fate is favored in the native myocardium).

Furthermore, engraftment in non-target organs has been reported by several authors (Kurtz, 2008). Therefore, more thorough screenings are necessary to discard teratogenic risks (Michael A Laflamme & Murry, 2005). Additionally, one of the main differences between clinical trials and preclinical studies is the time elapsed between MI and cell injection. In general, for animal models, the extraction, purification, and expansion or differentiation of stem cells are performed before induction of MI, where the cells are injected within a timeframe of a few hours. However, in the case of human patients, it can take several weeks from the extraction of the primary tissue to the final expansion of stem cells, where it has been suggested that the time immediately after MI might be a critical window of opportunity to obtain an efficient outcome (S. L. Chen et al., 2004; X. Wang, Xi, & Wang, 2014). It is also well accepted that the recellularization of damaged tissue is dependent on the extent of the scar or fibrotic area. Yet, there is no consensus on the number of cells necessary for injection. In clinical settings, this proves to be more

challenging to optimize and standardize since each case presents different localization and extent of damage, contrary to the preclinical models, where the extent and type of cardiac injury are precisely controlled following well-defined protocols. Ultimately, the issue of controlling stem cell fate *in vivo* has led researchers to differentiate stem cells into cardiac lineage *in vitro*, then evaluate the efficacy of implanted stem cell-derived cells for their therapeutic potential. The use of autograft hiPSCs or hiPSC-derived cells for regenerative cardiac therapy may potentially reduce the risk of incompatibility and immune reaction upon cellular or tissue implantation as compared to other cells (Rezai et al., 2005). However, it is known that one of the main disadvantages of using either hiPSC- or hESC-CMs for regenerative medicine is their relatively immature phenotype, resembling more a fetal state than an adult phenotype (Claire Robertson, David D Tran, & Steven C George, 2013), characterized by poor development of sarcomeric apparatus (Kamakura et al., 2013), smaller size than adult CMs, and inadequate electrophysiological activity (Ca^{2+} handling and action potential) (Claire Robertson et al., 2013). The immature profile of hiPSC- or hESC-CMs may also lead to several complications after implantation due to the failure of engraftment and synchronization with the native tissue. In addition, there have been some reports discussing the potential risk of tumor formation upon injection of stem cell-derived cells (Volarevic et al., 2018). To address these limitations, tissue engineering approaches have been widely investigated for the development of mature cellular aggregates or tissue surrogates for repair and regeneration of damaged myocardium. In the next section, we discuss tissue engineering technologies, highlighting the advantages and disadvantages of each approach, with a particular focus on scaffold-free strategies.

2.4 MICROSCALE TISSUE ENGINEERING FOR CARDIAC REGENERATION

Tissue engineering approaches have emerged in the past decades to develop functional cellular structures *in vitro* that can be readily integrated into the host myocardium as a potentially powerful alternatives strategy for the treatment of MI (Hirt, Hansen, & Eschenhagen, 2014). While early attempts focused on engineering of macroscale tissue constructs, the advancements in microscale technologies (i.e., microengineering) in the past few years have provided a unique ability to develop biomimetic tissue models with native-like properties and cellular/ECM organization for regenerative medicine and disease modeling applications (e.g. cancer) (Benam et al., 2015; Huh, Torisawa, Hamilton, Kim, & Ingber, 2012; Nagaraju, Truong, Mouneimne, & Nikkhah, 2018; Pedde et al., 2017; D. Truong et al., 2019; D. D. Truong et al., 2019; Jaimeson Veldhuizen, Raymond Q Migrino, & Mehdi Nikkhah, 2019). The use of microengineering technologies for cardiac disease modeling and drug screening, in recent years, has been demonstrated and discussed extensively (J. Veldhuizen, J. Cutts, D. Brafman, R. Q. Migrino, & M. Nikkhah, 2020a; Jaimeson Veldhuizen et al., 2019; Voges et al., 2017; L. Wang et al., 2014; Zuppinger, 2019). The scope of the current manuscript is to provide a review on microscale engineered cardiac tissues or, in other words, engineering *"cardiac microtissues"* (CMTs) for myocardial replacement therapy. A microtissue can be broadly defined as an engineered 3D biological structure within the micrometer range, which is formed by the functional aggregation of one or more cell types. Assembly of microtissues may or may not be supported by natural or synthetic biomaterials, such as ECM proteins and hydrogels (Huang et al., 2020). Engineered microtissues can be generally categorized into two different groups: scaffold-based and scaffold-free microtissues. The 3D environment

within the engineered microtissues provides a natural niche for cellular assembly with enhanced cell-cell interactions, physiologically relevant autocrine and paracrine signaling, as well as an improved function that mimic the *in vivo* conditions (Ravi, Paramesh, Kaviya, Anuradha, & Solomon, 2015). A key advantage in utilizing microscale technologies for engineering cardiac tissues is the induction of precise cellular organization and architecture, often in conjunction with modulated electromechanical cues (Annabi et al., 2013). Particularly, in the native heart, the structural anisotropy and architecture of the myocardium are as critical as the cellular and ECM composition of the tissue, which modulate normal tissue-level homeostasis and function. This 3D cellular organization is paramount to produce synchronized and unidirectional contractions. Conversely, cell misalignment has been linked to disruption of tissue homeostasis and emergence of several cardiovascular diseases (Kowalski et al., 2017; Maron, 1983). To that end, tissue engineering and specifically microscale tissue engineering approaches provide more robust methods to precisely modulate cellular and tissue-level structure and function to address limitations of the cell-based cardiac therapies.

2.4.1 Optimized cell culture for engineering of cardiac microtissues (CMTS)

Although numerous cell types have been used to engineer CMTs, not all cells are suitable for the use in cardiac regeneration to achieve the desired function and structural outcomes. The use of donor primary stem cells, such as those extracted from BM, adipose tissue, or cardiac muscle, represents a significant challenge due to the need for extensive *in vitro* expansion procedures. The use of ESCs also raises ethical concerns (Zacharias, Nelson, Mueller, & Hook, 2011). To that end, in recent years, there has been significant

attention toward the use of hiPSC in cardiovascular regeneration, similar to cell-based cardiac therapy. Different strategies thus far have been proposed to improve the maturation state of hiPSC-CMs for their use in engineering of functional CMTs. These approaches have aimed to mimic the microenvironment of the heart by introducing specific cues to the cell culture, which has been thoroughly reviewed by several authors (Jiang, Park, Hong, & Ban, 2018; Keung, Boheler, & Li, 2014); Scuderi and Butcher (2017); (Xiulan Yang, Lil Pabon, & Charles E. Murry, 2014). Evaluation of the maturation state of hiPSC-CMs is not trivial, and different markers have been utilized to determine their maturity level. Functional maturation has been traditionally defined by three principal factors: a) structural features, as measured by increased cell size, elongated morphology (Lundy, Zhu, Regnier, & Laflamme, 2013), organization of sarcomeric structures (Dias et al., 2018), and upregulation of cellular ultrastructure-related genes (MYH7, GJA1, TNNI3, AKAP6, GJA5, JPH2) (Ronaldson-Bouchard et al., 2018); b) enhanced electrophysiological properties, such as increased action potential amplitude, lower resting membrane potential, and increased conduction velocity (Jiang et al., 2018) and Ca^{2+} handling (increased calcium release and reuptake rates)(Lundy et al., 2013) along with upregulation of Ca^{2+} handling genes (CAV3, BIN1, ATP2A2, RYR2, ITPR3) (Ronaldson-Bouchard et al., 2018); and finally c) increased mechanical function, measured through higher contraction force (Ribeiro et al., 2015) when compared to fetal-state CMs along with regulation of contractile function-related genes, such as upregulation of the ones encoding for cTnT, αMHC, CASQ2, SERCA2 (D. Zhang et al., 2013), ITPR3, KCNH2 and downregulation of HCN4 (Ronaldson-Bouchard et al., 2018). At the molecular level, metabolic changes and regulation of genetic programs have also been among the critical markers of hiPSC-CMs

maturation. For example, a shift from glycolytic to oxidative metabolism is a marker for metabolic maturation, which indicates an increase in the oxidative capacity of the mitochondria (Cláudia Correia et al., 2018; Lopaschuk & Jaswal, 2010). This better resembles the energy sourcing and utilization of CMs in the native myocardium after birth. Other metabolic markers, including the enrichment of phospholipid metabolism and pantothenate and Coenzyme A metabolism, have been also identified as indicators of maturation (Bhute et al., 2017).

It has been reported that the presence of a 3D microenvironment within engineered CMTs can notably improve the structural and functional maturation of hiPSC-CMs. For example, in a recent study, Correia et al. characterized and compared the metabolic function of hiPSC-CMs cultured in 3D cell aggregates compared to 2D cell culture (Cláudia Correia et al., 2018). hiPSC-CMs cultured within the 3D environment shifted towards an oxidative metabolism, whereas 2D cultured cells exhibited glycolytic metabolism, which is less energy-efficient and is associated with a more immature phenotype. Electrophysiological properties, as defined through extended action potential duration, were also improved in the 3D cell aggregates. While the complete mechanism of metabolic regulation has not been well understood yet, it was suggested that 3D cell culture favors the paracrine, autocrine, and endocrine communication. Therefore, it was proposed that maturation of hiPSC-CMs was driven by downregulation of the PI3K/AKT/insulin pathway and upregulation of genes involved in fatty acid metabolism. A combination of maturation-inducing techniques has been another viable strategy to enhance the maturation of hiPSC-CMs, similar to the native myocardium. A prominent example is the Biowire platform created by Nunes et al., which combined the use of two different scaffolds, namely

a surgical suture and type I collagen matrix, along with electrical stimulation to improve the functional maturation of hiPSC-CMs (Nunes et al., 2013). Using this platform, the electrophysiological features of the hiPSC-CMs improved, resembling more closely the characteristics of the native adult CMs.

Overall, it is paramount to utilize strategies to induce a more mature phenotype in hiPSC-CMs within engineered CMTs to enable safer and more efficient engraftment as well as synchronization upon implantation or injection into the native myocardium.

2.4.2 Engineering Scaffold-Based Cardiac Microtissues (SB-CMTs)

Engineering of SB-CMTs requires at least two primary components: first, a biomaterial matrix that serves as scaffolding support and offers a 3D ECM-like structure within the engineered tissues, and second, cells of interest to populate within the 3D environment of the matrix. The use of scaffolding biomaterials for the creation of engineered CMTs serves several purposes. Primarily, the scaffold matrix could mimic the native tissue ECM, offering mechanical support for the cells to undergo morphogenesis and assemble in a 3D architecture. Integrated architectural and topographical cues can also be introduced within the engineered scaffolds (Cutts, Nikkhah, & Brafman, 2015; Nikkhah, Edalat, Manoucheri, & Khademhosseini, 2012; Zorlutuna et al., 2012). For example, anisotropy in engineered CMTs enables enhanced CMs alignment, contractile stress generation, and improved electrophysiological functions (Saini, Sam, Kharaziha, & Nikkhah, 2018). It has been also demonstrated that scaffold stiffness plays a crucial role in the biological function and metabolism of encapsulated cells in general (Pal, Vernon, & Nikkhah, 2018) and particularly CMs. Independent studies have shown that, when encapsulating CMs or CPCs,

the amplitude of contraction and expression of specific genes (e.g., vWF and CNN1 in case of CPCs) can be modulated by changes in the stiffness of the scaffolding matrix (Marsano et al., 2010; Harpinder Saini, Ali Navaei, Alison Van Putten, & Mehdi Nikkhah, 2015; Shapira-Schweitzer & Seliktar, 2007; Williams et al., 2015). Biochemical signaling cues have also been introduced to SB-CMTs through modification of the chemical moieties and composition of scaffolds (Chun et al., 2015; Sreejit & Verma, 2013) or incorporation of growth factors (Miyagi et al., 2011). Recently, it was demonstrated that cellular constructs fabricated with varying types of cells, for instance hESC-derived CMs in coculture with hESC-derived epicardial cells, embedded in collagen matrices, present a more mature state and improved capacity for remuscularization of infarcted myocardium (Bargehr et al., 2019). Additional components, such as vascular-like structures (Lux et al., 2016; Thomson et al., 2013), can also be integrated within the SB-CMTs through different fabrication strategies (e.g., bioprinting, micropatterning) (Pedde et al., 2017). The use of scaffolding biomaterials also enables precise manipulation of electrical or mechanical cues within the 3D tissue environment through exogenous signals, such as conductive nanomaterials or cyclic mechanical stretch, for improved cellular- and tissue-level functions (Baei, Hosseini, Baharvand, & Pahlavan, 2020; Kharaziha et al., 2014; Liaw & Zimmermann, 2016; Lux et al., 2016; Navaei et al., 2017; Ali Navaei, Harpinder Saini, et al., 2016; Nunes et al., 2013; Shin et al., 2016).

To date, several natural and synthetic materials have been identified as biocompatible candidates for cardiac tissue engineering (Cutts et al., 2015). For example, fibrin (Barsotti, Felice, Balbarini, & Di Stefano, 2011) and collagen (Z. Li & Guan, 2011) have been among the natural-derived hydrogels used for the development of SB-CMTs

construction. Some of the frequently used synthetic polymers for cardiovascular tissue engineering poly(N-isopropylacrylamide) (poly(NIPAAm) (D. J. Lee et al., 2019; Nagase, Yamato, Kanazawa, & Okano, 2018; Ali Navaei, Danh Truong, et al., 2016; Pal et al., 2020) are polylactic acid (PLA), polyglycolic acid (PGA), poly(glycerol sebacate) (PGS), among others (Mathur, Ma, Loskill, Jeeawoody, & Healy, 2016). There has also been extensive work in the development of composite (Shapira, Feiner, & Dvir, 2016), electrospun (Kharaziha et al., 2013; Kitsara, Agbulut, Kontziampasis, Chen, & Menasché, 2017), and nanoengineered (Holzwarth & Ma, 2011; Kharaziha et al., 2014) scaffolds with well-tuned mechanical and electrical properties to engineer highly functional SB-CMTs. While there have been numerous review articles providing excellent overviews on the types and characteristics of scaffolding biomaterials for cardiac tissue engineering, the subject of SB-CMTs is out of the scope of the present review article, and the readers are referred to earlier works (Pomeroy, Helfer, & Bursac, 2019).

2.4.2.1 Challenges of Scaffold-Based Cardiac Tissue Engineering

The use of scaffolding biomaterials, in cardiac tissue engineering, offers a robust strategy for cellular delivery and engraftment of the engineered tissue with the host myocardium. Moreover, it has been observed in preclinical trials that the implantation of SB-CMTs (i.e., cardiac patches) can have paracrine effects in the myocardium, that could lead to angiogenesis and reduced infarct size (Jianyi Zhang, Zhu, Radisic, & Vunjak-Novakovic, 2018). However, the delivery method of SB-CMTs to the target site within the host myocardium is subjected to factors such as the size and geometry of the tissue. Generally, SB-CMTs are constructed in the form of patches or sheets and are implanted in

the heart via thoracotomy, which is a highly invasive surgery. Moreover, there is no agreement on the optimal implantation location of patches (Feric & Radisic, 2016). Furthermore, engineering of SB-CMTs that are compatible with the host myocardium and its complex microenvironment is not a trivial task. It is well known that the stiffness of the myocardium can change according to the developmental stage, age, and stage of the cardiac disease of the patient. While immature hiPSC-CMs adapt better to scaffolds resembling the neonatal stiffness of the heart, the performance of SB-CMTs may benefit from a well-tuned stiffness similar to the one of the adult heart (Jacot, Martin, & Hunt, 2010). Cell behavior is also heavily influenced by the mechanical properties (stiffness, swelling, cross-link density) of the scaffolding matrix, causing the cells to behave differently as compared to the native tissues (Rajabi-Zeleti et al., 2014; van Spreeuwel et al., 2014; Zong et al., 2005). Degradation of scaffolding biomaterials may also pose another challenge in the implantation of SB-CMTs. For instance, a delicate balance between degradation rate and cellular interconnection and deposition of new ECM needs to be achieved. If the scaffold degrades too quickly, the delivered cells will not have the opportunity to form sufficient cell-to-cell and cell-to-ECM interactions to support their engraftment. On the other hand, if the scaffold does not degrade fast enough, it can elicit a foreign body reaction and fibrotic encapsulation (Bar & Cohen, 2020). In either case, there is a need for better optimization of a suitable degradation rate of the matrix. Also, it has been reported that ECM-derived scaffolds may exhibit immunogenic activity (Jawad et al., 2007) and elicit immune response (chronic inflammation, implant rejection) within the native tissue upon implantation. To that end, the clearance pathways and potential toxicity of the degradation byproducts need to be well studied prior to proceeding clinical trials.

2.5 SCAFFOLD-FREE CARDIAC TISSUE ENGINEERING

With the advancements in innovative tissue engineering strategies aided by micro- and nanoscale technologies, engineering of scaffold-free cardiac microtissues (SF-CMTs) have been proposed as a potentially attractive alternative to bridge the existing gap between cell-based cardiac therapy and scaffold-based tissue engineering approaches. Engineering of SF-CMTs offers the robustness and enhanced organization of SB-CMTs with the potential for less-invasive delivery methods, similar to cell-based cardiac therapies (W. Y. Lee et al., 2009), without the introduction of exogenous biomaterials. SF-CMTs can range from basic self-assembled spheroid cell aggregates, formed exclusively from primary CMs or stem cell-derived cells (W. Y. Lee et al., 2011; D. C. Nguyen et al., 2014) to more complex organoid structures composed of different cell types, such as CMs, cardiac fibroblasts (CFs), ECs, and even CPCs (Desroches et al., 2012; Emmert, Wolint, Wickboldt, et al., 2013; T. Y. Kim et al., 2018). In addition, through the incorporation of microengineering technologies, it has been possible to precisely control the architecture, cellular organization, and size/geometry of SF-CMTs. In the following sections, we discuss the relevant properties and features of SF-CMTs as well as the main fabrication strategies and will highlight the key study cases in the engineering of SF-CMTs for cardiac repair.

2.5.1 Size and geometry

It is well accepted that a gradient of oxygen and nutrients is formed within engineered tissue constructs due to the lack of proper vascularization and packing cellular density (Rouwkema, Koopman, Blitterswijk, Dhert, & Malda, 2009). Induction of hypoxic or necrotic cores is desirable for disease modeling (i.e., MI, ischemia, etc.) and drug screening

(Dylan J Richards et al., 2020). However, in the case of regenerative medicine, microtissues, and specifically SF-CMTs, must be engineered carefully to maintain cell viability to allow for engraftment and survival after implantation within the host myocardium. Different mathematical models have been developed in order to predict and optimize the best size-to-diffusion limit ratio of microtissues and organoids (Di Costanzo et al., 2018; McMurtrey, 2016; Milica Radisic, William Deen, Robert Langer, & Gordana Vunjak-Novakovic, 2005). Still, that ratio might vary according to the metabolic demands of the various cell types used for the fabrication of SF-CMTs. For instance, it has been reported that hiPSC-CMs cultured in 3D microenvironments have a higher metabolic rate than in 2D cultures (Yu Tan et al., 2017). As a consequence, higher concentrations of oxygen and nutrients, as well as a higher waste product removal are required (Cláudia Correia et al., 2018; Ulmer et al., 2018). In order to elucidate the optimal size for enhanced cell-to-cell interactions and diffusion limitations, Tan et al. constructed hiPSC-CMs spheroids of varying sizes and measured oxygen consumption rates, and their metabolic and electrophysiological activity (Yu Tan et al., 2017). It was demonstrated that spheroids with a radius of ~150μm (about 3000 cells/spheroid) presented the optimal metabolic activity while maximizing the benefits from the 3D microenvironment created within the microtissue.

The introduction of ECs has been proposed as an alternative to overcome the diffusion restriction in order to produce SF-CMTs with physiologically relevant sizes. The goal is to form vasculature-like structures within the microtissues that can carry oxygen and nutrients to the inner-most areas, allowing for the formation of larger, healthier scaffold-free tissues (Griffith et al., 2005; Noguchi et al., 2016; Sakaguchi, Shimizu, & Okano, 2015). In a

recent study, Pitaktong et al. fabricated spherical SF-CMTs with hiPSC-CMs, CFs, and hiPSC-derived early vascular cells (EVCs) (which can differentiate into ECs or pericytes) in a ratio of 7:1.5:1.5 respectively (Pitaktong et al., 2020). Spheroids with diameters up to 500μm were viable and exhibited organized vasculature-like structures. In addition to enhanced cell organization and primitive microvasculature, it was believed that the presence of ECs and CFs increased the resistance of the CMs to hypoxic conditions via paracrine signaling. Similarly, Beauchamp et al. created scaffold-free 3D cocultures of hiPSC-CMs and primary embryonic CFs (Beauchamp et al., 2020) (**Figure 2.3 A(i-ii)**) to elucidate the influence and role of CFs in the formation of SF-CMTs. It was found that the presence of CFs in the 3D coculture influenced the morphology (elongated) and maturation stage (higher expression of cTnI) of the hiPSC-CMs, making them more similar to adult CMs. Noguchi et al. also proposed the use of ECs and fibroblasts to create vascularized scaffold-free cardiac patches (Noguchi et al., 2016). For this purpose, they used neonatal rat CMs, human ECs, and human fibroblasts to create spheroids (**Figure 2.3 B(i)**). Vasculature formation was observed within the spheroids, which were further assembled to form cardiac patches of up to 10 mm of diameter (**Figure 2.3 B(ii-vi)**). It was reported that the ratio of CMs:ECs:CFs affects the functionality of SF-CMTs, with an optimal cellular ratio of 7:1.5:1.5 (CMs:ECs:CFs). Fractional shortening (FS) was directly proportional to the percentage of CMs in the spheroid, with a higher FS in pure CM-derived SF-CMTs when compared to multicellular SF-CMTs. However, multicellular constructs displayed enhanced cell organization and functioning microvascular structures. When implanted in mouse hearts, the optimized multicellular SF-CMTs successfully adhered to the native LV with the presence of blood flow within the microtissues. They concluded

that the SF-CMTs displayed enhanced properties with potential for recellularization and repairment of the heart. Similarly, Ong et al. created scaffold-free cardiac patches using multicellular (hiPSC-CMS, CFs, and ECs) cardiac spheroids as building blocks through 3D bioprinting technique(Ong et al., 2017). Primitive vessels ($CD31^+$ structures) were found, and implantation onto rat hearts suggested engraftment and vascularization (erythrocytes found in the explanted patch). Overall, these studies demonstrated that the introduction of ECs and CFs in SF-CMTs favors the formation of vascular structures and facilitates the fabrication of cellular constructs with increased sizes.

Other alternatives for enhanced size and tissue vascularization are based on the creation of SF-CMTs with geometries that favor cellular distribution over two dimensions and limit it over the third dimension, resulting in sheet-like constructs (Joseph Yang et al., 2005). Since the thickness of these constructs does not exceed the diffusion limits (~20μm), the cells remain viable. For instance, Okano's group demonstrated that sheet-like SF-CMTs, formed with CMs and ECs (ratio 9:1), expressed angiogenesis-related genes (vascular endothelial growth factor (VEGF), cyclooxygenase, tyrosine kinase, angiopoietin-1 (Ang-1) and angiopoietin-2 (Ang-2)) (Sekiya, Shimizu, Yamato, Kikuchi, & Okano, 2006). Histological analysis further revealed neovascular networks that were maintained and engrafted with the native myocardial tissue upon implantation. The contribution of the cell sheets to neovascularization of the native mouse heart was observed after implantation. Thus, the inclusion of non-CMs in the fabrication of SF-CMTs has proven beneficial as they can help induce neovascularization, paracrine crosstalk with CMs, as well as help to overcome size limitations and engraftment issues.

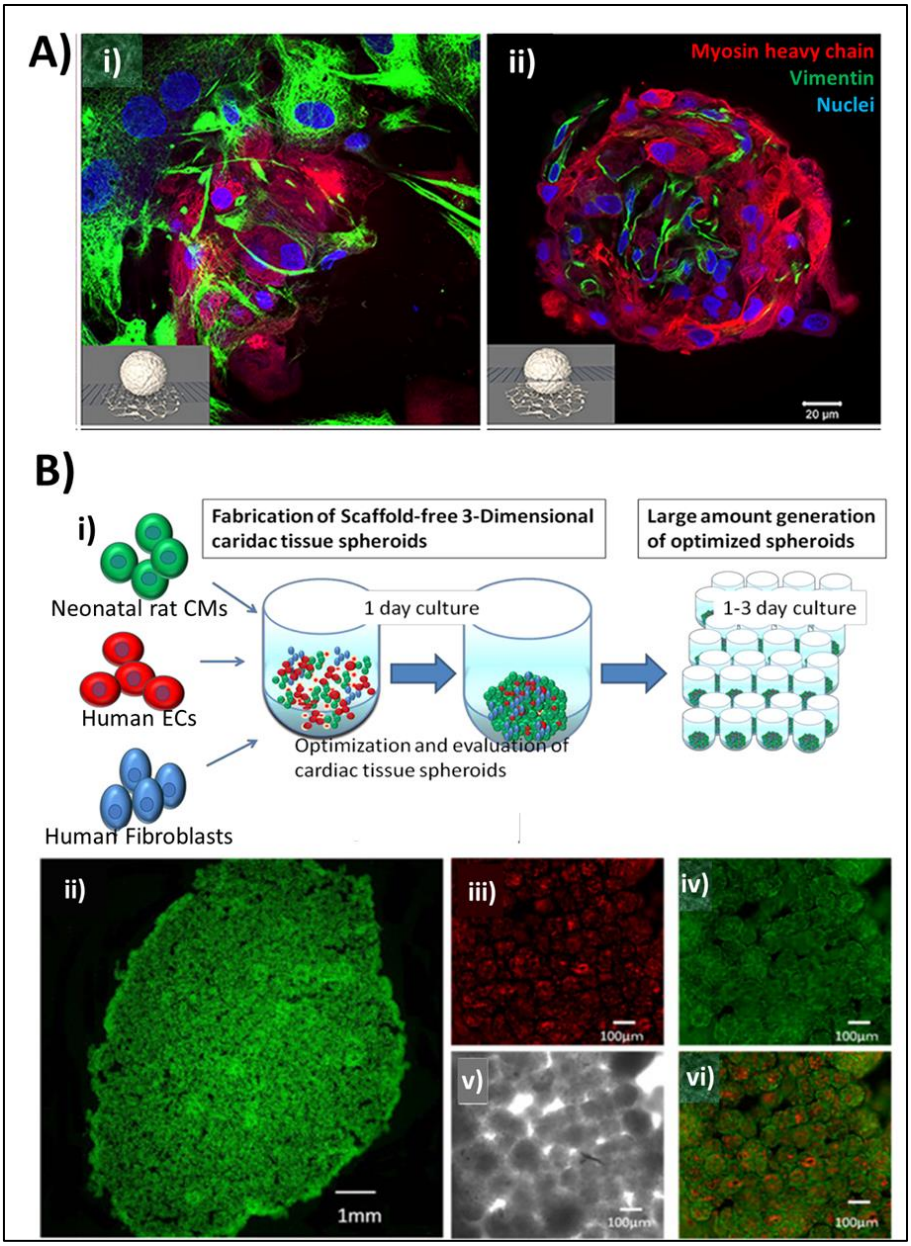

Figure 2.3. 3D coculture enhances the features of SF-CMTs. A) Confocal imaging of multicellular cardiac spheroid showing i) an optical section of the substrate level and ii) an optical section above the substrate level. (Myosin heavy chain: red, vimentin: green, and nuclei: blue (scale bar=20µm)). *Adapted with permission from The Authors (Beauchamp et al., 2020). Copyright © (2020).* B) Formation of a vascularized cardiac patch, composed of multicellular cardiac spheroids, showing i) schematic for the fabrication of cardiac spheroids, ii) contractile cardiac graft fabricated using the prevascularized spheroids, rat neonatal CMs showed in green, iii) ECs within the cardiac graft (red), iv) amplification of the rat neonatal CMs (green), v) phase contrast amplification and vi) merged image. *Adapted with permission from The Authors (Noguchi et al., 2016). Copyright © (2016).*

2.5.2 Cell composition and fabrication methods of SF-CMTs

There have been mainly two approaches to the fabrication of SF-CMTs. The first is based on guided self-aggregation of terminally differentiated cells, and the second requires the formation of stem cell aggregates and further differentiation into cardiac cells. In either case, the formation of self-assembled cellular aggregates is believed to be driven by thermodynamic processes. In particular, cell culture conditions for the production of SF-CMTs are required to achieve a balance such that the interfacial tensions and adhesion forces between the cells are smaller than those of the cells with the substrate; therefore, the cells are forced to attach between them and arrange in a manner that minimizes the free energy of the system (Brodland, 2002). The availability of adhesion proteins (connexins and cadherins) on the cell surface also plays an important role in minimizing the free energy of the system (Bhute et al., 2017; Matthys, Hookway, & McDevitt, 2016). In 1971, Halbert et al. reported for the first time that primary CMs have the potential to form self-assembled cell aggregates when cultured on non-adhesive polystyrene surfaces (Halbert, Bruderer, & Lin, 1971). Since then, several methods have been proposed based on those principles.

One of the early methods utilized for scaffold-free cell culture was the hanging drop technique. The basic principle behind this method consists of placing a cell suspension in a cover glass and inverting it (Halbert et al., 1971). By doing so, the superficial tension allows for the liquid of the cell suspension to hang from the cover glass. At the same time, gravity forces the cells to gather at the bottom of the droplet, promoting cell-to-cell adhesions and deposition of ECM proteins. For the specific case of cardiac tissue engineering, SF-CMTs can be formed using only CMs or cocultures of CMs with other cell

types (Polonchuk et al., 2017). To date, more sophisticated mechanisms have been developed to allow high-throughput and prolonged culture periods (Frey, Misun, Fluri, Hengstler, & Hierlemann, 2014; Neto et al., 2015). Sectioning of these SF-CMTs and further staining enables for the identification of cell types and their distribution within the CMT. Usually, a homogeneous cellular distribution can be found when using terminally differentiated cells. In addition, the deposition of ECM proteins can be confirmed in these spheroids. Beauchamp et al. created cardiac spheroids from hiPSC-CMs with varying sizes (2500, 5000, and 10000 cells/spheroid) using the hanging drop cell culture approach (Beauchamp et al., 2015). After three weeks in culture, sectioning, and immunostaining for cardiac-relevant proteins (Cx43, myomesin), and a Ca^{2+} handling assay were performed to evaluate the viability and electrophysiological function of the formed SF-CMTs. A homogeneous cell distribution with partially aligned myofibrils was demonstrated, with the cells presenting rounded morphology, reminiscent of those found in the fetal heart. Despite the rounded morphology, the developed SF-CMTs were responsive to pharmacological and electrical stimulations, measured through Ca^{2+} transients. Therefore, they confirmed that it is possible to form cell aggregates from hiPSC-CMs, using the hanging drop method, that respond to exogenous stimuli, rendering this technique a promising approach for the fabrication of SF-CMTs. However, the use of this method presents some disadvantages, for example, changing the culture media and collecting the SF-CMTs can be troublesome due to the small volume of the samples (Breslin & O'Driscoll, 2013), as well as the obstacle of enhancing CM maturation state.

Microengineered platforms have widely been utilized or designed as a more modern and innovative approach for the development of SF-CMTs in order to overcome some of

the challenges of more traditional methods such as hanging drop technique (Napolitano et al., 2007). Microfabrication techniques would specifically enable controlled cellular aggregation, uniform size, and geometry of SF-CMTs and continuous media change. Such fabrication methods have permitted the creation of microscale features, such as microwells, with high fidelity and reproducibility to generate SF-CMTs in a high throughput manner (Napolitano et al., 2007). For example, Cha et al. utilized photolithography and soft lithography methods to create cylindrical microwells with inverted-pyramidal openings (Cha et al., 2017). They created a silicon (Si) master mold through a series of etching steps. Then, polydimethylsiloxane (PDMS) was used to create a negative replica of the Si master mold, which was in turn used as a stamp over polyethylene glycol (PEG) hydrogel to cast the final microwell array. Human MSCs were seeded at a density of $2x10^5$ to $6x10^5$ cells/array to test the feasibility of the platform. Uniform-sized spheroids with diameters ranging from 100 to 180 μm were created, depending on the cellular seeding density. This platform offered a simple method for the creation of spheroids with highly controlled cell number and size. Other similar approaches based on soft-lithography were also implemented by casting agarose hydrogel using elastomeric stamps or molds (Dahlmann et al., 2013; Fennema, Rivron, Rouwkema, van Blitterswijk, & de Boer, 2013). The low cellular adhesion to the agarose surface enables self-cellular aggregation, inducing cell-to-cell adhesions for the formation of cellular constructs. Additionally, the high fidelity of agarose casting (down to micrometer scale) allows for the precise creation of microwells of varying shapes and sizes.

Agarose and other hydrogels (i.e., methylcellulose hydrogel) have been alternatively used for coating cell culture plates, producing ultra-low adhesion surfaces for

inducing cell aggregation. It is also feasible to induce self-aggregation and form SF-CMTs using polystyrene culture dishes. For instance, Giacomelli et al. seeded hiPSC-CMs and hiPSC-derived ECs ($CD34^+$) on conical 96-well plates in order to fabricate complex multicellular SF-CMTs (Giacomelli et al., 2017). They used different ratios of hiPSC-CMs:ECs to evaluate the optimal composition. It was found that the composition that led to the best organization and distribution of the $CD34^+$ was 85%:15% (of hiPSC-CMs:ECs, respectively) (**Figure 2.4 A(i-ii)**). Further qRT-PCR analysis of hiPSC-CMs:ECs SF-CMTs showed significant changes in expression of genes relevant for the cardiac function, specifically, the upregulation of sarcomeric structural genes, ion-channel genes, and Ca^{2+} handling genes, as compared to the 2D culture of hiPSC-CMs. In a more recent study by the same group, isogenic hiPSC-derived CMs, CFs and ECs were used to form tri-cellular SF-CMTs (Giacomelli et al., 2020). It was demonstrated that the inclusion of hiPSC-CFs improved the maturation of the hiPSC-CMs (enhanced cellular structures, mitochondrial metabolism, and electrophysiological features), through the cellular coupling mediated by gap junctions between the hiPSC-CMs and hiPSC-CFs and tri-cellular crosstalk. These results confirmed that the coculture of cells can enhance features relevant for SF-CMTs. In a similar fashion, Ravenscroft et al. formed spheroids composed of hiPSC-CMs and non-myocyte cells (dermal ECs, coronary artery ECs, and CFs) using round bottom ultra-low adhesion plates (**Figure 2.4 B(i-vi)**) (Ravenscroft, Pointon, Williams, Cross, and Sidaway (2016)). They assessed the contribution of non-myocytes to the state of maturation of both hESC-CMs and hiPSC-CMs cultured in SF-CMTs. Cardiac-marker immunostaining of SF-CMTs revealed enhanced striations in the CMs cocultured with ECs and CFs (**Figure 2.4 B(iv)**). Significantly increased expression of S100A1 and TCAP (markers for sarcomere

assembly), PDE3A and KCND3 (markers for cardiovascular function), and NOS3 (nitric oxide production) were found in multicellular SF-CMTs, suggesting crosstalk between non-myocytes and hiPSC-CMs. Also, higher amplitude Ca^{2+} transients and improved caffeine response was found in multicellular SF-CMTs when compared to SF-CMTs composed of monoculture of CMs. However, CMs in the multicellular SF-CMTs still lacked structural maturity.

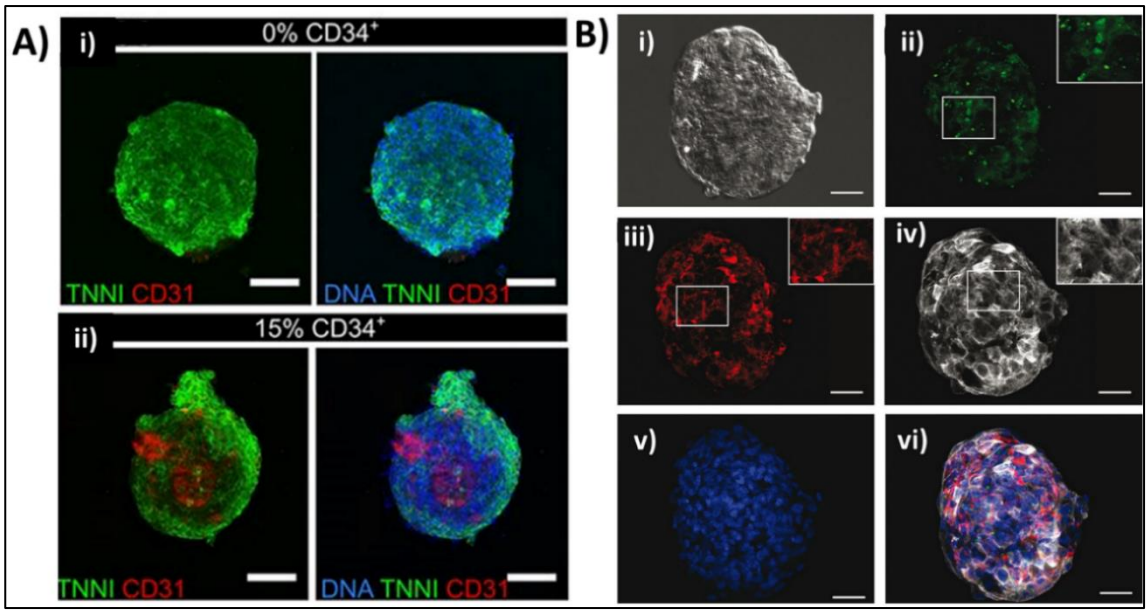

Figure 2.4. Fabrication of SF-CMT using low-adhesion surfaces. A) SF-CMT formed using hiPSC-CMs i) only (green) and ii) SF-CMT formed using a ratio of 85% of hiPSC-CMs and 15% of $CD34^+$ (green and red respectively). (Scale bars: 100µm). *Adapted with permission from The Company Of Biologists Ltd (Giacomelli et al., 2017). Copyright © (2017).* B) Multicellular SF-CMT fabricated using low-adhesion surfaces i) DIC image of a multicellular SF-CMT formed with ii) ECs (CD31: green), iii) fibroblasts (collagen I: red) and iv) CMs (ACTN2: white), v) the nuclei of the cells (blue), and vi) merged image. (Scale bars: 50µm). *Adapted with permission from Oxford University Press (Ravenscroft et al., 2016). Copyright © (2016).*

A different approach for the fabrication of SF-CMTs involves the use of a temperature-responsive polymer, namely poly(N-isopropyl acrylamide) (PIPAAm) (Shimizu et al., 2002). In a relevant work by Okano's group, PIPAAm was used for coating polystyrene culture dishes to create a surface that was slightly hydrophobic and promoted

cell adhesion at 37°C but reversed to hydrophilic and non-adhesive at 20°C(Masuda & Shimizu, 2016) (**Figure 2.5 A(i)**). When MSCs were seeded on these surfaces, they formed cell-to-cell adhesions and coupling, resulting in the formation of scaffold-free microtissues. In a similar work, Sakaguchi et al. (2015) demonstrated that multicellular sheets could be stacked, up to 12-layers, to form thicker microtissues. When layered, the cell sheets formed networks of vascular capillaries interspersed between layers. In another study, Chang et al. created multilayered cell sheets formed with MSCs and transplanted them on the surface of the LV of porcine models (Chang et al., 2015). It was demonstrated that the implanted cell sheets successfully adhered to the host cardiac tissue (**Figure 2.5 A(ii-v)**). Furthermore, Masumoto et al. demonstrated the possibility to form cardiac cell sheets with unpurified hiPSC-CMs (Masumoto et al., 2014). The engineered hiPSC-CM cell sheets were transplanted to a rat model of sub-acute MI to test their regenerative capacity, leading to improved systolic function and LV FS after transplantation. Notably, the implants were able to engraft with the host myocardium, with an accumulation of vWF^{+} ECs around the graft, suggesting neovascularization mediated by the transplanted cells (**Figure 2.5 B(i-ii)**). These approaches confirmed the efficacy of cell sheets as an efficient strategy for the fabrication of SF-CMTs with multicellular constructs and controlled size for cardiac regeneration. However, no direct evidence of electrical coupling has been found between the SF-CMTs and the host myocardium upon implantation.

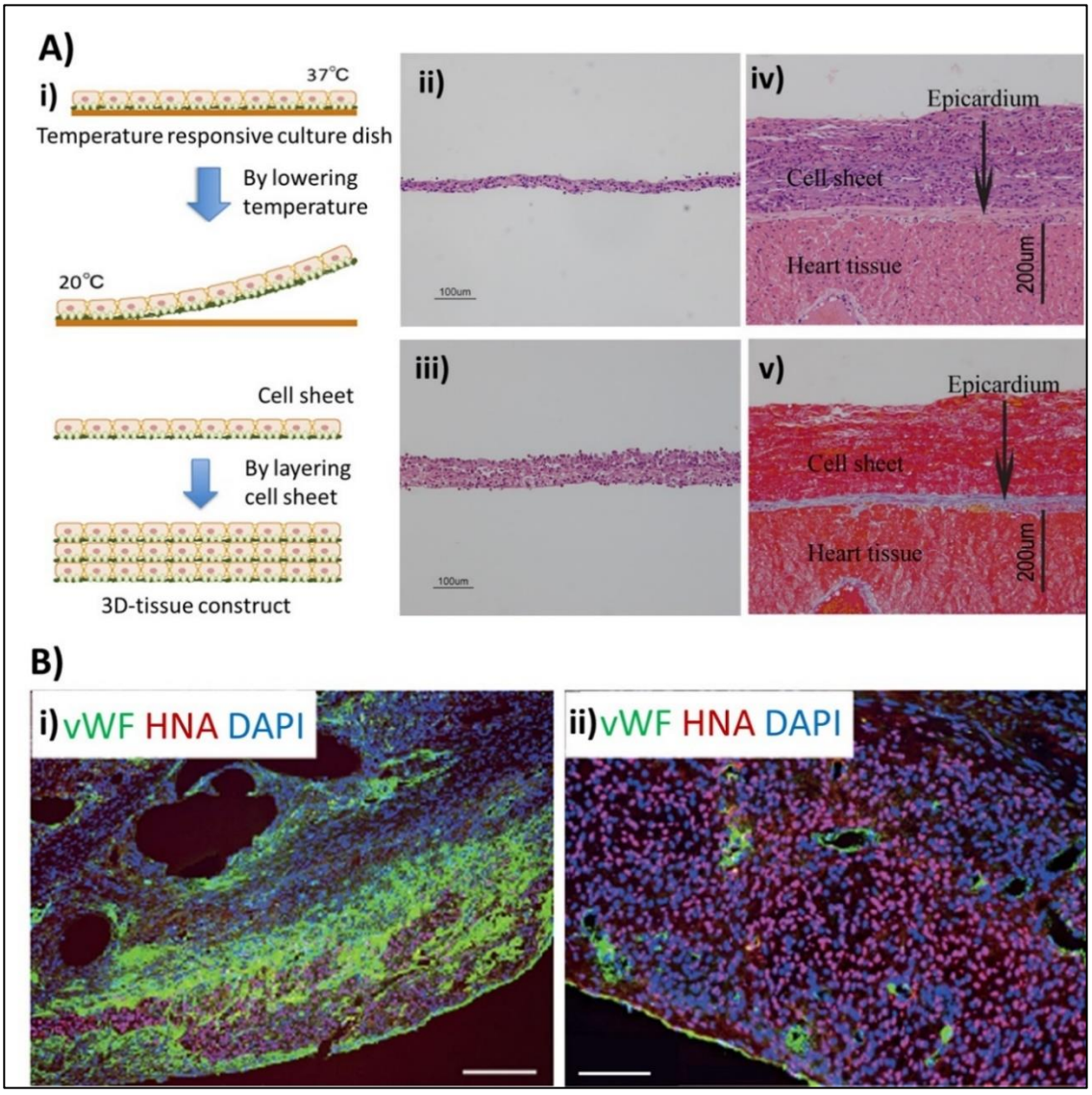

Figure 2.5. Fabrication and implantation of SF-CMTs in the form of cell sheets. A) SF-CMT formed layer by layer using the cell sheet technique i) Diagram for the formation of cardiac cell sheets using temperature-responsive polymeric surfaces. *Adapted with permission from Elsevier B.V (Masuda & Shimizu, 2016). Copyright © (2015).* ii) H&E staining of a cross-section of a monolayer MSC cell sheet and iii) three-layered MSC cell sheet. iv) H&E staining and v) Azan staining (collagen-rich areas showed in blue) for three-layered MSC cell sheet 60 minutes after implantation on porcine heart, showing adhesion to the epicardium. *Adapted with permission from Chang et al. (2015). Copyright © (2015).* B) Engraftment of hiPSC-CM sheets in mouse MI model at i) 3 days, and ii) 28 days after implantation (green: vWF, red: human cell nuclei (HNA), blue: all nuclei (DAPI)) (Scale bars: i) 200µm, ii) 100µm). *Adapted with permission from Springer Nature (Masumoto et al., 2014). Copyright © (2014).*

SF-CMTs can also be derived from the directed differentiation of embryoid bodies (EBs). EBs, usually in spherical geometry, are cellular aggregates formed from pluripotent/multipotent stem cells. EBs were first created for the study of organogenesis and developmental biology, but later their use was expanded for disease modeling, drug screening, and regenerative medicine (Davies, 2018; Dylan J Richards et al., 2017). Conventionally, SF-CMTs derived from EBs are referred to as cardiac organoids as they are composed of multiple types of self-organized cardiac cells that resemble the cell-to-cell interactions of the native myocardium. Adaptations from 2D cardiac differentiation have been implemented to form cardiac organoids from EBs. For example, Yan et al. optimized the traditional GiWi protocol (Xiaojun Lian et al., 2013) (modulation of Wnt/β-catenin canonical signaling pathway) for CM differentiation and applied it to EBs formed with hiPSCs in ultra-low adhesion plates (Yan et al. (2019)). The spontaneous beating of the organoids was observed upon day ten after initial differentiation, with enhanced expression of sarcomeric α-actinin (SAC) and mature sarcomeric structures when compared with 2D hiPSC-CMs. Cells expressing endothelial markers (CD31 and VE-cadherin) were also found within the organoids, demonstrating the co-differentiation of CMs and EBs in the 3D environment, showing their potential for regenerative medicine due to neovascularization. Different sizes of EBs led to different cell compositions under the same culture and differentiation conditions. This suggests that complex cell-to-cell interactions can influence the Wnt signaling pathway and therefore affect the outcome of 3D differentiation.

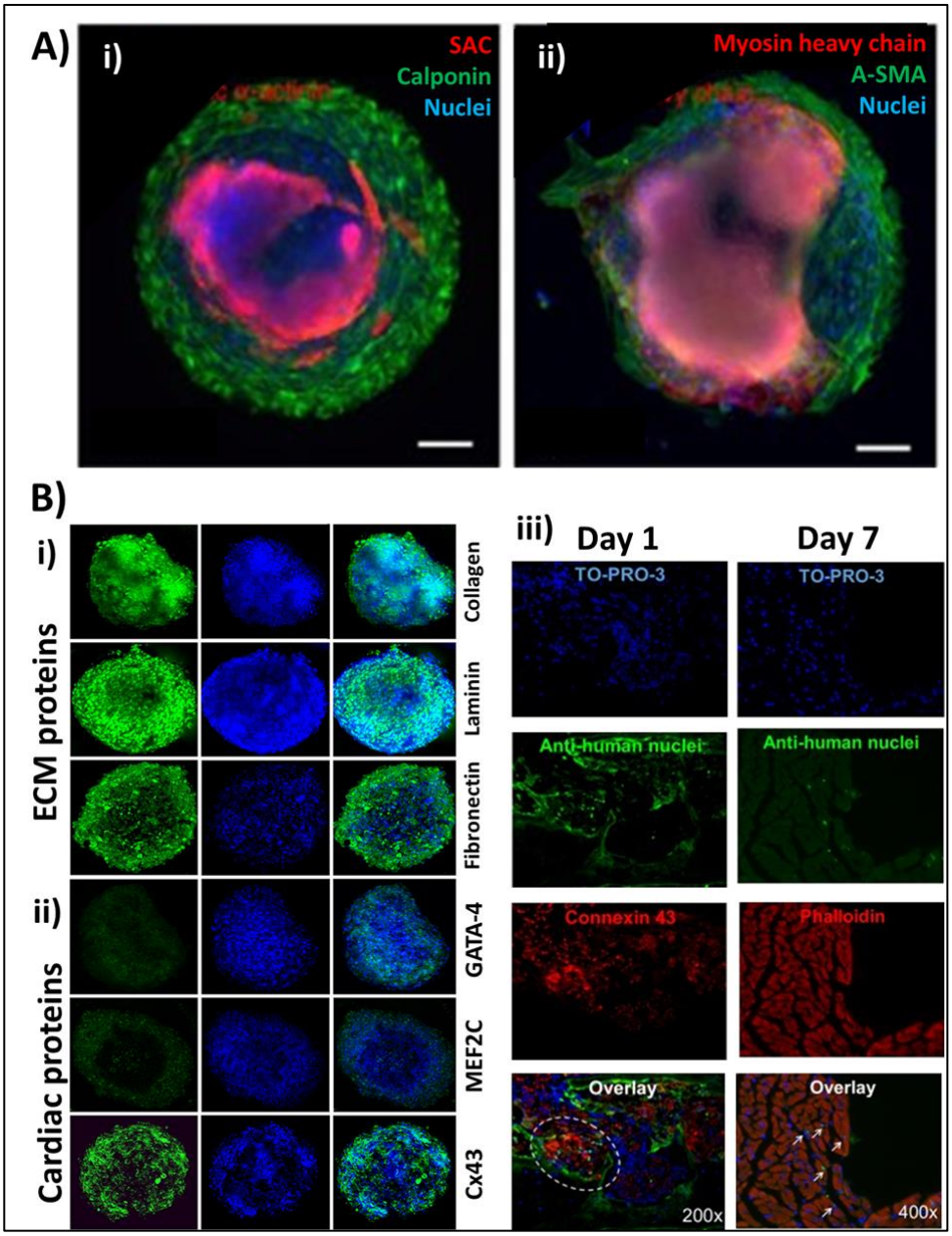

Figure 2.6. Spatial cellular organization within EB-derived SF-CMTs. A) SF-CMT fabrication from the differentiation of EBs, showing CMs in the center and myofibroblasts in the perimeter. i) SAC: red, calponin: green and DAPI: blue. ii) Myosin heavy chain: red, smooth muscle actin: green, DAPI: blue. (Scale bars: 100µm). *Adapted with permission from Springer Nature (Ma et al., 2015). Copyright © (2015).* B) Immunostaining of hCPCs-derived SF-CMT, showing expression of i) ECM proteins, and ii) Cardiac proteins (Scale bar: 50µm). iii) Sections of injured mice myocardium implanted with hCPCs-derived SF-CMT (showed in green) at 1 day (left panel) and 7 days (right panel) after implantation. Circle showing engrafted spheroids and arrows showing dispersed hCPCs. *Adapted with permission from Oltolina et al. (2015). Copyright © (2015).*

The self-organization that occurs within the EBs-derived cardiac organoids has been widely studied to gain a better understanding of how these SF-CMTs can be used for biomedical applications. For instance, it was documented by Ma et al. that the introduction of biophysical (substrate surface patterned and cell confinement) and biochemical (small molecules for directed differentiation) cues in hiPSC-EBs led to spatial cardiac differentiation (Ma et al., 2015). It was observed that the cells in the center of the SF-CMTs expressed cardiac-specific markers (cTnT, SAC, and myosin heavy chain), and the cells in the perimeter expressed myofibroblast markers (SM22, calponin, and smooth muscle actin) (**Figure 2.6 A(i-ii)**). The self-organization characteristics prove useful for the development of pre-vascularized SF-CMTs, which in turn may enhance performance for MI treatment (Dylan J Richards et al., 2017). In a different study, Oltolina et al. created EBs using human CPCs (hCPCs) obtained from patient samples, using methylcellulose-coated culture wells to induce cell clustering and self-aggregation (Oltolina et al., 2015). Immunostaining of the cell aggregates showed the expression of CPC-related proteins (F-actin, vimentin, CD44, C90, c-Kit, and Sca-1) and ECM proteins (collagen, laminin, and fibronectin) (**Figure 2.6 B(i)**). Additionally, expression of cardiac proteins (Cx43, GATA-4 and MEF2C) (**Figure 2.6 B(ii)**) and proteins involved in cardiomyogenic programs (YAP and HGF) were found within the SF-CMTs. *In vivo* experiments showed that the SF-CMTs were engrafted after implantation in mice models of MI, and that the hCPCs were able to migrate to the host myocardium and were detectable 7 days after implantation (**Figure 2.6B (iii)**).

The use of dynamic cultures has also been applied for the formation of EBs and differentiation towards cardiac-specific lineage (Rungarunlert et al., 2011; S. Zhao et al., 2016). For example, Niebruegge et al. created an integrative bioprocess using soft-

lithography stamping and a bioreactor system with controlled oxygen concentration for promoting controlled cell expansion, and aggregation and differentiation of hESCs (Niebruegge et al., 2009). The differentiation was performed through suspending the cells in differentiation medium within the bioreactor. Upregulation of cardiac-specific genes, specifically SAC, cTnT, and MLC2v, was found in the microtissues formed 14 days after the start of differentiation. It was suggested that this system could be translated for cardiac differentiation of hiPSCs as well. Hence, the formation of EBs and further 3D cardiac differentiation proves to be another viable method in the obtention of multicellular SF-CMTs with tissue-level relevant characteristics including function and structure.

2.6 NANOENGINEERING APPROACHES IN CARDIAC TISSUE ENGINEERING

The unique characteristics of nano-scaled materials (i.e., nanomaterials) and their integration with tissue engineering approaches have proven their potential to enhance the functionalities of engineered CMT (Kharaziha, Memic, Akbari, Brafman, & Nikkhah, 2016). Through improving the microenvironment of the SF-CMTs, in particular using nanomaterials, it is possible to better mimic the characteristics of the native myocardium, toward a more mature phenotype of *in vitro* and better functionalities *in vivo*. The addition of nanomaterials to stem cell culture, specifically, can modulate their differentiation and fate (Chimene, Alge, & Gaharwar, 2015). Carbon-based and gold-based nanomaterials have been amongst the most popular nanomaterials for cardiac tissue engineering due to their conductive electrical properties (Amezcua, Shirolkar, Fraze, & Stout, 2016; Karperien et al., 2019; Kharaziha et al., 2014; Mehrali et al., 2017; Ali Navaei et al., 2019; Ali Navaei,

Harpinder Saini, et al., 2016; Paul et al., 2014; Shin et al., 2013; Shin et al., 2016). Other nanomaterials have also been used for the construction of CMTs, for example, silica nanoparticles, polymeric nanofibers, and iron-based magnetic nanoparticles (Kankala et al., 2018). Whereas a myriad of nanomaterials exists, not all may be suitable for interactions with cardiac cells, as these nanomaterials need to meet specific criteria such as biocompatibility, lack of immunogenicity and cytotoxicity, etc. For example, it has been reported that carbon-based nanomaterials such as carbon nanotubes (CNTs) are more prone to elicit immune reactions (inflammation and formation of granulation tissue) and toxicity (Amezcua et al., 2016) as opposed to gold-based nanomaterials, which show better biocompatibility (Alaaldin M Alkilany & Murphy, 2010; Connor, Mwamuka, Gole, Murphy, & Wyatt, 2005; Kharaziha et al., 2016; Khlebtsov & Dykman, 2011; Shukla et al., 2005). In addition, key advantages of gold nanomaterials include a diverse nanoscale architecture, in the form of nanoparticles, nanorods, or nanowires, facile fabrication processes, as well as excellent surface properties amenable for assembly of functional groups (Dykman & Khlebtsov, 2012; Frens, 1973). The extent of the immune reaction and cytotoxicity to some nanomaterials has also been linked to their size, geometry, surface chemistry, concentration and the rate at which they are cleared by the immune system (Ashtari et al., 2019). The main cytotoxic mechanism is due to the cellular uptake of the nanoparticles and their capacity to induce cellular oxidative stress, causing damage to the DNA and cytoplasmic components, and triggering apoptosis (Holgate, 2010). In order to increase the biocompatibility of nanomaterials, several alterations have been proposed, such as surface modification and functionalization with biocompatible polymers, since polymers play an important role in protein adsorption (Nie, Xu, Huang, Ye, & Wu, 2003),

cell membrane interactions, and cellular uptake. For example, PEG, poly(ethylene glycol)-co-poly(d,l-lactide) (PELA) (L. Sun, Huang, Gong, & Zhou, 2010), and poly(acrylic acid) (M. Xu et al., 2016) are among some of the polymers used for surface functionalization of nanomaterials. In the following section, we discuss reports of diverse approaches for the utilization of nanomaterials towards the engineering of SF-CMTs.

2.6.1 Integration of scaffold-free cardiac microtissues (SF-CMTs) with nanomaterials

To date, several approaches have proposed the use of nanomaterials in conjunction with SF-CMTs to enhance their function and maturation. For instance, Tan et al. utilized agarose microwells to create SF-CMTs composed of neonatal rat CMs or hiPSC-CMs and added electrically conductive Si nanowires (SiNWs) (diameter≈100nm; length≈10μm) at a ratio of 1:1 to the cells (CMs:SiNWs) (Tan et al., 2015) (**Figure 2.7 A**). TEM imaging revealed that the SiNWs localized in the intercellular space within SF-CMTs, which has been suggested to improve cell-to-cell coupling. The influence of the synergistic effect of 3D culture and the addition of SiNWs to CMs maturation was then evaluated. It was found that the presence of SiNWs promoted the expression of SAC, cTnI, Cx43, and beta myosin heavy chain (β-MHC) (**Figure 2.7 B**), and the upregulation of Ca^{2+} channel coding genes (CACNA1C/CACNA1G), which led to improved Ca^{2+} handling. Additionally, enhanced sarcomere ultrastructure (increased Z-line width and alignment and increased SAC length) were observed in SF-CMTs fabricated with hiPSC-CMs. Furthermore, the authors investigated the effect of electrical stimulation on the neonatal rat SF-CMTs, with a stimulation regime of 15V at 1Hz, 2ms pulses to mimic electrical signals within the heart.

SF-CMTs with SiNWs were found to have significantly improved amplitude contraction and synchronization (measured through fractional area change) upon exposure to electrical stimulation. Also, a significantly higher expression of Cx43 was present in SF-CMTs incorporated with SiNWs, which potentially explained the improved electrical propagation within the cellular construct. It was hypothesized that the SiNWs propitiated the formation of an anisotropic mechanical microenvironment, thereby inducing an enhanced alignment of the intracellular contractile apparatus, and therefore improved electrical features of the SF-CMTs. In another study by the same group, they investigated the effect of electrical stimulation in SF-CMTs composed of hiPSC-CMs and SiNWs (Dylan J. Richards et al., 2016) (**Figure 2.7 C-E**). An electrical stimulation regime (2.5 V/cm, 1Hz, 5ms pulses) was used to mimic the electrical signals generated by the sinoatrial node in the heart. The hiPSC-CMs that were incorporated with SiNWs and exposed to electrical stimulation displayed significantly higher expression of Cx43 (**Figure 2.7 F**) and N-cadherin (N-cad) (**Figure 2.7 G**) when compared to the control groups, suggesting the formation of functional cell-to-cell junctions that allow for improved electrical signal propagation and mechanical coupling. Cardiac-specific marker immunostaining further revealed that the addition of SiNWs improved sarcomere quality (denoted by SAC striation) and induced an increase in the ratio of β-MHC to alpha myosin heavy chain (α-MHC), demonstrating a more mature phenotype. Significantly higher levels of ventricular myosin light chain protein were observed in the electrically stimulated groups, suggesting that the electrical stimulation induced a ventricular-like phenotype in hiPSC-CMs, as further corroborated with an observed reduction in the spontaneous beating rate. In general, the authors demonstrated that the effects of electrical stimulation on hiPSC-CMs can be enhanced by

the presence of an electrically conductive microenvironment induced by SiNWs, where the combination of electrically conductive nanoparticles and electrical stimulation in SF-CMTs led to a more mature ventricle-like phenotype in hiPSC-CMs.

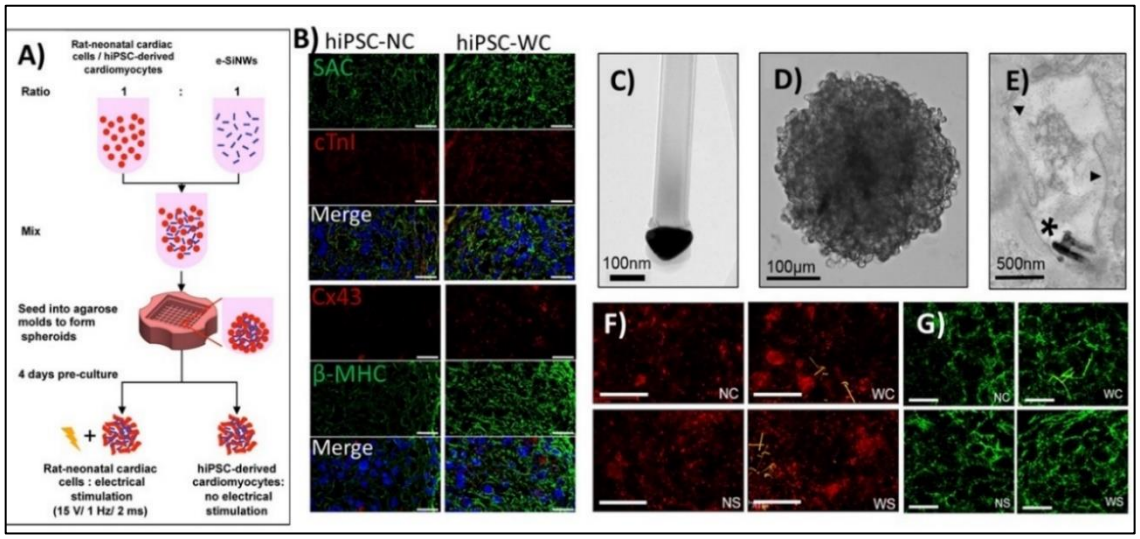

Figure 2.7. Fabrication of rat and hiPSC-CM spheroids with SiNWs. A) Diagram for the fabrication of the SF-CMTs with SiNWs. B) Immunostaining for SAC and cTnI, Cx43 and β-MHC in hiPSC-CM spheroids with and without SiNWs (Scale bars: 20µm). Experimental groups: hiPSC-CMs spheroids without SiNWs and no stimulation (hiPSC-NC); hiPSC-CMs spheroids with SiNWs and no stimulation (hiPSC-WC). *Adapted with permission from American Chemical Society (Tan et al., 2015). Copyright © (2015).* C) TEM image of the SiNWs. D) hiPSC SF-CMT with SiNWs on Day 0 after fabrication. E) TEM image of a spheroid section and SiNWs localization in the extracellular space. Asterisk, nanowire location; triangle, cell membrane. F) Immunostaining for Cx43 (red) expression (SiNWs shown in yellow). G) Immunostaining for N-cad (green) expression. Experimental groups: Spheroids without SiNWs and unstimulated at Day 19 (NC); Spheroids with SiNWs and unstimulated at Day 19 (WC); Spheroids without SiNWs and stimulated at Day 19 (NS); Spheroids with SiNWs and stimulated at Day 19 (WS). *Adapted with permission from American Chemical Society (Dylan J. Richards et al., 2016). Copyright © (2016).*

In a study by Park et al., scaffold-free tissue spheroids were formed from MSCs using the hanging drop technique, and further enriched with reduced graphene oxide flakes (RGO) (Park et al., 2015b) (**Figure 2.8 B(i-ii)**). The addition of RGO increased the expression of VEGF and Cx43 within the spheroids. An enhanced vascularization of the infarcted myocardium was found after the implantation of the hybrid MSC-RGO spheroids

in mice MI model, presumably due to the secretion of growth factors (i.e., vWF) (**Figure 2.8 B(iii)**). Additionally, LVEF was improved, and fibrosis was decreased in the infarct zone (**Figure 2.8 B(iv)**). Increased expression of Cx43 was also found in the infarct border zone (**Figure 2.8 B(v)**).

In a study by Ahadian et al., EBs were created from 129/SEV-derived mouse stem cells using hanging drop technique, and the influence of the addition of graphene on directed cardiac differentiation was investigated (Ahadian et al., 2016) (**Figure 2.8 A**). During cell seeding, the EBs were enriched with graphene, at a concentration of either 0.1 mg/ml or 0.2 mg/Ml. Phase-contrast imaging after three days of culture showed the presence of fragments of graphene sheets distributed throughout the EBs. Lower impedance was found in the EBs enriched with 0.2 mg/ml (298 KΩ) or 0.1 mg/ml (665 KΩ) of graphene when compared to the control group (0 mg/ml of graphene) (928KΩ). Stiffness of the EBs was further measured using atomic force microscopy (AFM), revealing that the addition of graphene increased the Young's modulus of the microtissues (31±1.7 kPa, compared to control=26.8±4.4 kPa). Four days after seeding, the 0.2 mg/ml graphene-incorporated EBs were subjected to an electrical stimulation regime (4V, 1Hz, 10ms). Significantly higher expression of cTnT was found in electrically stimulated EBs, while within this group, the graphene-incorporated EBs exhibited significantly enhanced expression of cTnT as compared to the control condition (EBs with no graphene) (**Figure 2.8 C**). Significant upregulation of cardiac-specific genes (Cctc1, MYH6, MYH7, and TNNT2) and spontaneous beating was also found in graphene-incorporated EBs. Additionally, more organized sarcomeric structures were observed in the cells within the stimulated EBs incorporated with graphene as compared to pristine EBs. The outcome of

this study demonstrated that inducing an electromechanical microenvironment, relevant to the myocardium, by the combination of graphene sheets and electrical stimulation can lead to cardiac differentiation without the need of soluble factor or small molecule addition.

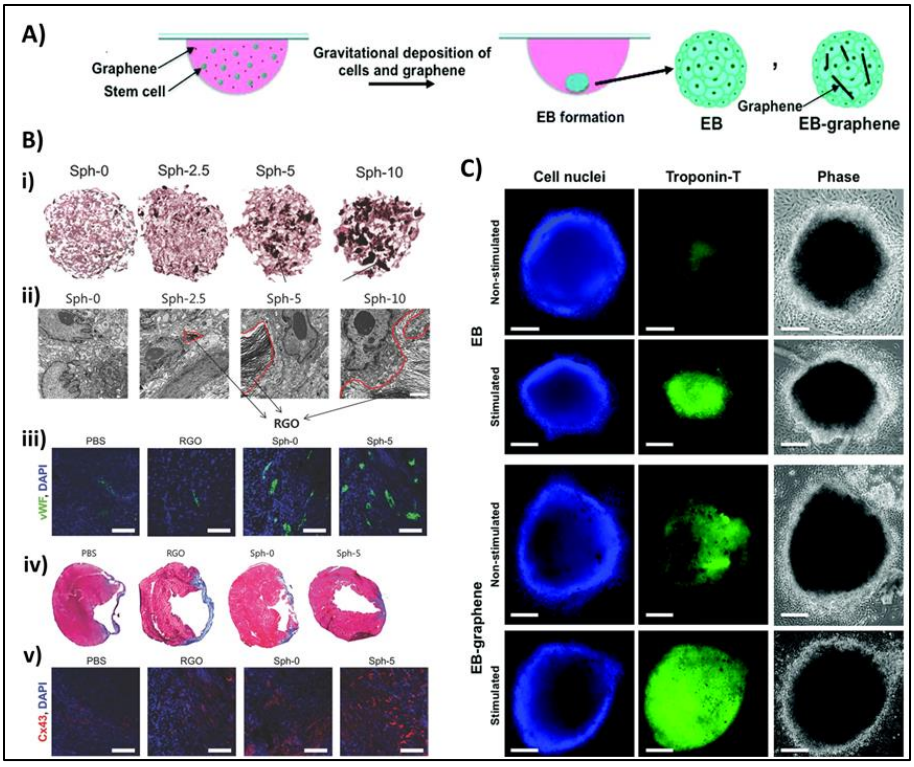

Figure 2.8. Integration of graphene sheets and RGO flakes into EBs. A) Diagram of EB formation through hanging-drop technique. *Adapted with permission from Royal Society of Chemistry (Ahadian et al., 2016). Copyright © (2016).* B) Formation and implantation of hybrid SF-CMTs with RGO flakes i) Hematoxylin and Eosin stain of spheroids formed with different concentrations of RGO (shown in black) (Scale bar: 100µm). ii)TEM images of spheroids formed with different concentrations of RGO (arrows). (Scale bar: 2µm). iii) Assessment of capillary density by immunostaining of VWF (Scale bars: 100µm). iv) Masson's trichrome staining of explanted hearts indicating fibrotic areas (blue). v) Expression of Cx43 in the infarct border zone (Scale bars: 100µm). Experimental groups: injection of PBS (PBS), injection of RGO flakes (RGO), injection of MSC spheroids (Sph-0), and injection of MSC–RGO hybrid spheroids (Sph-5). *Adapted with permission from WILEY-VCH Verlag GmbH & Co. KgaA, Weinheim (Park et al., 2015b). Copyright © (2015). C*) Expression of cTnT (green) in EB-derived SF-CMTs. (Scale bars: 100µm). Experimental groups: EBs formed without the addition of graphene without and with electrical stimulation respectively: EB (Non-Stimulated and Stimulated). EBs formed adding graphene without and with electrical stimulation respectively: EB-graphene (Non-stimulated and stimulated). *Adapted with permission from Royal Society of Chemistry (Ahadian et al., 2016). Copyright © (2016).*

Overall, the integration of nanomaterials and SF-CMTs has shown enhanced cell-to-cell interactions (Dylan J. Richards et al., 2016; Tan et al., 2015), and cell-to-ECM interactions (Park et al., 2015b). Specifically, the integration of electrical stimulation to the SF-CMTs enriched with nanomaterials has proven beneficial to improve their electrophysiological properties and increase the expression of cardiac-specific proteins. It has been suggested that the introduction of physiologically relevant electrical cues in combination with electrically conductive nanomaterials creates a microenvironment within the SF-CMTs that facilitates electrical propagation and closely mimics the microenvironment of the heart (Ahadian et al., 2016). Improving the different cellular interactions and the microenvironment within the SF-CMTs is paramount to overcome the current challenges of cell-based therapies as well as engineering of mature and functional SF-CMTs for cardiac therapy. Before these approaches proceed to clinical trials, more fundamental investigations are needed to elucidate the action mechanism of specific nanoparticles and the influence of other possible biochemical or biophysical signaling cues in a more complex tissue environment (i.e., at an organ level). Moreover, it is necessary to reach a consensus on the optimal concentration of nanoparticles to be added to SF-CMTs since it has been demonstrated that the outcome is highly dose-dependent. So far, the concentrations used vary widely from study to study, and while the main objective is to avoid cytotoxicity, there is still room for optimization. In addition, the long-term effects towards the hosting myocardium need to be investigated. So far, bioaccumulation of nanomaterials in the cardiac tissue and the possible side effects due to the implantation of SF-CMTs enriched with nanomaterials have not yet been reported, since those studies were

performed *in vitro*. Thus, a balance between having the maximal beneficial effect and avoiding cytotoxic concentrations needs to be reached.

2.7 SUMMARY AND FUTURE DIRECTIONS

In this review article, we summarized different regenerative-medicine approaches developed towards cardiac repair therapies. Traditional therapies based on drug treatment are focused mainly on the protection of the remaining viable myocardium and deceleration of fibrotic remodeling. Currently, when drug-based therapies fail, few alternatives remain(Bhatt et al., 2017). Inducing regeneration of the damaged myocardium is not trivial and presents several challenges. Thus, emerging alternative treatments have mainly focused on the recellularization of the damaged cardiac tissue and promote endogenous repair mechanisms (**Table 2.1**). The more straightforward methods are based on the delivery of dissociated cells in suspension to the myocardium. The findings of several cell-based cardiac therapies have suggested that the main role of the implanted cells resides in paracrine signaling and crosstalk with the native tissue. Therefore, it has been shown that independent of the source, cell-based therapies moderately promote neovascularization and repress the formation of fibrotic tissue, thus providing cardioprotective effects but not fully recellularization of the myocardium. The main challenges of cell-based therapies are the stress induced on cells from delivery to the myocardium that leads to low cellular survival and retention, poor engraftment, and the risk of delivery to non-target sites/organs.

Table 2.1

Summary table of the main characteristics of alternative approaches for cardiac repair.

	Cell-based cardiac therapy	**Scaffold-based cardiac microtissues**	**Scaffold-free cardiac microtissues**
Size and geometry	Dissociated cells in suspension	Patches or sheet-like tissues (up to 1-2 cm per side and up to 1-2 mm thickness)	Spheroids (up to 500µm diameter) or sheet-like tissues (up to 400µm thickness)
Cellular composition	Single cell type administered at a time	Mainly CMs (hiPSC- or hESC-derived), occasionally enriched with other types of cells such as endothelial cells, and cardiac fibroblasts	Mainly CMs (hiPSC- or hESC-derived), enriched with endothelial cells, cardiac fibroblasts and occasionally stem cells.
Delivery Method	Intracoronary or intramyocardial injection	Thoracotomy surgery or thoracoscopy	Intramyocardial injection or thoracotomy surgery
Exogenous materials	Not common	Scaffolds from diverse types of biomaterials such as natural or synthetic polymers, hydrogels, electrospun fibers, composite biomaterials often incorporated with nanomaterials.	Occasional inclusion of electrically conductive nanomaterials, such as graphene and graphene oxide flakes, and conductive Si nanowires.
Preparation and fabrication method	*In vitro* cellular purification and expansion, followed by dissociation prior injection.	*In vitro* cellular expansion, differentiation, and purification (when applicable) followed by encapsulation or seeding on the scaffold. Electrical stimulation in some cases.	*In vitro* cellular expansion, differentiation, and purification (when applicable) followed by induced self-aggregation. Or formation of EBs followed by 3D differentiation. Electrical stimulation in some cases.

Trial phase	Several preclinical studies have been performed and some Phase I clinical trials.	Several preclinical studies have been performed and few Phase I clinical trials.	Several preclinical studies have been performed.
Reported effects	Paracrine signaling inducing neovascularization in the borders of the infarcted zone.	Potential for remuscularization, paracrine signaling, induction of neovascularization, reduction of infarct size.	Cardioprotection, paracrine signaling, induction of neovascularization, reduced fibrotic remodeling.
Main challenges	Poor cellular survival and retention after implantation. Non-targeted delivery. Poor remuscularization potential. Lack of control of cellular differentiation after implantation.	Invasive delivery, optimal engineering of scaffold in terms of chemical composition, stiffness, degradation rate and immunogenic activity. Immature state of hiPSC- and hESC-derived cells.	Immature state of hiPSC- and hESC-derived cells. Need of further optimization for size and cellular composition. Need of further investigation regarding the use of nanomaterials.

Tissue engineering approaches have mainly focused on integrating engineering and biology for the development of robust cellular constructs and tissue surrogates in order to overcome the critical challenges of cell-based therapeutic methods. The prominent recent cell types used in this category are stem cell-derived cells (CMs, ECs, CFs), recently hiPSC-CMs due to the potential use of allograft cells for regeneration. The optimized culture of hiPSC-derived cells has helped to make advancements towards the formation of functional CMTs. At the same time, enhancing the resemblance of the architecture of CMTs to the native myocardium has led to enhanced maturation of hiPSC-derived cells and promoted cell-to-cell interactions within the tissue environment. Biomaterials from diverse origins, natural or synthetic with precisely controlled stiffness, chemical moieties, etc., have been used as scaffolding matrices in the formation of SB-CMTs. However, challenges for the use of SB-CMTs in clinical applications include the introduction of exogenous biomaterials to the host tissue that can elicit immune responses or cytotoxicity,

lack of engraftment and cellular coupling, and often the requirement of surgically invasive interventions to implant the engineered tissue constructs.

To address the current limitations of cell-based and scaffold-based tissue engineering strategies, in the past few years, engineering of SF-CMTs has emerged as a potentially powerful approach for the treatment of MI with minimally invasive implantation procedures. The use of co-culture and fabrication of multicellular constructs/organoids has proven optimal, as such cellular composition could better resemble the native myocardium. Also, paracrine and endocrine signaling is enhanced in SF-CMTs, which lead to a more maturation state of hiPSC-derived cells. Several methods for the construction of SF-CMTs have been proposed, based on the promotion of cell aggregation through inducing cell-to-cell adhesion and electromechanical coupling. These methods can be divided into three broad categories, with the first group consisting of gravity-assisted methods, either using conventional hanging drop technique or microengineered platforms, that rely on gravity to form cellular aggregates out of cell suspensions(Halbert et al., 1971; Neto et al., 2015). Usually, these methods offer great control on SF-CMTs size and cell number, allowing for homogeneous formation of spheroids. The second group involves the use of ultra-low adherent surfaces, such as PIPAAm-coated surfaces, to promote cell aggregation through the balance of electrostatic forces and reduction of free-energy. The fabrication of SF-CMTs using low attachment substrates requires minimal manipulation of the cell aggregates, which translates to lower stress induced by handling. The last group is based on the obtention of SF-CMTs through the differentiation of EBs. The main advantages of this method are the resultant physiologically-relevant cellular composition and

organization(Hoang, Wang, Conklin, Healy, & Ma, 2018),(Ma et al., 2015), and to the ease of scaling to high-throughput output; however, controlling the size can be problematic.

Despite significant promises, before the extended use of SF-CMTs in clinical trials, several remaining challenges need to be addressed. First, the maturation state of the stem cell-derived CMs needs to be improved. The advancement of *in vitro* maturation techniques may lead to more robust SF-CMTs that better resemble the adult myocardium, and consequently, may lead to better engraftment and retention within the native tissue. In Addition, there is a need to elucidate the mechanisms of the delivery of the SF-CMTs since it has been reported that it can have consequences in the engraftment and electrical coupling of the implanted cells. According to some studies, the intramyocardial delivery of spherical SF-CMTs may be the best option for enhanced electrical coupling (Emmert, Wolint, Winklhofer, et al., 2013; Gerbin, Yang, Murry, & Coulombe, 2015). Still, more studies are necessary in order to standardize the optimal size and delivery method to the infarcted myocardium. Recent approaches have utilized exogenous cues such as nanomaterials to enhance the structural maturity and functionalities of SF-CMTs. However, detailed studies are required to unveil the nanomaterials' specific mechanism of action on cellular- and tissue-level function within the heart, since it has been reported that some nanomaterials can elicit toxic reactions, such as foreign body reaction, inflammation, and apoptosis among others, in different organs in preclinical studies (Kermanizadeh, Balharry, Wallin, Loft, & Møller, 2015). The cellular composition within the engineered SF-CMTs needs to be determined in a manner that optimizes the electromechanical properties as well as the paracrine signaling of the tissue. Additionally, non-targeted delivery and teratogenic potential of the implanted cells need to be thoroughly studied and addressed, since it has

been reported that hiPSC-derived SF-CMTs can induce immune rejection in some cases and can also lead to the formation of malignant teratocarcinomas *in vivo* (Kawamura et al., 2016). Overall, the development of SF-CMTs holds great potential for myocardial replacement therapy and treatment of MI, due to their enhanced structure, tissue organization, and cellular composition, and the lack of exogenous bulk materials. Additionally, the effects of the introduction of nanomaterials to the fabrication of SF-CMT are worthy of further investigation due to their proven potential for the enhancement of their electrophysiological features. With this, we anticipate that the inclusion of nanomaterials and nanoengineering methods will lead to the next generation of SF-CMT for cardiac regenerative medicine.

2.8 REFERENCES

Ahadian, S., Zhou, Y., Yamada, S., Estili, M., Liang, X., Nakajima, K., . . . Matsue, T. (2016). Graphene induces spontaneous cardiac differentiation in embryoid bodies. *Nanoscale, 8*(13), 7075-7084. doi:10.1039/C5NR07059G

Alkilany, A. M., & Murphy, C. J. (2010). Toxicity and cellular uptake of gold nanoparticles: what we have learned so far? *Journal of Nanoparticle Research, 12*(7), 2313-2333.

Amezcua, R., Shirolkar, A., Fraze, C., & Stout, D. A. (2016). Nanomaterials for Cardiac Myocyte Tissue Engineering. *Nanomaterials, 6*(7), 133. Retrieved from https://www.mdpi.com/2079-4991/6/7/133

Annabi, N., Tsang, K., Mithieux, S. M., Nikkhah, M., Ameri, A., Khademhosseini, A., & Weiss, A. S. (2013). Highly elastic micropatterned hydrogel for engineering functional cardiac tissue. *Advanced Functional Materials, 23*(39), 4950-4959.

Ashtari, K., Nazari, H., Ko, H., Tebon, P., Akhshik, M., Akbari, M., . . . Soleimani, M. (2019). Electrically conductive nanomaterials for cardiac tissue engineering. *Advanced Drug Delivery Reviews, 144*, 162-179.

Baei, P., Hosseini, M., Baharvand, H., & Pahlavan, S. (2020). Electrically conductive materials for in vitro cardiac microtissue engineering. *Journal of Biomedical Materials Research Part A*.

Ban, K., Bae, S., & Yoon, Y.-s. (2017). Current strategies and challenges for purification of cardiomyocytes derived from human pluripotent stem cells. *Theranostics*, *7*(7), 2067.

Bar, A., & Cohen, S. (2020). Inducing Endogenous Cardiac Regeneration: Can Biomaterials Connect the Dots? *Frontiers in Bioengineering and Biotechnology*, *8*, 126.

Bargehr, J., Ong, L. P., Colzani, M., Davaapil, H., Hofsteen, P., Bhandari, S., . . . Sampaziotis, F. (2019). Epicardial cells derived from human embryonic stem cells augment cardiomyocyte-driven heart regeneration. *Nature Biotechnology, 37*(8), 895-906.

Barsotti, M. C., Felice, F., Balbarini, A., & Di Stefano, R. (2011). Fibrin as a scaffold for cardiac tissue engineering. *Biotechnology and Applied Biochemistry, 58*(5), 301-310.

Beauchamp, P., Jackson, C. B., Ozhathil, L. C., Agarkova, I., Galindo, C. L., Sawyer, D. B., . . . Zuppinger, C. (2020). 3D Co-culture of hiPSC-Derived Cardiomyocytes With Cardiac Fibroblasts Improves Tissue-Like Features of Cardiac Spheroids. *Frontiers in Molecular Biosciences, 7*. doi:10.3389/fmolb.2020.00014

Beauchamp, P., Moritz, W., Kelm, J. M., Ullrich, N. D., Agarkova, I., Anson, B. D., . . . Zuppinger, C. (2015). Development and Characterization of a Scaffold-Free 3D Spheroid Model of Induced Pluripotent Stem Cell-Derived Human Cardiomyocytes. *Tissue Engineering Part C: Methods, 21*(8), 852-861. doi:10.1089/ten.tec.2014.0376

Behfar, A., Crespo-Diaz, R., Terzic, A., & Gersh, B. J. (2014). Cell therapy for cardiac repair—lessons from clinical trials. *Nature Reviews Cardiology, 11*(4), 232.

Belostotskaya, G., Hendrikx, M., Galagudza, M., & Suchkov, S. (2020). How to Stimulate Myocardial Regeneration in Adult Mammalian Heart: Existing Views and New Approaches. *BioMed Research International, 2020*.

Benam, K. H., Dauth, S., Hassell, B., Herland, A., Jain, A., Jang, K.-J., . . . Ingber, D. E. (2015). Engineered In Vitro Disease Models. *Annual Review of Pathology: Mechanisms of Disease, 10*(1), 195-262. doi:10.1146/annurev-pathol-012414-040418

Benjamin, E. J., Blaha, M. J., Chiuve, S. E., Cushman, M., Das, S. R., Deo, R., . . . Stroke Stat, S. (2017). Heart Disease and Stroke Statistics-2017 Update A Report From

the American Heart Association. *Circulation, 135*(10), E146-E603. doi:10.1161/cir.0000000000000485

Bergmann, O., Bhardwaj, R. D., Bernard, S., Zdunek, S., Barnabé-Heider, F., Walsh, S., . . . Frisén, J. (2009). Evidence for Cardiomyocyte Renewal in Humans. *Science, 324*(5923), 98-102. doi:10.1126/science.1164680

Bhatt, A. S., Ambrosy, A. P., & Velazquez, E. J. (2017). Adverse remodeling and reverse remodeling after myocardial infarction. *Current Cardiology Reports, 19*(8), 71.

Bhute, V. J., Bao, X., Dunn, K. K., Knutson, K. R., McCurry, E. C., Jin, G., . . . Palecek, S. P. (2017). Metabolomics identifies metabolic markers of maturation in human pluripotent stem cell-derived cardiomyocytes. *Theranostics, 7*(7), 2078.

Braunwald, E. (2013). Heart failure. *JACC Heart Fail, 1*(1), 1-20. doi:10.1016/j.jchf.2012.10.002

Breslin, S., & O'Driscoll, L. (2013). Three-dimensional cell culture: the missing link in drug discovery. *Drug Discovery Today, 18*(5-6), 240-249.

Bretzner, F., Gilbert, F., Baylis, F., & Brownstone, R. M. (2011). Target populations for first-in-human embryonic stem cell research in spinal cord injury. *Cell Stem Cell, 8*(5), 468-475.

Brodland, G. W. (2002). The differential interfacial tension hypothesis (DITH): a comprehensive theory for the self-rearrangement of embryonic cells and tissues. *J. Biomech. Eng., 124*(2), 188-197.

Cha, J. M., Park, H., Shin, E. K., Sung, J. H., Kim, O., Jung, W., . . . Kim, J. (2017). A novel cylindrical microwell featuring inverted-pyramidal opening for efficient cell spheroid formation without cell loss. *Biofabrication, 9*(3), 035006.

Chang, D., Shimizu, T., Haraguchi, Y., Gao, S., Sakaguchi, K., Umezu, M., . . . Okano, T. (2015). Time course of cell sheet adhesion to porcine heart tissue after transplantation. *PLOS ONE, 10*(10).

Chen, S. L., Fang, W. W., Ye, F., Liu, Y. H., Qian, J., Shan, S. J., . . . Sun, J. P. (2004). Effect on left ventricular function of intracoronary transplantation of autologous bone marrow mesenchymal stem cell in patients with acute myocardial infarction. *Am J Cardiol, 94*(1), 92-95. doi:10.1016/j.amjcard.2004.03.034

Chimene, D., Alge, D. L., & Gaharwar, A. K. (2015). Two-dimensional nanomaterials for biomedical applications: Emerging trends and future prospects. *Advanced Materials, 27*(45), 7261-7284.

Chong, J. J., Yang, X., Don, C. W., Minami, E., Liu, Y.-W., Weyers, J. J., . . . Palpant, N. J. (2014). Human embryonic-stem-cell-derived cardiomyocytes regenerate non-human primate hearts. *Nature, 510*(7504), 273-277.

Chun, Y. W., Balikov, D. A., Feaster, T. K., Williams, C. H., Sheng, C. C., Lee, J.-B., . . . Ess, K. C. (2015). Combinatorial polymer matrices enhance in vitro maturation of human induced pluripotent stem cell-derived cardiomyocytes. *Biomaterials, 67*, 52-64.

Cleutjens, J. P., & Creemers, E. E. (2002). Integration of concepts: cardiac extracellular matrix remodeling after myocardial infarction. *Journal of Cardiac Failure, 8*(6), S344-S348.

Connor, E. E., Mwamuka, J., Gole, A., Murphy, C. J., & Wyatt, M. D. (2005). Gold Nanoparticles Are Taken Up by Human Cells but Do Not Cause Acute Cytotoxicity. *Small, 1*(3), 325-327. doi:https://doi.org/10.1002/smll.200400093

Correia, C., Koshkin, A., Duarte, P., Hu, D., Carido, M., Sebastião, M. J., . . . Teixeira, A. P. (2018). 3D aggregate culture improves metabolic maturation of human pluripotent stem cell derived cardiomyocytes. *Biotechnology and Bioengineering, 115*(3), 630-644.

Cutts, J., Nikkhah, M., & Brafman, D. A. (2015). Biomaterial approaches for stem cell-based myocardial tissue engineering: supplementary issue: stem cell biology. *Biomarker insights, 10*, BMI. S20313.

Dahlmann, J., Kensah, G., Kempf, H., Skvorc, D., Gawol, A., Elliott, D. A., . . . Gruh, I. (2013). The use of agarose microwells for scalable embryoid body formation and cardiac differentiation of human and murine pluripotent stem cells. *Biomaterials, 34*(10), 2463-2471.

Davies, J. A. (2018). Chapter 1 - Organoids and mini-organs: Introduction, history, and potential. In J. A. Davies & M. L. Lawrence (Eds.), *Organoids and Mini-Organs* (pp. 3-23): Academic Press.

De Angelis, E., Pecoraro, M., Rusciano, M. R., Ciccarelli, M., & Popolo, A. (2019). Cross-Talk between Neurohormonal Pathways and the Immune System in Heart Failure: A Review of the Literature. *Int J Mol Sci, 20*(7). doi:10.3390/ijms20071698

Desroches, B. R., Zhang, P., Choi, B.-R., King, M. E., Maldonado, A. E., Li, W., . . . Hartmann, K. M. (2012). Functional scaffold-free 3-D cardiac microtissues: a novel model for the investigation of heart cells. *American Journal of Physiology-Heart and Circulatory Physiology, 302*(10), H2031-H2042.

Di Costanzo, E., Giacomello, A., Messina, E., Natalini, R., Pontrelli, G., Rossi, F., . . . Twarogowska, M. (2018). A discrete in continuous mathematical model of cardiac

progenitor cells formation and growth as spheroid clusters (Cardiospheres). *Mathematical Medicine and Biology: a Journal of the IMA, 35*(1), 121-144.

Dias, T. P., Pinto, S. N., Santos, J. I., Fernandes, T. G., Fernandes, F., Diogo, M. M., . . . Cabral, J. M. (2018). Biophysical study of human induced Pluripotent Stem Cell-Derived cardiomyocyte structural maturation during long-term culture. *Biochemical and Biophysical Research Communications, 499*(3), 611-617.

Dykman, L., & Khlebtsov, N. (2012). Gold nanoparticles in biomedical applications: recent advances and perspectives. *Chemical Society Reviews, 41*(6), 2256-2282.

Emmert, M. Y., Wolint, P., Wickboldt, N., Gemayel, G., Weber, B., Brokopp, C. E., . . . Jaconi, M. E. (2013). Human stem cell-based three-dimensional microtissues for advanced cardiac cell therapies. *Biomaterials, 34*(27), 6339-6354.

Emmert, M. Y., Wolint, P., Winklhofer, S., Stolzmann, P., Cesarovic, N., Fleischmann, T., . . . Scherman, J. (2013). Transcatheter based electromechanical mapping guided intramyocardial transplantation and in vivo tracking of human stem cell based three dimensional microtissues in the porcine heart. *Biomaterials, 34*(10), 2428-2441.

Fennema, E., Rivron, N., Rouwkema, J., van Blitterswijk, C., & de Boer, J. (2013). Spheroid culture as a tool for creating 3D complex tissues. *Trends in Biotechnology, 31*(2), 108-115. doi:https://doi.org/10.1016/j.tibtech.2012.12.003

Feric, N. T., & Radisic, M. (2016). Strategies and Challenges to Myocardial Replacement Therapy. *Stem Cells Translational Medicine, 5*(4), 410-416. doi:10.5966/sctm.2015-0288

Frens, G. (1973). Controlled nucleation for the regulation of the particle size in monodisperse gold suspensions. *Nature Physical Science, 241*(105), 20-22.

Frey, O., Misun, P. M., Fluri, D. A., Hengstler, J. G., & Hierlemann, A. (2014). Reconfigurable microfluidic hanging drop network for multi-tissue interaction and analysis. *Nature Communications, 5*(1), 1-11.

Gerbin, K. A., Yang, X., Murry, C. E., & Coulombe, K. L. (2015). Enhanced electrical integration of engineered human myocardium via intramyocardial versus epicardial delivery in infarcted rat hearts. *PLOS ONE, 10*(7).

Ghiroldi, A., Piccoli, M., Cirillo, F., Monasky, M. M., Ciconte, G., Pappone, C., & Anastasia, L. (2018). Cell-based therapies for cardiac regeneration: A comprehensive review of past and ongoing strategies. *International Journal of Molecular Sciences, 19*(10), 3194.

Giacomelli, E., Bellin, M., Sala, L., Van Meer, B. J., Tertoolen, L. G., Orlova, V. V., & Mummery, C. L. (2017). Three-dimensional cardiac microtissues composed of cardiomyocytes and endothelial cells co-differentiated from human pluripotent stem cells. *Development, 144*(6), 1008-1017.

Giacomelli, E., Meraviglia, V., Campostrini, G., Cochrane, A., Cao, X., van Helden, R. W., . . . Davis, R. P. (2020). Human-iPSC-Derived Cardiac Stromal Cells Enhance Maturation in 3D Cardiac Microtissues and Reveal Non-cardiomyocyte Contributions to Heart Disease. *Cell Stem Cell*.

Golpanian, S., Wolf, A., Hatzistergos, K. E., & Hare, J. M. (2016). Rebuilding the damaged heart: mesenchymal stem cells, cell-based therapy, and engineered heart tissue. *Physiological Reviews, 96*(3), 1127-1168.

Griffith, C. K., Miller, C., Sainson, R. C., Calvert, J. W., Jeon, N. L., Hughes, C. C., & George, S. C. (2005). Diffusion limits of an in vitro thick prevascularized tissue. *Tissue Engineering, 11*(1-2), 257-266.

Halbert, S., Bruderer, R., & Lin, T. (1971). In vitro organization of dissociated rat cardiac cells into beating three-dimensional structures. *The Journal of Experimental Medicine, 133*(4), 677-695.

Hirt, M. N., Hansen, A., & Eschenhagen, T. (2014). Cardiac tissue engineering: state of the art. *Circulation Research, 114*(2), 354-367.

Hoang, P., Wang, J., Conklin, B. R., Healy, K. E., & Ma, Z. (2018). Generation of spatial-patterned early-developing cardiac organoids using human pluripotent stem cells. *Nature protocols, 13*(4), 723.

Holgate, S. T. (2010). Exposure, uptake, distribution and toxicity of nanomaterials in humans. *Journal of Biomedical Nanotechnology, 6*(1), 1-19.

Holzwarth, J. M., & Ma, P. X. (2011). 3D nanofibrous scaffolds for tissue engineering. *Journal of Materials Chemistry, 21*(28), 10243-10251. doi:10.1039/C1JM10522A

Huang, J., Jiang, Y., Ren, Y., Liu, Y., Wu, X., Li, Z., & Ren, J. (2020). Biomaterials and biosensors in intestinal organoid culture, a progress review. *Journal of Biomedical Materials Research Part A, 108*(7), 1501-1508. doi:10.1002/jbm.a.36921

Huh, D., Torisawa, Y.-s., Hamilton, G. A., Kim, H. J., & Ingber, D. E. (2012). Microengineered physiological biomimicry: Organs-on-Chips. *Lab on a Chip, 12*(12), 2156-2164. doi:10.1039/C2LC40089H

Inamdar, A. A., & Inamdar, A. C. (2016). Heart failure: diagnosis, management and utilization. *Journal of Clinical Medicine, 5*(7), 62.

Jackson, S. L., Tong, X., King, R. J., Loustalot, F., Hong, Y., & Ritchey, M. D. (2018). National Burden of Heart Failure Events in the United States, 2006 to 2014. *Circ Heart Fail, 11*(12), e004873. doi:10.1161/CIRCHEARTFAILURE.117.004873

Jacot, J. G., Martin, J. C., & Hunt, D. L. (2010). Mechanobiology of cardiomyocyte development. *Journal of Biomechanics, 43*(1), 93-98.

Jawad, H., Ali, N. N., Lyon, A. R., Chen, Q. Z., Harding, S. E., & Boccaccini, A. R. (2007). Myocardial tissue engineering: a review. *Journal of Tissue Engineering and Regenerative Medicine, 1*(5), 327-342. doi:10.1002/term.46

Jiang, Y., Park, P., Hong, S. M., & Ban, K. (2018). Maturation of Cardiomyocytes Derived from Human Pluripotent Stem Cells: Current Strategies and Limitations. *Molecules and cells, 41*(7), 613-621. doi:10.14348/molcells.2018.0143

Kamakura, T., Makiyama, T., Sasaki, K., Yoshida, Y., Wuriyanghai, Y., Chen, J., . . . Horie, M. (2013). Ultrastructural maturation of human-induced pluripotent stem cell-derived cardiomyocytes in a long-term culture. *Circulation Journal, 77*(5), 1307-1314.

Kankala, R. K., Zhu, K., Sun, X.-N., Liu, C.-G., Wang, S.-B., & Chen, A.-Z. (2018). Cardiac tissue engineering on the nanoscale. *ACS Biomaterials Science & Engineering, 4*(3), 800-818.

Karperien, L., Navaei, A., Godau, B., Dolatshahi-Pirouz, A., Akbari, M., & Nikkhah, M. (2019). Nanoengineered biomaterials for cardiac regeneration. In *Nanoengineered Biomaterials for Regenerative Medicine* (pp. 95-124): Elsevier.

Kawamura, A., Miyagawa, S., Fukushima, S., Kawamura, T., Kashiyama, N., Ito, E., . . . Hatazawa, J. (2016). Teratocarcinomas arising from allogeneic induced pluripotent stem cell-derived cardiac tissue constructs provoked host immune rejection in mice. *Scientific Reports, 6*, 19464.

Kehat, I., Kenyagin-Karsenti, D., Snir, M., Segev, H., Amit, M., Gepstein, A., . . . Gepstein, L. (2001). Human embryonic stem cells can differentiate into myocytes with structural and functional properties of cardiomyocytes. *The Journal of Clinical Investigation, 108*(3), 407-414.

Kermanizadeh, A., Balharry, D., Wallin, H., Loft, S., & Møller, P. (2015). Nanomaterial translocation–the biokinetics, tissue accumulation, toxicity and fate of materials in secondary organs–a review. *Critical Reviews in Toxicology, 45*(10), 837-872.

Keung, W., Boheler, K. R., & Li, R. A. (2014). Developmental cues for the maturation of metabolic, electrophysiological and calcium handling properties of human pluripotent stem cell-derived cardiomyocytes. *Stem Cell Research & Therapy, 5*(1), 17.

Kharaziha, M., Memic, A., Akbari, M., Brafman, D. A., & Nikkhah, M. (2016). Nano-Enabled Approaches for Stem Cell-Based Cardiac Tissue Engineering. *Advanced Healthcare Materials, 5*(13), 1533-1553. doi:https://doi.org/10.1002/adhm.201600088

Kharaziha, M., Nikkhah, M., Shin, S.-R., Annabi, N., Masoumi, N., Gaharwar, A. K., . . . Khademhosseini, A. (2013). PGS: Gelatin nanofibrous scaffolds with tunable mechanical and structural properties for engineering cardiac tissues. *Biomaterials, 34*(27), 6355-6366.

Kharaziha, M., Shin, S. R., Nikkhah, M., Topkaya, S. N., Masoumi, N., Annabi, N., . . . Khademhosseini, A. (2014). Tough and flexible CNT–polymeric hybrid scaffolds for engineering cardiac constructs. *Biomaterials, 35*(26), 7346-7354.

Khlebtsov, N., & Dykman, L. (2011). Biodistribution and toxicity of engineered gold nanoparticles: a review of in vitro and in vivo studies. *Chemical Society Reviews, 40*(3), 1647-1671.

Kholia, S., Ranghino, A., Garnieri, P., Lopatina, T., Deregibus, M. C., Rispoli, P., . . . Camussi, G. (2016). Extracellular vesicles as new players in angiogenesis. *Vascular Pharmacology, 86*, 64-70.

Kim, T. Y., Kofron, C. M., King, M. E., Markes, A. R., Okundaye, A. O., Qu, Z., . . . Choi, B.-R. (2018). Directed fusion of cardiac spheroids into larger heterocellular microtissues enables investigation of cardiac action potential propagation via cardiac fibroblasts. *PloS one, 13*(5).

Kitsara, M., Agbulut, O., Kontziampasis, D., Chen, Y., & Menasché, P. (2017). Fibers for hearts: a critical review on electrospinning for cardiac tissue engineering. *Acta Biomaterialia, 48*, 20-40.

Klotz, S., Foronjy, R. F., Dickstein, M. L., Gu, A., Garrelds, I. M., Jan Danser, A., . . . Burkhoff, D. (2005). Mechanical unloading during left ventricular assist device support increases left ventricular collagen cross-linking and myocardial stiffness. *Circulation, 112*(3), 364-374.

Kowalski, W. J., Yuan, F., Nakane, T., Masumoto, H., Dwenger, M., Ye, F., . . . Keller, B. B. (2017). Quantification of cardiomyocyte alignment from three-dimensional (3D) confocal microscopy of engineered tissue. *Microscopy and Microanalysis, 23*(4), 826-842.

Kurtz, A. (2008). Mesenchymal stem cell delivery routes and fate. *International Journal of Stem Cells, 1*(1), 1.

Laflamme, M. A., Chen, K. Y., Naumova, A. V., Muskheli, V., Fugate, J. A., Dupras, S. K., . . . Police, S. (2007). Cardiomyocytes derived from human embryonic stem

cells in pro-survival factors enhance function of infarcted rat hearts. *Nature Biotechnology, 25*(9), 1015-1024.

Laflamme, M. A., & Murry, C. E. (2005). Regenerating the heart. *Nature Biotechnology, 23*(7), 845-856.

Laflamme, M. A., & Murry, C. E. (2011). Heart regeneration. *Nature, 473*(7347), 326-335. doi:10.1038/nature10147

Lee, D. J., Cavasin, M. A., Rocker, A. J., Soranno, D. E., Meng, X., Shandas, R., & Park, D. (2019). An injectable sulfonated reversible thermal gel for therapeutic angiogenesis to protect cardiac function after a myocardial infarction. *Journal of Biological Engineering, 13*(1), 6.

Lee, R. H., Kim, B., Choi, I., Kim, H., Choi, H. S., Suh, K., . . . Jung, J. S. (2004). Characterization and expression analysis of mesenchymal stem cells from human bone marrow and adipose tissue. *Cellular Physiology and Biochemistry, 14*(4-6), 311-324.

Lee, W. Y., Chang, Y. H., Yeh, Y. C., Chen, C. H., Lin, K. M., Huang, C. C., . . . Sung, H. W. (2009). The use of injectable spherically symmetric cell aggregates self-assembled in a thermo-responsive hydrogel for enhanced cell transplantation. *Biomaterials, 30*(29), 5505-5513. doi:10.1016/j.biomaterials.2009.07.006

Lee, W. Y., Wei, H. J., Lin, W. W., Yeh, Y. C., Hwang, S. M., Wang, J. J., . . . Sung, H. W. (2011). Enhancement of cell retention and functional benefits in myocardial infarction using human amniotic-fluid stem-cell bodies enriched with endogenous ECM. *Biomaterials, 32*(24), 5558-5567. doi:10.1016/j.biomaterials.2011.04.031

Li, Z., & Guan, J. (2011). Hydrogels for cardiac tissue engineering. *Polymers, 3*(2), 740-761.

Lian, X., Zhang, J., Azarin, S. M., Zhu, K., Hazeltine, L. B., Bao, X., . . . Palecek, S. P. (2013). Directed cardiomyocyte differentiation from human pluripotent stem cells by modulating Wnt/β-catenin signaling under fully defined conditions. *Nature Protocols, 8*(1), 162.

Liaw, N. Y., & Zimmermann, W.-H. (2016). Mechanical stimulation in the engineering of heart muscle. *Advanced Drug Delivery Reviews, 96*, 156-160.

Liu, Y.-W., Chen, B., Yang, X., Fugate, J. A., Kalucki, F. A., Futakuchi-Tsuchida, A., . . . Baldessari, A. (2018). Human embryonic stem cell–derived cardiomyocytes restore function in infarcted hearts of non-human primates. *Nature Biotechnology, 36*(7), 597-605.

Lopaschuk, G. D., & Jaswal, J. S. (2010). Energy metabolic phenotype of the cardiomyocyte during development, differentiation, and postnatal maturation. *Journal of cardiovascular pharmacology, 56*(2), 130-140.

Lundy, S. D., Zhu, W.-Z., Regnier, M., & Laflamme, M. A. (2013). Structural and functional maturation of cardiomyocytes derived from human pluripotent stem cells. *Stem Cells and Development, 22*(14), 1991-2002.

Lux, M., Andrée, B., Horvath, T., Nosko, A., Manikowski, D., Hilfiker-Kleiner, D., . . . Hilfiker, A. (2016). In vitro maturation of large-scale cardiac patches based on a perfusable starter matrix by cyclic mechanical stimulation. *Acta Biomaterialia, 30*, 177-187.

Ma, Z., Wang, J., Loskill, P., Huebsch, N., Koo, S., Svedlund, F. L., . . . Conklin, B. R. (2015). Self-organizing human cardiac microchambers mediated by geometric confinement. *Nature Communications, 6*(1), 1-10.

Makkar, R. R., Smith, R. R., Cheng, K., Malliaras, K., Thomson, L. E., Berman, D., . . . Johnston, P. V. (2012). Intracoronary cardiosphere-derived cells for heart regeneration after myocardial infarction (CADUCEUS): a prospective, randomised phase 1 trial. *The Lancet, 379*(9819), 895-904.

Mallapaty, S. (2020). Revealed: two men in China were first to receive pioneering stem-cell treatment for heart-disease. *Nature*.

Maron, B. (1983). Myocardial disorganisation in hypertrophic cardiomyopathy. Another point of view. *British Heart Journal, 50*(1), 1.

Marsano, A., Maidhof, R., Wan, L. Q., Wang, Y., Gao, J., Tandon, N., & Vunjak-Novakovic, G. (2010). Scaffold stiffness affects the contractile function of three-dimensional engineered cardiac constructs. *Biotechnology Progress, 26*(5), 1382-1390.

Masuda, S., & Shimizu, T. (2016). Three-dimensional cardiac tissue fabrication based on cell sheet technology. *Advanced Drug Delivery Reviews, 96*, 103-109.

Masumoto, H., Ikuno, T., Takeda, M., Fukushima, H., Marui, A., Katayama, S., . . . Sakata, R. (2014). Human iPS cell-engineered cardiac tissue sheets with cardiomyocytes and vascular cells for cardiac regeneration. *Scientific Reports, 4*, 6716.

Mathur, A., Ma, Z., Loskill, P., Jeeawoody, S., & Healy, K. E. (2016). In vitro cardiac tissue models: current status and future prospects. *Advanced Drug Delivery Reviews, 96*, 203-213.

Matthys, O. B., Hookway, T. A., & McDevitt, T. C. (2016). Design principles for engineering of tissues from human pluripotent stem cells. *Current Stem Cell Reports, 2*(1), 43-51.

Maxeiner, H., Krehbiehl, N., Müller, A., Woitasky, N., Akintürk, H., Müller, M., . . . Wenzel, S. (2010). New insights into paracrine mechanisms of human cardiac progenitor cells. *European Journal of Heart Failure, 12*(7), 730-737. doi:10.1093/eurjhf/hfq063

McMurtrey, R. J. (2016). Analytic models of oxygen and nutrient diffusion, metabolism dynamics, and architecture optimization in three-dimensional tissue constructs with applications and insights in cerebral organoids. *Tissue Engineering Part C: Methods, 22*(3), 221-249.

Mehrali, M., Thakur, A., Pennisi, C. P., Talebian, S., Arpanaei, A., Nikkhah, M., & Dolatshahi-Pirouz, A. (2017). Nanoreinforced hydrogels for tissue engineering: Biomaterials that are compatible with load-bearing and electroactive tissues. *Advanced Materials, 29*(8), 1603612.

Miyagi, Y., Chiu, L. L., Cimini, M., Weisel, R. D., Radisic, M., & Li, R.-K. (2011). Biodegradable collagen patch with covalently immobilized VEGF for myocardial repair. *Biomaterials, 32*(5), 1280-1290.

Mueller, X. M. (2004). Drug immunosuppression therapy for adult heart transplantation. Part 1: immune response to allograft and mechanism of action of immunosuppressants. *The Annals of Thoracic Surgery, 77*(1), 354-362.

Nabel, E. G., & Braunwald, E. (2012). A tale of coronary artery disease and myocardial infarction. *N Engl J Med, 366*(1), 54-63. doi:10.1056/NEJMra1112570

Nagaraju, S., Truong, D., Mouneimne, G., & Nikkhah, M. (2018). Microfluidic tumor–vascular model to study breast cancer cell invasion and intravasation. *Advanced Healthcare Materials, 7*(9), 1701257.

Nagase, K., Yamato, M., Kanazawa, H., & Okano, T. (2018). Poly (N-isopropylacrylamide)-based thermoresponsive surfaces provide new types of biomedical applications. *Biomaterials, 153*, 27-48.

Napolitano, A. P., Dean, D. M., Man, A. J., Youssef, J., Ho, D. N., Rago, A. P., . . . Morgan, J. R. (2007). Scaffold-free three-dimensional cell culture utilizing micromolded nonadhesive hydrogels. *Biotechniques, 43*(4), 494-500.

Navaei, A., Eliato, K. R., Ros, R., Migrino, R. Q., Willis, B. C., & Nikkhah, M. (2019). The influence of electrically conductive and non-conductive nanocomposite scaffolds on the maturation and excitability of engineered cardiac tissues. *Biomaterials Science, 7*(2), 585-595.

Navaei, A., Moore, N., Sullivan, R. T., Truong, D., Migrino, R. Q., & Nikkhah, M. (2017). Electrically conductive hydrogel-based micro-topographies for the development of organized cardiac tissues. *RSC advances, 7*(6), 3302-3312.

Navaei, A., Saini, H., Christenson, W., Sullivan, R. T., Ros, R., & Nikkhah, M. (2016). Gold nanorod-incorporated gelatin-based conductive hydrogels for engineering cardiac tissue constructs. *Acta biomaterialia, 41*, 133-146.

Navaei, A., Truong, D., Heffernan, J., Cutts, J., Brafman, D., Sirianni, R. W., . . . Nikkhah, M. (2016). PNIPAAm-based biohybrid injectable hydrogel for cardiac tissue engineering. *Acta Biomaterialia, 32*, 10-23.

Neto, A., Correia, C., Oliveira, M., Rial-Hermida, M., Alvarez-Lorenzo, C., Reis, R., & Mano, J. (2015). A novel hanging spherical drop system for the generation of cellular spheroids and high throughput combinatorial drug screening. *Biomaterials Science, 3*(4), 581-585.

Nguyen, D. C., Hookway, T. A., Wu, Q., Jha, R., Preininger, M. K., Chen, X., . . . Maher, K. (2014). Microscale generation of cardiospheres promotes robust enrichment of cardiomyocytes derived from human pluripotent stem cells. *Stem Cell Reports, 3*(2), 260-268.

Nie, F.-Q., Xu, Z.-K., Huang, X.-J., Ye, P., & Wu, J. (2003). Acrylonitrile-based copolymer membranes containing reactive groups: surface modification by the immobilization of poly (ethylene glycol) for improving antifouling property and biocompatibility. *Langmuir, 19*(23), 9889-9895.

Niebruegge, S., Bauwens, C. L., Peerani, R., Thavandiran, N., Masse, S., Sevaptisidis, E., . . . Kumacheva, E. (2009). Generation of human embryonic stem cell-derived mesoderm and cardiac cells using size-specified aggregates in an oxygen-controlled bioreactor. *Biotechnology and Bioengineering, 102*(2), 493-507.

Nikkhah, M., Edalat, F., Manoucheri, S., & Khademhosseini, A. (2012). Engineering microscale topographies to control the cell–substrate interface. *Biomaterials, 33*(21), 5230-5246.

Noguchi, R., Nakayama, K., Itoh, M., Kamohara, K., Furukawa, K., Oyama, J.-i., . . . Morita, S. (2016). Development of a three-dimensional pre-vascularized scaffold-free contractile cardiac patch for treating heart disease. *The Journal of Heart and Lung Transplantation, 35*(1), 137-145.

Nunes, S. S., Miklas, J. W., Liu, J., Aschar-Sobbi, R., Xiao, Y., Zhang, B., . . . Hsieh, A. (2013). Biowire: a platform for maturation of human pluripotent stem cell–derived cardiomyocytes. *Nature Methods, 10*(8), 781.

Oltolina, F., Zamperone, A., Colangelo, D., Gregoletto, L., Reano, S., Pietronave, S., . . . Diena, M. (2015). Human cardiac progenitor spheroids exhibit enhanced engraftment potential. *PLOS ONE, 10*(9).

Ong, C. S., Fukunishi, T., Zhang, H., Huang, C. Y., Nashed, A., Blazeski, A., . . . Tung, L. (2017). Biomaterial-free three-dimensional bioprinting of cardiac tissue using

human induced pluripotent stem cell derived cardiomyocytes. *Scientific Reports, 7*(1), 1-11.

Pagano, F., Picchio, V., Chimenti, I., Sordano, A., De Falco, E., Peruzzi, M., . . . Sciarretta, S. (2019). On the Road to Regeneration:"Tools" and "Routes" Towards Efficient Cardiac Cell Therapy for Ischemic Cardiomyopathy. *Current Cardiology Reports, 21*(11), 133.

Pal, A., Smith, C. I., Palade, J., Nagaraju, S., Alarcon-Benedetto, B. A., Kilbourne, J., . . . Nikkhah, M. (2020). Poly (N-isopropylacrylamide)-based dual-crosslinking biohybrid injectable hydrogels for vascularization. *Acta Biomaterialia, 107*, 138-151.

Pal, A., Vernon, B. L., & Nikkhah, M. (2018). Therapeutic neovascularization promoted by injectable hydrogels. *Bioactive Materials, 3*(4), 389-400.

Park, J., Kim, Y. S., Ryu, S., Kang, W. S., Park, S., Han, J., . . . Kim, B. S. (2015b). Graphene potentiates the myocardial repair efficacy of mesenchymal stem cells by stimulating the expression of angiogenic growth factors and gap junction protein. *Advanced Functional Materials, 25*(17), 2590-2600.

Paul, A., Hasan, A., Kindi, H. A., Gaharwar, A. K., Rao, V. T., Nikkhah, M., . . . Shum-Tim, D. (2014). Injectable graphene oxide/hydrogel-based angiogenic gene delivery system for vasculogenesis and cardiac repair. *ACS Nano, 8*(8), 8050-8062.

Pedde, R. D., Mirani, B., Navaei, A., Styan, T., Wong, S., Mehrali, M., . . . Dolatshahi-Pirouz, A. (2017). Emerging biofabrication strategies for engineering complex tissue constructs. *Advanced Materials, 29*(19), 1606061.

Perin, E. C., & López, J. (2006). Methods of stem cell delivery in cardiac diseases. *Nature Clinical Practice Cardiovascular Medicine, 3*(1), S110-S113.

Pitaktong, I., Lui, C., Lowenthal, J., Mattson, G., Jung, W.-H., Bai, Y., . . . Gerecht, S. (2020). Early Vascular Cells Improve Microvascularization Within 3D Cardiac Spheroids. *Tissue Engineering Part C: Methods, 26*(2), 80-90.

Polonchuk, L., Chabria, M., Badi, L., Hoflack, J.-C., Figtree, G., Davies, M. J., & Gentile, C. (2017). Cardiac spheroids as promising in vitro models to study the human heart microenvironment. *Scientific Reports, 7*(1), 1-12.

Pomeroy, J. E., Helfer, A., & Bursac, N. (2019). Biomaterializing the promise of cardiac tissue engineering. *Biotechnology Advances*.

Prabhu, S. D., & Frangogiannis, N. G. (2016). The Biological Basis for Cardiac Repair After Myocardial Infarction. *Circulation Research, 119*(1), 91-112. doi:doi:10.1161/CIRCRESAHA.116.303577

Radisic, M., Deen, W., Langer, R., & Vunjak-Novakovic, G. (2005). Mathematical model of oxygen distribution in engineered cardiac tissue with parallel channel array perfused with culture medium containing oxygen carriers. *American Journal of Physiology-Heart and Circulatory Physiology, 288*(3), H1278-H1289.

Rajabi-Zeleti, S., Jalili-Firoozinezhad, S., Azarnia, M., Khayyatan, F., Vahdat, S., Nikeghbalian, S., . . . Aghdami, N. (2014). The behavior of cardiac progenitor cells on macroporous pericardium-derived scaffolds. *Biomaterials, 35*(3), 970-982.

Ravenscroft, S. M., Pointon, A., Williams, A. W., Cross, M. J., & Sidaway, J. E. (2016). Cardiac Non-myocyte Cells Show Enhanced Pharmacological Function Suggestive of Contractile Maturity in Stem Cell Derived Cardiomyocyte Microtissues. *Toxicological Sciences, 152*(1), 99-112. doi:10.1093/toxsci/kfw069

Ravi, M., Paramesh, V., Kaviya, S., Anuradha, E., & Solomon, F. P. (2015). 3D cell culture systems: advantages and applications. *Journal of Cellular Physiology, 230*(1), 16-26.

Rezai, N., Corbel, S. Y., Dabiri, D., Kerjner, A., Rossi, F. M., McManus, B. M., & Podor, T. J. (2005). Bone marrow-derived recipient cells in murine transplanted hearts: potential roles and the effect of immunosuppression. *Laboratory Investigation, 85*(8), 982-991.

Ribeiro, M. C., Tertoolen, L. G., Guadix, J. A., Bellin, M., Kosmidis, G., D'Aniello, C., . . . Feinberg, A. W. (2015). Functional maturation of human pluripotent stem cell derived cardiomyocytes in vitro–correlation between contraction force and electrophysiology. *Biomaterials, 51*, 138-150.

Richards, D. J., Coyle, R. C., Tan, Y., Jia, J., Wong, K., Toomer, K., . . . Mei, Y. (2017). Inspiration from heart development: Biomimetic development of functional human cardiac organoids. *Biomaterials, 142*, 112-123.

Richards, D. J., Li, Y., Kerr, C. M., Yao, J., Beeson, G. C., Coyle, R. C., . . . Wilson, R. (2020). Human cardiac organoids for the modelling of myocardial infarction and drug cardiotoxicity. *Nature Biomedical Engineering*, 1-17.

Richards, D. J., Tan, Y., Coyle, R., Li, Y., Xu, R., Yeung, N., . . . Mei, Y. (2016). Nanowires and Electrical Stimulation Synergistically Improve Functions of hiPSC Cardiac Spheroids. *Nano Letters, 16*(7), 4670-4678. doi:10.1021/acs.nanolett.6b02093

Robertson, C., Tran, D. D., & George, S. C. (2013). Concise review: Maturation phases of human pluripotent stem cell-derived cardiomyocytes. *Stem Cells, 31*(5), 829-837.

Rodriguez, A., Elabd, C., Amri, E., Ailhaud, G., & Dani, C. (2005). The human adipose tissue is a source of multipotent stem cells. *Biochimie, 87*(1), 125-128.

Ronaldson-Bouchard, K., Ma, S. P., Yeager, K., Chen, T., Song, L., Sirabella, D., . . . Vunjak-Novakovic, G. (2018). Advanced maturation of human cardiac tissue grown from pluripotent stem cells. *Nature, 556*(7700), 239-243.

Rouwkema, J., Koopman, B. F., Blitterswijk, C. A. V., Dhert, W. J., & Malda, J. (2009). Supply of nutrients to cells in engineered tissues. *Biotechnology and Genetic Engineering Reviews, 26*(1), 163-178.

Rungarunlert, S., Klincumhom, N., Bock, I., Nemes, C., Techakumphu, M., Pirity, M. K., & Dinnyes, A. (2011). Enhanced cardiac differentiation of mouse embryonic stem cells by use of the slow-turning, lateral vessel (STLV) bioreactor. *Biotechnology Letters, 33*(8), 1565-1573.

Saini, H., Navaei, A., Van Putten, A., & Nikkhah, M. (2015). 3D Cardiac Microtissues Encapsulated with the Co-Culture of Cardiomyocytes and Cardiac Fibroblasts. *Advanced healthcare materials, 4*(13), 1961-1971. doi:10.1002/adhm.201500331

Saini, H., Sam, F. S., Kharaziha, M., & Nikkhah, M. (2018). 8 Micropatterning. *Cell and Material Interface: Advances in Tissue Engineering, Biosensor, Implant, and Imaging Technologies*, 187.

Sakaguchi, K., Shimizu, T., & Okano, T. (2015). Construction of three-dimensional vascularized cardiac tissue with cell sheet engineering. *Journal of Controlled Release, 205*, 83-88. doi:https://doi.org/10.1016/j.jconrel.2014.12.016

Savarese, G., & Lund, L. H. (2017). Global public health burden of heart failure. *Cardiac failure review, 3*(1), 7.

Schwartz, S. D., Hubschman, J.-P., Heilwell, G., Franco-Cardenas, V., Pan, C. K., Ostrick, R. M., . . . Lanza, R. (2012). Embryonic stem cell trials for macular degeneration: a preliminary report. *The Lancet, 379*(9817), 713-720.

Scuderi, G. J., & Butcher, J. (2017). Naturally Engineered Maturation of Cardiomyocytes. *Frontiers in Cell and Developmental Biology, 5*(50). doi:10.3389/fcell.2017.00050

Segers, V. F., & Lee, R. T. (2008). Stem-cell therapy for cardiac disease. *Nature, 451*(7181), 937-942.

Sekiya, S., Shimizu, T., Yamato, M., Kikuchi, A., & Okano, T. (2006). Bioengineered cardiac cell sheet grafts have intrinsic angiogenic potential. *Biochemical and Biophysical Research Communications, 341*(2), 573-582.

Shafei, A. E. S., Ali, M. A., Ghanem, H. G., Shehata, A. I., Abdelgawad, A. A., Handal, H. R., . . . El-Shal, A. S. (2017). Mesenchymal stem cell therapy: A promising cell-

based therapy for treatment of myocardial infarction. *The journal of Gene Medicine, 19*(12), e2995.

Shapira-Schweitzer, K., & Seliktar, D. (2007). Matrix stiffness affects spontaneous contraction of cardiomyocytes cultured within a PEGylated fibrinogen biomaterial. *Acta Biomaterialia, 3*(1), 33-41.

Shapira, A., Feiner, R., & Dvir, T. (2016). Composite biomaterial scaffolds for cardiac tissue engineering. *International Materials Reviews, 61*(1), 1-19.

Shimizu, T., Yamato, M., Isoi, Y., Akutsu, T., Setomaru, T., Abe, K., . . . Okano, T. (2002). Fabrication of pulsatile cardiac tissue grafts using a novel 3-dimensional cell sheet manipulation technique and temperature-responsive cell culture surfaces. *Circulation Research, 90*(3), e40-e48.

Shin, S. R., Jung, S. M., Zalabany, M., Kim, K., Zorlutuna, P., Kim, S. b., . . . Kong, J. (2013). Carbon-nanotube-embedded hydrogel sheets for engineering cardiac constructs and bioactuators. *ACS Nano, 7*(3), 2369-2380.

Shin, S. R., Zihlmann, C., Akbari, M., Assawes, P., Cheung, L., Zhang, K., . . . Wan, K. t. (2016). Reduced graphene oxide-gelMA hybrid hydrogels as scaffolds for cardiac tissue engineering. *Small, 12*(27), 3677-3689.

Shukla, R., Bansal, V., Chaudhary, M., Basu, A., Bhonde, R. R., & Sastry, M. (2005). Biocompatibility of gold nanoparticles and their endocytotic fate inside the cellular compartment: a microscopic overview. *Langmuir, 21*(23), 10644-10654.

Sreejit, P., & Verma, R. (2013). Natural ECM as biomaterial for scaffold based cardiac regeneration using adult bone marrow derived stem cells. *Stem Cell Reviews and Reports, 9*(2), 158-171.

Sun, L., Huang, C., Gong, T., & Zhou, S. (2010). A biocompatible approach to surface modification: biodegradable polymer functionalized super-paramagnetic iron oxide nanoparticles. *Materials Science and Engineering: C, 30*(4), 583-589.

Sun, Q., Zhang, Z., & Sun, Z. (2014). The potential and challenges of using stem cells for cardiovascular repair and regeneration. *Genes & Diseases, 1*(1), 113-119.

Takahashi, K., Tanabe, K., Ohnuki, M., Narita, M., Ichisaka, T., Tomoda, K., & Yamanaka, S. (2007). Induction of pluripotent stem cells from adult human fibroblasts by defined factors. *Cell, 131*(5), 861-872.

Tan, Y., Richards, D., Coyle, R. C., Yao, J., Xu, R., Gou, W., . . . Mei, Y. (2017). Cell number per spheroid and electrical conductivity of nanowires influence the function of silicon nanowired human cardiac spheroids. *Acta biomaterialia, 51*, 495-504.

Tan, Y., Richards, D., Xu, R., Stewart-Clark, S., Mani, S. K., Borg, T. K., . . . Mei, Y. (2015). Silicon nanowire-induced maturation of cardiomyocytes derived from human induced pluripotent stem cells. *Nano Letters, 15*(5), 2765-2772.

Thomson, K. S., Korte, F. S., Giachelli, C. M., Ratner, B. D., Regnier, M., & Scatena, M. (2013). Prevascularized microtemplated fibrin scaffolds for cardiac tissue engineering applications. *Tissue Engineering Part A, 19*(7-8), 967-977.

Thygesen, K., Alpert, J. S., & White, H. D. (2007). Universal Definition of Myocardial Infarction. *Circulation, 116*(22), 2634-2653. doi:doi:10.1161/CIRCULATIONAHA.107.187397

Tonsho, M., Michel, S., Ahmed, Z., Alessandrini, A., & Madsen, J. C. (2014). Heart transplantation: challenges facing the field. *Cold Spring Harbor Perspectives in Medicine, 4*(5), a015636.

Torella, D., Ellison, G. M., Méndez-Ferrer, S., Ibanez, B., & Nadal-Ginard, B. (2006). Resident human cardiac stem cells: role in cardiac cellular homeostasis and potential for myocardial regeneration. *Nature Clinical Practice Cardiovascular Medicine, 3*(1), S8-S13.

Truong, D., Fiorelli, R., Barrientos, E. S., Melendez, E. L., Sanai, N., Mehta, S., & Nikkhah, M. (2019). A three-dimensional (3D) organotypic microfluidic model for glioma stem cells–Vascular interactions. *Biomaterials, 198*, 63-77.

Truong, D. D., Kratz, A., Park, J. G., Barrientos, E. S., Saini, H., Nguyen, T., . . . Nikkhah, M. (2019). A human organotypic microfluidic tumor model permits investigation of the interplay between patient-derived fibroblasts and breast cancer cells. *Cancer Research, 79*(12), 3139-3151.

Ulmer, B. M., Stoehr, A., Schulze, M. L., Patel, S., Gucek, M., Mannhardt, I., . . . Hansen, A. (2018). Contractile work contributes to maturation of energy metabolism in hiPSC-derived cardiomyocytes. *Stem Cell Reports, 10*(3), 834-847.

van Spreeuwel, A., Bax, N., Bastiaens, A., Foolen, J., Loerakker, S., Borochin, M., . . . Bouten, C. (2014). The influence of matrix (an) isotropy on cardiomyocyte contraction in engineered cardiac microtissues. *Integrative Biology, 6*(4), 422-429.

Veldhuizen, J., Cutts, J., Brafman, D., Migrino, R. Q., & Nikkhah, M. (2020a). Engineering anisotropic human stem cell-derived three-dimensional cardiac tissue on-a-chip. *Biomaterials*, 120195.

Veldhuizen, J., Migrino, R. Q., & Nikkhah, M. (2019). Three-dimensional microengineered models of human cardiac diseases. *Journal of biological engineering, 13*(1), 29.

Virag, J. I., & Murry, C. E. (2003). Myofibroblast and endothelial cell proliferation during murine myocardial infarct repair. *The American Journal of Pathology, 163*(6), 2433-2440.

Virani, S. S., Alonso, A., Benjamin, E. J., Bittencourt, M. S., Callaway, C. W., Carson, A. P., . . . Delling, F. N. (2020). Heart disease and stroke statistics—2020 update: a report from the American Heart Association. *Circulation*, E139-E596.

Voges, H. K., Mills, R. J., Elliott, D. A., Parton, R. G., Porrello, E. R., & Hudson, J. E. (2017). Development of a human cardiac organoid injury model reveals innate regenerative potential. *Development, 144*(6), 1118-1127.

Volarevic, V., Markovic, B. S., Gazdic, M., Volarevic, A., Jovicic, N., Arsenijevic, N., . . . Stojkovic, M. (2018). Ethical and safety issues of stem cell-based therapy. *International Journal of Medical Sciences, 15*(1), 36.

Wang, L., Huang, G., Sha, B., Wang, S., Han, Y., Wu, J., . . . Xu, F. (2014). Engineering three-dimensional cardiac microtissues for potential drug screening applications. *Current Medicinal Chemistry, 21*(22), 2497-2509.

Wang, X., Xi, W.-c., & Wang, F. (2014). The beneficial effects of intracoronary autologous bone marrow stem cell transfer as an adjunct to percutaneous coronary intervention in patients with acute myocardial infarction. *Biotechnology Letters, 36*(11), 2163-2168.

Williams, C., Budina, E., Stoppel, W. L., Sullivan, K. E., Emani, S., Emani, S. M., & Black III, L. D. (2015). Cardiac extracellular matrix–fibrin hybrid scaffolds with tunable properties for cardiovascular tissue engineering. *Acta Biomaterialia, 14*, 84-95.

Xu, M., Zhu, J., Wang, F., Xiong, Y., Wu, Y., Wang, Q., . . . Liu, S. (2016). Improved in vitro and in vivo biocompatibility of graphene oxide through surface modification: poly (acrylic acid)-functionalization is superior to PEGylation. *ACS Nano, 10*(3), 3267-3281.

Yan, Y., Bejoy, J., Xia, J., Griffin, K., Guan, J., & Li, Y. (2019). Cell population balance of cardiovascular spheroids derived from human induced pluripotent stem cells. *Scientific Reports, 9*(1), 1-12.

Yang, J., Yamato, M., Kohno, C., Nishimoto, A., Sekine, H., Fukai, F., & Okano, T. (2005). Cell sheet engineering: recreating tissues without biodegradable scaffolds. *Biomaterials, 26*(33), 6415-6422.

Yang, X., Pabon, L., & Murry, C. E. (2014). Engineering Adolescence. *Circulation Research, 114*(3), 511-523. doi:doi:10.1161/CIRCRESAHA.114.300558

Yu, J., Vodyanik, M. A., Smuga-Otto, K., Antosiewicz-Bourget, J., Frane, J. L., Tian, S., . . . Stewart, R. (2007). Induced pluripotent stem cell lines derived from human somatic cells. *Science, 318*(5858), 1917-1920.

Zacharias, D. G., Nelson, T. J., Mueller, P. S., & Hook, C. C. (2011). *The science and ethics of induced pluripotency: what will become of embryonic stem cells?* Paper presented at the Mayo Clinic Proceedings.

Zhang, D., Shadrin, I. Y., Lam, J., Xian, H.-Q., Snodgrass, H. R., & Bursac, N. (2013). Tissue-engineered cardiac patch for advanced functional maturation of human ESC-derived cardiomyocytes. *Biomaterials, 34*(23), 5813-5820.

Zhang, H. Z., Kim, M. H., Lim, J. H., & Bae, H.-R. (2013). Time-dependent expression patterns of cardiac aquaporins following myocardial infarction. *Journal of Korean Medical Science, 28*(3), 402-408.

Zhang, J., Wilson, G. F., Soerens, A. G., Koonce, C. H., Yu, J., Palecek, S. P., . . . Kamp, T. J. (2009). Functional cardiomyocytes derived from human induced pluripotent stem cells. *Circulation Research, 104*(4), e30-e41.

Zhang, J., Zhu, W., Radisic, M., & Vunjak-Novakovic, G. (2018). Can we engineer a human cardiac patch for therapy? *Circulation Research, 123*(2), 244-265.

Zhao, S., Xu, Z., Wang, H., Reese, B. E., Gushchina, L. V., Jiang, M., . . . Shen, R. (2016). Bioengineering of injectable encapsulated aggregates of pluripotent stem cells for therapy of myocardial infarction. *Nature Communications, 7*(1), 1-12.

Ziaeian, B., & Fonarow, G. C. (2016). Epidemiology and aetiology of heart failure. *Nature Reviews Cardiology, 13*(6), 368-378.

Zong, X., Bien, H., Chung, C.-Y., Yin, L., Fang, D., Hsiao, B. S., . . . Entcheva, E. (2005). Electrospun fine-textured scaffolds for heart tissue constructs. *Biomaterials, 26*(26), 5330-5338.

Zorlutuna, P., Annabi, N., Camci-Unal, G., Nikkhah, M., Cha, J. M., Nichol, J. W., . . . Khademhosseini, A. (2012). Microfabricated biomaterials for engineering 3D tissues. *Advanced Materials, 24*(14), 1782-1804.

Zuppinger, C. (2019). 3D Cardiac Cell Culture: A Critical Review of Current Technologies and Applications. *Frontiers in Cardiovascular Medicine, 6*(87). doi:10.3389/fcvm.2019.00087

CHAPTER 3

NANOENGINEERING OF GOLD NANORIBBON-EMBEDDED ISOGENIC STEM CELL-DERIVED CARDIAC ORGANOIDS

3.1 ABSTRACT

Cardiac tissue engineering is an emerging field providing tools to treat and study cardiovascular diseases (CVDs). In the past years, the integration of stem cell technologies with micro- and nanoengineering techniques have enabled creation of novel engineered cardiac tissues (ECTs) with potential applications in disease modeling, drug screening, and regenerative medicine. However, a major unaddressed limitation of stem cell-derived ECTs is their immature state, resembling a neonatal phenotype and genotype. The modulation of the cellular microenvironment within the ECTs has been proposed as efficient mechanism to promote cellular maturation and improve features such as cellular coupling and synchronization. The integration of biological and nanoscale cues in the ECTs could serve as a tool for the modification and control of engineered tissue microenvironment. Here we present a proof-of-concept study for the integration of biofunctionalized gold nanoribbons (AuNRs) with hiPSC-derived isogenic cardiac organoids to enhance tissue function and maturation. We first present extensive characterization of the synthesized AuNRs, their PEGylation and cytotoxicity evaluation. We then evaluated the functional contractility and transcriptomic profile of cardiac organoids fabricated with hiPSC-derived cardiomyocytes (mono-culture) as well as with hiPSC-derived cardiomyocytes and cardiac fibroblasts (co-culture). We demonstrated that PEGylated AuNRs are biocompatible and do not induce cell death in hiPSC-derived

cardiac cells and organoids. We also found an improved transcriptomic profile of the co-cultured organoids indicating maturation of the hiPSC-derived cardiomyocytes in presence of cardiac fibroblasts. Overall, we present for the first time the integration of AuNRs into cardiac organoids, showing promising results for improved tissue function.

3.2 INTRODUCTION

Cardiovascular diseases (CVDs) are the primary cause of deaths around the world (Mc Namara, Alzubaidi, & Jackson, 2019). Moreover, the risk factors associated with CVDs are expected to increase in the near future (G. A. Roth et al., 2020). Studying the mechanisms underlying CVDs are limited by the reduced availability of primary human cardiac tissues cells. Therefore preclinical cardiac research have mainly relied on animal models (J. Veldhuizen, R. Q. Migrino, & M. Nikkhah, 2019). However, with the increasing utilization of stem cell technologies, it is now easy to source human cardiac cells for advanced *in vitro* studies (Hartman, Dai, & Laflamme, 2016). Protocols for the directed differentiation of human cardiomyocytes (CMs), cardiac fibroblasts (CFs), and other cell types have been developed and refined to produce these cells within a short period of time in order of few weeks (X. Lian et al., 2013; J. Zhang et al., 2019). While these advancements have provided access to unlimited number of cardiac cells, one remaining main disadvantage is that these stem cells are usually in an immature state and phenotype (Bedada, Wheelwright, & Metzger, 2016).

The refinement of micro and nanoengineering technologies has allowed for the manufacturing of highly reproducible engineered tissues. This, in combination with stem cell technologies, has resulted in powerful protocols for the fabrication of complex and

biomimetic human cardiac tissues *in vitro* (Esmaeili et al., 2022; A. Patino-Guerrero et al., 2020; J. Veldhuizen et al., 2019). Different cardiac tissues have been engineered with specific applications such as disease modeling, drug screening (J. Li et al., 2020), or myocardial regeneration (D. Yu, Wang, & Ye, 2021). Regardless of a specific application, the following general principles still apply: a) it is desirable that the hiPSC-derived cardiac cells reach an adult-like phenotype and genotype in order to better represent adult human myocardium (Ahmed, Anzai, Chanthra, & Uosaki, 2020; Bedada et al., 2016); b) the design and control of microenvironmental cues is one of the key factors promoting cellular maturation and enhancing physiologic performance of the engineered tissues (Augustine et al., 2021; Wanjare & Huang, 2017); and c) the manipulation of the microenvironment within the engineered tissues can be achieved through physical, chemical, and biological cues, or more often, by a combination of two or more of these methods (Augustine et al., 2021; Besser et al., 2018; Wanjare & Huang, 2017).

The introduction of advanced biomaterials with unique properties has been proposed as a practical approach for the fabrication of engineered cardiac tissues (ECTs) within a controlled microenvironment (Cutts et al., 2015; Dolatshahi-Pirouz, Nikkhah, Kolind, Dokmeci, & Khademhosseini, 2011; Esmaeili et al., 2022). Specifically, nanoengineered biomaterials are of particular interest due to their unique physical and chemical properties (Kharaziha et al., 2016). Their size allows for intimate interaction with cellular structures and the intercellular microenvironment. Recently, high aspect ratio nanoparticles, also known as one-dimensional (1D) nanoparticles, have been of special interest for tissue engineering applications due to their morphological features. On one hand, they may present attractive nanoscale features, such as electrical conductivity and surface plasmon

resonance (Hong, Tan, Chen, Xu, & Zhang, 2015). Additionally, their larger size, compared to nanoparticles with smaller aspect ratios, allow them to remain and integrated within the intercellular space while continuing to modify the cellular microenvironment (Lopez-Chaves et al., 2018).

One of the most relevant functions of the cardiac tissue relates to its electrical activity and the ability of cardiac cells to conduct electrical signals (Sundnes et al., 2007). This signal propagation is possible due to the formation of a syncytium that transmits electrical and mechanical pulses.(Slotvitsky, Tsvelaya, Podgurskaya, & Agladze, 2020). Often, ECTs do not closely mimic, if at all, the electrophysiological features of the native myocardium (Veerman et al., 2015). In this regard, electrically conductive nanoparticles could be interest of cardiac tissue engineering as it is believed that they can enhance the maturation and functionality of hiPSC-derived ECTs by creating a more electrically conductive extracellular microenvironment (Esmaeili et al., 2022). Since ECTs fabricated with hiPSC-derived cardiac cells present an immature phenotype with poor cell-cell coupling and inefficient electrical activity, incorporating electrically conductive nanoparticles could also represent a promising approach to modulate the microenvironment of ECT and improve the physiologic performance of cardiac tissues (A. Patino-Guerrero et al., 2020). For example, it has been reported that the integration of Si nanowires into cardiac spheroids improved their gene expression profile and cell-to-cell connection (Dylan J. Richards et al., 2016; Y. Tan et al., 2017). The integration of graphene and graphene oxide has also been found to upregulate the expression of cardiac-relevant genes (Ahadian et al., 2016; Park et al., 2015a).

The incorporation of different cardiac cell types has also been widely proposed as another key factor affecting the ECTs microenvironment (Campostrini et al., 2021; Alejandra Patino-Guerrero et al., 2023; H. Saini, A. Navaei, A. Van Putten, & M. Nikkhah, 2015). It was demonstrated that CFs play an important role in the secretion of growth factors and cytokines that regulate the activity of CMs (W. Chen, Bian, Zhou, & Zhang, 2021; Souders, Bowers, & Baudino, 2009). Moreover, CFs are the main producers of extracellular matrix (ECM) proteins in the cardiac tissue (Daseke, Tenkorang, Chalise, Konfrst, & Lindsey, 2020). To that end, isogenic cardiac organoids are of special interest in the tissue engineering due to the lack of exogenic biomaterials, recapitulation of cardiac tissue composition, feasible application in disease modeling and regeneration through minimally invasive route (A. Patino-Guerrero et al., 2020). The benefits of co-culture of CMs and CFs for the formation of cardiac organoids have been widely studied and reported, and in our recent work, the CMs:CFs ratio was optimized for the creation of isogenic cardiac organoids (Alejandra Patino-Guerrero et al., 2023). Thus, the integration of hiPSC-CFs in ECTs serves as another relevant tool for the regulation of the microenvironment and the fabrication of cardiac organoids.

In this manuscript we present a proof-of-concept study for the integration of gold nanoribbons (AuNRs) with scaffold-free isogenic hiPSC-derived cardiac organoids. We hypothesize that the inclusion of 1D gold nanoparticles, namely AuNRs, in combination with the co-culture of isogenic hiPSC-derived cardiac cells (CMs and CFs), can lead to the improved maturation of the cells and an overall enhanced physiologic performance of the cardiac organoids. First, we adapted a seed-mediated growth synthesis method for the fabrication and characterization of the AuNRs with desired length and geometry. We

further functionalized the surface of the AuNRs with polyethylene glycol (PEG) to render them biocompatible and suitable for cardiac tissue engineering applications. We differentiated CMs and CFs from a hiPSC line to generate isogenic lines of cells for tissue formation. By seeding these cells (7:3 CM:CF ratio) along with AuNRs (10 µg/ml) in agarose microwells, we induced cellular aggregation and the formation of scaffold-free cardiac organoids. We analyzed the effect of the AuNRs in the formation of the cardiac organoids by examining the integrity and viability of the cardiac organoids and evaluating electrophysiological features as well as the resulting transcriptomic profile.

3.3 EXPERIMENTAL METHODS

3.3.1 Materials

All the materials, as wells as their working concentrations, brands and identifier numbers are provided in the supplementary "Table A1. Table of resources" in **APPENDIX A**.

3.3.2 Synthesis of gold nanoribbons (AuNRs)

The protocol for the synthesis of AuNRs was adapted from Xu, et. al. (Y. Xu et al., 2015). This method is based in the seed-mediated aggregation of gold atoms, guided by a bisurfactant system. First, the gold seed solution was prepared as follows. In a 15 ml conical tube, 7.5 ml of 0.1 M of Cetrimonium bromide (CTAB) solution were mixed with 250 µl of $HAuCl_4$ (0.01 M). Then, 600 µl of ice-cold $NaBH_4$ (0.01M) was added to the seed solution and vigorously vortexed for two minutes. This solution was then incubated at 35°C for 1 hour, resulting in a reddish-maroon solution. After the incubation period, the solution was diluted to a 1:10 ratio.

The growth solution was prepared in a 50 ml conical tube. First 230 mg of CTAB and 48.5 mg of sodium oleate (NaOL) were dissolved in 384 ml of deionized water (DIW). Then, 250 µl of $HAuCl_4$ (0.01 M) was added to this solution which immediately turned the growth solution color to bright yellow. This solution was incubated at 35 °C for 15 minutes or until it turned colorless. Finally, 3.8 ml of an ascorbic acid solution (0.1 M) were added to the growth solution to reduce all ionic gold to metallic gold. 20 µl of the diluted seed solution were added to the final growth solution and vortexed for 30 s. The solution was incubated undisturbed at 35°C for 8 hrs. The synthesized AuNRs solution had a characteristic pink to maroon color after the incubation period.

3.3.3 Purification and characterization of the AuNRs

In order to purify and obtain a highly concentrated AuNRs solution, the synthesized AuNRs solution was washed three times. For this, the samples were centrifuged at 3000x*g* for 17 minutes, the supernatant was removed and replaced by DIW. Gold nanoparticles present optical properties, namely surface plasmon resonance (SPR) phenomenon, that allows for their characterization using UV-Visible spectrophotometry (UV-Vis). A sample of the concentrated AuNRs solution was measured through UV-Vis to corroborate that the synthesis was successful.

To evaluate the morphology of the AuNRs the samples were mounted in a copper mesh grid (Ted Pella). The samples were visualized through transmission electronic microscope (TEM) (Phillips JEOL 2010). To determine the average size of the ribbon-like nanoparticles a total of 100 particles above 0.6 µm length were measured using FIJI ImageJ. The average size was calculated as the arithmetic mean of these particles.

A standard concentration curve was generated to measure the concentration of the AuNRs. For this, serial dilutions of the AuNRs were prepared and the concentration of each of the dilutions was measured using inductively coupled plasma mass spectrometry (ICP-MS). Each of the measured concentrations was correlated to the optical density (O.D.) at 450 nm of the corresponding AuNRs dilution. Finally, the linear regression of the obtained curve was calculated. Subsequently, the concentration of AuNRs was obtained by inserting the O.D. in the equation generated from the linear regression.

3.3.4 PEGylation of AuNRs

A surface molecule exchange was performed to substitute the residual CTAB and NaOL on the surface of the AuNRs with polyethylene glycol (PEG) (**Figure 3.1 A**). This PEGylation reaction was adapted from Zhang, et. al. (Z. Zhang & Lin, 2014). For this purpose, the concentrated AuNRs solution was centrifuged at 3000*xg* for 17 minutes. The supernatant was removed and replaced with 400 µl of Tris buffer (pH: 3.0). Then, 30 µl of a solution of 2 mM PEG in Tris buffer was added to the AuNRs solution and vortexed vigorously for 2 minutes. The resultant solution was incubated undisturbed at room temperature for 24 hours. After this incubation period, the AuNRs solution was centrifuged again, and the supernatant was replaced with 400 µl of 20% ethanol (VWR). Then 30 µl of PEG (2mM) in 20% ethanol was added to the solution and vortex vigorously. The solution was incubated undisturbed at room temperature for 24 hours. Then, the samples were washed twice with sterilize 1x DPBS (Dulbecco's phosphate buffered solution). Finally, the AuNRs were resuspended in sterile 1x DPBS for concentration measurement analysis and stored at room temperature until their use.

3.3.5 Human induced pluripotent stem cells maintenance

The hiPSCs (IMR90-4, WiCell) were maintained in mTeSR-1 media (StemCell Technologies) with daily changes. The cells were seeded on hESC-Matrigel (Corning)-coated plates to help to maintain the pluripotency state of the cells. The hiPSC colonies were allowed to reach ~85% confluency before replating. When the cells reached confluency, they were incubated in a 0.5 mM EDTA (Corning) in 1x DPBS solution for 6-7 minutes and mechanical dissociation with 1 ml of mTeSR-1 media was performed to remove the cells from the plates. The cells were replated at a seeding density of 150-250K cells per well. To ensure the well maintenance of the hiPSCs, they were stained for the stemness factors Nanog and Sox2 (**Figure 3.1 B**).

3.3.6 Directed differentiation of hiPSC-derived cardiomyocytes

The hiPSC-CMs differentiation protocol was adapted from the GiWi protocol (X. Lian et al., 2013), which is based on the regulation of the Wnt canonical pathway. Briefly, when the hiPSCs reached 80-95% confluency, the maintenance media was substituted with of RPMI 1640 supplemented with 2% B27 minus insulin (Gibco), 1% Pen/Strep (Gibco) (RPMI-) and 7-9 µM of CHIR99021 (BioVision) in order to induce the activation of the Wnt pathway in the cells (designated as day 0). After 24 hours, the media was substituted for RPMI- media only. Then, 72 hours after day 0, the media was substituted by a 1:1 mix of conditioned media and fresh RPMI- supplemented with 5 µM IWP2 (Sigma) in order to inhibit the Wnt signaling within the cells. Culture media was refreshed 48 hours after this. Finally, the hiPSC-CM were maintained in RPMI 1640 supplemented with 2% B27 plus

insulin (Gibco) and 1% Pen/Strep (Gibco) (RPMI+) until day 13 after day 0, the media was refreshed every 48 hours. The cells typically presented spontaneous beating around day 10.

In order to increase the purity of the obtained hiPSC-CMs, the differentiated cells were submitted to a glucose starvation period (Binah et al., 2007). On day 13 of differentiation, the cell culture media was exchanged to RPMI 1640 minus glucose supplemented with 2% B27 plus insulin (Gibco), 1% Pen/Strep (Gibco), and 4mM sodium lactate (Sigma). Media was refreshed every 72 hours up to day 19. On day 19, the media was substitute with RPMI+ to allow for the recovery of the cells. To eliminate the debris generated from the purification of the hiPSC-CMs, the cells were dissociated on day 21 using TrypLE Express (LifeTech) for 10-12 minutes, followed by mechanical dissociation. The hiPSC-CMs were replated on Matrigel with a cell seeding density of 1-1.5 million cells per well (**Figure 3.1 B**). Cells were maintained with RPMI+ until their utilization for the experiments, and the media was refreshed every 48 hours.

3.3.7 Directed differentiation of hiPSC-derived cardiac fibroblasts

The differentiation of isogenic human cardiac fibroblast (CF) was adapted from Fan, et. al. (C. Fan et al., 2020). It is based on the modulation of Wnt canonical pathway to produce cardiac progenitor cells, followed by the introduction of fibroblast growth factor (FGF). Briefly, the CFs differentiation was initiated when the hiPSCs reached around 80% confluency. On day 0, the hiPSCs basal media was changed to RPMI 1640 which was supplemented with 7µM CHIR99021 (BioVision). After 24 hours (day 1), the media was replaced by RPMI-. Upon day 1, the hiPSC-CFs differentiation was carried out with a basal media, with changes every 48 hours. The basal media consisted of high-glucose (4.5 g/l)

DMEM with L-glutamine (4 mM) (Gibco), supplemented with HLL supplement (human serum albumin (500 µg/ml), linoleic acid (0.6µM), lecithin (0.6 µg/ml), and β-fibroblast growth factor (β-FGF) (70 ng/µl); this stage was carried for 20 days. Then, the hiPSC-CFs were dissociated with 1x Trypsin and replated in uncoated plates to remove cellular debris. After this, the cells were maintained with Fibroblast Growth Media 3 (FGM-3), with media changes every 48 hours. The CFs were replated when reached ~85% confluency. The hiPSC-CFs used for all of the experiments were between passage number P6 and P12 to avoid further differentiation into myofibroblasts.

3.3.8 Fabrication of isogenic scaffold-free cardiac organoids embedded with AuNRs

Commercially available silicone molds (Microtissues, #35-24) were used to cast agarose microwells (800 µm diameter, 800 µm depth). Briefly, ~350 µl of a 2% agarose in saline solution were deposited in the silicone molds. After the agarose was solidified, it was removed from the molds. The agarose microwells were conditioned with RPMI+ media prior their utilization for organoid fabrication.

The hiPSC-CMs were incubated at 37°C for 10-12 minutes with Tryple Express (LifeTech), followed by mechanical dissociation. The Tryple was neutralized with RPMI/B27 plus insulin. Additionally, the hiPSC-CFs were incubated with 1x Trypsin (Gibco) for 3-4 minutes at 37°C followed by neutralization with FGM3. The cells were manually counted to determine the concentration and were centrifuged (300x*g* for 3 minutes) to remove the supernatant. The cells were resuspended in RPMI/B27 plus insulin to a final concentration of 175K cells per 75 µl (**Figure 3.1 C**). The cells were seeded in

the agarose microwells and were incubated undisturbed for 1 hour at 37°C to allow the cells to settle in the microwells. Then, the culture wells were filled with RPMI/B27 plus and the media was changed every 48 hours until the end of the experiment.

3.3.9 Imaging and video signal acquisition and analysis

Phase-contrast images and videos were acquired with a Zeiss Axio Observer Z1 microscope. The Apotome2 complement was used for all fluorescent images. ZenPro and ImageJ (FIJI) software were used for image and video processing. A custom-made MATLAB code was used for extracting the spontaneous beating signals from the cardiac organoids. The beating rate of the cardiac organoids was calculated by detecting the peaks presented in the acquired signals. The inter-beat interval variability (IIV) was calculated as the standard deviation of the variation in time between the presented peaks.

3.3.10 Viability assay

The viability assay was performed with the Viability/Cytotoxicity assay kit for animal live & dead cells (Biotium), according to the instructions of the kit. Briefly, CFs were seeded on 6-well plates and were allowed to reach ~80% confluency. Then, the cell culture media was replaced by media supplemented with AuNBs (PEGylated and non-PEGylated) at a concentration of 20 μg/ml. The CFs were incubated for 96 hours without media changes. At the end of the 96 hours a solution of 2 μM calcein AM and 4 μM EthD-III in DPBS was prepared. The cells were washed twice with 1x DPBS followed by a 30 minutes incubation with the viability assay solution at 37°C. Finally, the solution was replaced by 1x DPBS before imaging.

Additionally, on day 7 after seeding the cardiac cells in the agarose microwells, the viability assay solution was prepared, and the organoids were incubated for 30 minutes at 37°C. The cardiac organoids were harvested from the agarose microwells and the solution was replaced by 1x DPBS before imaging.

3.3.11 TUNEL assay

In order to complete TUNEL assay within the cardiac organoids, cryosectioning of the tissues was performed prior the staining. The cryosectioning was performed on cardiac organoids seven days after seeding on the agarose microwells. First, the tissues were harvested and washed twice with 1x DPBS. Then a solution of 4% paraformaldehyde (PFA) was used to fix the organoids, which were incubated in the solution for 45 minutes at 37°C. To prevent image artifacts from freezing the tissues, a cryoprotection stage was performed. This consisted of a 15% sucrose (VWR) incubation at room temperature for 1 hour, followed by a 30% sucrose incubation at 4°C overnight. After this, the cardiac organoids were flash-frozen using OCT (Tissue-Tek). The tissues were sectioned at 10 µm thickness with the CryoStar NX70 cryostat (ThermoScientific) and preserve at -20°C until their utilization.

The clik-iT Plus TUNEL assay (Invitrogen) was used for evaluating early apoptosis inside the cardiac organoids. The staining was performed according to the instructions of the kit without any modifications.

3.3.12 qRT-PCR

The qRT-PCR reaction was performed similar to our previous publication.(Alejandra Patino-Guerrero et al., 2023) Briefly, the organoids were collected from the agarose

microwells seven days after seeding and washed with 1x DPBS twice to remove cellular debris. Then the tissues were digested and RNA was extracted utilizing the RNA microprep kit (Zymo). NanoDrop UV-Vis Spectrophotometer was utilized to evaluate the RNA quality and calculate RNA concentration. iScript Reverse Transcription Supermix (BioRad) was used to performed the cDNA conversion with a normalized amount of RNA from each sample.

Validated primers were used for the qRT-PCR reaction and 18s was used as housekeeping gene for data normalization (**Table A2**). The PCR master mix reaction consisted of 5µl of iTaq Universal SYBR Green Supermix (BioRad), 1µl of 8µM forward and reverse primers in NF water, 3.9µl of NF water, 0.1µl of the cDNA sample. The reaction was carried on using the q-Tower real time thermocycler (Analitik Jena). dCT values were normalized to their corresponding day 0 values.

3.3.13 Statistical analysis

All the statistical analyses were performed using the GraphPad Prism software. T-test or one-way ANOVA test, with post-hoc pairwise analysis using Tukey test, with alpha=0.05 were utilized to determine statistical differences between the study groups. For all the assays presented in this manuscript, at least 3 biological replicates (N=3) were performed.

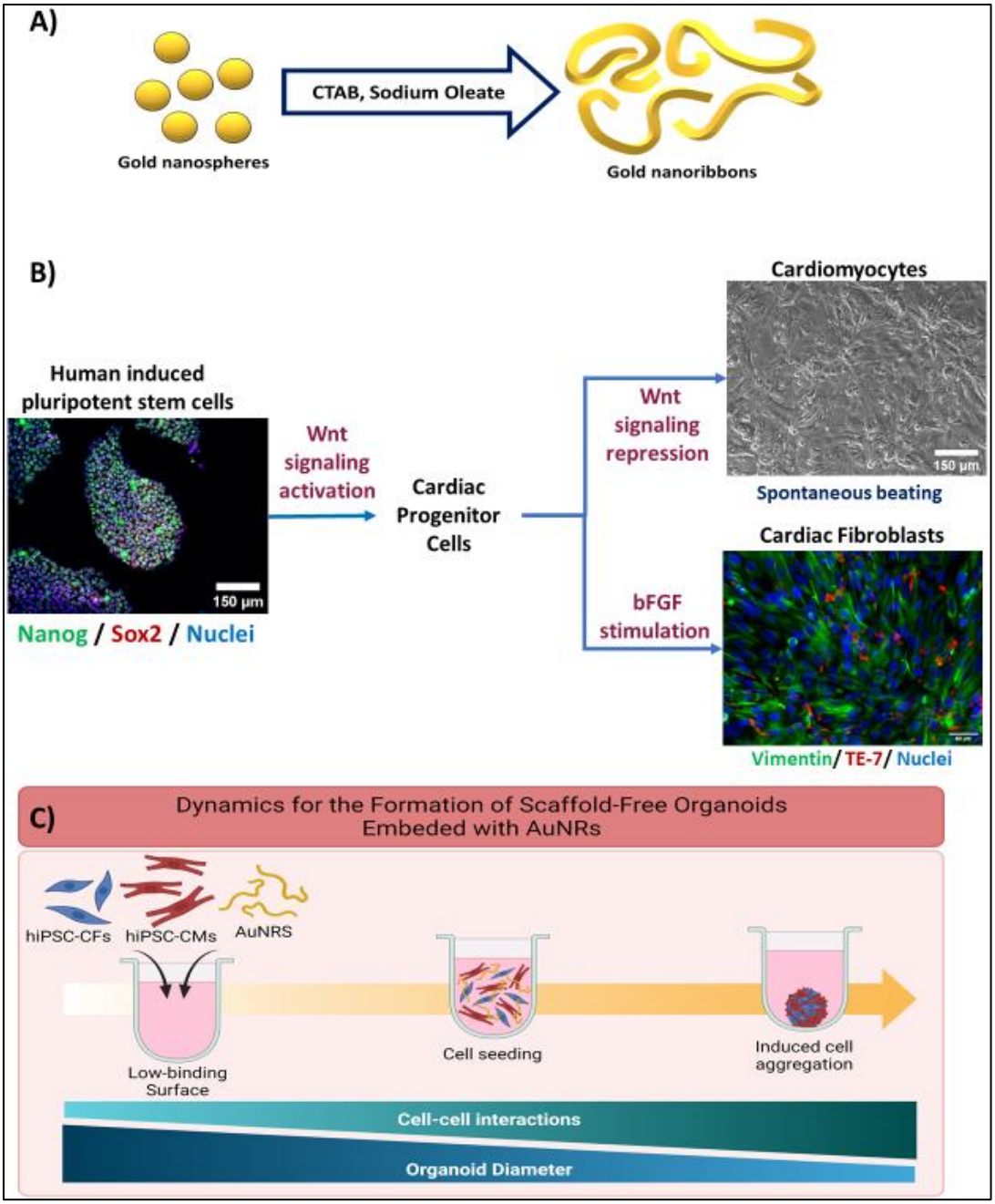

Figure 3.1. Schematics for the formation of scaffold-free cardiac organoids integrated with gold nanoribbons. A) Seed-mediated growth method for the fabrication of AuNRs. B) Isogenic differentiation of hiPSC-CMs and hiPSC-CFs through the regulation of the Wnt signaling pathway and fibroblast growth factor stimulation. Spontaneous beating was observed in the hiPSC-CMs. Vimentin and TE-7 staining was used for the confirmation of the differentiation of hiPSC-CFs. C) Formation of cardiac organoids by seeding hiPSC-derived cardiac cells and AuNRs in agarose microwells. The cardiac organoids were formed by the integration of hiPSC-CMs, hiPSC-CFs (7:3 respectively), and AuNRs (10µg/ml). Diameter reduction and spontaneous beating were observed on day seven after seeding.

3.4 RESULTS AND DISCUSSION

3.4.1 Synthesis and characterization of gold nanoribbons (AuNRs)

High aspect ratio one dimensional (1D) gold nanoparticles, such as AuNRs are often fabricated through complex processes, for example, electrospinning, lithography, ad chemical reductions (Hong et al., 2015; C. Zhao et al., 2020). However, some of these technologies are not widely accessible and require dedicated equipment. Thus, we have adapted a synthesis protocol based on the directed aggregation of gold, guided by a bi-surfactant template system (Y. Xu et al., 2015) to produce AuNRs with suitable features for integration into the scaffold-free organoids. This protocol presents several advantages over other synthesis methods. First, all the reactions can be performed with benchtop equipment and reagents that are commercially available and easy to handle. Second, all the reactions are carried at either room temperature or temperatures that are easily achievable with conventional lab equipment. Finally, and most important, the length of the AuNRs can be tuned by controlling the reaction time and purification method.

The length of the AuNRs is dictated by several factors throughout the synthesis process. For example, different template molecules can potentially limit the aggregation of gold atoms at determined lengths. Also, the availability of gold in the growth solution can act as a limiting factor. The growth of the AuNRs is a time-dependent reaction (Y. Xu et al., 2015); therefore, by controlling the synthesis time, i.e., the incubation time after of the growth solution after the gold seeds have been introduced, it is possible to tune the length of the AuNRs. Finally, the purification of the AuNRs is performed by precipitation through centrifugation, thus, it is possible to select particles of certain size based on the

centrifugation settings. The original reported protocol for the synthesis of AuNRs yielded particles of about 40μm in length. However, nanoparticles of this length can negatively impact the cellular aggregation and the formation of a cardiac syncytium as they can hinder cell-cell interactions and the formation of gap junctions in ECTs (Dylan J. Richards et al., 2016).

The morphology of the synthesized nanoparticles herein was verified through TEM imaging. Ribbon-like particles where observed (**Figure 3.2 A**), and the morphology was consistent through different batches of AuNRs. In order to increase the yield of the reaction we performed a centrifugation swipe by varying the speed and time of the precipitation (not shown). We observed that the highest nanoparticle concentration, based on UV-Vis spectrophotometry, was achieved when the nanoparticle solution was centrifuged at 3000x*g* for 17 minutes. Measurement of the length of ~100 nanoparticles showed a range from 0.6 μm up to 6.0 μm and larger, with an average length of 2.4±0.99 μm (**Figure 3.2 B**). While previous studies have demonstrated some advantages in the integration of nanoparticles for the fabrication of scaffold-free cardiac microtissues, there is a wide range of utilized nanoparticle materials, geometries, sizes, and concentrations (A. Patino-Guerrero et al., 2020). Despite these variations, there are two common factors for all of these studies. First, the nanomaterials are selected for their electroconductivity characteristics; and second, the size and geometry of the nanoparticles are tuned in order to prevent uptake by the cells. Additionally, it has been demonstrated that even small concentrations of gold nanoparticles have a positive effect in the electrophysiological behavior and formation of cardiac engineered tissues (A. Navaei et al., 2016).

1D gold nanoparticles typically present the surface plasmon resonance phenomenon (SPR). SPR is a complex phenomenon that occurs in some metals due to the availability of free electrons in the material lattice. This phenomenon is more easily observed in nanoparticles due to their high surface-to-volume ratio (Amendola, Pilot, Frasconi, Maragò, & Iatì, 2017). Specifically, the resonance frequencies of gold nanoparticles are presented within the visible range of the electromagnetic spectrum (Apyari, Dmitrienko, & Zolotov, 2013). Therefore, when gold nanoparticles are found in suspension, optical methods can be used for detecting their SPR frequency. For example, UV-visible spectrophotometry can be used as an accessible method for evaluating SPR of AuNRs.

The SPR spectral signature of gold nanoparticles is dependent of their size, geometry, and concentration (Amendola et al., 2017; Willets & Van Duyne, 2007); and therefore, can be used for the characterization of the AuNRs. For instance, in suspensions of high aspect ratio nanoparticles usually only one peak is observed for the SPR phenomenon in the UV-visible spectrophotometric analysis. This peak corresponds to the cross-section of the AuNRs, that is within the nanometer scale. For our synthesized AuNRs, this peak was consistently presented at around 520 nm (**Figure 3.2 C**). While SPR have many applications (Amendola et al., 2017), in our particular application, this phenomenon served as a tool for confirming the effective synthesis of AuNRs through UV-Vis spectrophotometry. Moreover, the correlation of the absorbance of the AuNRs suspension with the nanoparticle concentration allowed us to create a standard concentration curve that permitted to calculate the concentration of any AuNRs solution based on its absorbance (**Figure 3.2 D and E**).

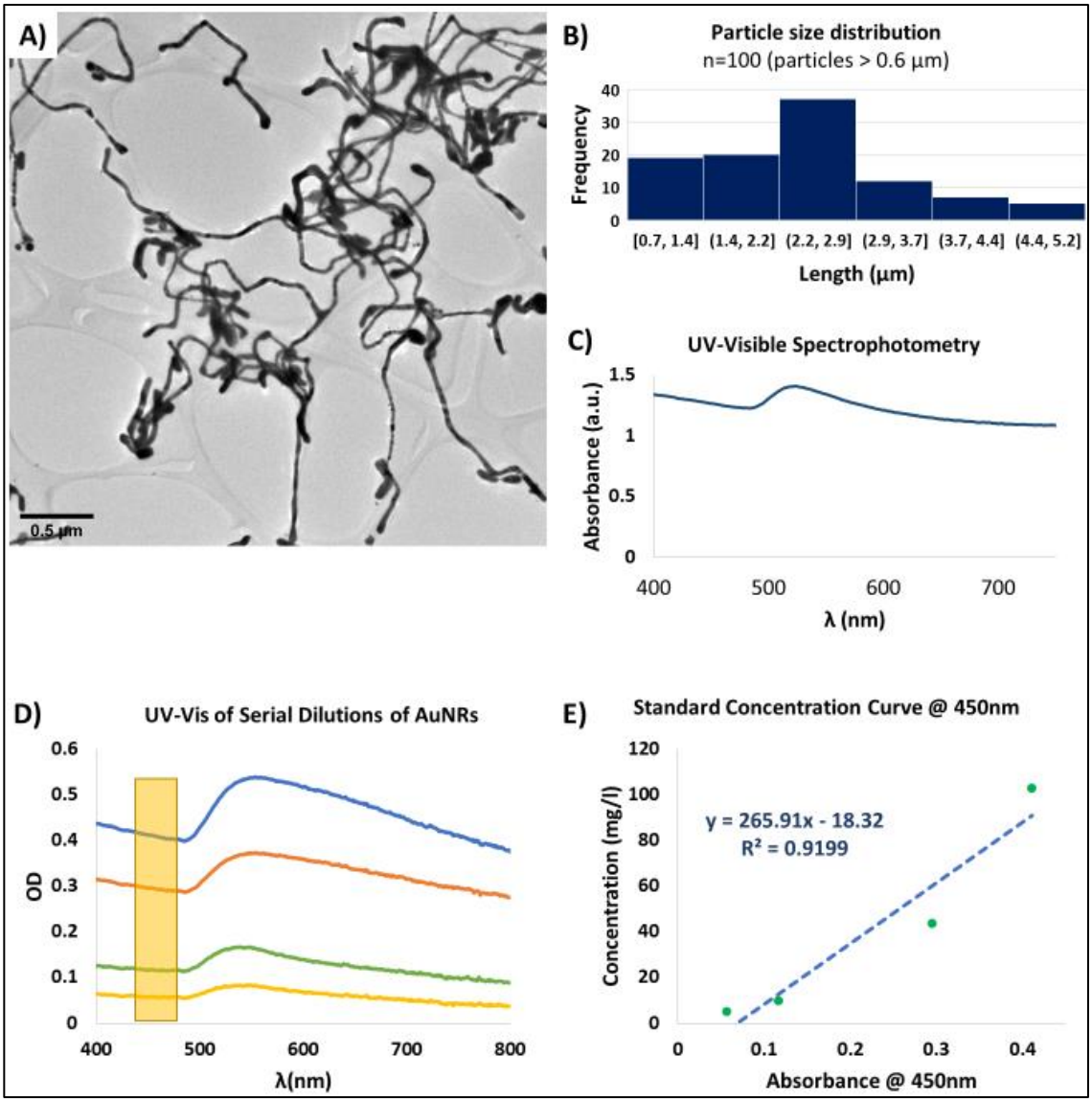

Figure 3.2. Characterization of gold nanoribbons (AuNRs). A) Representative TEM image of AuNRs (Scale bar: 0.5µm). B) Particle size distribution of 100 AuNRs with length>0.6µm. C) Representative UV-visible spectrum of the synthesized AuNRs. The characteristic SPR peak is presented at ~520 nm. D) UV-visible spectrum of serial dilutions of a suspension of AuNRs. The yellow rectangle represents the region within the spectra (450 nm) that was utilized for creating the standard curve for measuring AuNRs concentration. E) Standard concentration curved obtained by measuring the concentration of the AuNRs generated from ICP-MS, and its correlation with the UV-Vis optical density at 450 nm.

In order to obtain a concentration standard curve, we first performed serial dilutions of a colloidal suspension within the working range of AuNRs. These diluted suspensions

where then analyzed by UV-vis spectrophotometry (**Figure 3.2 D**) and ICP-MS. While our AuNRs synthesis method proved to be a robust and consistent technique, based on the TEM images and UV-vis spectra, there were minor batch-to-batch variations in the readings of the SPR peak wavelength. Therefore, in order to standardize the concentration measurements based on the UV-vis spectrum, we selected the region localized at 450 nm as it has been reported to be a suitable wavelength for measuring the concentration of gold nanoparticles (Shard, Wright, & Minelli, 2018). Based on this approach, we were able to calculate the linear correlation between the reported absorbance at 450 nm and the nanoparticle concentration found by mass spectrometry (ICP-MS) (**Figure 3.2 E**). With this, we achieved a non-destructive and straightforward method for faithful measuring the concentration of the resultant AuNRs suspensions. Therefore, we were able to prepare working solutions with specific and desired concentrations for the integration of the AuNRs into the scaffold-free cardiac organoids.

3.4.2 PEGylation and cytotoxicity evaluation of AuNRs

Cytotoxicity and bioaccumulation of gold nanoparticles has been studied previously due to their promising applications for various tissue engineering and therapeutics applications *in vitro* and *in vivo* (Lopez-Chaves et al., 2018). It has been found that gold nanoparticles are bioinert and biostable by itself (Connor et al., 2005; Rambanapasi et al., 2016). However, the template molecules (CTAB and sodium oleate) used for the synthesis of the AuNRs may exhibit some cytotoxic effects (Alaaldin M. Alkilany et al., 2009; L. Wang et al., 2013). Thus, in order to render the AuNRs usable for our cardiac tissue

engineering applications it was necessary to modify the surface of the nanoparticles and replace the original template molecules by biocompatible ones (**Figure 3.3 A**).

Polyethylene glycol (PEG) has been widely accepted as a biocompatible biomaterial (Santos-Martinez et al., 2014; Shi et al., 2021). Moreover, several protocols have been developed and adapted for its use as a replacing surface molecule specifically for gold nanoparticles (Z. Zhang & Lin, 2014). Besides being biocompatible, PEG has several other attractive features for its use in fabrication of nanoparticles. For example, it has been proven that the PEGylation of nanoparticles can affect their interaction with surrounding cells, by improving their biocompatibility (Santos-Martinez et al., 2014) and modifying their internalization rate (Shi et al., 2021). In this specific case, we were interested in performing the exchange of the surface molecules of the AuNRs.

Due to a similar surface chemistry of the AuNRs, developed in our work, to the nanoparticles used in another work by Zhang and Lin (Z. Zhang & Lin, 2014), we were able to adapt the methodology by modifying the concentrations of the reagents in order to ensure the availability of PEG molecules to perform a total surface exchange. In order to confirm the successful PEGylation of the AuNRs, we performed FTIR analysis to lyophilized samples. The FTIR spectra of CTAB and PEG were well characterized and presented distinctive peaks for both substances. One hand, the FTIR spectrum for CTAB was characterized by presence of two peaks around 2849.77 cm^{-1} and 2918.24 cm^{-1} corresponding to the stretching of C-H bonds. Additionally, several peaks were present around 1470 cm^{-1} (Shettigar, Misra, & Patel, 2018). The analyzed CTAB-capped AuNRs presented the same FTIR spectrum as those reported in the literature (**Figure 3.3 B**).

Similarly, the PEGylated samples presented a FTIR pattern that correlated to reported studies (Vrandečić, Erceg, Jakić, & Klarić, 2010), consisting of absorption bands between 840 cm^{-1} and 1466 cm^{-1} that correspond to C-C stretching and CH_2 rocking (Vrandečić et al., 2010) (**Figure 3.3 A**). Thus, this analysis provided a clear fingerprint to determine the successful exchange of the molecules on the surface of the synthesized AuNRs.

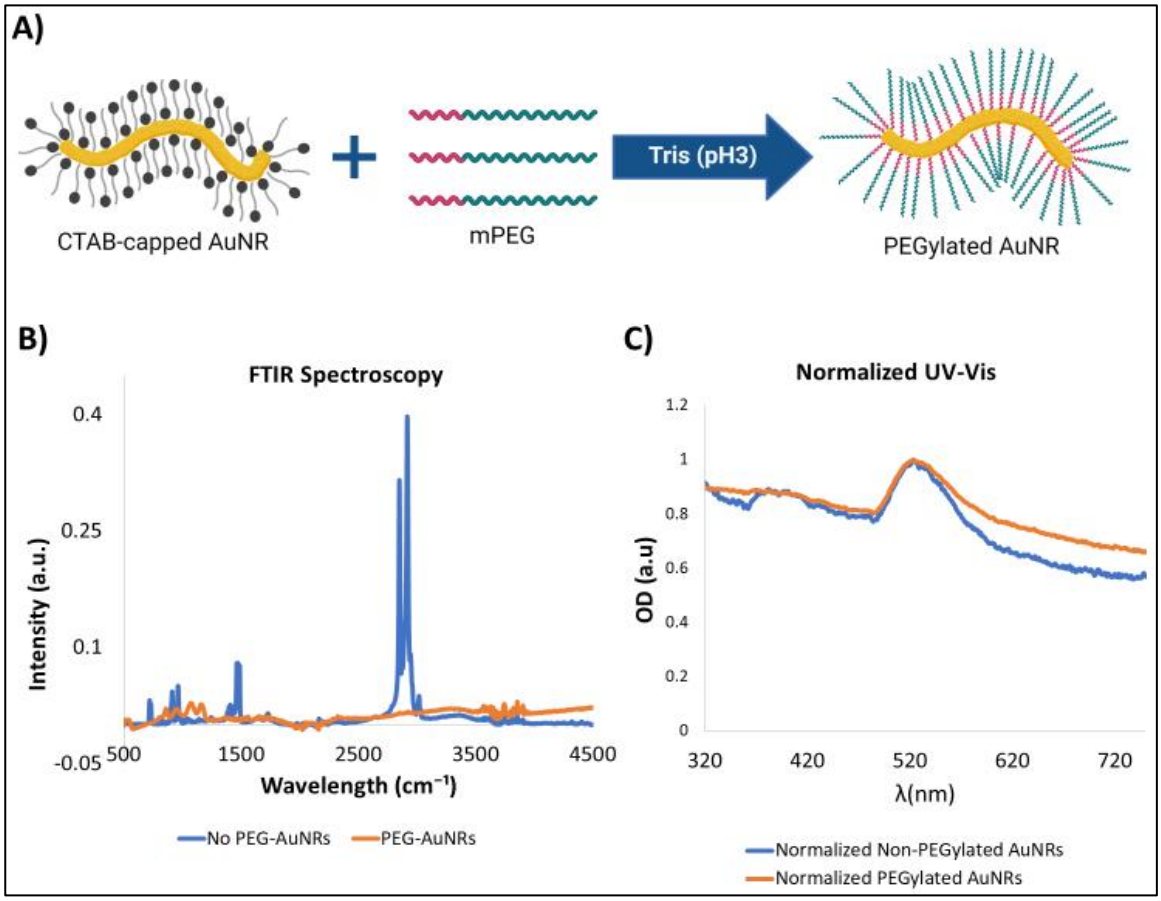

Figure 3.3. PEGylation of AuNRs. A) Representative schematic for the exchange of CTAB with PEG on the surface of the AuNRs. B) Representative FTIR spectroscopy of the AuNRs before (blue) and after (orange) the PEGylation. Characteristic peaks corresponding to CTAB and PEG molecules are observed for each of the spectrum. C) Normalized UV-Vis spectra for AuNRs before (blue) and after (orange) PEGylation. Similar spectrum for each of the conditions suggests that there are no significant changes in the morphology or particle aggregation of the AuNRs due to the PEGylation.

Spectrophotometric analysis of gold nanoparticles has been deem extremely sensitive to changes in their morphology, surface chemistry, and physical aggregation

(Murphy et al., 2008). Notably, UV-vis spectrophotometry of AuNRs before and after PEGylation demonstrated that the SPR peak and overall UV-Vis spectrum of the PEGylated nanoparticles remained almost unchanged, suggesting that significant changes to the morphology of the nanoparticles or particle aggregation did not occur during the process of surface modification through PEG exchange (**Figure 3.3 C**).

To investigate the effect of PEGylated and non-PEGylated AuNRs on the viability of cells, we performed an acute cytotoxicity assay on two dimensional (2D) monolayers of hiPSC-CFs. We carried the assay with a concentration that was double the concentration of the working solution for the fabrication of the cardiac organoids to ensure the feasibility of using PEG-AuNRs in the formation of cardiac organoids. To the best of our knowledge, this is the first study to present the integration of AuNRs with scaffold-free cardiac tissues. Thus, the selected working concentration of the PEG-AuNRs (10μg/ml) was based on similar studies that utilized nanoparticles embedded in cardiac organoids (Park et al., 2015a).

We evaluated the viability of the cells through co-staining with calcein AM and ethidium homodimer III (EthD-III). Calcein AM is a cell-permeable molecule, that is retained in the cytoplasm of the cells and is cleaved by the action of esterases. When is cleaved, this causes the calcein dye to be released and in consequence the live healthy cells appear fluorescent green. On the other hand, EthD-III is membrane permeable and is fluorescent when binds to DNA molecules. Thus, EthD-III will only stain the nuclei of cells with defective cellular membranes, appearing as fluorescent red.

The acute cytotoxicity test for PEGylated and non-PEGylated AuNRs at 48 and 96 hours of exposure showed differences in the viability of the cells. Similar cellular density was observed for PEG-AuNRs and the control cellular populations for both timepoints (**Figure 3.4 A and B**). Moreover, the quantification of viable cells reflected statistical differences between non-PEG and PEG-AuNRs (**Figure 3.4 C and D**). It has been reported that the cytotoxicity of CTAB-capped gold nanoparticles is mainly due to traces of free CTAB found in the suspension of the nanoparticles (Alaaldin M. Alkilany et al., 2009). The desorption of CTAB molecules from the surface of the nanoparticles has also been proposed as a probable theory behind the toxic effect of gold nanoparticles (Murphy et al., 2008), causing microtubule damage of the cells (Q. Li, Huang, Liu, Hu, & Qu, 2018). However, IF images demonstrated that there is a significant difference between the PEGylated and non-PEGylated AuNRs, and that the cellular densities are similar between the groups with PEGylated AuNRs and without AuNRs (**Figure 3.4 B**).

Overall, primarily, we demonstrated the feasibility for the surface modification of AuNRs synthesized by seed-mediated growth method, which to the best of our knowledge, has not been reported before. Additionally, we showed that the PEGylation of AuNRs significantly reduced their acute cytotoxicity in human cardiac cells, rendering them safe for integration into cardiac engineered tissues after the surface molecule exchange is completed and the AuNRs have been biofunctionalized.

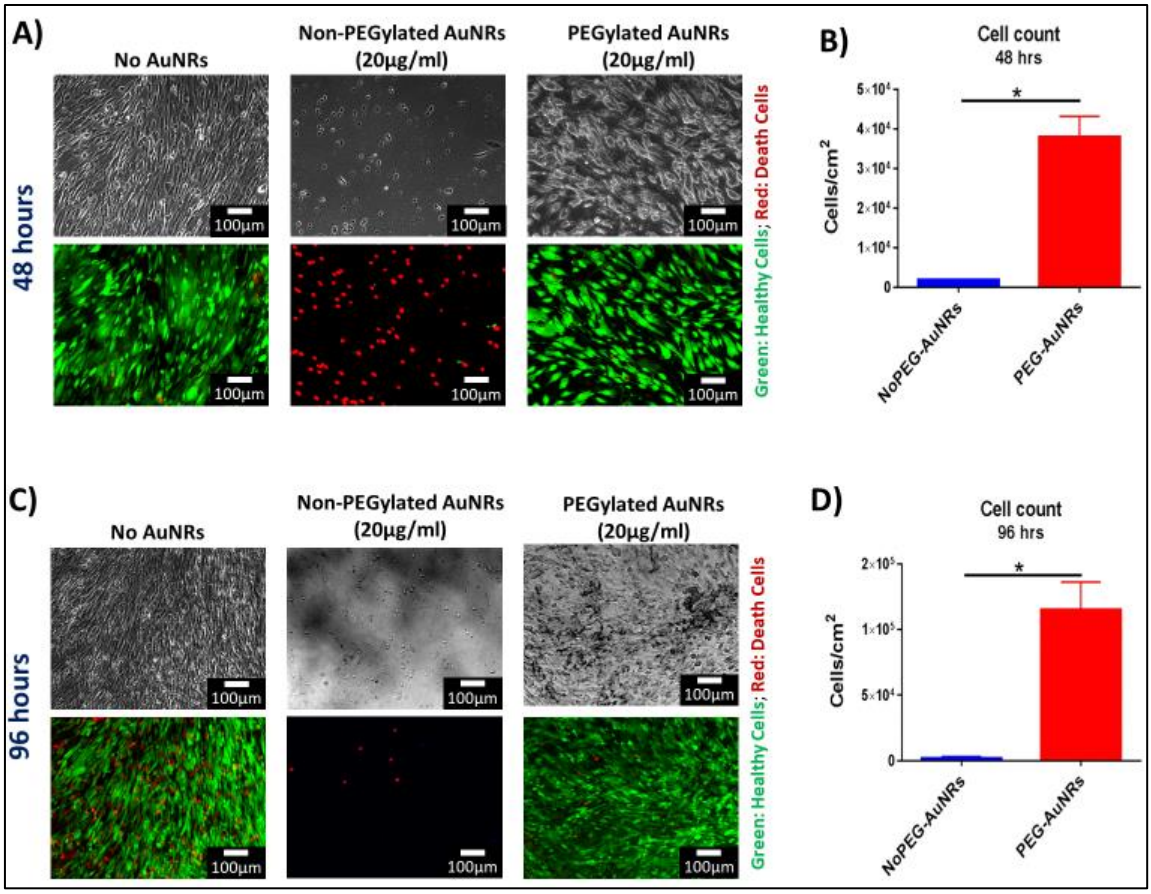

Figure 3.4. Cytotoxicity evaluation of PEGylated AuNRs. A) Representative images of viability assay at 48 hours of hiPSC-CFs cultured with 20µg/ml of non-PEGylated and PEGylated AuNRs (Top row: phase-contrast; bottom row: fluorescence) (Green: healthy cells; red: death cells) (Scale bars: 100 µm). B) Quantification of viable hiPSC-CFs after 48 hours cultured with AuNRs. (*: P-value≤0.05) C) Representative images of viability assay at 96 hours of hiPSC-CFs cultured with 20 µg/ml of AuNRs (Top row: phase-contrast; bottom row: fluorescence) (Green: healthy cells; red: death cells) (Scale bars: 100 µm). D) Quantification of viable hiPSC-CFs after 96 hours cultured with AuNRs. (*: P-value≤0.05).

3.4.3 Viability evaluation of 3D scaffold-free cardiac organoids integrated with AuNRs

While the low cytotoxicity of the PEG-AuNRs was demonstrated on 2D monolayers of hiPSC-CFs (**Figure 3.4**), it was still crucial to validate that the fabricated 3D cardiac organoids remained viable upon integration and exposure to PEG-AuNRs. Additionally, harvesting the cardiac organoids from the agarose microwells is a key factor for

downstream analyses and applications. Therefore, it was important to evaluate that the integrity of the tissues was not influenced by their removal from the agarose microwells.

To investigate the cellular viability and 3D tissue integrity, a viability assay was performed on the cardiac organoids. After staining, the microtissues were removed from the microwells by gently pipetting with culture media and washed with 1x PBS. After rinsing, the vast majority of the cardiac cells appeared viable, denoted by the green staining after viability assay, with no apparent differences between the experimental conditions (**Figure 3.5 A**). Additionally, it is well known that one of the mechanisms that induce apoptosis in adherent cells is the anoikis phenomenon, driven by the lack of anchorage sites to the cells (Frisch & Screaton, 2001). Therefore, it is possible that some cell death is also generated during the formation of the cardiac organoids in the microwells. These dead cells are deposited at the bottom of the microwells and due to their depth (800 µm), it is not possible for these debris to be washed during routinely media changes, being present until the cardiac organoids are harvested. This cellular debris was washed when the organoids were removed from the microwells and does not seem to negatively affect in any of the parameters analyzed in this study.

After harvesting, the morphology of the organoids was preserved and the cardiac microtissues presented spontaneous beating after harvesting (**Videos A1-A4**), corroborating that the contractile activity of the tissues was also preserved. Many features of these organoids are dependent on their morphology. For example, it has been reported that oxygen and nutrient gradients generated within the organoids depends on their diameter (Dylan J. Richards et al., 2020; Y. Tan et al., 2017). The oxygen and nutrient

gradients within the microtissues have been leveraged to model pathologic conditions, such as hypoxia (Dylan J. Richards et al., 2020). Studies have proposed utilizing cardiac organoids for manufacture of cardiac engineered tissues at bigger scales (Arai et al., 2018; Kawai et al., 2022). These techniques rely on maintaining uniformity of the cardiac organoids. Therefore, creating and preserving cardiac organoids with specific diameters is important for their utilization in disease modeling and drug screening applications. We have demonstrated in this study that our proposed method leads to the formation of cardiac organoids with uniform size and morphology (**Figure A1 and A2**). Moreover, we have confirmed, for the first time, that it is feasible to integrate AuNRs in the fabrication of cardiac organoids. These organoids remained viable and maintained their morphology and electrophysiological activity after being removed from the agarose microwells.

Diffusion of oxygen and nutrients has been a critical concern in the tissue engineering field to facilitate the transport of these molecules. It has been reported that cellular density, cellular origin and organoid size can affect the oxygen consumption rate and can lead to the creation of hypoxic or necrotic cores (Dylan J. Richards et al., 2020; Y. Tan et al., 2017). To that end, we further evaluate early apoptosis of the cells within the cryosectioned slices of the cardiac organoids using TUNEL (**Figure 3.5 B**). This is to demonstrate that the diameter and cellular density of the cardiac organoids were appropriate and that the AuNRs did not cause any cytotoxic effect in the hiPSC-CMs due to the 3D microenvironment. Based on our obtained images, we did not find significant cell death due to early apoptosis in any of the analyzed tissues (**Figure 3.5 C**). This indicates that the nutrient diffusion within the organoids was appropriate and hypoxic cores were not generated. These secondary analyses were indeed consistent with our primary viability

assay, confirming that the synthesized and PEGylated AuNRs (PEG-AuNRs) did not induce any toxicity effects on cardiac organoids.

Opaque spots (**Figure 3.5 B, yellow arrows**) were found in the phase-contrast images of the organoids integrated with the AuNRs but were not seen in organoids without gold nanoparticles. These opaque areas are presumably regions were the AuNRs were concentrated. This suggests that the gold nanoparticles were integrated through the entire body of the organoids. However, it remains to be elucidated in our future work whether the AuNRs underwent aggregation due their integration in the cellular microenvironment.

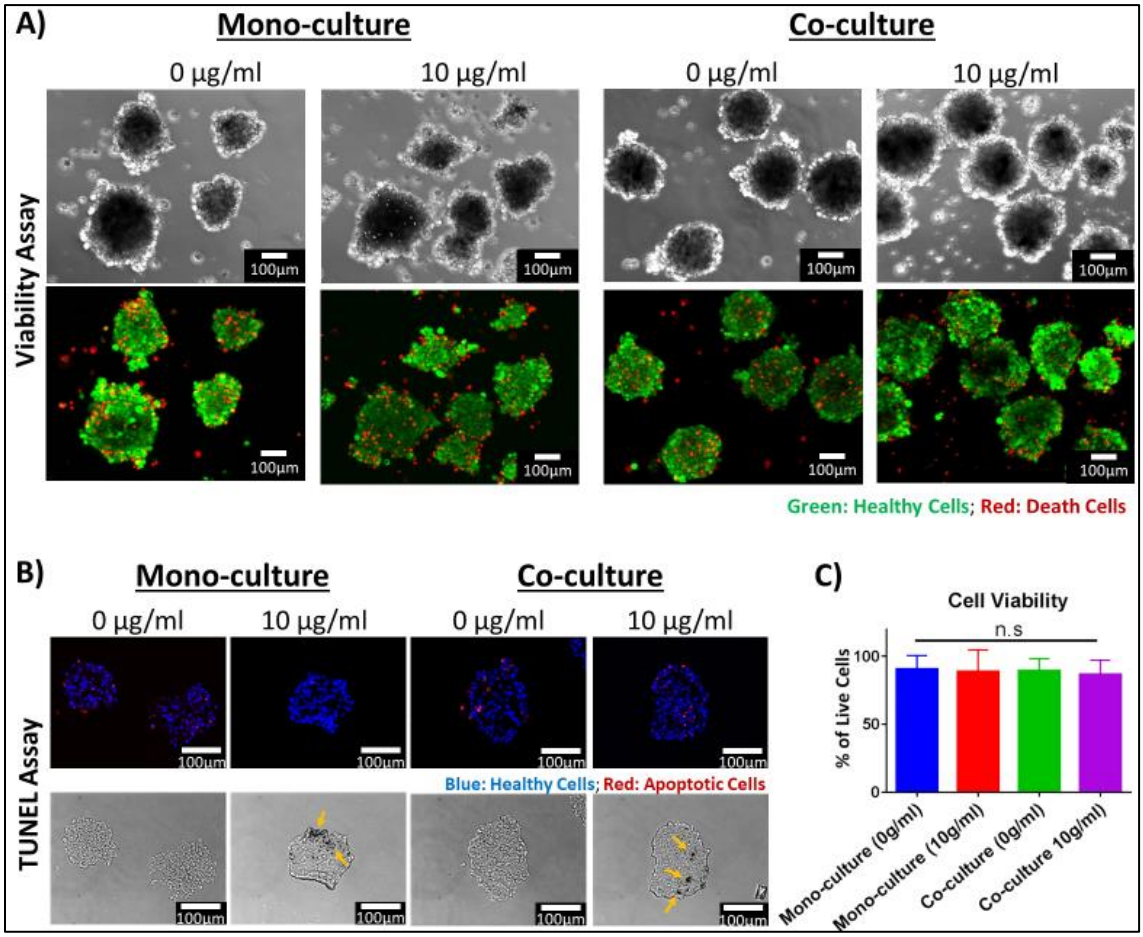

Figure 3.5. Viability evaluation of isogenic cardiac organoids integrated with PEGylated AuNRs. A) Viability assay of isogenic cardiac organoids on day 7 after harvesting from agarose microwells (Scale bars: 100µm). The top row: Phase-contrast images; bottom row: fluorescent images (Green: healthy cells; red: dead cells). B) TUNEL assay of

cryosectioned slices of cardiac organoids after being harvested from the agarose microwells (Scale bars: 100 µm). Top row: fluorescent images corresponding to TUNEL assay (Blue: healthy cells; red: apoptotic cells). Bottom row: Phase contrast images, the yellow arrows point to opaque areas that are suspected to correspond to regions where AuNRs have concentrated. C) Quantification of cell viability based on TUNEL assay (n.s.: p-value >0.05).

3.4.4 Functional contractility analysis of isogenic cardiac organoids embedded with AuNRs

The integration of nanoparticles in cardiac organoids has been of keen interest in the cardiac tissue engineering field (A. Patino-Guerrero et al., 2020; Dylan J. Richards et al., 2016; Y. Tan et al., 2017). One of the proposed hypotheses across these studies is that enriching the intercellular microenvironment with electrically conductive nanomaterials and nanoscale topographical cues can enhance the performance of the engineered microtissues (Esmaeili et al., 2022; Navaei et al., 2017; A. Navaei et al., 2019; A. Navaei et al., 2016). Additionally, it is well accepted that co-culture of cardiac cells in engineered tissues can improve the maturation of hiPSC-derived cardiac cells (Beauchamp et al., 2020; Alejandra Patino-Guerrero et al., 2023). The creation of isogenic engineered tissues for the purpose of drug screening and disease modeling has been extensively discussed (Cho, Lee, Skylar-Scott, Heilshorn, & Wu, 2021). Specifically, scaffold-free engineered tissues present a particular complexity due to the lack of extracellular matrix (ECM) or ECM-like materials that can provide support to the cells. Therefore, cellular aggregation and tissue compaction would be relevant in the fabrication of cardiac organoids (Alejandra Patino-Guerrero et al., 2023). First, the cellular ratio for co-culture groups was thoroughly optimized, as it was shown that it leads to improved tissue compaction (Alejandra Patino-Guerrero et al., 2023). Additionally, it was necessary to corroborate the presence of the

PEG-AuNRs in the engineered tissues after their fabrication. The phase-contrast images of the cardiac organoids taken seven days after seeding in the agarose microwells showed rounded and dense tissues that presented spontaneous beating (**Figure 3.6 A, top row**). For the organoids fabricated with PEG-AuNRs, opaque regions were observed in magnified images (**Figure 3.6 A, bottom row**) as also shown in **Figure 3.5 B**, that the gold nanoparticles were effectively integrated within the cardiac tissues.

Contractile activity of the cardiac engineered tissues is one of the main features that needs to be evaluated, as most of their tissue engineering applications rely on an effective electromechanical function (Cho, Discher, Leong, Vunjak-Novakovic, & Wu, 2022). After signal extraction from time-lapse images, it was found that all the experimental groups showed a similar spontaneous beating behavior (**Figure 3.6 B**). The organoids presented comparable beating per rates (beat per minute; BPM) (**Figure 3.6 C**) ranging from 12.19 to 18.23 BPM (**Figure 3.6 D**). The inter-beat interval variability (IIV) has been described as an indirect measure of tissue synchronicity (Iseoka et al., 2017; J. Veldhuizen, J. Cutts, D. A. Brafman, R. Q. Migrino, & M. Nikkhah, 2020b). Tissue synchronicity is a relevant biomarker of functionality of hiPSC-derived tissues (Jaimeson Veldhuizen et al., 2020b), as it requires the formation of gap junctions and the capability of cardiac cells to be paced by endogenous or exogenous electrical stimulation (Wu & Guo, 2018). Thus, decreased IIV is a desirable feature of engineered cardiac tissues. Our analysis did not show a significant difference in the IIV of the four experimental groups (**Figure 3.6 D and 3.6 E**). Overall, this suggests that the PEG-AuNRs had negligible effect in the contractility of the cardiac organoids.

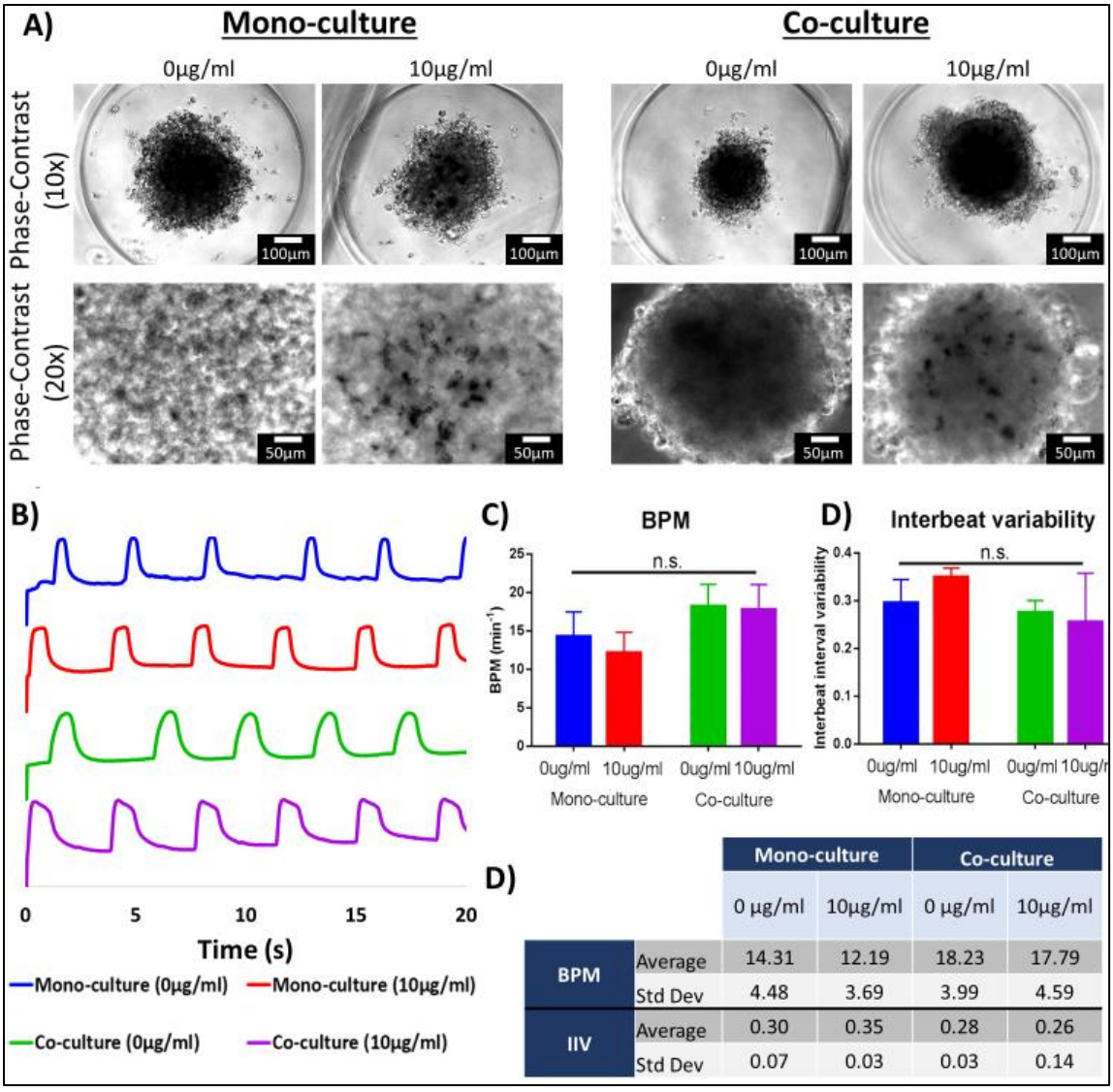

D)

		Mono-culture		Co-culture	
		0 µg/ml	10µg/ml	0 µg/ml	10µg/ml
BPM	Average	14.31	12.19	18.23	17.79
	Std Dev	4.48	3.69	3.99	4.59
IIV	Average	0.30	0.35	0.28	0.26
	Std Dev	0.07	0.03	0.03	0.14

Figure 3.6. Contractility evaluation of isogenic cardiac organoids embedded with PEGylated AuNRs. A) Phase-contrast images of cardiac organoids in the agarose microwells. Top row: low magnification images (Scale bars: 100 µm); bottom row: high magnification images where opaque regions are found. It is believed that these regions correspond to areas where PEG-AuNRs were concentrated (Scale bars: 50µm). B) Representative spontaneous beating signals extracted from time-lapse videos (y-axis represents arbitrary units). C) Quantification of spontaneous beating rates extracted from phase-contrast videos. D) Summary of beating rate (BPM) and inter-beat interval variability (IIV) values calculated from the extracted spontaneous beating signals. E) Quantification of inter-beat interval variability (IIV) extracted from phase-contrast videos. (n.s.= p-value>0.05).

Previous studies focused on the integration of nanoparticles in scaffold-free cardiac tissues demonstrated a wide range of concentrations. Moreover, the methods for measuring

the concentrations of those nanoparticles and integrating them with cardiac organoids were not consistent across different studies. Therefore, moving forward with future studies, we aim to optimize the PEG-AuNRs concentration in order to maximize their interaction with cardiac cells.

3.4.5 Analysis of transcriptomic profile of cardiac organoids

The evaluation of the transcriptomic profile has become one of the gold standard molecular-level methods for evaluating the overall performance of engineered tissues. The assessment of gene expression levels is of particular interest for cells and cardiac tissues derived from human stem cells to evaluate their maturity. Genes relevant for the cardiac function, such as those involved in the formation of the contractile machinery of the CMs (i.e., ACTN2, TNN2, TNNI3, MYH6, and MYH7) and calcium handling (i.e., RYR2) are utmost of interest as surrogate biomarkers for maturation and performance of engineered tissues (Ahmed et al., 2020). Herein, the transcriptomic profile of the scaffold-free cardiac organoids was evaluated through a panel of seven cardiac-relevant genes with the purpose of assessing the effect of the co-culture versus mono-culture conditions. In addition, we were interested in comparing the gene expression profile of the cardiac organoids in presence or absence of PEG-AuNRs.

It has been reported that one of the main factors contributing to the maturation of hiPSC-CMs is the presence of non-cardiomyocyte cells (i.e., hiPSC-CFs) (Campostrini et al., 2021; Alejandra Patino-Guerrero et al., 2023). When CFs are integrated into ECTs, these cells secrete growth factors and cytokines that lead to cellular crosstalk with CMs, and ultimately lead to improved maturation of hiPSC-CMs in engineered tissues (Colliva,

Braga, Giacca, & Zacchigna, 2020). Moreover, it has been demonstrated that hiPSC-CFs can potentially modulate electromechanical properties of 3D ECTs (Rupert, Kim, Choi, & Coulombe, 2020). Similar to those reports, in our study, we found that sarcomere-related genes, namely ACTN2, TNNT2, and TNNI3, were upregulated in the co-culture (0 µg/ml) cardiac organoids (**Figure 3.7 A**). For four of the other evaluated genes (GJA1, RYR2, MYH6, and MYH7) we did not find any significant difference between any of the experimental conditions. However, there was a trend for higher expression of the analyzed gene panel for both co-culture conditions (0 µg/ml and 10 µg/ml) **(Figure 3.7 B**). Thus, our results are consistent with previous findings in the literature, indicating the beneficial effect of the integration of hiPSC-CFs in ECTs.

Alternatively, the integration of the PEG-AuNRs overall appeared to be negligible for the effects of modifying the transcriptomic profile of the cardiac organoids. Specifically, we did not find any significant difference in the expression of any of the analyzed genes for the mono-culture conditions (0µg/ml vs. 10µg/ml) (**Figure 3.7 A**). However, For the co-culture conditions (0µg/ml vs. 10µg/ml) we found significant differences for the expression of ACTN2, TNNT2, and TNNI3, with higher expression in the group without PEG-AuNRs (co-culture, 0g/ml). These observations show the dominant effect of co-culture groups in maturation of the organoids. We suspect that the negligible effect of the PEG-AuNRs in the gene expression of the cardiac organoids is related to the possible particle aggregation observed previously (**Figure 3.6 A**). Overall, we have demonstrated the feasibility of the integration of PEG-AuNRs within cardiac organoids;

however, variables such as nanoparticle concentration, aggregation, and other external factors (i.e., electrical stimulation) need to be further studied in future works.

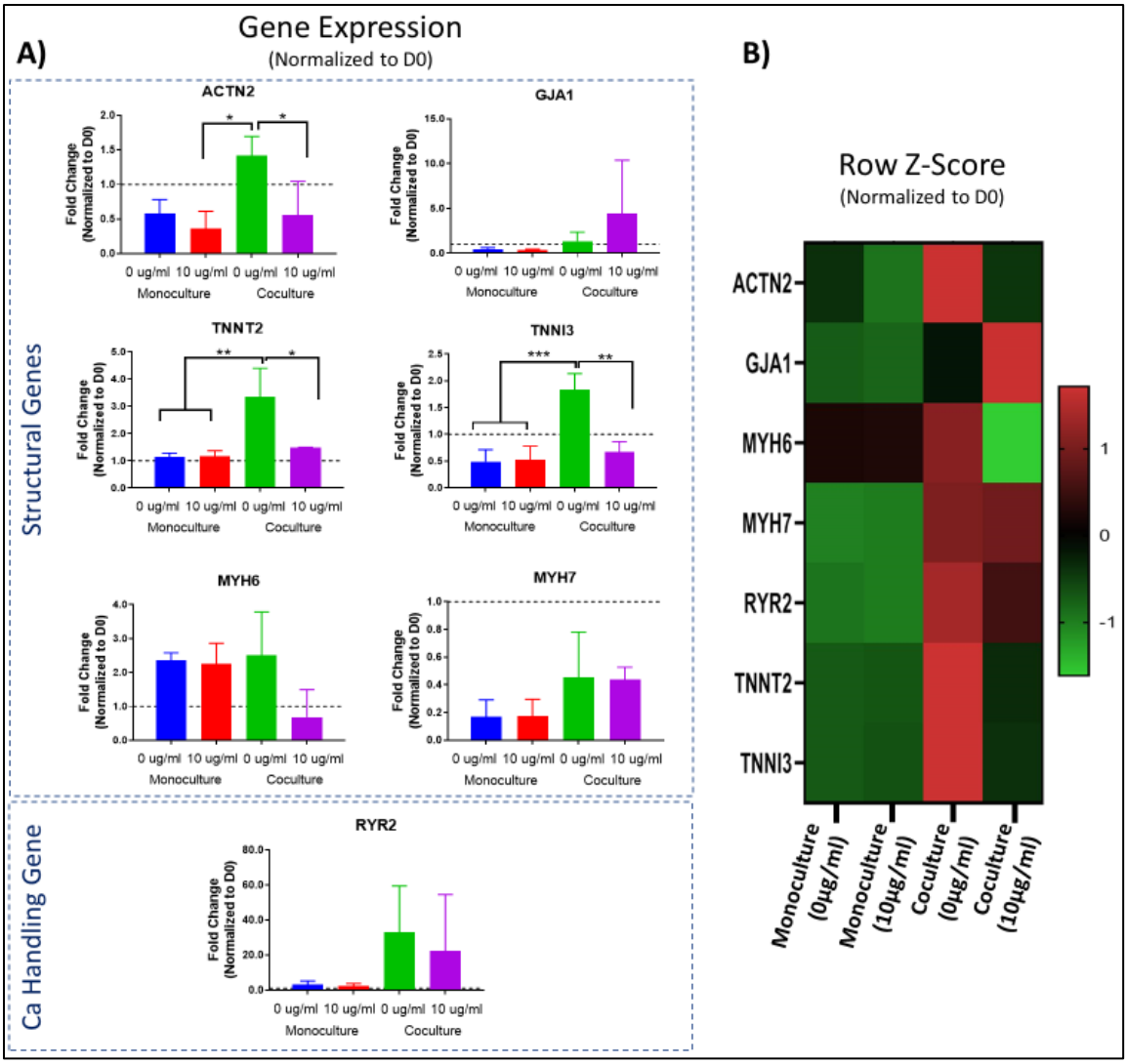

Figure 3.7. Transcriptomic profile of isogenic cardiac organoids integrated with PEGylated AuNRs. A) Gene expression values obtained from qRT-PCR analysis. All the values were normalized to D0 of the experiment (day when cells were seeded in agarose microwells) (*: p-value≤0.05, **: p-value≤0.01, ***: p-value≤0.001). B) Row Z-Score heatmap for gene expression levels, based on qRT-PCR fold change values.

3.5 CONCLUSION

The integration of nanomaterials has been widely proposed for various applications in tissue engineering. It is speculated that the electroconductive properties of some of the utilized nanoparticles, along with the biophysical cues that they provide when introduced

in engineered tissues can enhance their structure and function. To the best of our knowledge, this is the first study to evaluate the integration of 1D gold nanoparticles with scaffold-free isogenic cardiac organoids.

We first presented a modified method for the generation of 1D gold nanoparticles, namely gold nanoribbons (AuNRs). These nanoribbons have been extensively characterized and have been biofunctionalized by performing a surface molecule exchange through a PEGylation reaction. The feasibility for utilizing these nanoribbons was primarily demonstrated through cytotoxicity assays in 2D monolayers of hiPSC-CFs and 3D isogenic cardiac organoids derived from mono-culture and co-culture of and hiPSC-CMs and hiPSC-CFs. We verified the presence of the AuNRs within the engineered organoids by phase-contrast imaging of the surface and cryosectioned slices of the cardiac organoids. We then performed contractility evaluation, as well as analysis of the transcriptomic profile of the isogenic cardiac organoids embedded with the AuNRs. Although we did not find any significant difference in the spontaneous beating behavior of the engineered tissues, we found significant upregulation of some cardiac-relevant genes, specifically ACTN2, TNNT2, and TNNI3 for the co-culture (0µg/ml) cardiac organoids. These observations demonstrated the critical influence of hiPSC-CFs on maturation and function of isogenic cardiac organoids regardless of the presence of AuNRs.

We speculate that the lack of an observable effect from the PEG-AuNRs can be due to two main factors: a) the selected concentration for this proof-of-concept needs to be optimized, and b) there is possible aggregation of the AuNRs when they interact with the cardiac cells in the 3D microenvironment. Thus, our future studies will be focused on

elucidating the aggregation mechanism of the AuNRs, in order to promote a more homogeneous distribution of the nanoparticles within organoids. Additionally, optimization of the concentration of the AuNRs may result in the enhanced cell-particle interactions and the overall function of hiPSC-derived isogenic cardiac organoids. Overall, the findings of this study have potential for applications in cardiac tissue engineering for the creation of physiologically relevant scaffold-free tissues for disease modeling and regenerative medicine applications.

3.6 REFERENCES

Ahadian, S., Zhou, Y., Yamada, S., Estili, M., Liang, X., Nakajima, K., . . . Matsue, T. (2016). Graphene induces spontaneous cardiac differentiation in embryoid bodies. *Nanoscale, 8*(13), 7075-7084. doi:10.1039/C5NR07059G

Ahmed, R. E., Anzai, T., Chanthra, N., & Uosaki, H. (2020). A Brief Review of Current Maturation Methods for Human Induced Pluripotent Stem Cells-Derived Cardiomyocytes. *Frontiers in Cell and Developmental Biology, 8*. doi:10.3389/fcell.2020.00178

Alkilany, A. M., Nagaria, P. K., Hexel, C. R., Shaw, T. J., Murphy, C. J., & Wyatt, M. D. (2009). Cellular Uptake and Cytotoxicity of Gold Nanorods: Molecular Origin of Cytotoxicity and Surface Effects. *Small, 5*(6), 701-708. doi:https://doi.org/10.1002/smll.200801546

Amendola, V., Pilot, R., Frasconi, M., Maragò, O. M., & Iatì, M. A. (2017). Surface plasmon resonance in gold nanoparticles: a review. *Journal of Physics: Condensed Matter, 29*(20), 203002. doi:10.1088/1361-648X/aa60f3

Apyari, V. V., Dmitrienko, S. G., & Zolotov, Y. A. (2013). Unusual application of common digital devices: Potentialities of Eye-One Pro mini-spectrophotometer – A monitor calibrator for registration of surface plasmon resonance bands of silver and gold nanoparticles in solid matrices. *Sensors and Actuators B: Chemical, 188*, 1109-1115. doi:https://doi.org/10.1016/j.snb.2013.07.097

Arai, K., Murata, D., Verissimo, A. R., Mukae, Y., Itoh, M., Nakamura, A., . . . Nakayama, K. (2018). Fabrication of scaffold-free tubular cardiac constructs using a Bio-3D printer. *PLOS ONE, 13*(12), e0209162. doi:10.1371/journal.pone.0209162

Augustine, R., Dan, P., Hasan, A., Khalaf, I. M., Prasad, P., Ghosal, K., . . . Maureira, P. (2021). Stem cell-based approaches in cardiac tissue engineering: controlling the microenvironment for autologous cells. *Biomedicine & Pharmacotherapy, 138*, 111425. doi:https://doi.org/10.1016/j.biopha.2021.111425

Beauchamp, P., Jackson, C. B., Ozhathil, L. C., Agarkova, I., Galindo, C. L., Sawyer, D. B., . . . Zuppinger, C. (2020). 3D Co-culture of hiPSC-Derived Cardiomyocytes With Cardiac Fibroblasts Improves Tissue-Like Features of Cardiac Spheroids. *Frontiers in Molecular Biosciences, 7*. doi:10.3389/fmolb.2020.00014

Bedada, F. B., Wheelwright, M., & Metzger, J. M. (2016). Maturation status of sarcomere structure and function in human iPSC-derived cardiac myocytes. *Biochimica et Biophysica Acta (BBA) - Molecular Cell Research, 1863*(7, Part B), 1829-1838. doi:https://doi.org/10.1016/j.bbamcr.2015.11.005

Besser, R. R., Ishahak, M., Mayo, V., Carbonero, D., Claure, I., & Agarwal, A. (2018). Engineered Microenvironments for Maturation of Stem Cell Derived Cardiac Myocytes. *Theranostics, 8*(1), 124-140. doi:10.7150/thno.19441

Binah, O., Dolnikov, K., Sadan, O., Shilkrut, M., Zeevi-Levin, N., Amit, M., . . . Itskovitz-Eldor, J. (2007). Functional and developmental properties of human embryonic stem cells-derived cardiomyocytes. *J Electrocardiol, 40*(6 Suppl), S192-196. doi:10.1016/j.jelectrocard.2007.05.035

Campostrini, G., Meraviglia, V., Giacomelli, E., van Helden, R. W. J., Yiangou, L., Davis, R. P., . . . Mummery, C. L. (2021). Generation, functional analysis and applications of isogenic three-dimensional self-aggregating cardiac microtissues from human pluripotent stem cells. *Nat Protoc, 16*(4), 2213-2256. doi:10.1038/s41596-021-00497-2

Chen, W., Bian, W., Zhou, Y., & Zhang, J. (2021). Cardiac Fibroblasts and Myocardial Regeneration. *Frontiers in Bioengineering and Biotechnology, 9*. doi:10.3389/fbioe.2021.599928

Cho, S., Discher, D. E., Leong, K. W., Vunjak-Novakovic, G., & Wu, J. C. (2022). Challenges and opportunities for the next generation of cardiovascular tissue engineering. *Nature Methods, 19*(9), 1064-1071. doi:10.1038/s41592-022-01591-3

Cho, S., Lee, C., Skylar-Scott, M. A., Heilshorn, S. C., & Wu, J. C. (2021). Reconstructing the heart using iPSCs: Engineering strategies and applications. *Journal of Molecular and Cellular Cardiology, 157*, 56-65. doi:https://doi.org/10.1016/j.yjmcc.2021.04.006

Colliva, A., Braga, L., Giacca, M., & Zacchigna, S. (2020). Endothelial cell–cardiomyocyte crosstalk in heart development and disease. *The Journal of Physiology, 598*(14), 2923-2939. doi:https://doi.org/10.1113/JP276758

Connor, E. E., Mwamuka, J., Gole, A., Murphy, C. J., & Wyatt, M. D. (2005). Gold Nanoparticles Are Taken Up by Human Cells but Do Not Cause Acute Cytotoxicity. *Small, 1*(3), 325-327. doi:https://doi.org/10.1002/smll.200400093

Cutts, J., Nikkhah, M., & Brafman, D. A. (2015). Biomaterial approaches for stem cell-based myocardial tissue engineering: supplementary issue: stem cell biology. *Biomarker insights, 10*, BMI. S20313.

Daseke, M. J., Tenkorang, M. A. A., Chalise, U., Konfrst, S. R., & Lindsey, M. L. (2020). Cardiac fibroblast activation during myocardial infarction wound healing: Fibroblast polarization after MI. *Matrix Biology, 91-92*, 109-116. doi:https://doi.org/10.1016/j.matbio.2020.03.010

Dolatshahi-Pirouz, A., Nikkhah, M., Kolind, K., Dokmeci, M. R., & Khademhosseini, A. (2011). Micro- and Nanoengineering Approaches to Control Stem Cell-Biomaterial Interactions. *Journal of Functional Biomaterials, 2*(3), 88-106. doi:10.3390/jfb2030088

Esmaeili, H., Patino-Guerrero, A., Hasany, M., Ansari, M. O., Memic, A., Dolatshahi-Pirouz, A., & Nikkhah, M. (2022). Electroconductive biomaterials for cardiac tissue engineering. *Acta Biomater, 139*, 118-140. doi:10.1016/j.actbio.2021.08.031

Fan, C., Tang, Y., Zhao, M., Lou, X., Pretorius, D., Menasche, P., . . . Zhang, J. (2020). CHIR99021 and fibroblast growth factor 1 enhance the regenerative potency of human cardiac muscle patch after myocardial infarction in mice. *J Mol Cell Cardiol, 141*, 1-10. doi:10.1016/j.yjmcc.2020.03.003

Frisch, S. M., & Screaton, R. A. (2001). Anoikis mechanisms. *Current Opinion in Cell Biology, 13*(5), 555-562. doi:https://doi.org/10.1016/S0955-0674(00)00251-9

Hartman, M. E., Dai, D.-F., & Laflamme, M. A. (2016). Human pluripotent stem cells: Prospects and challenges as a source of cardiomyocytes for in vitro modeling and cell-based cardiac repair. *Advanced Drug Delivery Reviews, 96*, 3-17. doi:https://doi.org/10.1016/j.addr.2015.05.004

Hong, X., Tan, C., Chen, J., Xu, Z., & Zhang, H. (2015). Synthesis, properties and applications of one- and two-dimensional gold nanostructures. *Nano Research, 8*(1), 40-55. doi:10.1007/s12274-014-0636-3

Iseoka, H., Miyagawa, S., Fukushima, S., Saito, A., Masuda, S., Yajima, S., . . . Sawa, Y. (2017). Pivotal Role of Non-cardiomyocytes in Electromechanical and Therapeutic Potential of Induced Pluripotent Stem Cell-Derived Engineered Cardiac Tissue. *Tissue Engineering Part A, 24*(3-4), 287-300. doi:10.1089/ten.tea.2016.0535

Kawai, Y., Tohyama, S., Arai, K., Tamura, T., Soma, Y., Fukuda, K., . . . Kobayashi, E. (2022). Scaffold-Free Tubular Engineered Heart Tissue From Human Induced

Pluripotent Stem Cells Using Bio-3D Printing Technology in vivo. *Frontiers in Cardiovascular Medicine, 8*. doi:10.3389/fcvm.2021.806215

Kharaziha, M., Memic, A., Akbari, M., Brafman, D. A., & Nikkhah, M. (2016). Nano-Enabled Approaches for Stem Cell-Based Cardiac Tissue Engineering. *Advanced Healthcare Materials, 5*(13), 1533-1553. doi:https://doi.org/10.1002/adhm.201600088

Li, J., Hua, Y., Miyagawa, S., Zhang, J., Li, L., Liu, L., & Sawa, Y. (2020). hiPSC-Derived Cardiac Tissue for Disease Modeling and Drug Discovery. *International Journal of Molecular Sciences, 21*(23). doi:10.3390/ijms21238893

Li, Q., Huang, C., Liu, L., Hu, R., & Qu, J. (2018). Effect of Surface Coating of Gold Nanoparticles on Cytotoxicity and Cell Cycle Progression. *Nanomaterials, 8*(12). doi:10.3390/nano8121063

Lian, X., Zhang, J., Azarin, S. M., Zhu, K., Hazeltine, L. B., Bao, X., . . . Palecek, S. P. (2013). Directed cardiomyocyte differentiation from human pluripotent stem cells by modulating Wnt/beta-catenin signaling under fully defined conditions. *Nat Protoc, 8*(1), 162-175. doi:10.1038/nprot.2012.150

Lopez-Chaves, C., Soto-Alvaredo, J., Montes-Bayon, M., Bettmer, J., Llopis, J., & Sanchez-Gonzalez, C. (2018). Gold nanoparticles: Distribution, bioaccumulation and toxicity. In vitro and in vivo studies. *Nanomedicine: Nanotechnology, Biology and Medicine, 14*(1), 1-12. doi:https://doi.org/10.1016/j.nano.2017.08.011

Mc Namara, K., Alzubaidi, H., & Jackson, J. K. (2019). Cardiovascular disease as a leading cause of death: how are pharmacists getting involved? *Integrated Pharmacy Research and Practice, 8*, 1-11. doi:10.2147/IPRP.S133088

Murphy, C. J., Gole, A. M., Stone, J. W., Sisco, P. N., Alkilany, A. M., Goldsmith, E. C., & Baxter, S. C. (2008). Gold Nanoparticles in Biology: Beyond Toxicity to Cellular Imaging. *Accounts of Chemical Research, 41*(12), 1721-1730. doi:10.1021/ar800035u

Navaei, A., Moore, N., Sullivan, R. T., Truong, D., Migrino, R. Q., & Nikkhah, M. (2017). Electrically conductive hydrogel-based micro-topographies for the development of organized cardiac tissues. *RSC advances, 7*(6), 3302-3312.

Navaei, A., Rahmani Eliato, K., Ros, R., Migrino, R. Q., Willis, B. C., & Nikkhah, M. (2019). The influence of electrically conductive and non-conductive nanocomposite scaffolds on the maturation and excitability of engineered cardiac tissues. *Biomater Sci, 7*(2), 585-595. doi:10.1039/c8bm01050a

Navaei, A., Saini, H., Christenson, W., Sullivan, R. T., Ros, R., & Nikkhah, M. (2016). Gold nanorod-incorporated gelatin-based conductive hydrogels for engineering cardiac tissue constructs. *Acta Biomater, 41*, 133-146. doi:10.1016/j.actbio.2016.05.027

Park, J., Kim, Y. S., Ryu, S., Kang, W. S., Park, S., Han, J., . . . Kim, B.-S. (2015a). Graphene Potentiates the Myocardial Repair Efficacy of Mesenchymal Stem Cells by Stimulating the Expression of Angiogenic Growth Factors and Gap Junction Protein. *Advanced Functional Materials, 25*(17), 2590-2600. doi:https://doi.org/10.1002/adfm.201500365

Patino-Guerrero, A., Ponce Wong, R. D., Kodibagkar, V. D., Zhu, W., Migrino, R. Q., Graudejus, O., & Nikkhah, M. (2023). Development and Characterization of Isogenic Cardiac Organoids from Human-Induced Pluripotent Stem Cells Under Supplement Starvation Regimen. *ACS Biomaterials Science & Engineering, 9*(2), 944-958. doi:10.1021/acsbiomaterials.2c01290

Patino-Guerrero, A., Veldhuizen, J., Zhu, W., Migrino, R. Q., & Nikkhah, M. (2020). Three-dimensional scaffold-free microtissues engineered for cardiac repair. *J Mater Chem B, 8*(34), 7571-7590. doi:10.1039/d0tb01528h

Rambanapasi, C., Zeevaart, J. R., Buntting, H., Bester, C., Kotze, D., Hayeshi, R., & Grobler, A. (2016). Bioaccumulation and Subchronic Toxicity of 14 nm Gold Nanoparticles in Rats. *Molecules, 21*(6). doi:10.3390/molecules21060763

Richards, D. J., Li, Y., Kerr, C. M., Yao, J., Beeson, G. C., Coyle, R. C., . . . Mei, Y. (2020). Human cardiac organoids for the modelling of myocardial infarction and drug cardiotoxicity. *Nature Biomedical Engineering, 4*(4), 446-462. doi:10.1038/s41551-020-0539-4

Richards, D. J., Tan, Y., Coyle, R., Li, Y., Xu, R., Yeung, N., . . . Mei, Y. (2016). Nanowires and Electrical Stimulation Synergistically Improve Functions of hiPSC Cardiac Spheroids. *Nano Letters, 16*(7), 4670-4678. doi:10.1021/acs.nanolett.6b02093

Roth, G. A., Mensah, G. A., Johnson, C. O., Addolorato, G., Ammirati, E., Baddour, L. M., . . . Group, G.-N.-J. G. B. o. C. D. W. (2020). Global Burden of Cardiovascular Diseases and Risk Factors, 1990-2019: Update From the GBD 2019 Study. *J Am Coll Cardiol, 76*(25), 2982-3021. doi:10.1016/j.jacc.2020.11.010

Rupert, C. E., Kim, T. Y., Choi, B.-R., & Coulombe, K. L. K. (2020). Human Cardiac Fibroblast Number and Activation State Modulate Electromechanical Function of hiPSC-Cardiomyocytes in Engineered Myocardium. *Stem Cells International, 2020*, 9363809. doi:10.1155/2020/9363809

Saini, H., Navaei, A., Van Putten, A., & Nikkhah, M. (2015). 3D cardiac microtissues encapsulated with the co-culture of cardiomyocytes and cardiac fibroblasts. *Adv Healthc Mater, 4*(13), 1961-1971. doi:10.1002/adhm.201500331

Santos-Martinez, M. J., Rahme, K., Corbalan, J. J., Faulkner, C., Holmes, J. D., Tajber, L., . . . Radomski, M. W. (2014). Pegylation Increases Platelet Biocompatibility of Gold Nanoparticles. *Journal of Biomedical Nanotechnology, 10*(6), 1004-1015. doi:10.1166/jbn.2014.1813

Shard, A. G., Wright, L., & Minelli, C. (2018). Robust and accurate measurements of gold nanoparticle concentrations using UV-visible spectrophotometry. *Biointerphases, 13*(6), 061002. doi:10.1116/1.5054780

Shettigar, R. R., Misra, N. M., & Patel, K. (2018). Cationic surfactant (CTAB) a multipurpose additive in polymer-based drilling fluids. *Journal of Petroleum Exploration and Production Technology, 8*(2), 597-606. doi:10.1007/s13202-017-0357-8

Shi, L., Zhang, J., Zhao, M., Tang, S., Cheng, X., Zhang, W., . . . Wang, Q. (2021). Effects of polyethylene glycol on the surface of nanoparticles for targeted drug delivery. *Nanoscale, 13*(24), 10748-10764. doi:10.1039/D1NR02065J

Slotvitsky, M. M., Tsvelaya, V. A., Podgurskaya, A. D., & Agladze, K. I. (2020). Formation of an electrical coupling between differentiating cardiomyocytes. *Scientific Reports, 10*(1), 7774. doi:10.1038/s41598-020-64581-5

Souders, C. A., Bowers, S. L., & Baudino, T. A. (2009). Cardiac fibroblast: the renaissance cell. *Circ Res, 105*(12), 1164-1176. doi:10.1161/CIRCRESAHA.109.209809

Sundnes, J., Lines, G. T., Cai, X., Nielsen, B. F., Mardal, K.-A., & Tveito, A. (2007). *Computing the electrical activity in the heart* (Vol. 1): Springer Science & Business Media.

Tan, Y., Richards, D., Coyle, R. C., Yao, J., Xu, R., Gou, W., . . . Mei, Y. (2017). Cell number per spheroid and electrical conductivity of nanowires influence the function of silicon nanowired human cardiac spheroids. *Acta Biomater, 51*, 495-504. doi:10.1016/j.actbio.2017.01.029

Veerman, C. C., Kosmidis, G., Mummery, C. L., Casini, S., Verkerk, A. O., & Bellin, M. (2015). Immaturity of human stem-cell-derived cardiomyocytes in culture: fatal flaw or soluble problem? *Stem Cells Dev, 24*(9), 1035-1052. doi:10.1089/scd.2014.0533

Veldhuizen, J., Cutts, J., Brafman, D. A., Migrino, R. Q., & Nikkhah, M. (2020b). Engineering anisotropic human stem cell-derived three-dimensional cardiac tissue on-a-chip. *Biomaterials, 256*, 120195. doi:https://doi.org/10.1016/j.biomaterials.2020.120195

Veldhuizen, J., Migrino, R. Q., & Nikkhah, M. (2019). Three-dimensional microengineered models of human cardiac diseases. *J Biol Eng*, *13*(1), 29. doi:10.1186/s13036-019-0155-6

Vrandečić, N. S., Erceg, M., Jakić, M., & Klarić, I. (2010). Kinetic analysis of thermal degradation of poly(ethylene glycol) and poly(ethylene oxide)s of different molecular weight. *Thermochimica Acta*, *498*(1), 71-80. doi:https://doi.org/10.1016/j.tca.2009.10.005

Wang, L., Jiang, X., Ji, Y., Bai, R., Zhao, Y., Wu, X., & Chen, C. (2013). Surface chemistry of gold nanorods: origin of cell membrane damage and cytotoxicity. *Nanoscale*, *5*(18), 8384-8391. doi:10.1039/C3NR01626A

Wanjare, M., & Huang, N. F. (2017). Regulation of the microenvironment for cardiac tissue engineering. *Regenerative Medicine, 12*(2), 187-201. doi:10.2217/rme-2016-0132

Willets, K. A., & Van Duyne, R. P. (2007). Localized surface plasmon resonance spectroscopy and sensing. *Annual review of physical chemistry*, *58*(1), 267-297.

Wu, Y., & Guo, L. (2018). Enhancement of Intercellular Electrical Synchronization by Conductive Materials in Cardiac Tissue Engineering. *IEEE Transactions on Biomedical Engineering, 65*(2), 264-272. doi:10.1109/TBME.2017.2764000

Xu, Y., Wang, X., Chen, L., Zhao, Y., He, L., Yang, P., . . . Zhang, Q. (2015). High-yield synthesis of gold nanoribbons by using binary surfactants. *Journal of Materials Chemistry C, 3*(7), 1447-1451. doi:10.1039/C4TC02603A

Yu, D., Wang, X., & Ye, L. (2021). Cardiac Tissue Engineering for the Treatment of Myocardial Infarction. *Journal of Cardiovascular Development and Disease*, *8*(11). doi:10.3390/jcdd8110153

Zhang, J., Tao, R., Campbell, K. F., Carvalho, J. L., Ruiz, E. C., Kim, G. C., . . . Kamp, T. J. (2019). Functional cardiac fibroblasts derived from human pluripotent stem cells via second heart field progenitors. *Nat Commun, 10*(1), 2238. doi:10.1038/s41467-019-09831-5

Zhang, Z., & Lin, M. (2014). Fast loading of PEG–SH on CTAB-protected gold nanorods. *RSC Advances, 4*(34), 17760-17767. doi:10.1039/C3RA48061E

Zhao, C., Xu, X., Ferhan, A. R., Chiang, N., Jackman, J. A., Yang, Q., . . . Weiss, P. S. (2020). Scalable Fabrication of Quasi-One-Dimensional Gold Nanoribbons for Plasmonic Sensing. *Nano Letters*, *20*(3), 1747-1754. doi:10.1021/acs.nanolett.9b04963

CHAPTER 4

DEVELOPMENT AND CHARACTERIZATION OF ISOGENIC CARDIAC ORGANOIDS FROM HUMAN-INDUCED PLURIPOTENT STEM CELLS UNDER SUPPLEMENT STARVATION REGIMEN

4.1 ABSTRACT

The prevalence of cardiovascular risk factors is expected to increase the occurrence of cardiovascular diseases (CVDs) worldwide. Cardiac organoids are promising candidates for bridging the gap between *in vitro* experimentation and translational applications in drug development, and cardiac repair due to their attractive features. Here we present the fabrication and characterization of isogenic scaffold-free cardiac organoids derived from human induced pluripotent stem cells (hiPSCs) formed under a supplement-deprivation regimen that allows for metabolic synchronization and maturation of hiPSC-derived cardiac cells. We propose the formation of coculture cardiac organoids that include hiPSC-derived cardiomyocytes and hiPSC-derived cardiac fibroblasts (hiPSC-CMs and hiPSC-CFs respectively). The cardiac organoids were characterized through extensive morphological assessment, evaluation of cellular ultrastructures, and analysis of transcriptomic and electrophysiological profiles. Morphology and transcriptomic profile of the organoids were improved by coculture of hiPSC-CMs with hiPSC-CFs. Specifically, upregulation of Ca^{+2} handling-related genes, such as RYR2, and SERCA, and structure-related genes such as TNNT2 and MYH6 was observed. Additionally, the electrophysiological characterization of the organoids under supplement deprivation shows a trend for reduced conduction velocity for coculture organoids. These studies help to gain better understanding of the role of other isogenic cells such as hiPSC-CFs in the formation

of mature cardiac organoids, along with the introduction of exogenous chemical cues, such as supplement starvation.

4.2 INTRODUCTION

Cardiovascular diseases (CVDs) have been consistently the leading cause of mortality worldwide. Additionally, the risk factors for CVDs continue to rise globally (G. A. Roth et al., 2020). The development of novel technologies for addressing CVDs is imperative to improve the outcome and life expectancy of these diseases. Cardiac tissue engineering has emerged as a promising powerful approach to address the elevated prevalence, economic burden, and death toll caused by CVDs. However, there are remaining challenges that need to be addressed.

In the past few years, the surge and refinement of stem cell technologies have advanced cardiac tissue engineering. The discovery of human-induced pluripotent stem cells (hiPSCs) has allowed for the derivation of a myriad of different cell types from the same donor, namely isogenic cells. Additionally, protocols for the directed differentiation of human cardiac cells have resulted in virtually unlimited availability of cardiac cells for use in *in vitro* experimentation. However, one of the main disadvantages of using hiPSC-derived cardiac cells, and specifically hiPSC-derived cardiomyocytes (hiPSC-CMs) is their immature state and phenotype (Binah et al., 2007; C. Robertson, D. D. Tran, & S. C. George, 2013; G. A. Roth et al., 2020; Snir et al., 2003; Veerman et al., 2015; X. Yang, L. Pabon, & C. E. Murry, 2014), leading to poor representation of structural, mechanical, and electrical properties of the native heart in cellular constructs engineered from these cells.

Maturation of hiPSC-CMs is of special interest for tissue engineering due to their main role in the mechanical and electrical performance in the cardiac tissue (J. Veldhuizen

et al., 2019). To that end, in the past few years, numerous strategies have been proposed to improve the maturation state of hiPSC-derived cells including electrical and mechanical stimulation, prolonged culture periods and coculture with different types of cells, introduction of chemical cues such hormones and growth factors and modified topographical signaling (Esmaeili et al., 2022; Gomez-Garcia, Quesnel, Al-Attar, Laskary, & Laflamme, 2021; Navaei et al., 2017; A. Navaei et al., 2019; A. Navaei et al., 2016; Nikkhah et al., 2016; Jaimeson Veldhuizen et al., 2020b). Overall these findings have demonstrated that the control of the microenvironment within the engineered cardiac tissues (ECTs) is necessary for improved cell maturation and overall performance of these tissues.

The adult myocardium is formed by several types of cells. Two of the most abundant types of cells are CMs and cardiac fibroblasts (CFs). CMs generate synchronized contraction of the tissue (Woodcock & Matkovich, 2005) and occupy the majority of the myocardium volume (Radisic et al., 2007). While, CFs are the main producers of extracellular matrix (ECM) proteins which play an important role in the integrity of the cardiac tissue and contribute to the propagation of mechanical and electrical signaling. CFs also secrete growth factors and other signaling molecules that contribute to the cross-talk among the different cells types within the myocardium (Souders et al., 2009). Therefore, recapitulation of cardiac tissue cellular composition is of central importance in the fabrication of physiologically relevant ECTs (Nugraha, Buono, von Boehmer, Hoerstrup, & Emmert, 2019).

The innovations in microfabrication techniques along with derivation of hiPSC into cardiac cells have led to significant advances in the creation of cardiac organoids

(Beauchamp et al., 2020; A. Patino-Guerrero et al., 2020). However, some characteristics of these tissues and the mechanics for their formation require further investigation. For example, the integration of isogenic cardiac cells is of very recent application and some aspects, such as cellular crosstalk and electrophysiological behavior, have not been fully evaluated yet. Additionally, there is no consensus on the optimal cellular composition of cardiac organoids (Nugraha et al., 2019; Pinto et al., 2016). Therefore, improving our understanding of the mechanisms for the fabrication, maturation and overall functioning of cardiac organoids requires basic investigation at the cellular and molecular level.

In this study, we propose the development and characterization of scaffold-free isogenic cardiac organoids under supplement starvation regimen. There is evidence, for example, that the deprivation of serum and other supplements in the culture media, can induce cellular synchronization (C. Fan et al., 2020; Khammanit, Chantakru, Kitiyanant, & Saikhun, 2008). Also, it has been reported that serum starvation can induce maturation of CMs derived from embryonic stem cells (J. Yang et al., 2021). Conventionally, hiPSC-CMs and ECTs fabricated with these cells maintained in a high-glucose media, enhanced with a complex nutrient mixture, can support the high-metabolic needs of the hiPSC-CMs (X. Lian et al., 2013). Thus, it is hypothesized that replacing this nutrient-rich media with a supplement-free, low-glucose basal media can induce a latent state in the hiPSC-CMs causing metabolic synchronization of the cell culture due to a starvation state.

We present the formation and characterization of scaffold-free isogenic cardiac organoids, fabricated with hiPSC-CMs and hiPSC-derived CFs (hiPSC-CFs). We introduce a 24-hour supplement starvation regimen to hiPSC-CMs upon the formation of the cardiac organoids. The ECTs were fabricated under monoculture (only hiPSC-CMs)

and coculture (hiPSC-CMs and hiPSC-CFs, 7:3 respectively) conditions. We subsequently compared the phenotype and the function of cardiac organoids formed under the supplement starvation regimen to organoids formed with hiPSC-CMs that did not undergo the supplement-free period. Specifically, morphological, structural, molecular, and electrophysiological evaluation of the microtissues were performed in order to assess their maturation state, and overall performance for potential applications in cardiac repair, disease modeling and drug screening.

4.3 EXPERIMENTAL SECTION

For the convenience of the reader we have created a "Table of resources" (**APPENDIX B**), including all the materials used in this manuscript, along with their working concentrations and identifier numbers.

4.3.1 Methods

4.3.1.1 Human Stem Cell culture

Human-induced pluripotent stem cells (IMR90-4) were obtained from WiCell (Wisconsin, USA). The cells were cultured in mTeSR-1 media (Stem Cell Technologies) on hESC-Matrigel (Corning)-coated plates. The media was changed every day, and the cells were replated when reaching ~80% confluency. For replating, the culture media was removed and 0.5mM EDTA (Corning) in 1x DPBS (Dulbecco's phosphate buffered solution) was added. The cell culture was incubated with the EDTA solution for 6-7 minutes at room temperature. After this, the EDTA was removed, and the cells were mechanically dissociated with mTeSR-1 and replated at the desired cell density (150-250K cell per well of a 6-well plate). Cryopreservation of the cells was performed in 90%FBS, 10%DMSO.

4.3.1.2 Differentiation of hiPSC-derived cardiomyocytes

The differentiation of the hiPSC-CMs was performed under the GiWi protocol (X. Lian et al., 2013). This protocol is specific for ventricular CMs and is based in the introduction of small molecules for the regulation of the canonical Wnt signaling. The differentiation process was started when the hiPSCs reached at least 80% confluency. On day 0 (D0) the culture media was changed to RPMI+B27 minus insulin (RPMI 1640, 2%B27 minus insulin (Gibco), 1%Pen/Strep (Gibco)). Additionally, 7-9μM CHIR99021 (BioVision) was integrated to the media in order to inhibit the Glycogen Synthase Kinase-3 (GSK) pathway and activate the canonical Wnt pathway. Exactly 24 hours later (day 1), the media was changed to RPMI+B27 minus insulin. 72 hours post-initiation of the differentiation (day 3), a 1:1 mixture of conditioned media from the cell culture, and fresh RPMI+B27 minus insulin was supplemented with 5μM IWP-2 (Sigma) for inducing the inhibition of the Wnt pathway in the cells. On day 5 the media was changed to RPMI+B27 minus insulin to allow for cell recovery. After this, the media was changed every 48 hours with RPMI+B27 to promote cell maturation (**Figure 4.1 A**). The hiPSC-CMs presented spontaneous beating typically around day 9 (**Video B1**)

In order to increase the yield of the differentiation of the hiPSC-CMs, on day 13, glucose-free media (RPMI 1640, B27, 4mM sodium lactate, 1%Pen/Strep) was used to allow for hiPSC-CM enrichment through glucose starvation (Binah et al., 2007). The media was changed every 72 hours. On day 19, the media was switched to RPMI+B27 to allow for cell recovery. After this, the obtained hiPSC-CMs were dissociated using TrypLE Express (LifeTech) and replated in Matrigel-coated plates. Following this, the media was changed every 48 hours upon starting all the experiments.

4.3.1.3 Differentiation of hiPSC-derived cardiac fibroblasts

The differentiation of hiPSC-CF was based in the consecutive modulation of the canonical Wnt and fibroblast growth factor (FGF) signaling through the introduction of small molecules and growth factors to the culture medium (J. Zhang et al., 2019). The hiPSCs were allowed to reach at least 80% confluency before starting the differentiation process. The hiPSC-CFs differentiation protocol was started by changing cell culture medium for RPMI+B27 minus insulin, conditioned with 7μM CHIR99021 (BioVision). On day 1, culture media was changed to RPMI+B27 minus insulin simple to allow for cell to recovery.

On day 2 of the differentiation the medium was changed to the basal CF differentiation medium, consisting of high glucose (4.5g/l) DMEM with L-glutamine (4mM) (Gibco), and complemented with HLL supplement (human serum albumin (500μg/ml), linoleic acid (0.6μM), and lecithin (0.6μg/ml). This medium was supplemented with 70 ng/μl of β-fibroblast growth factor (β-FGF). Next, the culture media was changed every 48 hours with basal CF differentiation medium supplemented with β-FGF (70ng/μl). The hiPSC-CFs were dissociated with 1x Trypsin and replated on uncoated plates on day 20. From this point the cells were maintain with Fibroblast Growth Media-3 (FGM-3) (Fisher Scientific), changing the medium every 48 hours. The fibroblasts were passaged when they reached ~85% confluency. Freezing media was composed by 80%FGM3, 10%FBS, and 10%DMSO. For all of our experiments, hiPSC-CFs were used between passage numbers P8 and P12 to avoid the differentiation of the CFs into myofibroblasts.

4.3.1.4 Supplement Starvation regimen for hiPSC-CMs

Prior to the formation of the cardiac organoids, the hiPSC-CM were introduced to a 24-hour supplement-free period to induce the metabolic synchronization of the cellular population due to low availability of nutrients (C. Fan et al., 2020; Khammanit et al., 2008). On day 25 after initiated the hiPSC-CM differentiation, the cells were washed with 1x DPBS twice. Then, the basal culture media was substituted by serum free medium (Serum free Dulbecco's modified Eagle's Medium (DMEM) supplemented with glucose (4.5g/l), L-glutamine (584mg/l), and sodium pyruvate (110mg/l)). Exactly after 24 hours these cells were used for the formation of the cardiac organoids (**Video B2 and B3**).

4.3.1.5 Casting of agarose microwells

The cardiac organoids were fabricated using of agarose microwells (800µm diameter, 800µm depth). The microwells were casted using commercially available silicon molds (Microtissues), yielding to 35-microwell devices. For this, a solution of 2% agarose in sterile saline (0.9% (w/v) NaCl) was prepared. Then, 330µl of the agarose solution were deposited in the silicon molds and allowed to solidify at room temperature. The agarose microwells were demolded carefully, placed in 24-well culture plates, and 1ml of RPMI+B27 plus insulin was deposited in each well. The microwells were incubated for at least 1 hour at 37°C to allow the conditioning of the microwells, this step was repeated one more time before using the microwells for cardiac tissue formation.

4.3.1.6 **Fabrication of scaffold-free cardiac organoids**

The hiPSC-CMs were dissociated using TrypLE Express for 12 minutes at 37°C followed by mechanical dissociation with a micropipette. After this, the TrypLE Express was neutralized with basal culture medium and the cells were centrifuged at 300g for 3

minutes. The supernatant was replaced by basal RPMI 1640 medium. Likewise, the hiPSC-CFs were dissociated from the culture plates by using 0.05% Trypsin-EDTA (Thermo) and incubated for 3-4 minutes at 37°C. After mechanical dissociation the trypsin was neutralized with FGM3 and the cells were centrifuged at 250g for 4 minutes. For monoculture organoids, hiPSC-CM were resuspended at a concentration of $175x10^3$ cells per 75µl of basal RPMI 1640 medium. For coculture organoids, the cells were mixed at a ratio of 70%:30% hiPSC-CM and hiPSC-CFs respectively, to an equal concentration of $175x10^3$ cells per 75µl. This with the aim of creating cardiac organoids of $5x10^3$ cardiac cells each. The cellular ratio for the coculture organoids was carefully selected after the extensive optimization experiments of the proportion of the cellular population (data not shown).

The cells were allowed to sit undisturbed in the agarose microwells for 1 hour at 37°C before adding 1 ml of basal RPMI medium to each well. After this, the culture media was changed every 48 hours. The cardiac organoids were allowed to aggregate in the agarose microwells for 7 days before harvesting (**Figure 4.1 B, video B4-B7**). Four different experimental conditions were produced as follow:

- B27M: Monoculture organoids formed with supplemented hiPSC-CMs.
- B27C: Coculture organoids formed with supplemented hiPSC-CMs and hiPSC-CFs.
- SFM: Monoculture organoids, formed with supplement-free hiPSC-CMs.
- SFC: Coculture organoids, formed with supplement-free hiPSC-CMs and hiPSC-CFs.

4.3.1.7 Microscopy imaging and morphological characterization

Phase-contrast and fluorescence images were acquired by Zeiss Axio Observer Z1 equipped with Apotome2 (Zeiss) and ZenPro software. The samples were imaged at 2.5x

in the agarose microwells on day 1 and day 7 after seeding the cells in order to track the size change. Additionally, on day 7, time-lapse imaging of individual organoids was recorded at 10x for 20 seconds at 34℃ for spontaneous beating behavior characterization. Time-lapse images were analyzed with a custom MATLAB code in order to extract the spontaneous beating rate. Also, the inter-beat intervals were measured from the extracted signals; then inter-beat interval variability (IIV) parameter was calculated as the standard deviation of this measure. We performed one-way ANOVA analysis to the extracted beating rate and IIV signals in order to evaluate the statistical differences between groups.

Morphological characterization of the cardiac organoids was performed by analyzing and processing the phase-contrast images with the "Measure" and "Shape descriptors" tools of FIJI software (Daghero et al., 2022; Kopanja, Kralj, Zunic, Loncar, & Tadic, 2016; Phelan, Gianforcaro, Gerstenhaber, & Lelkes, 2019). Specifically, tracing straight lines for measuring the diameter and using the "freehand selection" tool to trace the edges of individual organoids (Khan et al., 2020). A total of 15-20 cardiac organoids were evaluated per experimental group. A total of three biological replicates (N=3) were evaluated in order to perform statistical analysis.

4.3.1.8 Cardiac organoid cryosectioning

In order to perform the immunohistochemistry, the formed tissues were cryosectioned. First, the cardiac organoids were harvested on day 7 after seeding in the agarose microwells. The samples were washed with 1x DPBS to remove cellular debris accumulated in the agarose microwells. Then, the tissues were fixed with 4% paraformaldehyde (4% PF) (ThermoScientific) for 45 minutes at 37℃. Next, the samples

were rinsed twice with PBS-glycine (100 mM), followed by one rinse with PBS-Tween20 (0.05% (v/v)).

To prevent ice crystal formation when freezing the cardiac organoids, sucrose cryoprotection was performed. Briefly, after the PBS-Tween 20 wash, the tissues were submerged in a solution of 15%(w/v) sucrose in DI water for 1 hour at room temperature. Then, the sucrose solution was replaced by a 30%(w/v) sucrose solution overnight at 4℃. The next day, the sucrose solution was removed, and the tissues were fast-frozen by embedding in Tissue-Tek OCT compound (Tissue-Tek). The OCT-embedded tissues were deposited in specimen holders and the placed in a freezing bath formed with 95% ethanol and dry ice nuggets. The OCT was allowed to completely solidify before removing from the ethanol bath. The samples were preserved at -80℃ until ready for cryosectioning.

The cryosectioning was performed with the CryoStar NX70 cryostat (ThermoScientific). It was setup to make tissue slices of a thickness of 10 µm. With the holder at a temperature of -10℃ and the blade at -14℃. The tissue slices were collected in positively charged glass slides and were preserved at -20℃ until further processing.

4.3.1.9 Immunohistochemistry

After cryosectioning, the tissue slices were rinse once with PBS-Tween 20 to eliminate remaining OCT from the glass slides. The tissues were permeabilized using an IF buffer (0.2% Triton X-100, 0.1% BSA (radioimmunoassay grade), 0.05% Tween 20, 0.02% NaN3 in 1x DPBS) for 30 minutes at room temperature. In order to prevent unspecific antibody binding, sample blocking was performed with 10% goat serum (ImmunoReagents) for 1 hour at room temperature. Primary antibodies were diluted in 10% goat serum as follow: sarcomeric alpha actinin (SAA) (Thermo Fisher, Cat#: MA1-

22863) 1:100; Connexin 43 (Abcam, Cat#: ab11370) 1:125; Vimentin (Cell Signaling, Cat#: D24H3) 1:100. The samples were incubated at 4℃ overnight with the primary antibody solution; a sample incubated with only 10% goat serum was used as secondary antibody control.

The next day, the samples were washed with DPBS-Tween20 for 15 minutes four times at room temperature. The secondary antibodies and 4',6-diamidino-1-phenylindole (DAPI) were diluted in 1x DPBS (1:500 and 1:1000 respectively) and the solution was centrifuged at 14,000 RPM for 10 minutes in order to eliminate antibody aggregates. The secondary antibodies plus DAPI were added to the samples and incubated for 1 hour at 37℃. Finally, the samples were washed three times with 1x DPBS-Tween20 for 15 minutes protected from light. The samples were mounted using VectaShield (Vector) to prevent fading and bleaching of the fluorophores. Imaging was performed with the Leica SP8 Confocal Microscope at 63x and 100x. The z-stack projection was then reconstructed using FIJI software. The assay was repeated for N=3 biological replicates.

In order to evaluate the sarcomere length of the hiPSC-CMs within the cardiac organoids the "Measure" tool of the FIJI software was used. Individual sarcomere lengths were measured by tracing a straight line from consecutive Z-discs, stained with the anti-SAA antibody as shown in **Figure B4**. A total of 35-50 measurements per experimental group, per biological replicate were calculated in order to performed the statistical analysis.

4.3.1.10 TUNEL Assay

The samples for TUNEL assay were harvested from the agarose microwells on day 7 after seeding. Then, the samples were fixed and cryosectioned, and stained using the commercially available Click-iT Plus TUNEL assay (Invitrogen), following the

instructions indicated by the kit. Briefly, the samples were permeabilized with a proteinase-K solution. Followed by a DI water rinse and incubation with the TdT buffer for 10 minutes. Then, the TdT solution was added to the samples and incubated for 60 minutes. Next, the samples were rinsed with DI water and 3% BSA ,0.1% TritonX-100 in PBS. The Click-iT Plus TUNEL reaction cocktail was added to the samples and incubated for 30 minutes. After rinsing, a DAPI staining was performed for 15 minutes. All the incubations were completed at 37℃. A sample treated with DNAse-1 for 30 minutes was used as positive control. The samples were imaged with the Zeiss Axio Observer Z1 microscope equipped with Apotome2 (Zeiss) and ZenPro software at 20x. The z-stack projections were reconstructed with FIJI software. The assay was repeated for N=3 biological replicates.

4.3.1.11 Quantitative real-time reverse transcription-PCR (qRT-PCR)

After seven days in the agarose microwells the cardiac organoids were harvested and rinsed twice with 1x DPBS to eliminate cellular debris accumulated in the microwells. After this, the RNA from the samples was extracted using the RNA MicroPrep kit (Zymo). The RNA quality and concentrations were evaluated using the NanoDrop UV-Vis Spectrophotometer. Nuclease-free (NF) water was used as a blank, then 2 µl of the sample were used for the measurement. Total RNA was used for the cDNA synthesis along with iScript Reverse Transcription Supermix (BioRad).

For qRT-PCR, melting curve analysis and PCR product size quantification were used for primer validation (**Table B2**). 18S was used as housekeeping gene for dCt normalization as previously optimized by our group.(Jaimeson Veldhuizen et al., 2020b) A qPCR master mix reaction was created by combining the 5 µl of iTaq Universal SYBR Green Supermix (BioRad), 3.9 µl of NF water, 0.1 µl of the cDNA sample, and 1 µl of the

primer working solution (8µM of forward and reverse primers in NF water). The qRT-PCR reactions were performed in 96-wells plates using the q-Tower real time thermocycler (Analitik Jena). All dCt values were normalized to the respective sample collected on D-1 (before starting supplement starvation). The assay was repeated for N=3 biological replicates.

4.3.1.12 Microelectrode array (MEA) electrophysiological analysis

Glass microelectrode arrays (MEAs) with 59 electrodes plus one reference electrode were used for the MEA electrophysiological analysis. The array consists of an 8x8 grid of electrodes, spaced by 200µm (center-to-center), with a recording diameter of 30 µm. The MEAs were prepared prior the electrophysiology analysis to allow for adhesion of the cardiac organoids to the surface and induce the contact of the cardiac cells with the microelectrodes. First the devices were sterilized with UV-radiation for at least 1 hour. Then, the MEAs were rinsed twice with DI water. The MEAs were coated with Matrigel (Corning) overnight at 37℃ to provide anchorage sites to the cells. After harvesting, the tissues were rinsed twice with 1x DPBS. Then, the cardiac organoids were deposited on the MEA devices with RPMI basal media. The devices were swirled gently to promote the localization of the cardiac tissues on top the electrodes and ensure the acquisition of the electrophysiological signals. The organoids were allowed to sit undisturbed for at least 24 hours before the electrophysiological signal acquisition.

A custom-made interface board (PLEXON) with temperature control (BMSEED LLC.) was used for obtaining the signals from the MEAs. The INTAN Stimulation/Recording controller was used in combination with the RHX software as the user interface. The field potentials (FPs) of spontaneous beating signals were recorded for

30 second for each sample. The signals were mapped by correlation with phase contrast images at 2.5x (Zeiss Axio Observer Z1 microscope and ZenPro software) and analyzed using a custom MATLAB code.

Regions of interest (ROIs) for the evaluation of electrophysiological signals were determined through the creation of FPs heatmaps. ROIs were selected as the more active areas according to the FPs heatmaps and corroborated with phase-contrast imaging as the electrodes that were in contact with localized organoids. The conduction velocity (CV) was calculated by first measuring the signal propagation time ($\Delta t_{average}$) between channels within the ROIs. For this, the time of occurrence for beating peaks was detected for all ROIs, then Δt was calculated by:

$$\boldsymbol{\Delta t = |t_{ocurrence\ of\ ChannelA} - t_{ocurrence\ of\ ChannelB}|.} \qquad (1)$$

Then:

$$\boldsymbol{\Delta t_{average} = \frac{1}{n}\sum_{i=1}^{n} \Delta t} \qquad (2)$$

Where n is the number of peaks detected per channel. The CV for pair of channels was calculated by:

$$\boldsymbol{CV_{AB} = \frac{distance\ between\ channels}{\Delta t_{average}}} \qquad (3)$$

Finally, the average CV per ROI was calculated as the average of all the CV_{AB}s found within ROI. The CV of 2 to 3 ROIs was averaged per samples, and this was taken as the CV of the sample. CV_{AB}s outliers were identified through Grubb's test (GraphPad Prism), and were not used for the calculation of the final CV.

4.3.1.13 Statistical analysis

All the statistical analyses were carried using GraphPad Prism. Two-way ANOVA was used for analyzing the diameter changed of the cardiac organoids. One-way ANOVA was performed in circularity and roundness analysis, as well as for qRT-PCR. Two-tailed t-test was used for analysis of the CV. Significance level was of $\alpha=0.05$ for all cases. All results are presented in the form of mean ± SEM. A minimum of three biological replicates (N=3) were analyzed for all the experimental assays, except for MEA analysis, for which two biological replicates (N=2) were utilized for the experiments.

4.4 RESULTS AND DISCUSSION

4.4.1 Isogenic differentiation of hiPSC-derived cardiomyocytes and cardiac fibroblasts

Derivation of cardiac cells from one hiPSC source, namely isogenic cardiac cells, is of relevance for several applications within the cardiac engineering field (Campostrini et al., 2021). On one hand, it allows for the creation of ECTs fabricated with different types of cells, contributing to a closer resemblance of the native myocardium composition. Additionally, the inclusion of different types of cardiac cells allows for cell to cell communication through growth factors, cytokines, and other chemical cues which promote maturation of the ECTs (Tirziu, Giordano, & Simons, 2010).

Moreover, multicellular ECTs are of physiological relevance for numerous *in vitro* applications. For instance, while CMs are responsible of the contraction and main mechanical function of the heart, a number of cardiac diseases are mediated by the activation of CFs and their deposition of ECM proteins (D. Fan, Takawale, Lee, & Kassiri,

2012). Therefore, *in vitro* models that accurately recapitulate myocardium cellular composition are necessary for disease modeling and drug screening applications. Moreover, the potential for using patient-derived cells in the ECTs can help to overcome challenges such as engraftment to the host myocardium and biocompatibility and rejection issues.

The cardiac cells utilized herein for the formation of the cardiac organoids were obtained from the differentiation of hiPSC monolayers (**Figure 4.1 A**). The selected cell line presented a pluripotency state (**Figure B1A**) that allowed for the induction of the hiPSCs into cardiogenic mesodermal progenitor cells through the activation of the canonical Wnt signaling. This activation was mediated by the introduction of the CHIR99021 small molecule. Further chemical cues allowed for the successful derivation of CMs and CFs. For example, the introduction of the IWP-2 small molecule on D3 after initiated the differentiation acts repressing the Wnt signaling, which leads to the commitment of the cells towards a cardiac progenitor cell fate, and finally CMs with immature state (Doyle et al., 2015). On the other side, the presence of FGF in the environment of cardiac mesodermal progenitor cells interacts with the BMP signaling, directing the cells to a non-myocyte fate; thus, leading to the commitment towards CFs (J. Zhang et al., 2019).

Based on our utilized protocol, typically the hiPSC-CMs presented spontaneous beating around day 10 after the initiation of differentiation. After metabolic selection through glucose starvation and replating of the cells, we obtained uniform monolayers of beating cells (**Video B1**). Besides the spontaneous beating, the successful differentiation of hiPSC-CMs was confirmed through immunostaining for cardiac relevant markers, such

as SAA. Additionally, the yield of our differentiation protocol (>90% hiPSC-CMs) has been analyzed by flow cytometry previously.(Jaimeson Veldhuizen et al., 2020b) The differentiation of the hiPSC-CFs was validated by cell morphology evaluation and immunostaining for TE7 and vimentin (**Figure B1B)**.

It has been reported that supplement starvation can help with hiPSC-CM maturation by inducing a structural and metabolic changes, and overall improved performance of ECTs (C. Fan et al., 2020; Khammanit et al., 2008; J. Yang et al., 2021). Traditional protocols for differentiation of hiPSC-CMs require RPMI 1640 with B27 supplement as basal cell culture media for cell maintenance after day seven of differentiation. B27 is a serum-free supplement that was originally formulated and optimized by Brewer, et. al. for the survival of hippocampal neurons (Gregory J. Brewer & Cotman, 1989; G. J. Brewer, Torricelli, Evege, & Price, 1993). It contains antioxidants, proteins, fatty acids, and vitamins that help support cells in a neonatal state. The metabolism of hiPSC-CMs is dependent on the presence of fatty acids, among other nutrients, and it has been reported that the change in the culture media composition can lead to changes in the metabolism of neonatal CMs (C. Correia et al., 2017). Thus, it was shown that nutrient deprivation can lead to a homogeneous cell culture composition, via metabolic cell synchronization (C. Fan et al., 2020). By substituting the basal culture media with a supplement-free media we aimed to induce a metabolic shift in the hiPSC-CMs, as it has been previously demonstrated that nutrient deprivation leads to cellular maturation (J. Yang et al., 2021).

4.4.2 Formation of isogenic cardiac organoids

When forming scaffold-free ECTs, cellular aggregation is an important consideration. The lack of a matrix that provides mechanical support to the cells can

ultimately lead to induction of apoptosis through anoikis (Ogasawara et al., 2017; Taddei, Giannoni, Fiaschi, & Chiarugi, 2012), causing the failure of the ECTs. Additionally, cell coupling within the ECTs allows for the propagation of chemical, electrical, and mechanical cues that are necessary for its proper function (A. Patino-Guerrero et al., 2020). Therefore, it is necessary to evaluate the cellular aggregation of the cardiac organoids in order to elucidate the effects of the coculture and supplement-free regimen. Despite the importance of cellular aggregation in scaffold-free cardiac tissues, the progressive change in size of cardiac organoids has not been thoroughly described previously and it is often overlooked, focusing only on the final size of cardiac organoids. However, the progressive size change can be helpful to characterize the dynamics of cellular adhesions and aggregation, contingent upon the different cellular compositions in ECTs. In this study, we performed a 24-hour supplement starvation regimen for the hiPSC-CMs prior the formation of the scaffold-free cardiac organoids (**Figure 4.1 B, Figure B2A**). Additionally, we fabricated coculture cardiac organoids, formed with 70% hiPSC-CMs and 30% hiPSC-CFs. We hypothesized that the supplement starvation regimen in conjugation with coculture with hiPSC-CFs will lead to an improved formation and functionality of the cardiac organoids.

Phase-contrast imaging and video recordings were used to evaluate the morphology of the cardiac organoids (**Figure B2B**). The diameter change of the microtissues was monitored within the agarose microwells from day 1 to day 7 after cell seeding. Briefly, the interfacial tensions between the agarose microwells surface and the culture media along with a relatively high availability of adhesion proteins (connexins and cadherins) promote the adhesion between the cells, leading to the formation of self-arranged ECTs (**Figure 4.2**

A, Video B4-B7). The cardiac organoids retained their morphology and size after harvesting from the agarose microwells, confirming the formation of cell-cell adhesions.

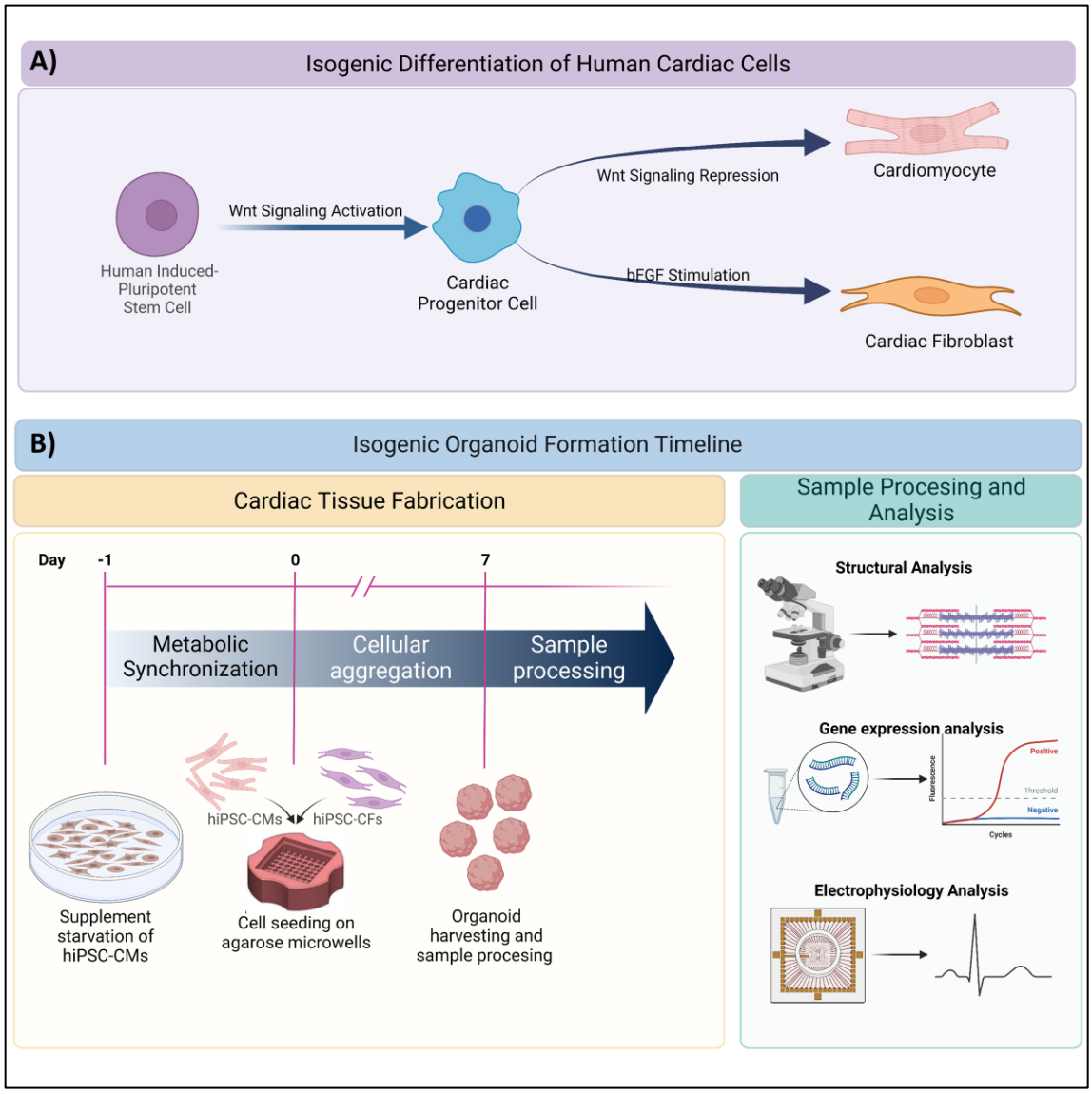

Figure 4.1. Schematic for the fabrication of scaffold-free isogenic cardiac organoids derived from human-induced pluripotent stem cells. A) Diagram for the isogenic differentiation of cardiac cells. B) Timeline for the fabrication of the cardiac organoids and sample processing after harvesting (Created with BioRender.com).

We observed an important change in the overall shape and size of the organoids from day one to day seven (**Figure 4.2 B, C**). First, we found that the final organoid diameter at day seven was similar for all the experimental conditions. However, diameter

evaluation at day 1 after seeding in the agarose microwells, showed a significantly reduced size for the coculture groups B27C and SFC (**Figure 4.2 C**). This suggests that the presence of hiPSC-CFs in the ECTs promote an accelerated cellular aggregation and microtissue compaction. Earlier cellular aggregation can be beneficial in the formation of cardiac organoids. First, the physical cell-to-cell adhesions and communication can help with cell survival by preventing anoikis (Taddei et al., 2012). Second, it has been previously demonstrated that CFs can deposit ECM proteins (Souders et al., 2009) that can also help with cell support and mechanical signal propagation. Thus, the presence of hiPSC-CFs in the formation of the cardiac organoids was seen to be beneficial for a rapid induced cellular aggregation, leading to the microtissue compaction, and resulting in a decrease in the size of the ECTs with time progression.

Circularity evaluation of the organoids on day seven revealed that B27C and SFC groups present a significantly more circular shape and smoother edges (**Figure 4.2 D**). Smoother organoid edges could be indicative of improved cellular compaction, which leads to a higher cell density within the ECTs, resulting in organoids of physiological-relevant cellular density. Additionally, the coculture groups showed a more circular morphology when compared to their monoculture counterparts.

A more rounded morphology and overall higher shape homogeneity across cardiac organoids could be beneficial for several applications (Fennema et al., 2013; Kang, Kim, Lee, Takayama, & Park, 2021; Velasco, Shariati, & Esfandyarpour, 2020). For example, the use of cardiac organoids has been proposed as the building blocks for bioprinting of large-scale cardiac tissues (Roche, Brereton, Ashton, Jackson, & Gentile, 2020). Thus, derivation of compact organoids with low diameter variability and reproducible size will

be optimal for 3D bioprinting processes. Additionally, rounder morphology, greater compaction and increased cellular density could facilitate the injection, survival, and engraftment of cardiac organoids within the diseased myocardium when used for cardiac repair and replacement.

After analyzing the spontaneous beating signals extracted from the phase-contrast videos, we found a similar beating pattern for all the experimental conditions (**Figure 4.2 E**). The calculated spontaneous beating rates (BPM) did not show significant differences between any of the groups (B27M:13.4±1.7; B27C:14.3±2.5; SFM:11.8±1.8; SFC:12.9±0.6) (**Figure 4.2 F**). Inter-beat interval variability (IIV) was calculated as the variation in the duration of the beat-to-beat intervals in the extracted signals (**Figure 4.2 G**). IIV is a measure of the periodic contractions of the cardiac tissue and has been used as a parameter to evaluate the synchronicity of the tissues, and as indirect measurement of mechanical and electrical coupling of the cardiac cells. Our evaluation did not show any significant difference between experimental groups, suggesting a similar degree of cell-to-cell coupling, regardless of the cellular composition of the cardiac organoids.

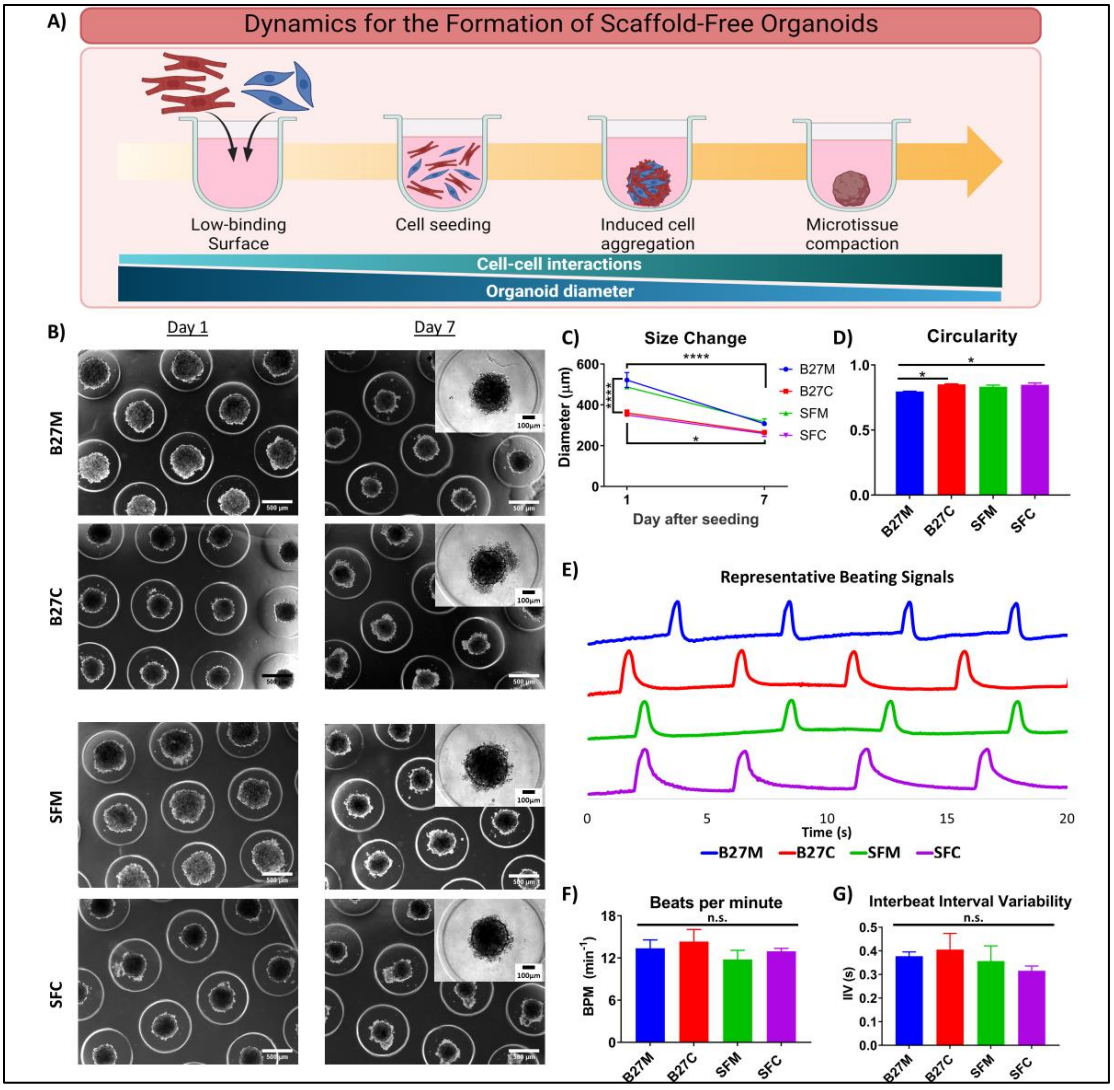

Figure 4.2. Morphological characterization of the isogenic cardiac organoids from phase-contrast imaging. A) Schematic representation of induced cell aggregation and compaction of isogenic cardiac organoids, showing increased intercellular interactions and decreased diameter with time progression (Created with Biorender.com). B) Representative phase-contrast images of the formed organoids (day 1 vs. day 7 after seeding) (Scale bars: 500µm). Insets: 10x phase-contrast images of single cardiac organoids on day 7 (Inset scale bar: 100µm). C) Size change of the cardiac organoids (day 1 vs. day 7 after seeding). D) Circularity evaluation of the cardiac organoids, measured on day 7 after seeding. E) Normalized representative spontaneous beating signals extracted from phase-contrast videos (Y-axis represent arbitrary units). F) Spontaneous beating rate of the cardiac organoids. G) Inter-beat interval variability calculated from the spontaneous beating signals obtained from the cardiac organoids. One-way ANOVA was performed for all the evaluations (n.s.=P-value>0.05, *=P-value≤0.05, ****=P-value≤0.0001). Abbreviations: B27M: monoculture supplemented organoids, B27C: coculture supplemented organoids, SFM: supplement starved monoculture organoids, SFC: supplement starved coculture organoids.

4.4.3 Evaluation of the cellular ultrastructure of cardiac organoids

One of the main challenges for engineering scaffold-free cardiac tissues is the limitation in size due to the lack of vascularization, the oxygen diffusion limit and meeting the metabolic requirements of the hiPSC-CMs (M. Radisic, W. Deen, R. Langer, & G. Vunjak-Novakovic, 2005; Y. Tan et al., 2017; J. Veldhuizen et al., 2022). To evaluate cell survival within the cardiac organoids, we performed TUNEL assay on cryosectioned slices of tissues harvested on day seven after seeding to evaluate early apoptotic cells (**Figure 4.3 A**). We did not find significant cell death for any of the conditions (**Figure 4.3 B**), suggesting that the size of the organoids allowed for the correct oxygen and nutrient diffusion and that the cells remained viable after the collection of the microtissues.

Through confocal imaging we observed the cellular ultrastructures of the cardiac organoids. Specifically, when co-staining the ECTs for cardiac biomarkers we were able to simultaneously visualize distinct cellular components that allowed for the structural characterization of the organoids. First, we performed immunohistochemistry (IHC) co-staining for sarcomeric alpha actinin (SAA) and vimentin in order to evaluate the cellular composition and distribution within the ECTs. Sarcomeric alpha actinin (SAA) is one of the vital protein components of the sarcomeric unit for mechanotransduction and is used as a gold standard biomarker for hiPSC-CMs. Additionally, vimentin is a structural protein that can be found within cardiac fibroblasts and is responsible for cell shape stabilization and cytoplasm integrity. Consequently, vimentin has been widely used as a biomarker for CFs (Souders et al., 2009).

One of the main attributes of the immature phenotype of hiPSC-CMs is poor sarcomeric structure development. Sarcomeres are the leading structures in the mechanical

functioning of the myocardium, critical in the synchronized contraction and relaxation of the cardiac muscle (Martin & Kirk, 2020; Sadayappan & de Tombe, 2012). Mature contractile machinery in CMs is characterized by the presence of elongated and robust sarcomeric units. SAA is found intertwined with myosin and actin within the sarcomeric unit and is localized in the so-called Z-discs (Pasqualini, Sheehy, Agarwal, Aratyn-Schaus, & Parker, 2015).

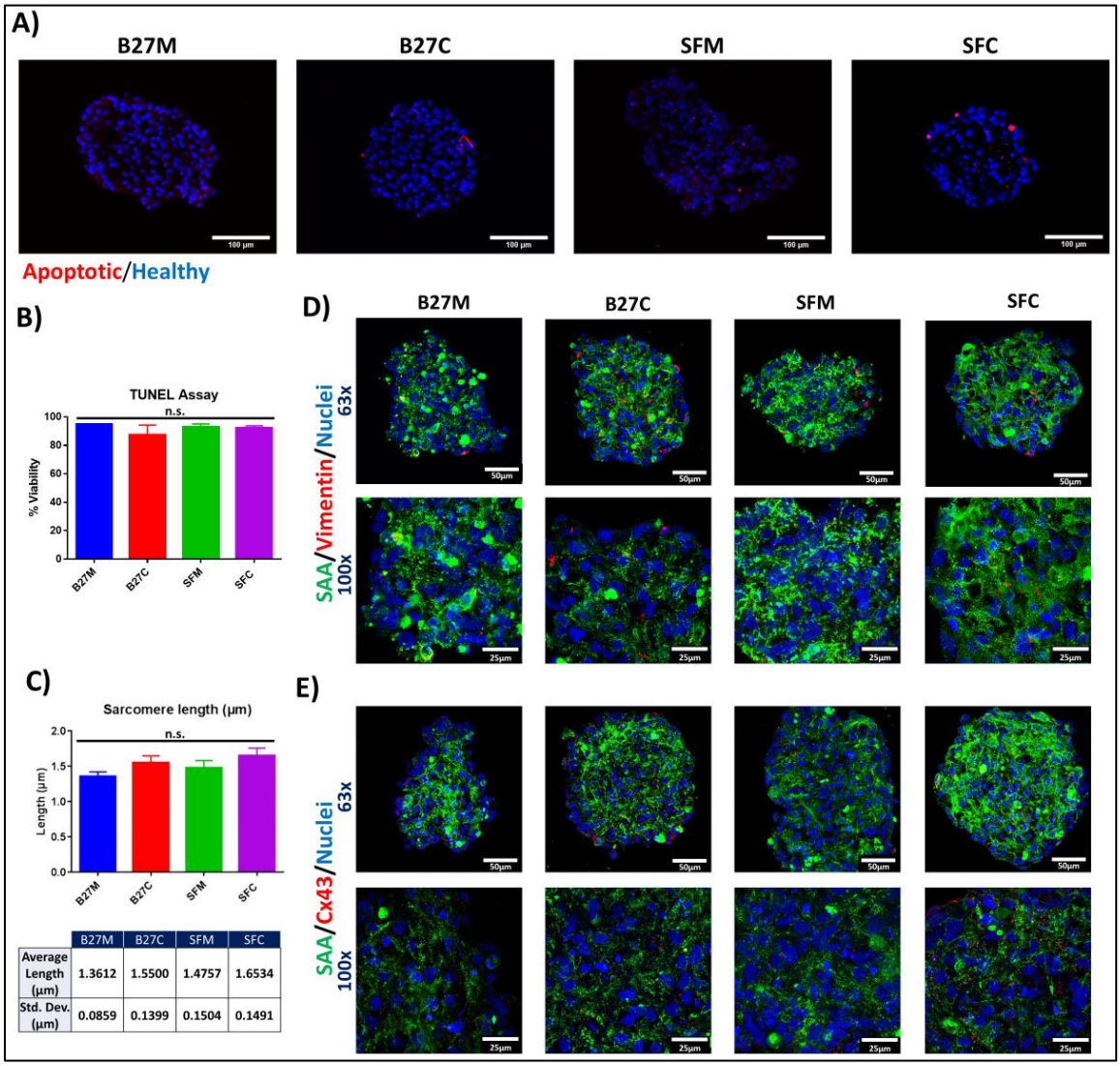

Figure 4.3. Structural characterization of the isogenic cardiac organoids from confocal imaging. A) Representative images for TUNEL assay performed over cryosectioned slices of the cardiac organoids on day 7 after seeding (Red: Apoptotic cells; Blue: Healthy cells) (Scale bars: 100 µm). B) Viability evaluation based on TUNEL assay. No significant cell

death was found on any of the experimental conditions. One-way ANOVA was performed for all the evaluations (n.s.=P-value> 0.05). C) Quantification of sarcomere length based on IHC images of cardiac organoids (n.s.=P-value> 0.05). D)Confocal imaging of 10µm cryosectioned slices of the cardiac organoids on day 7 after seeding. Top row: 63x magnification (Scale bar: 50 µm). Bottom row: 100x magnification (Scale bar: 25 µm) (Green: Sarcomeric alpha actinin; Red: Vimentin; Blue: Nuclei). E) Confocal imaging of IHC stained cryosectioned cardiac organoids for the visualization of the sarcomeric structures and Cx43 expression (Green: SAA; Red: Cx43; Blue: Nuclei) (Top row: scale bars: 50 µm; Bottom row: scale bars:25 µm).

Thus, when CMs are stained against SAA, the cells present striation bands, perpendicular to the main axis of the body of the cells. All our experimental groups showed these characteristic structures, with regions across all of the body of the organoids where SAA bands are present. These SAA bands correspond to the Z-discs of the sarcomeric structures and serve as a biomarker to detect the distribution of the hiPSC-CMs. Quantification of the sarcomere length, this is the average distance from band to band, showed an average length ranging from 1.36 µm to 1.65 µm for all the groups. Although the statistical analysis did not show significant differences, there is an apparent trend for an increase sarcomere length in the coculture groups (**Figure 4.3 C**). The stained hiPSC-CMs can be observed oriented in arbitrary positions within the organoids. Since the cellular aggregation of the ECTs was not directed by any external physical or chemical cue, cellular alignment was not anticipated. Moreover, SAA distribution is similar for all the experimental conditions (**Figure 4.3 D**).

As expected, higher expression of vimentin was found in the coculture organoids (B27C and SFC) by the enrichment of hiPSC-CFs in the formation of these. Similar to the distribution of the hiPSC-CMs, the presence of vimentin in the ECTs does not follow a specific alignment or localization, and it was observed throughout the entire cross-section of the organoids (**Figure 4.3 D**). A modest expression of vimentin in the monoculture

cardiac organoids (B27M and SFM) was observed. While our directed differentiation protocol and further metabolic selection of hiPSC-CMs has a high production yield (>90% hiPSC-CMS) (Jaimeson Veldhuizen et al., 2020b), it is possible that hiPSC-CFs and other cell types that are not specified were generated as a by-product of the CMs differentiation and that these cells survived the glucose starvation; thus, remaining present in the final form of the organoids.

The formation of cell-to-cell adhesions is vital for the fabrication of scaffold-free ECTs. In the native cardiac tissue, cells can be found forming a single syncytium that can conduct mechanical and electrical cues (Carmeliet, 2019; Napiwocki et al., 2021; A. H. Nguyen et al., 2019). The propagation of electrical signals is mainly due to the depolarization and repolarization of the cell membrane (Carmeliet, 2019). Thus, the formation of gap junctions is a main focus for the characterization of cardiac organoids since they are the main mechanism for electrical conduction in the cardiac tissue. One of the main gap junction proteins, expressed both by CMs and CFs, is connexin 43 (Cx43). Therefore, IHC co-staining of SAA and Cx43 was used to visualize the expression and localization of gap junctions in relation to the position of the cardiac cells (**Figure 4.3 E**). We observed that the expression of Cx43 does not present a specific pattern within the cardiac organoids, and it follows the arbitrary arrangement of the cells. Additionally, based on qualitative evaluation, there is no significant difference in the expression levels of Cx43 between experimental groups (**Figure 4.3 E, bottom**). This was further confirmed by gene expression analysis of the GJA1 gene (**Figure 4.4 A**). Overall, we demonstrated the formation to cell-cell adhesions through SAA and Cx43 co-staining, confirming our hypothesis for the aggregation and interaction of the cardiac cells.

4.4.4 Transcriptional profile of the cardiac organoids

The evaluation of the effects of coculture conditions and nutrient starvation at the transcriptional level was performed through qRT-PCR. We selected a panel of 12 genes relevant for cardiac structure (ACTN2, GJA1, MYH6, MYH7, TNNT2, TNNI3, MLC2V, and MLC2A) and genes involved in electrophysiological function and calcium (Ca^{2+}) handling (RYR2, SERCA, CASQ2, and S100A1). The cardiac organoids were harvested on day 7 after seeding and dissociated to extract the total mRNA. In order to include the effects of the nutrient deprivation in the hiPSC-CMs, the gene expression was normalized to a 2D cellular population on the day when the nutrient deprivation was started (D-1). Additionally, each group was matched to a D-1 control with similar cellular composition (i.e., monoculture and coculture conditions). We found that the B27C and SFC conditions presented a higher expression of most of these genes when compared to their monoculture counterpart (**Figure 4.4 A**). Specifically, we found statistically significant higher expression of MYH7, MLC2A, and MLC2V (only for SFC).

Even when the expression was significantly higher for coculture groups, when compared to the gene expression levels of D-1, there was an overall downregulation of most of CMs structural genes, for example GJA1, and MYH7 (**Figure 4.4 A, first and second columns**). The downregulation of some these genes when the hiPSC-CMs are exposed to a 3D microenvironment have also been reported previously such as GJA1, MYH6, and MYH7 (Takada et al., 2022). For example, GJA1 is the gene in charge for the transcription of Cx43, and as previously discussed, organized localization and translocation of Cx43 to the cell membrane allows for the formation of a 3D syncytium that allows for electrical signal propagation (Biendarra-Tiegs, Clemens, Secreto, & Nelson, 2020). The

downregulation of this and other genes in cardiac organoids has been attributed to the simplicity of monoculture and coculture models as well as to a transcriptomic shift related to the 3D microenvironment and the relative immaturity of the hiPSC-derived cells (Kerr, Richards, Menick, Deleon-Pennell, & Mei, 2021).

On the other hand, the majority of Ca^{2+}-handling genes, such as RYR2, SERCA, and S100A1, were upregulated for all experimental conditions, with no significant differences among the groups (**Figure 4.4 A, third column**). This may be an indication that a 3D microenvironment is sufficient for promoting an enhanced electrophysiological phenotype of the hiPSC-CMs. Additionally, upregulation of RYR2 has been correlated to a more mature hiPSC-CMs (Jiang et al., 2018).

The relative expression of each gene, compared to the other experimental groups was further evaluated through the calculation of the row Z-score (**Figure 4.4 B**). We found that coculture groups (B27C and SFC) presented a relatively higher expression of the cardiac-relevant genes. This is a consequence of several factors. On one hand, the combination of 3D microenvironment and the coculture with hiPSC-CFs has been demonstrated to promote ECM organization (Kerr et al., 2021), providing mechanical support and anchorage for the hiPSC-CMs. This mechanical support serves several purposes, for instance, cell-to-ECM interactions and adhesion points can provide positive feedback to the intracellular structure of the hiPSC-CMs (Valdoz et al., 2021) and therefore inducing improved sarcomeric machinery. Additionally, the secretion of growth factors and other chemical cues, along with the cell-to-cell coupling, promotes improved intercellular interactions, inducing enhanced maturation of the hiPSC-CMs through paracrine signaling and crosstalk (Kerr et al., 2021). These findings are aligned with the

rapid cardiac organoid compaction for our coculture experimental conditions, that we described during the morphological characterization of our ECTs.

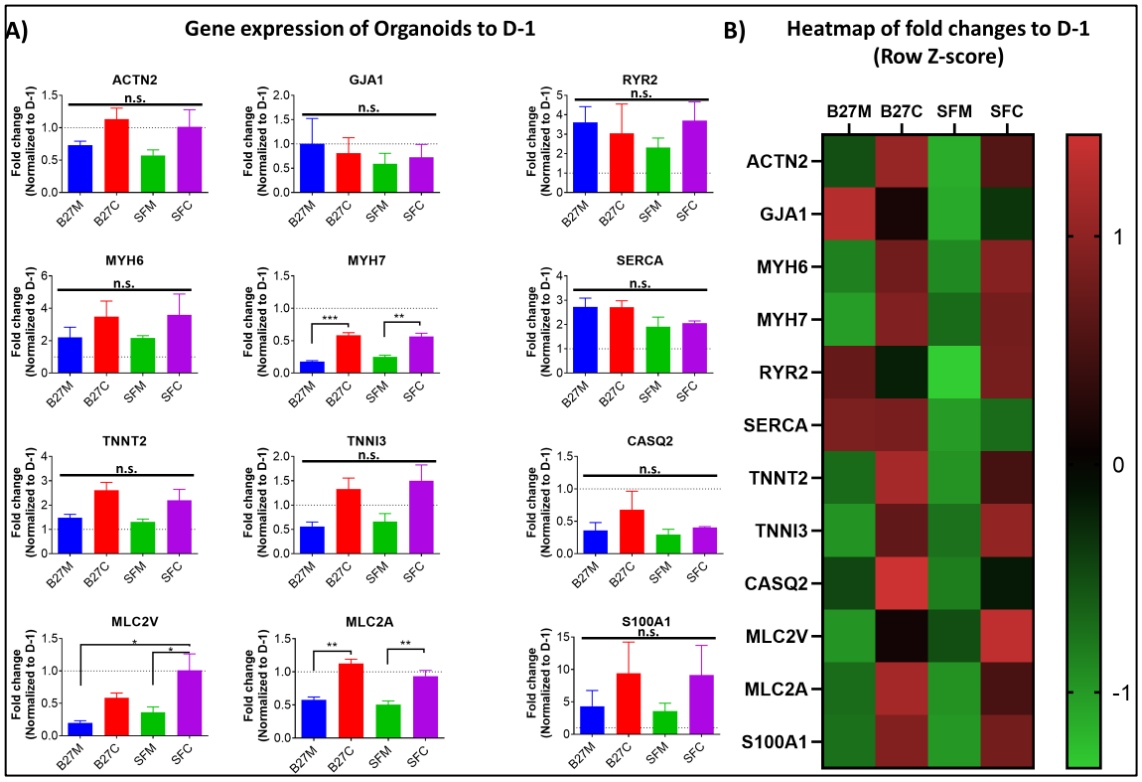

Figure 4.4. Gene expression profile of the isogenic cardiac organoids on day 7 after seeding. A) Fold-change values of a panel of 12 cardiac-relevant genes, evaluated through qRT-PCR. All the results from the experimental conditions were compared to the day before starting the supplement starvation (namely, D-1). One-way ANOVA was performed for finding statistical differences (n.s.=P-value>0.05, *=P-value≤0.05, **=P-value≤0.01, ***=P-value≤0.001). B) Heatmap for Z-score of gene expression of cardiac-relevant genes. A trend for higher expression on the coculture conditions is shown.

The presented qRT-PCR analyses enabled us to assess some of the key gene regulation as function of supplement starvation and coculture groups. Although, to broaden the gene expression evaluation utilizing more modern comprehensive, such as RNA-seq may be required in future work. With this we expect to evaluate not only the structural conformation of the cardiac organoids, but also address other aspects of these ECTs, such

as metabolic shifting and a closer assessment of the crosstalk between different cardiac cells.

4.4.5 Electrophysiological characterization of the cardiac organoids

The electrophysiological character of ECTs is paramount in increasing utility of cardiac organoids in a myriad of applications.(Choi, Lee, Rajaraman, & Kim, 2021) For example, the ability to recapitulate the action potentials of the native heart *in vitro* can facilitate the evaluation of the proarrhythmic effect of drugs and small molecules, resulting in better *in vitro* systems for disease modeling and drug screening (Kussauer, David, & Lemcke, 2019; Stella Stoter, Hirt, Stenzig, & Weinberger, 2020). When these models are created in combination with patient derived-hiPSCs, they can lead to personalized diagnosis and treatments (Choi et al., 2021). Furthermore, understanding the electrical properties of cardiac organoids can help elucidate the mechanisms for coupling and engraftment to native tissue for cardiac regeneration applications. However, the electrophysiological evaluation of 3D cardiac microtissues is not trivial due to their size and geometry. Here we have used an MEA platform for recording the extracellular field potentials (FPs) on the surface of the cardiac organoids. Evaluation of the electrophysiological characteristics of cardiac organoids under supplement starvation regimen has never been described before, to the best of our knowledge. Thus, the focus of the FPs evaluation is only on the SFM and SFC groups.

First, the cardiac organoids were harvested 7 days after seeding in the agarose microwells and placed on the MEA wells. The microtissues were left undisturbed for at least 24 hours to allow for recovery. After this period the FPs from the spontaneous beating were recorded (**Figure 4.5 A**). In order to promote cellular adhesions to the glass surface

of the MEA and to guarantee contact of the organoids with the microelectrodes the surface of the MEAs were coated with Matrigel. The surface treatment provided adhesion points to the cells in the microtissues that prevented the cardiac organoids from remaining in suspension and promoted a good contact between the tissues and the microelectrodes.

We observed that 24 hours after seeding on the MEAs, the cardiac organoids were attached to the surface and some cells started to spread from the microtissues (**Figure 4.5 B**). Additionally, the cardiac organoids presented spontaneous beating after the recovery period (**Videos B8 and B9**). The FPs from this spontaneous beating was recorded with the Intan stimulation/recording controller (**Figure B5A**).

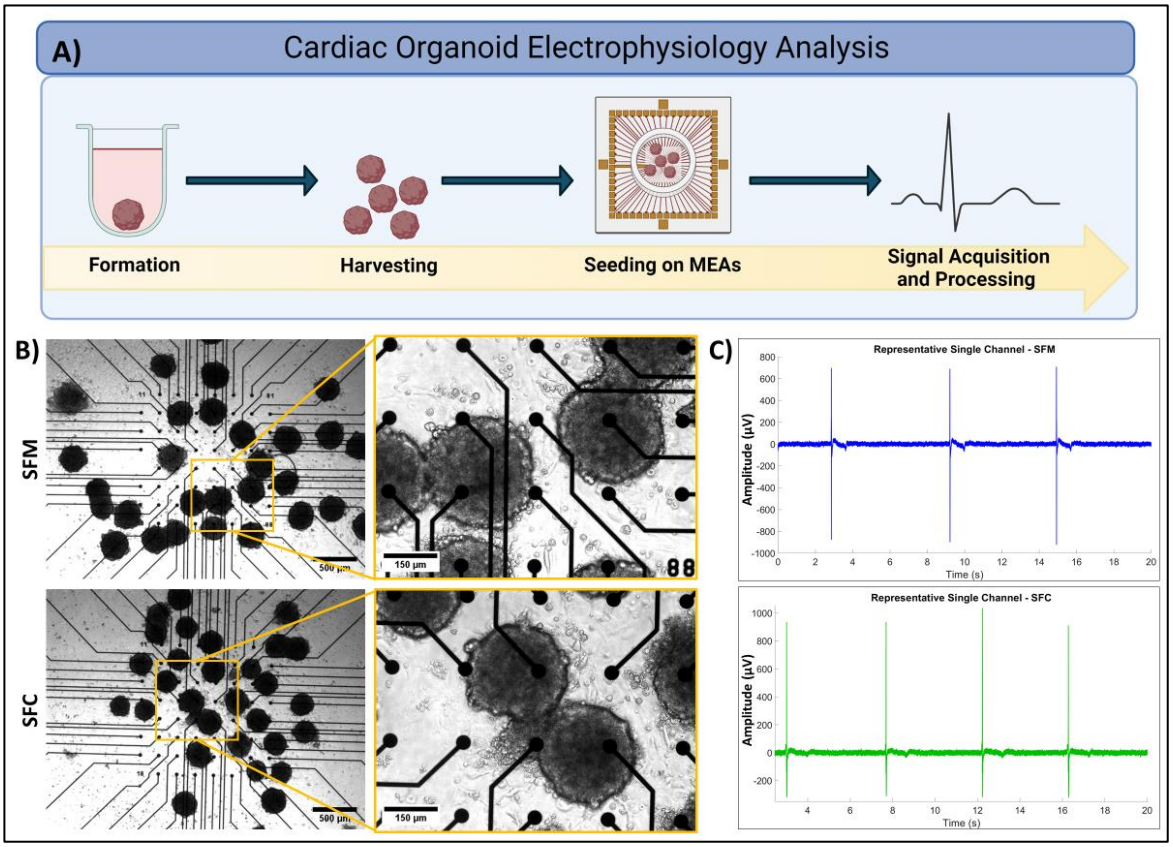

Figure 4.5. Electrophysiological characterization of cardiac organoids using MEAs. A) Schematic representation of the methodology for the acquisition of the FPs from the cardiac organoids harvested on day 7 after seeding (created with Biorender.com) B) Representative phase-contrast images of cardiac organoids seeded on MEAs (left: 2.5x, right:10x; scale

bars: 500µm and 150µm respectively). C) Representative FPs acquired from the cardiac organoids.

The recorded signals consisted of a total of 60 channels, corresponding to each of the MEAs recording electrodes and the reference electrode. The FPs were recorded for periods of 20 seconds and presented the typical waveform of cardiac FPs (**Figure 4.5 C, Figure B6 and Figure B7**) (Kussauer et al., 2019). In order to facilitate the visualization of the FPs, and moreover to correlate specific MEAs channels to the positioning of the cardiac organoids, we created heatmaps that represent the spatial localization of each electrode. This heatmaps represent features of the FPs that are paramount for the electrophysiological characterization of ECTs; for example, the FPs peak-to-peak amplitude, and maximum and minimum values for each channel (H. Kim, Kamm, Vunjak-Novakovic, & Wu, 2022; Kussauer et al., 2019). By overlaying these heatmaps on phase-contrast images of the corresponding groups (**Figure 4.6 A**), we were able to identify the areas that presented the higher electrophysiological activity, allowing us to select ROIs for further signal processing. Additionally, we integrated these heatmaps and the acquired FPs to create videos of each of our experimental samples (**Figure 4.6 B and Video B10 and B11,** the videos are shown at 0.5x speed to help with the visualization of the spontaneous beating). With this we have created a powerful tool to provide information about the spatiotemporal electrophysiological activity of the cardiac organoids seeded on the MEAs platform, which can offer more information about the activity of individual organoids in relation with neighboring organoids and the overall tissue synchronicity.

The signals selected from ROIs were further processed in order to calculate the average CV for each experimental condition (**Figure B8A and B8B**). With this approach we proposed a straightforward method for calculating the CV of the cardiac organoids

produced under supplement starvation regimen. We found CV values of 9.99±1.07 cm/s and 6.20±0.62 cm/s for the SFM and SFC organoids, respectively. Although the CV of the evaluated conditions was not significantly different (p=0.0918), we found a trend for a decreased signal propagation velocity in the SFC group (**Figure 4.6C**). This trend is in agreement with the rapid cellular aggregation and tissue compaction described earlier and is indicative of intercellular interactions between hiPSC-CMs and hiPSC-CFs. For example, it has been reported that CFs can electrically isolate the CMs in the tissue and obstructing the propagation of electrical signaling (Vasquez, Benamer, & Morley, 2011); thus, impeding a fast signal propagation and leading to a decreased CV. Also, it has been observed that this interference is dependent on the CFs density (Hall, Gehmlich, Denning, & Pavlovic, 2021).

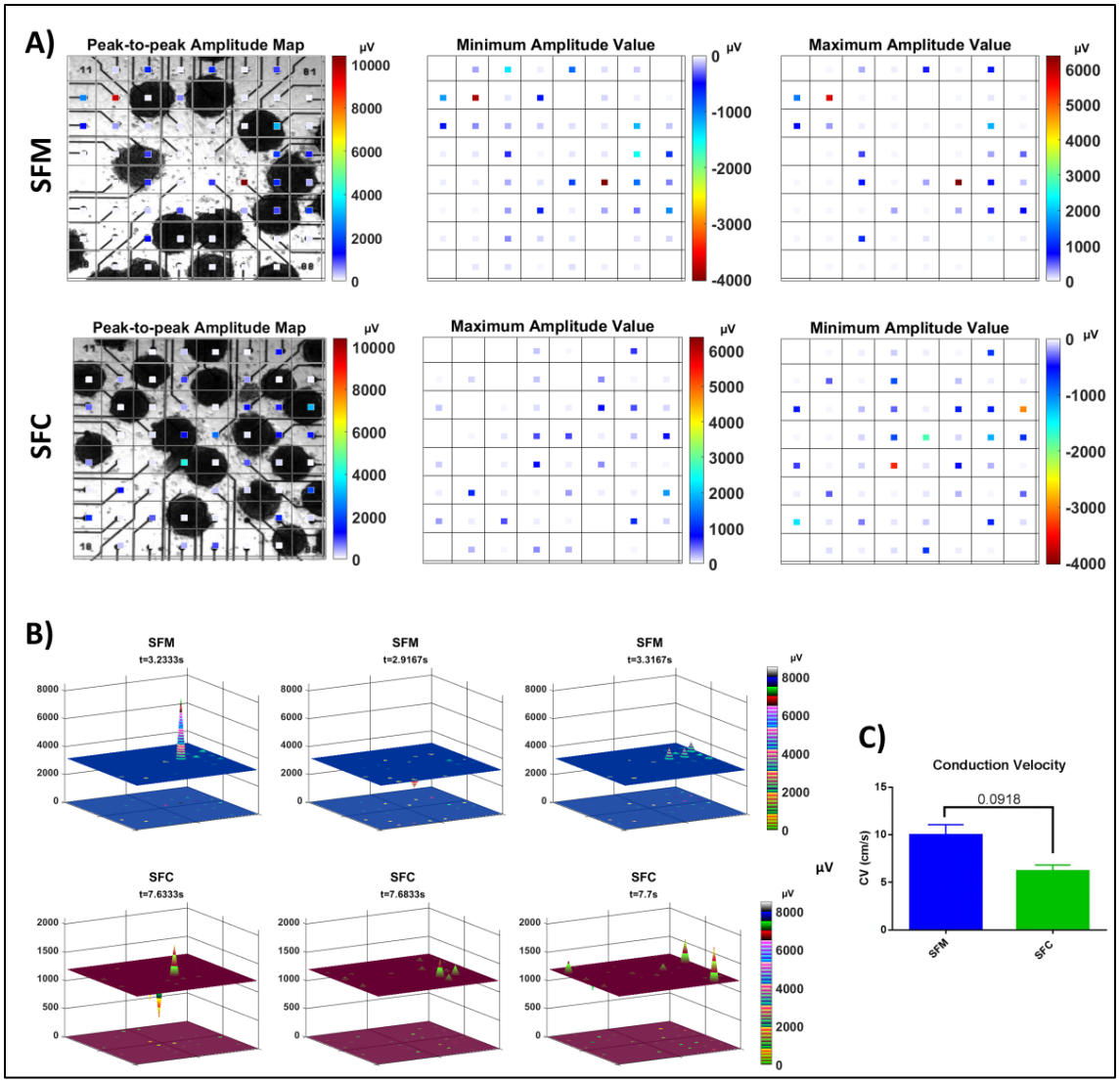

Figure 4.6. Evaluation of electrophysiological features of cardiac organoids from FPs. A) Heatmaps of the peak-to-peak amplitude, maximum and minimum values of the FPs acquired with each individual channel of the MEA platform. The heatmaps were overlaid on phase-contrast images to show the localization of individual cardiac organoids. B) Representative frames of the FPs amplitude videos generated from the acquired signals, extracted from **Video S10** and **Video S11**, respectively. C) CV values for each of the analyzed experimental conditions. (p-value for significance: 0.05).

Based on previous evidence, organoids enriched with hiPSC-CFs present a complex electromechanical behavior. On one hand, CFs provide mechanical and chemical cues that are important for cellular survival and maturation (Kerr et al., 2021; Valdoz et al., 2021). Also, it has been reported that CFs present conductance and membrane potential different

from those of the CMs, influencing in the overall electrical conduction of cardiac tissues (Bazhutina et al., 2021). In consequence, it was expected that our coculture experimental group showed a slower conduction velocity. These findings highlight the importance of an optimized coculture cellular ratio that can support the mechanical and chemical environment of the scaffold-free tissues, but also, do not hinder the desired electrophysiological properties of the organoids (H. Saini et al., 2015). The extraction of other features from the acquired signals, such as waveform, and plateau time are subject of future work. This will lead to a better understanding and characterization of the electrical properties of the cardiac organoids.

4.5 CONCLUSION

In this study we presented the formation of scaffold-free isogenic cardiac organoids derived from hiPSCs under a supplement starvation regimen. We demonstrated that the presence of hiPSC-CFs in the cardiac organoids significantly improved structural and physiological features of the cardiac organoids. This is reflected in enhanced gene expression of cardiac-relevant genes and improved morphology. These results are in alignment with the outcome of other isogenic and non-isogenic cardiac organoids reported in the literature (Beauchamp et al., 2020; Beauchamp et al., 2015; Campostrini et al., 2021). In summary, there is a consensus that co-culture cellular populations are beneficial to enhance maturation and other features of the cardiac organoids.

Additionally, we found a trend for decreased CV that appears to be related to the presence of hiPSC-CFs, but this requires further investigation. We showed a modest improvement with the proposed supplement-free regimen, supporting the need of further optimization of the conditions of nutrient deprivation to improve the functionality of

scaffold-free cardiac tissues. We confirmed that the inclusion of hiPSC-CFs in the cardiac organoids affects not only the morphology of the engineered tissues and their transcriptomic profile, but it also has an effect in the electrical behavior of the organoids. This trend is sufficient evidence to pursue a more thorough investigation regarding the features derived from the acquired FPs. Additionally, our approach demonstrates a straightforward method for a fast and simple evaluation of the basic electrophysiological characteristics of scaffold-free 3D cardiac organoids. The outcome of this study could be potentially utilized for the development of more physiologically relevant cardiac tissue models for disease modeling, drug testing and regenerative medicine applications (H. Kim et al., 2022; Y. Liu et al., 2022; Sakalem, De Sibio, da Costa, & de Oliveira, 2021).

4.6 REFERENCES

Bazhutina, A., Balakina-Vikulova, N. A., Kursanov, A., Solovyova, O., Panfilov, A., & Katsnelson, L. B. (2021). Mathematical modelling of the mechano-electric coupling in the human cardiomyocyte electrically connected with fibroblasts. *Prog Biophys Mol Biol, 159*, 46-57. doi:10.1016/j.pbiomolbio.2020.08.003

Beauchamp, P., Jackson, C. B., Ozhathil, L. C., Agarkova, I., Galindo, C. L., Sawyer, D. B., . . . Zuppinger, C. (2020). 3D Co-culture of hiPSC-Derived Cardiomyocytes With Cardiac Fibroblasts Improves Tissue-Like Features of Cardiac Spheroids. *Frontiers in Molecular Biosciences, 7*. doi:10.3389/fmolb.2020.00014

Beauchamp, P., Moritz, W., Kelm, J. M., Ullrich, N. D., Agarkova, I., Anson, B. D., . . . Zuppinger, C. (2015). Development and Characterization of a Scaffold-Free 3D Spheroid Model of Induced Pluripotent Stem Cell-Derived Human Cardiomyocytes. *Tissue Engineering Part C: Methods, 21*(8), 852-861. doi:10.1089/ten.tec.2014.0376

Biendarra-Tiegs, S. M., Clemens, D. J., Secreto, F. J., & Nelson, T. J. (2020). Human Induced Pluripotent Stem Cell-Derived Non-Cardiomyocytes Modulate Cardiac Electrophysiological Maturation Through Connexin 43-Mediated Cell-Cell Interactions. *Stem Cells Dev, 29*(2), 75-89. doi:10.1089/scd.2019.0098

Binah, O., Dolnikov, K., Sadan, O., Shilkrut, M., Zeevi-Levin, N., Amit, M., . . . Itskovitz-Eldor, J. (2007). Functional and developmental properties of human embryonic stem cells-derived cardiomyocytes. *J Electrocardiol, 40*(6 Suppl), S192-196. doi:10.1016/j.jelectrocard.2007.05.035

Brewer, G. J., & Cotman, C. W. (1989). Survival and growth of hippocampal neurons in defined medium at low density: advantages of a sandwich culture technique or low oxygen. *Brain Research, 494*(1), 65-74. doi:10.1016/0006-8993(89)90144-3

Brewer, G. J., Torricelli, J. R., Evege, E. K., & Price, P. J. (1993). Optimized survival of hippocampal neurons in B27-supplemented Neurobasal, a new serum-free medium combination. *J Neurosci Res, 35*(5), 567-576. doi:10.1002/jnr.490350513

Campostrini, G., Meraviglia, V., Giacomelli, E., van Helden, R. W. J., Yiangou, L., Davis, R. P., . . . Mummery, C. L. (2021). Generation, functional analysis and applications of isogenic three-dimensional self-aggregating cardiac microtissues from human pluripotent stem cells. *Nat Protoc, 16*(4), 2213-2256. doi:10.1038/s41596-021-00497-2

Carmeliet, E. (2019). Conduction in cardiac tissue. Historical reflections. *Physiological Reports, 7*(1), e13860. doi:https://doi.org/10.14814/phy2.13860

Choi, J. S., Lee, H. J., Rajaraman, S., & Kim, D. H. (2021). Recent advances in three-dimensional microelectrode array technologies for in vitro and in vivo cardiac and neuronal interfaces. *Biosens Bioelectron, 171*, 112687. doi:10.1016/j.bios.2020.112687

Correia, C., Koshkin, A., Duarte, P., Hu, D., Teixeira, A., Domian, I., . . . Alves, P. M. (2017). Distinct carbon sources affect structural and functional maturation of cardiomyocytes derived from human pluripotent stem cells. *Sci Rep, 7*(1), 8590. doi:10.1038/s41598-017-08713-4

Daghero, H., Doffe, F., Varela, B., Yozzi, V., Verdes, J. M., Crispo, M., . . . Pagotto, R. (2022). Jejunum-derived NF-κB reporter organoids as 3D models for the study of TNF-alpha-induced inflammation. *Scientific Reports, 12*(1), 14425. doi:10.1038/s41598-022-18556-3

Doyle, M. J., Lohr, J. L., Chapman, C. S., Koyano-Nakagawa, N., Garry, M. G., & Garry, D. J. (2015). Human Induced Pluripotent Stem Cell-Derived Cardiomyocytes as a Model for Heart Development and Congenital Heart Disease. *Stem Cell Rev Rep, 11*(5), 710-727. doi:10.1007/s12015-015-9596-6

Esmaeili, H., Patino-Guerrero, A., Hasany, M., Ansari, M. O., Memic, A., Dolatshahi-Pirouz, A., & Nikkhah, M. (2022). Electroconductive biomaterials for cardiac tissue engineering. *Acta Biomater, 139*, 118-140. doi:10.1016/j.actbio.2021.08.031

Fan, C., Tang, Y., Zhao, M., Lou, X., Pretorius, D., Menasche, P., . . . Zhang, J. (2020). CHIR99021 and fibroblast growth factor 1 enhance the regenerative potency of human cardiac muscle patch after myocardial infarction in mice. *J Mol Cell Cardiol, 141*, 1-10. doi:10.1016/j.yjmcc.2020.03.003

Fan, D., Takawale, A., Lee, J., & Kassiri, Z. (2012). Cardiac fibroblasts, fibrosis and extracellular matrix remodeling in heart disease. *Fibrogenesis Tissue Repair, 5*(1), 15. doi:10.1186/1755-1536-5-15

Fennema, E., Rivron, N., Rouwkema, J., van Blitterswijk, C., & de Boer, J. (2013). Spheroid culture as a tool for creating 3D complex tissues. *Trends in Biotechnology, 31*(2), 108-115. doi:https://doi.org/10.1016/j.tibtech.2012.12.003

Gomez-Garcia, M. J., Quesnel, E., Al-Attar, R., Laskary, A. R., & Laflamme, M. A. (2021). Maturation of human pluripotent stem cell derived cardiomyocytes in vitro and in vivo. *Semin Cell Dev Biol, 118*, 163-171. doi:10.1016/j.semcdb.2021.05.022

Hall, C., Gehmlich, K., Denning, C., & Pavlovic, D. (2021). Complex Relationship Between Cardiac Fibroblasts and Cardiomyocytes in Health and Disease. *J Am Heart Assoc, 10*(5), e019338. doi:10.1161/JAHA.120.019338

Jiang, Y., Park, P., Hong, S. M., & Ban, K. (2018). Maturation of Cardiomyocytes Derived from Human Pluripotent Stem Cells: Current Strategies and Limitations. *Molecules and cells, 41*(7), 613-621. doi:10.14348/molcells.2018.0143

Kang, S.-M., Kim, D., Lee, J.-H., Takayama, S., & Park, J. Y. (2021). Engineered Microsystems for Spheroid and Organoid Studies. *Advanced Healthcare Materials, 10*(2), 2001284. doi:https://doi.org/10.1002/adhm.202001284

Kerr, C. M., Richards, D., Menick, D. R., Deleon-Pennell, K. Y., & Mei, Y. (2021). Multicellular Human Cardiac Organoids Transcriptomically Model Distinct Tissue-Level Features of Adult Myocardium. *Int J Mol Sci, 22*(16). doi:10.3390/ijms22168482

Khammanit, R., Chantakru, S., Kitiyanant, Y., & Saikhun, J. (2008). Effect of serum starvation and chemical inhibitors on cell cycle synchronization of canine dermal fibroblasts. *Theriogenology, 70*(1), 27-34. doi:10.1016/j.theriogenology.2008.02.015

Khan, M. A., Hashim, M. J., Mustafa, H., Baniyas, M. Y., Al Suwaidi, S. K. B. M., AlKatheeri, R., . . . Al Darmaki, R. S. (2020). Global epidemiology of ischemic heart disease: results from the global burden of disease study. *Cureus, 12*(7).

Kim, H., Kamm, R. D., Vunjak-Novakovic, G., & Wu, J. C. (2022). Progress in multicellular human cardiac organoids for clinical applications. *Cell Stem Cell, 29*(4), 503-514. doi:10.1016/j.stem.2022.03.012

Kopanja, L., Kralj, S., Zunic, D., Loncar, B., & Tadic, M. (2016). Core–shell superparamagnetic iron oxide nanoparticle (SPION) clusters: TEM micrograph analysis, particle design and shape analysis. *Ceramics International, 42*(9), 10976-10984. doi:https://doi.org/10.1016/j.ceramint.2016.03.235

Kussauer, S., David, R., & Lemcke, H. (2019). hiPSCs Derived Cardiac Cells for Drug and Toxicity Screening and Disease Modeling: What Micro- Electrode-Array Analyses Can Tell Us. *Cells, 8*(11). doi:10.3390/cells8111331

Lian, X., Zhang, J., Azarin, S. M., Zhu, K., Hazeltine, L. B., Bao, X., . . . Palecek, S. P. (2013). Directed cardiomyocyte differentiation from human pluripotent stem cells by modulating Wnt/beta-catenin signaling under fully defined conditions. *Nat Protoc, 8*(1), 162-175. doi:10.1038/nprot.2012.150

Liu, Y., Zhang, Y., Mei, T., Cao, H., Hu, Y., Jia, W., . . . Liu, Z. (2022). hESCs-Derived Early Vascular Cell Spheroids for Cardiac Tissue Vascular Engineering and Myocardial Infarction Treatment. *Advanced Science, 9*(9), 2104299. doi:https://doi.org/10.1002/advs.202104299

Martin, T. G., & Kirk, J. A. (2020). Under construction: The dynamic assembly, maintenance, and degradation of the cardiac sarcomere. *J Mol Cell Cardiol, 148*, 89-102. doi:10.1016/j.yjmcc.2020.08.018

Napiwocki, B. N., Lang, D., Stempien, A., Zhang, J., Vaidyanathan, R., Makielski, J. C., . . . Crone, W. C. (2021). Aligned human cardiac syncytium for in vitro analysis of electrical, structural, and mechanical readouts. *Biotechnology and Bioengineering, 118*(1), 442-452. doi:https://doi.org/10.1002/bit.27582

Navaei, A., Moore, N., Sullivan, R. T., Truong, D., Migrino, R. Q., & Nikkhah, M. (2017). Electrically conductive hydrogel-based micro-topographies for the development of organized cardiac tissues. *RSC advances, 7*(6), 3302-3312.

Navaei, A., Rahmani Eliato, K., Ros, R., Migrino, R. Q., Willis, B. C., & Nikkhah, M. (2019). The influence of electrically conductive and non-conductive nanocomposite scaffolds on the maturation and excitability of engineered cardiac tissues. *Biomater Sci, 7*(2), 585-595. doi:10.1039/c8bm01050a

Navaei, A., Saini, H., Christenson, W., Sullivan, R. T., Ros, R., & Nikkhah, M. (2016). Gold nanorod-incorporated gelatin-based conductive hydrogels for engineering cardiac tissue constructs. *Acta Biomater, 41*, 133-146. doi:10.1016/j.actbio.2016.05.027

Nguyen, A. H., Marsh, P., Schmiess-Heine, L., Burke, P. J., Lee, A., Lee, J., & Cao, H. (2019). Cardiac tissue engineering: state-of-the-art methods and outlook. *Journal of Biological Engineering, 13*(1), 57. doi:10.1186/s13036-019-0185-0

Nikkhah, M., Akbari, M., Paul, A., Memic, A., Dolatshahi-Pirouz, A., & Khademhosseini, A. (2016). Gelatin-Based Biomaterials For Tissue Engineering And Stem Cell Bioengineering. *Biomaterials from Nature for Advanced Devices and Therapies*, 37-62. doi:https://doi.org/10.1002/9781119126218.ch3

Nugraha, B., Buono, M. F., von Boehmer, L., Hoerstrup, S. P., & Emmert, M. Y. (2019). Human Cardiac Organoids for Disease Modeling. *Clin Pharmacol Ther, 105*(1), 79-85. doi:10.1002/cpt.1286

Ogasawara, T., Okano, S., Ichimura, H., Kadota, S., Tanaka, Y., Minami, I., . . . Shiba, Y. (2017). Impact of extracellular matrix on engraftment and maturation of pluripotent stem cell-derived cardiomyocytes in a rat myocardial infarct model. *Sci Rep, 7*(1), 8630. doi:10.1038/s41598-017-09217-x

Pasqualini, F. S., Sheehy, S. P., Agarwal, A., Aratyn-Schaus, Y., & Parker, K. K. (2015). Structural phenotyping of stem cell-derived cardiomyocytes. *Stem Cell Reports, 4*(3), 340-347. doi:10.1016/j.stemcr.2015.01.020

Patino-Guerrero, A., Veldhuizen, J., Zhu, W., Migrino, R. Q., & Nikkhah, M. (2020). Three-dimensional scaffold-free microtissues engineered for cardiac repair. *J Mater Chem B, 8*(34), 7571-7590. doi:10.1039/d0tb01528h

Phelan, M. A., Gianforcaro, A. L., Gerstenhaber, J. A., & Lelkes, P. I. (2019). An Air Bubble-Isolating Rotating Wall Vessel Bioreactor for Improved Spheroid/Organoid Formation. *Tissue Engineering Part C: Methods, 25*(8), 479-488. doi:10.1089/ten.tec.2019.0088

Pinto, A. R., Ilinykh, A., Ivey, M. J., Kuwabara, J. T., D'Antoni, M. L., Debuque, R., . . . Tallquist, M. D. (2016). Revisiting Cardiac Cellular Composition. *Circ Res, 118*(3), 400-409. doi:10.1161/CIRCRESAHA.115.307778

Radisic, M., Deen, W., Langer, R., & Vunjak-Novakovic, G. (2005). Mathematical model of oxygen distribution in engineered cardiac tissue with parallel channel array perfused with culture medium containing oxygen carriers. *Am J Physiol Heart Circ Physiol, 288*(3), H1278-1289. doi:10.1152/ajpheart.00787.2004

Radisic, M., Park, H., Gerecht, S., Cannizzaro, C., Langer, R., & Vunjak-Novakovic, G. (2007). Biomimetic approach to cardiac tissue engineering. *Philosophical transactions of the Royal Society of London. Series B, Biological sciences, 362*(1484), 1357-1368. doi:10.1098/rstb.2007.2121

Robertson, C., Tran, D. D., & George, S. C. (2013). Concise review: maturation phases of human pluripotent stem cell-derived cardiomyocytes. *Stem Cells, 31*(5), 829-837. doi:10.1002/stem.1331

Roche, C. D., Brereton, R. J. L., Ashton, A. W., Jackson, C., & Gentile, C. (2020). Current challenges in three-dimensional bioprinting heart tissues for cardiac surgery. *Eur J Cardiothorac Surg, 58*(3), 500-510. doi:10.1093/ejcts/ezaa093

Roth, G. A., Mensah, G. A., Johnson, C. O., Addolorato, G., Ammirati, E., Baddour, L. M., . . . Group, G.-N.-J. G. B. o. C. D. W. (2020). Global Burden of Cardiovascular Diseases and Risk Factors, 1990-2019: Update From the GBD 2019 Study. *J Am Coll Cardiol, 76*(25), 2982-3021. doi:10.1016/j.jacc.2020.11.010

Sadayappan, S., & de Tombe, P. P. (2012). Cardiac myosin binding protein-C: redefining its structure and function. *Biophys Rev, 4*(2), 93-106. doi:10.1007/s12551-012-0067-x

Saini, H., Navaei, A., Van Putten, A., & Nikkhah, M. (2015). 3D cardiac microtissues encapsulated with the co-culture of cardiomyocytes and cardiac fibroblasts. *Adv Healthc Mater, 4*(13), 1961-1971. doi:10.1002/adhm.201500331

Sakalem, M. E., De Sibio, M. T., da Costa, F. A. d. S., & de Oliveira, M. (2021). Historical evolution of spheroids and organoids, and possibilities of use in life sciences and medicine. *Biotechnology Journal*, *16*(5), 2000463. doi:https://doi.org/10.1002/biot.202000463

Snir, M., Kehat, I., Gepstein, A., Coleman, R., Itskovitz-Eldor, J., Livne, E., & Gepstein, L. (2003). Assessment of the ultrastructural and proliferative properties of human embryonic stem cell-derived cardiomyocytes. *Am J Physiol Heart Circ Physiol, 285*(6), H2355-2363. doi:10.1152/ajpheart.00020.2003

Souders, C. A., Bowers, S. L., & Baudino, T. A. (2009). Cardiac fibroblast: the renaissance cell. *Circ Res, 105*(12), 1164-1176. doi:10.1161/CIRCRESAHA.109.209809

Stella Stoter, A. M., Hirt, M. N., Stenzig, J., & Weinberger, F. (2020). Assessment of Cardiotoxicity With Stem Cell-based Strategies. *Clin Ther, 42*(10), 1892-1910. doi:10.1016/j.clinthera.2020.08.012

Taddei, M. L., Giannoni, E., Fiaschi, T., & Chiarugi, P. (2012). Anoikis: an emerging hallmark in health and diseases. *J Pathol, 226*(2), 380-393. doi:10.1002/path.3000

Takada, T., Sasaki, D., Matsuura, K., Miura, K., Sakamoto, S., Goto, H., . . . Hagiwara, N. (2022). Aligned human induced pluripotent stem cell-derived cardiac tissue improves contractile properties through promoting unidirectional and synchronous cardiomyocyte contraction. *Biomaterials, 281*, 121351. doi:10.1016/j.biomaterials.2021.121351

Tan, Y., Richards, D., Coyle, R. C., Yao, J., Xu, R., Gou, W., . . . Mei, Y. (2017). Cell number per spheroid and electrical conductivity of nanowires influence the function of silicon nanowired human cardiac spheroids. *Acta Biomater, 51*, 495-504. doi:10.1016/j.actbio.2017.01.029

Tirziu, D., Giordano, F. J., & Simons, M. (2010). Cell communications in the heart. *Circulation, 122*(9), 928-937. doi:10.1161/CIRCULATIONAHA.108.847731

Valdoz, J. C., Johnson, B. C., Jacobs, D. J., Franks, N. A., Dodson, E. L., Sanders, C., . . . Van Ry, P. M. (2021). The ECM: To Scaffold, or Not to Scaffold, That Is the Question. *Int J Mol Sci, 22*(23). doi:10.3390/ijms222312690

Vasquez, C., Benamer, N., & Morley, G. E. (2011). The cardiac fibroblast: functional and electrophysiological considerations in healthy and diseased hearts. *Journal of cardiovascular pharmacology, 57*(4), 380-388. doi:10.1097/FJC.0b013e31820cda19

Veerman, C. C., Kosmidis, G., Mummery, C. L., Casini, S., Verkerk, A. O., & Bellin, M. (2015). Immaturity of human stem-cell-derived cardiomyocytes in culture: fatal flaw or soluble problem? *Stem Cells Dev, 24*(9), 1035-1052. doi:10.1089/scd.2014.0533

Velasco, V., Shariati, S. A., & Esfandyarpour, R. (2020). Microtechnology-based methods for organoid models. *Microsystems & Nanoengineering, 6*(1), 76. doi:10.1038/s41378-020-00185-3

Veldhuizen, J., Chavan, R., Moghadas, B., Park, J. G., Kodibagkar, V. D., Migrino, R. Q., & Nikkhah, M. (2022). Cardiac ischemia on-a-chip to investigate cellular and molecular response of myocardial tissue under hypoxia. *Biomaterials, 281*, 121336. doi:10.1016/j.biomaterials.2021.121336

Veldhuizen, J., Cutts, J., Brafman, D. A., Migrino, R. Q., & Nikkhah, M. (2020b). Engineering anisotropic human stem cell-derived three-dimensional cardiac tissue on-a-chip. *Biomaterials, 256*, 120195. doi:https://doi.org/10.1016/j.biomaterials.2020.120195

Veldhuizen, J., Migrino, R. Q., & Nikkhah, M. (2019). Three-dimensional microengineered models of human cardiac diseases. *J Biol Eng, 13*(1), 29. doi:10.1186/s13036-019-0155-6

Woodcock, E. A., & Matkovich, S. J. (2005). Cardiomyocytes structure, function and associated pathologies. *Int J Biochem Cell Biol, 37*(9), 1746-1751. doi:10.1016/j.biocel.2005.04.011

Yang, J., Ding, N., Zhao, D., Yu, Y., Shao, C., Ni, X., . . . Hu, S. (2021). Intermittent Starvation Promotes Maturation of Human Embryonic Stem Cell-Derived Cardiomyocytes. *Front Cell Dev Biol, 9*, 687769. doi:10.3389/fcell.2021.687769

Yang, X., Pabon, L., & Murry, C. E. (2014). Engineering adolescence: maturation of human pluripotent stem cell-derived cardiomyocytes. *Circ Res, 114*(3), 511-523. doi:10.1161/CIRCRESAHA.114.300558

Zhang, J., Tao, R., Campbell, K. F., Carvalho, J. L., Ruiz, E. C., Kim, G. C., . . . Kamp, T. J. (2019). Functional cardiac fibroblasts derived from human pluripotent stem cells via second heart field progenitors. *Nat Commun, 10*(1), 2238. doi:10.1038/s41467-019-09831-5

CHAPTER 5

ELECTROPHYSIOLOGICAL CHARACTERIZATION OF ISOGENIC CARDIAC ORGANOIDS USING A MICROELECTRODE ARRAY PLATFORM

5.1 ABSTRACT

The high prevalence of cardiovascular diseases (CVDs) has led to the development of in vitro models to increase our knowledge of their mechanisms. Specifically, cardiac tissues have been engineered to serve as models for applications in pharmaceutical research, disease modeling, and regenerative medicine. However, there is still a lack of complete understanding of their electrophysiological features. In recent years, cardiac organoids have surge as promising models for studying CVD, but their size and morphology present a particular challenge for electrophysiological characterization. Proposed methods for studying the electrical features of cardiac organoids include patch-clamp and fluorescence imaging. However, these methods required highly specialized equipment and manipulation, and often do not represent accurately the electrical activity at a tissue level. In this chapter, we expand the discussion on the electrophysiological characterization of cardiac organoids based on the novel approach for the evaluation of the electrophysiological features of cardiac organoids by implementing the use of microelectrode arrays (MEAs) presented in Chapter 3. We describe in-depth the development of specialized code to visualize these FPs and extracted physiological relevant features from these. We finally discussed the developed an algorithm to select regions of interest (ROIs) for the calculation of the conduction velocity (CV) of the cardiac organoids.

5.2 INTRODUCTION

Being cardiovascular diseases (CVDs) the primary cause of deaths around the globe, there is a current unmet need for models that allow the study of CVDs in vitro. Moreover, the existing models are usually not fully characterized, and there is a lack of understanding of physiological relevant characteristics. Recent advances in the field of tissue engineering have led to the creation of engineered tissues that can recapitulate some of the features of the native myocardium (Veldhuizen et al., 2022). Thus, there is a need for better methods and tools that help gain understanding of these physiological-relevant features, specifically those related to the electrical activity of engineered cardiac tissues (ECTs).

Some traditional approaches for acquiring and analyzing electrical signals extracted from cardiac organoids have include patch clamp and optical methods, such as calcium transients imaging (Chung et al., 2022; Joddar et al., 2022; H. Kim et al., 2022; Dylan J. Richards et al., 2020). While these methods provide some insight of the electrical mechanisms leading to the function of the ECTs, they often required specialized equipment and highly trained users.

The use of microelectrode array platforms (MEAs), has been recently proposed as a more modern approach for the electrophysiology analysis of ECTs, and specifically cardiac organoids (Chung et al., 2022). The MEAs systems usually consist of a grid of electrodes encapsulated in a biocompatible (and often transparent) substrate with open recording sites within the micrometer scale (Didier, Kundu, DeRoo, & Rajaraman, 2020). The substrate of the MEA platform serves as a surface for cell and tissue culture. Often,

these surfaces are biofunctionalized in order to serve as a cell-ECM interphase between the MEAs and the tissues or cells. This provide the ECTs with anchorage points on the MEA surface and encourages an intimate contact between the cardiac tissues and the microelectrodes, leading to a more accurate signal recording, and to an improved signal-to-noise ratio. Additionally, transparent substrates allow for the use of optical methods, such as microscopy imaging and video recording. The pairing of microscopy methods with MEA analysis allows for the monitoring of the tissue morphology, and the positioning of the tissues respective to the localization of the microelectrode grid (Simeonov & Schäffer, 2019).

While MEAs have been widely used for the study of brain organoids and brain tissues (Jeong, Choi, & Cho, 2023; J. Kim, Sullivan, & Park, 2021; Tasnim & Liu, 2022), their application in other 3D engineered tissues, such as cardiac organoids, is yet to be further explored. One obstacle for the use of MEAs for exploring electrophysiological features of cardiac organoids is the processing and interpretation of the acquired data. MEAs data recording provides a high temporal resolution, resulting in tens of thousands of data points per second, per electrode. Thus, processing the data resulting from the MEAs recording (i.e., field potentials (FPs)) can be time- and labor-intensive, requiring high computational power (Klempíř et al., 2020). Therefore, there is a pressing need for improved methods, algorithms, and software interfaces that allow for the efficient extraction of relevant features from the acquired FPs.

There has been reports for the use of MEAs for studying some cardiac organoids. However, the organoids used for those studies were limited in their representation of the

human myocardium. For example, some the organoids were generated utilizing a combination of human induced pluripotent stem cell (hiPSC)-derived cardiac cells and primary cells, leading to an inconsistent maturation state of the organoids (Varzideh, Mahmoudi, & Pahlavan, 2019). Also, the cellular composition of the cardiac organoids is not well defined due to the method utilized for their creation (i.e., directed differentiation of embryoid bodies) (S. G. Lee et al., 2022; Lewis-Israeli et al., 2021). These reports have provided some insight regarding some of the electrical features of cardiac organoids and are valuable proof-of-concept studies. However, there is still a need for gaining a better understanding of the electrical features of more physiologically relevant cardiac engineered models. For example, isogenic cardiac organoids with well-defined cellular compositions. Moreover, there is a major need for the development and adaption of approaches that lead to the easy and accurate electrophysiological characterization of these ECTs.

In this dissertation we have used an electrophysiology recording module developed by BMSEED company (Phoenix, AZ), for recording the extracellular field potentials (FPs) on the surface of the cardiac organoids. First, we developed a dedicated MATLAB code that has allowed to visualized important aspects of the FPs, such as peak-to-peak amplitude, and maximums and minimums. These aspects were then integrated in spatial and spatiotemporal heatmaps that represented the spatial organization of individual electrodes within the MEAs. These heatmaps, in combination with phase-contrast imaging, helped us to select regions of interest (ROIs), were the cardiac organoids presented the highest electrical activity. Finally, we proposed a novel algorithm for the calculation of the conduction velocity (CV) of the cardiac organoids. This approach was applied to the electrophysiological evaluation of cardiac organoids with defined cellular composition and

generated under a supplement starvation regimen, as previously reported by our group (Alejandra Patino-Guerrero et al., 2023).

5.3 MATERIALS AND METHODS

5.3.1 Differentiation of hiPSC-derived cardiac cells

Prior the fabrication of the cardiac organoids, the directed differentiation of hiSPC was implemented in order to obtain hiPSC-CMs and hiPSC-CFs, as detailed before (Alejandra Patino-Guerrero et al., 2023). Briefly, hiPSC-CMs were differentiated utilizing an optimized protocol adapted from the GiWi method (X. Lian et al., 2013). This method utilizes small molecules in the absence of insulin to regulate the Wnt canonical pathway, leading the stem cells to a cardiogenic mesoderm fate, and ultimately differentiating into human cardiomyocytes. First, the hiPSCs (IMR90-4, WiCell) were maintained on hESC-Matrigel-coated plates with mTeSR-1 plus media until they reached 80-90% confluency.

Then, on the initial day of the differentiation, the maintenance media was substituted by basal media minus insulin. This media composition was used the first five days of the differentiation and consisted of RPMI 1640 supplemented with 2% B27 minus insulin (Gibco), and 1% Penicillin/Streptomycin (P/S) (Gibco). On the initial day of the differentiation (Day 0), CHIR99021 (7-9µM, BioVision) was supplemented in the basal media minus insulin to activate the Wnt pathway in the hiPSCs. On Day 2, the media was substituted for the basal media minus insulin. In order to deactivate the Wnt pathway, on Day 3, IWP2 (5µM, Sigma) was supplemented in a 1:1 mix of conditioned media and fresh basal media minus insulin. After this, the media was replaced every 48 hours with basal

media, consisting of RPMI 1640, 2% B27, and 1% P/S. The cells typically presented spontaneous beating around Day 9.

On Day 13, glucose starvation was induced in the cell culture in order to increase the purity of the hiPSC-CMs (Binah et al., 2007). For this, the basal media was replaced by glucose-free media, consisting of RPMI 1640 minus glucose, 2% B27, 1% P/S, and sodium lactate (4mM, Sigma); The media was refreshed every 72 hours. After 6 days, the cells were fed with the basal media to allow for recovery. Then, the cells were dissociated using TrypLE Express and replated with a cell density of ~150K cells/cm². The differentiated hiPSC-CMs were maintained with the RPMI 1640 basal media until their use for experiments; the media was changed every 48 hours. In addition to the spontaneous beating, staining for sarcomeric alpha actinin was used as a biomarker to confirm the successful differentiation of the hiPSC-CMs.

For hiPSC-CF, a protocol from (C. Fan et al., 2020) was adapted as follow. Similar to hiPSC-CMs differentiation, the Wnt canonical pathway is regulated to direct the cells into a cardiogenic fate. Thus, on Day 0, when the cells reached ~80% confluency, the cell culture media was substituted by RPMI 1640 media supplemented with CHIR99020 (7μM). 24 hours after, the cell culture was refreshed with basal media minus insulin. Then fibroblast growth factor was introduced in the culture to induce the CFs differentiation. The media formulation for this contained high-glucose DMEM with L-glutamine (4 mM) (Gibco), supplemented with HLL supplement, and β-fibroblast growth factor (β-FGF) (70 ng/μl); this media was refreshed every 48 hrs. On Day 20 the cells were dissociated using 1x Trypsin and seeded on uncoated plates. The hiPSC-CFs were maintained in Fibroblast

Growth Media 3 (FGM-3) and replated every time they reached ~85% confluency. For this study the hiPSC-CFs were used between passages P6 and P12. The hiPSC-CFs differentiation was confirmed with staining using vimentin and the TE-7 (Cell Signaling) antibody (EMD Millipore) as biomarkers.

5.3.2 Fabrication of isogenic cardiac organoids

The fabrication of the isogenic cardiac organoids was based on our previously reported protocol (Alejandra Patino-Guerrero et al., 2023). Briefly, the hiPSC-CMs were submitted to a supplement starvation regime for 24 hours prior their use for organoid fabrication; then, hiPSC-CMs and hiPSC-CFs were dissociated. Two different experimental groups were created for this study, as follows:

- SFM: Monoculture, 100% hiPSC-CMs.
- SFC: Coculture, 70% hiPSC-CMs and 30% hiPSC-CFs.

Agarose microwells were casted using commercially available silicone molds (Microtissues) and deposited in 24-well plates. These microwells had dimensions of 800µm depth and 80µm diameter in which the cells were deposited at a cell density of 5K cells per well. After seeding, the cells were left undisturbed for one hour to allow them to sediment to the bottom of the microwells. Then the wells were filled with 1 ml of RPMI 1640/B27 basal media, and the media was refreshed every 48 hours until the end of the experiment.

After seven days in the agarose microwells, the cardiac organoids were collected by gently pipetting media up and down. Then, the organoids were collected in a

microcentrifuge tube and were allowed to sediment. The supernatant was removed and replaced with 1x DPBS in order to remove any cellular debris, this step was repeated twice. Finally, the 1x DPBS was replaced again with basal cell culture media.

5.3.3 Seeding cardiac organoids on MEAs

The fabricated cardiac organoids were seeded in a glass microelectrode array (MEA) platform (Naturmedizinisches Institute (NMI) of the University of Tubingen), consisting of 60 electrodes arranged in an 8x8 grid. The MEA was sterilized by UV radiation for at leas 1 hour. Then the glass surface was coated with Matrigel (Corning). Approximately 35 organoids were seeded per each MEA and were incubated for at least 24 hours before FPs acquisition to allow for the recovery of the microtissues.

5.3.4 MEA signal acquisition

The electrophysiology module with temperature control developed by BMSEED LLC (**Figure 5.1**) was used to record the FPs generated by the spontaneous beating for the cardiac organoids. The signals were acquired for 20 to 30 seconds, with a sampling rate of 30 kHz. After FPs recording, phase-contrast images of the MEAs with the cardiac organoids were obtained (Zeiss Axio Observer Z1 microscope and ZenPro software).

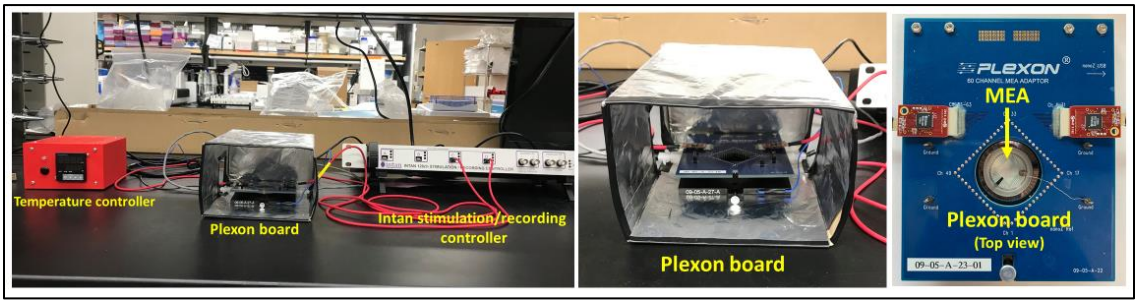

Figure 5.1. Electrophysiology equipment setup. A) System setup for the FP signal acquisition of the cardiac organoids, showing the temperature controller, the plexon board,

and the Intan stimulation/recording controller. *Adapted with permission from Alejandra Patino-Guerrero et al. (2023). Copyright 2023 American Chemical Society.*

5.3.5 MEA spatiotemporal heatmaps creation

In order to provide with a condensed visualization of the acquired FPs from the cardiac organoids, heatmaps were created. In correlation with phase contrast images of the MEAs, the heatmaps served as a tool for selecting regions of interest (ROIs). Thus, a custom MATLAB code was utilized to process the acquired signals and to generate the heatmaps. Detailed MATLAB code can be consulted in the **APPENDIX C.** Briefly, the "peak2peak", "min", and "max" functions were utilized to calculate the peak-to-peak amplitude and the minimum and maximum values for each of the individual channels corresponding to the MEAs electrodes. Then, a grid comprised of 8x8 squares was created to simulate the spatial configuration of the electrodes. A correlation matrix was created in order to associate the values of the MEA individual channels to their corresponding location in the 8x8 grid. The function "imagesc" was used in order to represent the calculated values as specific colors within a custom MATLAB color scale (**APPENDIX C**). Finally, the calculated values were plotted in the 8x8 grid accordingly.

The amplitude videos were created frame by frame, by plotting the amplitude values of each channel at every timepoint (**APPENDIX C**). First, similarly to the heatmaps, an 8x8 grid was created and the MEA channels were correlated to the grid according to their spatial location. Then, the amplitude values of each channel were plotted using the "imagesc" function. One frame was created for each acquired timepoint to create an array containing all the frames. The sampling rate of the INTAN (30 KHz) was taken into account in order to display the frames at the right rate and to create real-time videos of the acquired FPs.

5.3.6 Calculation of conduction velocity (CV)

A detailed description of the methodology for the calculation of the CV is provided in section "***4.3.1.12 Microelectrode array (MEA) electrophysiological analysis"*** of this dissertation. And the overall workflow for CV calculation is shown in **Figure 5.2 A**. Briefly, ROIs were selected based on the overlay of spatial heatmaps and phase-contrast images (**Figure 4.6**). Then the signal propagation time (Δt_average) for electrodes within the ROIs was calculated as the average time difference of the time of occurrence of FPs peaks (**Figure 5.2 B**). The distance between each pair of electrodes was calculated and divided by the Δt_average in order to obtain the CV for the pair of electrodes. Finally, the CV of the ROI was calculated as the average CV between each pair of electrodes. For each experimental condition the CV of 2 to 3 ROIs was calculated. Outlier values for CV between pairs of electrodes were detected by Grubb's test (GraphPad Prism) and were not taken into account for the final calculations.

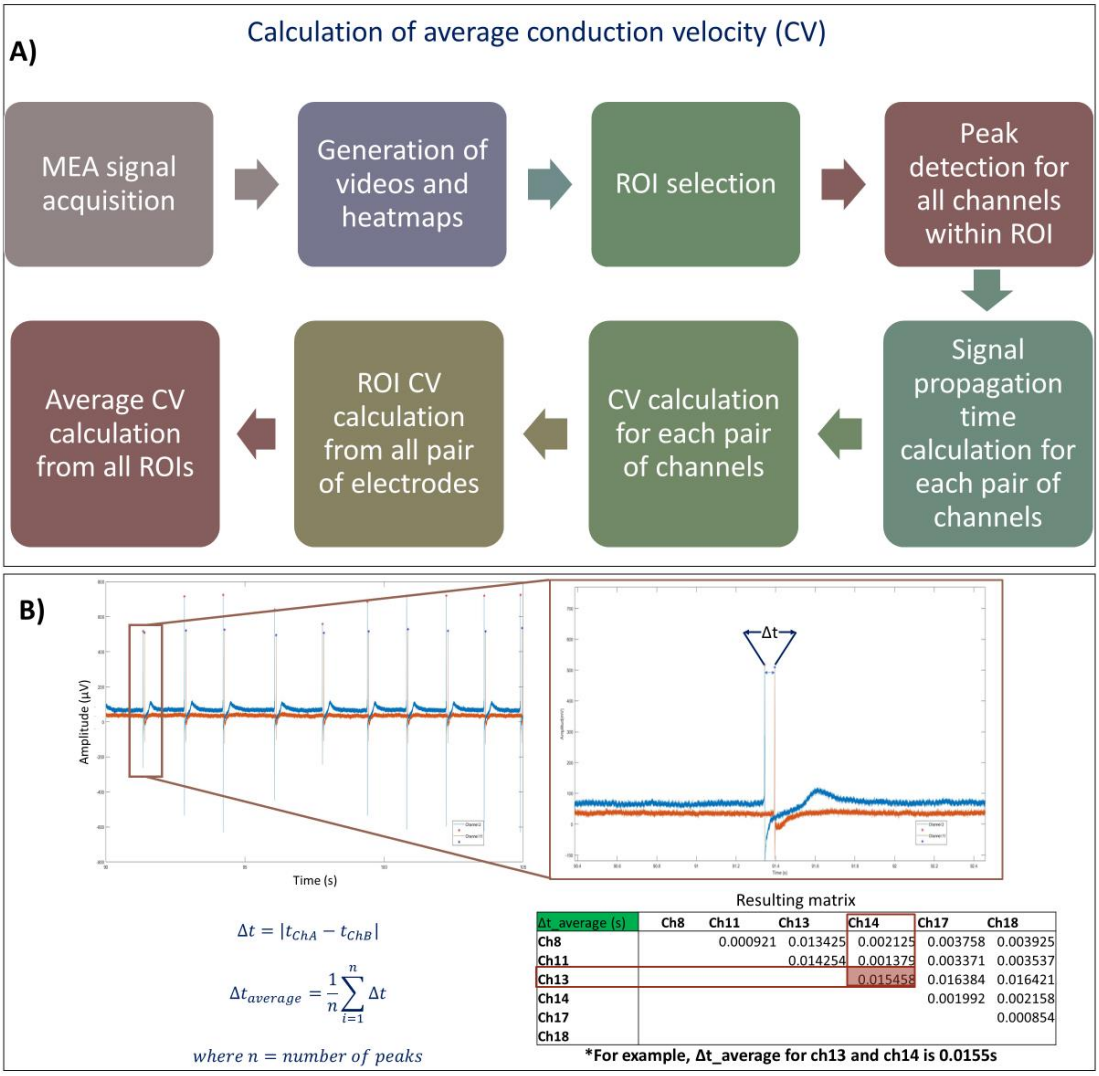

Figure 5.2. Calculation of the conduction velocity (CV). A) Algorithm for ROI selection and CV calculation. B) Representative calculations of the signal propagation time for a pair of MEA electrodes, including the equations for its calculation. *Adapted with permission from Alejandra Patino-Guerrero et al. (2023). Copyright 2023 American Chemical Society.*

5.4 RESULTS AND DISCUSSION

5.4.1 Field potentials (FPs) signal acquisition form the cardiac organoids

The electrical activity of cardiac cells is a complex phenomenon that is responsible of the synchronized contraction of the heart tissue, among other processes (Fozzard & Gibbons, 1973; Santana, Cheng, & Lederer, 2010). This electrical activity is primarily

regulated by ion transport through ion channels, causing the rapid depolarization and repolarization of the cellular membrane (Fozzard & Gibbons, 1973). This process causes a change of potential in the cellular membrane of the cardiac cells, known as action potentials (APs). Additionally, this potential change is also reflected in the intercellular space and in the ECM. Thus, these APs can be captured by microelectrodes in localized regions of cardiac tissue. These recorded signals are denoted as field potentials (FPs) (Chung et al., 2022). Therefore, FPs analysis serves as an indirect tool for the measurement of the electrical activity of the cardiac cells. Moreover, it has been reported that different types of cells present APs with varying shapes (He, Ma, Lee, Thomson, & Kamp, 2003; Santana et al., 2010). Thus, the characterization of FPs also serves as a method for evaluating differences in the electrical activity of tissues with varying cellular compositions. However, the FPs of hiPSC-derived cardiac tissues are still not well described (Chung et al., 2022).

Therefore, in this study the evaluation of electrophysiological features of isogenic cardiac organoids was performed through the analysis of the recorded field potentials (FPs). The FPs from the cardiac organoids were recorded 24 hours after seeding in the MEAs platforms (**Figure 4.5 A**). The cardiac organoids presented spontaneous beating after the recovery period (**Videos B8 and B9**). We were able to record FPs with observable and cyclic peaks that corresponded to the spontaneous beating of the cardiac organoids (**Figure 5.3 and 5.4**). Thus, we have confirmed that the MEAs present an adequate spatiotemporal resolution for recording FPs of several isogenic cardiac organoids at a time. Moreover, we have recorded for the first time, the FPs of isogenic cardiac organoids with defined cellular composition (i.e. SFM: 100% hiPSC-CMS, and SFC: 70% hiPSC-CMs and 30% hiPSC-CFs), generated under a supplement starvation regimen.

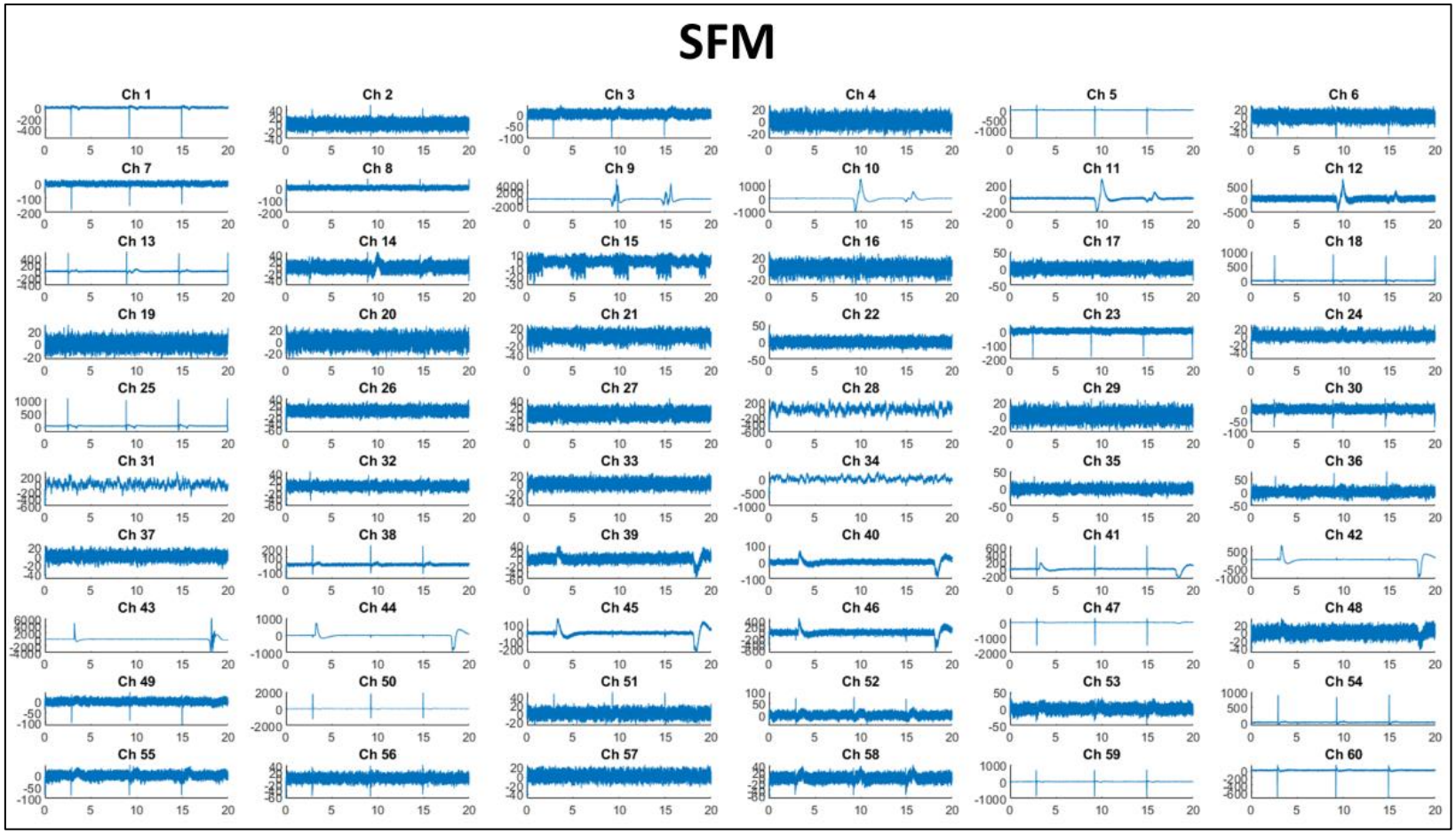

Figure 5.3. Representative FPs recorded from monoculture (SFM) cardiac organoids. The image shows the 60 channels, corresponding to the 60 electrodes of the MEA, for a span of 20 seconds of the recorded signals. (X-axis: time (s); Y-axis: Amplitude (μV)). *Adapted with permission from Alejandra Patino-Guerrero et al. (2023). Copyright 2023 American Chemical Society*

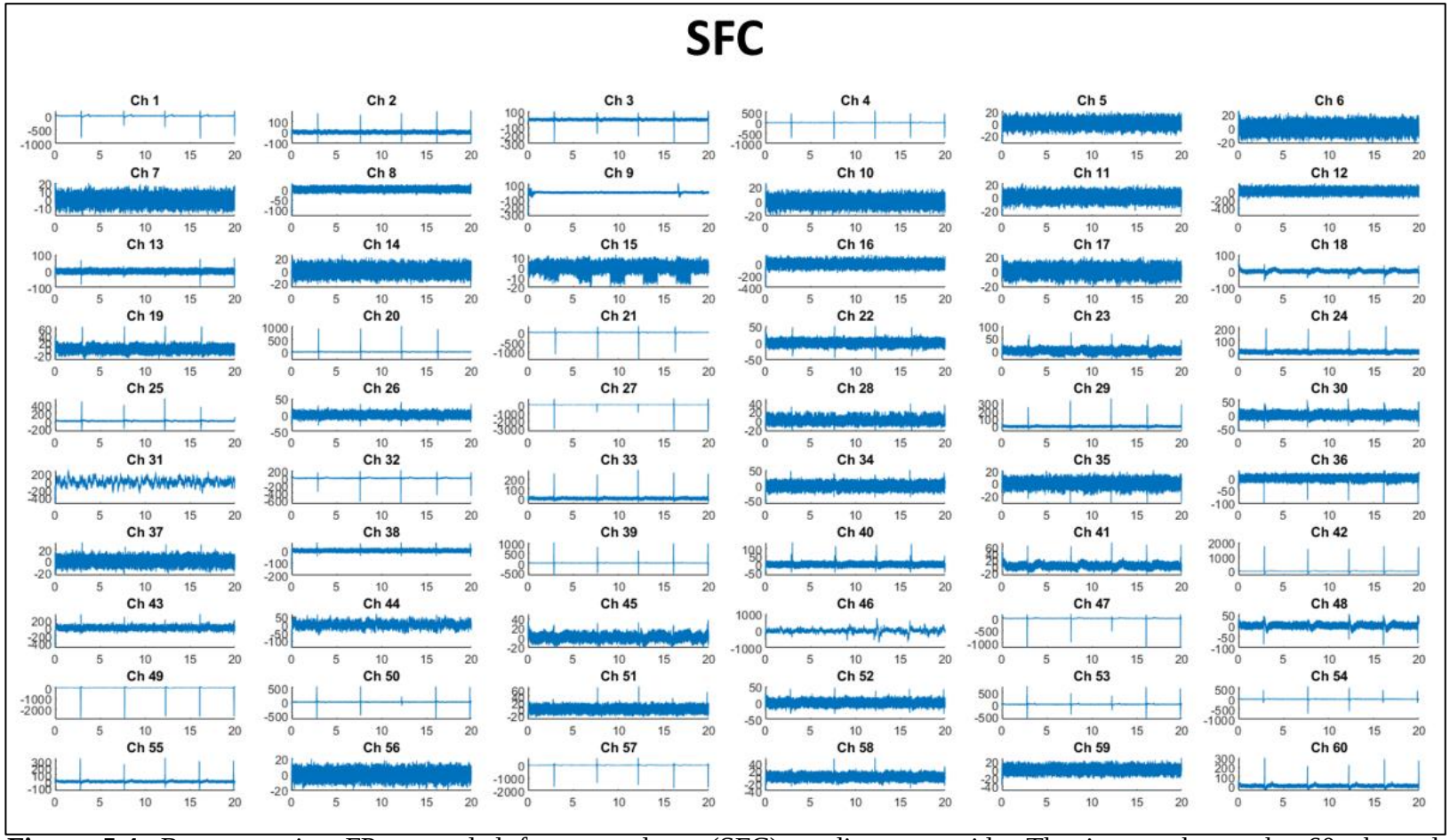

Figure 5.4. Representative FPs recorded from coculture (SFC) cardiac organoids. The image shows the 60 channels, corresponding to the 60 electrodes of the MEA, for a span of 20 seconds of the recorded signals (X-axis: time (s); Y-axis: Amplitude (μV)). *Adapted with permission from Alejandra Patino-Guerrero et al. (2023). Copyright 2023 American Chemical Society*

5.4.2 Creation of spatiotemporal heatmaps of FPs

While FPs plots allow to visualize the acquired signals in a specific timeframe, they are often difficult to interpret. Moreover, subtle features of the FPs cannot be easily visualized. Additionally, most of the MEAs interphases require the use of dedicated software that are usually expensive, difficult to use, and designed for applications outside cardiac tissue engineering (Bridges, Tovar, Wu, Hansma, & Kosik, 2018; Sala, Ward-van Oostwaard, Tertoolen, Mummery, & Bellin, 2017). Thus, the need to create better and more accessible tools to represent relevant electrophysiological features of the cardiac organoids.

The spatial distribution of the microelectrode grid was represented as heatmaps that contained represent key features of the acquired FPs; for example, the FPs peak-to-peak amplitude, and maximum and minimum values for each channel (**Figure 4.6 A**). It has been reported that these features are a direct translation of APs in cardiac cells (Tertoolen, Braam, van Meer, Passier, & Mummery, 2018). Moreover, these FPs features vary according to the cellular composition, maturation state, and cellular interconnectivity within the cardiac organoids (Chung et al., 2022). Thus, the evaluation of FPs features, offers an accessible approach for the electrophysiological characterization of cardiac organoids at tissue level.

While relevant and detailed, the data obtained from MEAs platforms can very quickly add to a considerable amount of information, requiring high computational power to process the acquired signals. For example, in this study, the standard sampling rate was performed at 30 kHz, using an array of 60 electrodes. This accounts for $1.8x10^6$ data points recorded per second. Additionally, in order to obtain a fair representation of the electrophysiological behavior of the cardiac organoids, it is necessary to record at least a

few APs bursts (i.e. organoid contractions), requiring the recording of the signal for several seconds (**Figure 5.3 and 5.4**). For example, we present here the FPs acquired for 20 seconds. Thus, this study comprises around $36x10^6$ data points for each of the experimental condition evaluated. However, the spatial localization of the cardiac organoids for each group is different and no homogeneous (**Figure 4.5 B**). Therefore, there are some regions of the MEAs that are of no interest for the electrophysiological analysis since the cardiac organoids are not in contact with those electrodes. Thus, the selection of regions of interest (ROIs) results convenient in order to minimize the information that requires processing, and to optimize the analysis of electrophysiological features.

We have demonstrated that the combination of key FPs features in spatial heatmaps with phase-contrast images (**Figure 4.6 A**), and the spatiotemporal heatmaps (**Figure 4.6 B** and **Video B10** and **B11**) of the acquired FPs allows for the identification of ROIs that significantly reduces the amount of data that needs to be processed. This opens the door for an efficient approach that requires little specialized methods and techniques for the electrophysiological analysis of 3D ECTs.

Often, FPs parameters, such as amplitude and duration, have serve to evaluate cardiac disease models and the effect of specific drugs (Chung et al., 2022; Tertoolen et al., 2018). While these parameters have been thoroughly described in 2D CMs monolayers (Chowdhury et al., 2018; Wells et al., 2019), there are very few reports on 3D scaffold-free cardiac tissues. Therefore, by creating these spatiotemporal heatmaps of MEAs we aim to characterize isogenic ECTs with defined cellular compositions (Alejandra Patino-Guerrero et al., 2023). But also, we seek to provide with tools to enable and facilitate the visualization and analysis of FPs for cardiac organoids. These spatiotemporal heatmaps can be

implemented in drug screening and cardiac disease modeling applications and can help further the understanding of the electrophysiological properties of ECTs.

5.4.3 Conduction velocity (CV) calculation from ROIs

The conduction velocity (CV) can be defined as the propagation time of the APs in cardiac tissues (Cantwell et al., 2015; Carmeliet, 2019). CV is an important parameter for the functional evaluation of ECTs at cellular and tissue levels. For example, it can be indicative of the tissue architecture or the cellular interconnectivity (Cantwell et al., 2015), and specific CV values have been used to describe healthy or diseased cardiac tissue (Cantwell et al., 2015; Spencer et al., 2017). Specifically, for hiPSC-derived cardiac tissues CV has been used as parameter of tissue maturation (Goldfracht et al., 2019; Shadrin et al., 2017).

While CV is a relevant measurement for the characterization of engineered tissues, the underlying mechanisms for the APs propagation are still not well understood (Carmeliet, 2019). Therefore, the CV characterization of isogenic cardiac organoids is pertinent to provide more insight regarding their electrophysiological features. Moreover, by developing a simple approach for the calculation of CV in cardiac organoids we look to expand the possible use of these engineered tissues for drug screening and disease modeling applications.

5.5 CONCLUSIONS

In this study we presented the electrophysiological characterization of isogenic human cardiac organoids derived from hiPSCs, with two different cellular compositions, generated under a supplement starvation regime. The acquisition of FPs was performed

using a glass MEA platform that allowed for the utilization of phase-contrast imaging. We have created spatiotemporal heatmaps that represent important FPs features. These features help to evaluate the electrical behavior of the presented organoids. Moreover, by using the spatiotemporal heatmaps in combination with the phase-contrast images we were able to select ROIs for the calculation of the CV. The selection of ROIs allowed for a more efficient method for data processing, requiring less time and computational power.

5.6 RFERENCES

Binah, O., Dolnikov, K., Sadan, O., Shilkrut, M., Zeevi-Levin, N., Amit, M., . . . Itskovitz-Eldor, J. (2007). Functional and developmental properties of human embryonic stem cells-derived cardiomyocytes. *J Electrocardiol, 40*(6 Suppl), S192-196. doi:10.1016/j.jelectrocard.2007.05.035

Bridges, D. C., Tovar, K. R., Wu, B., Hansma, P. K., & Kosik, K. S. (2018). MEA Viewer: A high-performance interactive application for visualizing electrophysiological data. *PLOS ONE, 13*(2), e0192477. doi:10.1371/journal.pone.0192477

Cantwell, C. D., Roney, C. H., Ng, F. S., Siggers, J. H., Sherwin, S. J., & Peters, N. S. (2015). Techniques for automated local activation time annotation and conduction velocity estimation in cardiac mapping. *Computers in Biology and Medicine, 65*, 229-242. doi:https://doi.org/10.1016/j.compbiomed.2015.04.027

Carmeliet, E. (2019). Conduction in cardiac tissue. Historical reflections. *Physiological Reports, 7*(1), e13860. doi:https://doi.org/10.14814/phy2.13860

Chowdhury, R. A., Tzortzis, K. N., Dupont, E., Selvadurai, S., Perbellini, F., Cantwell, C. D., . . . Peters, N. S. (2018). Concurrent micro- to macro-cardiac electrophysiology in myocyte cultures and human heart slices. *Scientific Reports, 8*(1), 6947. doi:10.1038/s41598-018-25170-9

Chung, W. G., Kim, E., Song, H., Lee, J., Lee, S., Lim, K., . . . Park, J.-U. (2022). Recent Advances in Electrophysiological Recording Platforms for Brain and Heart Organoids. *Advanced NanoBiomed Research, 2*(12), 2200081. doi:https://doi.org/10.1002/anbr.202200081

Didier, C. M., Kundu, A., DeRoo, D., & Rajaraman, S. (2020). Development of in vitro 2D and 3D microelectrode arrays and their role in advancing biomedical research. *Journal of Micromechanics and Microengineering, 30*(10), 103001. doi:10.1088/1361-6439/ab8e91

Fan, C., Tang, Y., Zhao, M., Lou, X., Pretorius, D., Menasche, P., . . . Zhang, J. (2020). CHIR99021 and fibroblast growth factor 1 enhance the regenerative potency of human cardiac muscle patch after myocardial infarction in mice. *J Mol Cell Cardiol, 141*, 1-10. doi:10.1016/j.yjmcc.2020.03.003

Fozzard, H. A., & Gibbons, W. R. (1973). Action potential and contraction of heart muscle. *The American Journal of Cardiology, 31*(2), 182-192. doi:https://doi.org/10.1016/0002-9149(73)91031-X

Goldfracht, I., Efraim, Y., Shinnawi, R., Kovalev, E., Huber, I., Gepstein, A., . . . Gepstein, L. (2019). Engineered heart tissue models from hiPSC-derived cardiomyocytes and cardiac ECM for disease modeling and drug testing applications. *Acta Biomaterialia, 92*, 145-159. doi:https://doi.org/10.1016/j.actbio.2019.05.016

He, J.-Q., Ma, Y., Lee, Y., Thomson, J. A., & Kamp, T. J. (2003). Human Embryonic Stem Cells Develop Into Multiple Types of Cardiac Myocytes. *Circulation Research, 93*(1), 32-39. doi:10.1161/01.RES.0000080317.92718.99

Jeong, E., Choi, S., & Cho, S.-W. (2023). Recent Advances in Brain Organoid Technology for Human Brain Research. *ACS Applied Materials & Interfaces, 15*(1), 200-219. doi:10.1021/acsami.2c17467

Joddar, B., Natividad-Diaz, S. L., Padilla, A. E., Esparza, A. A., Ramirez, S. P., Chambers, D. R., & Ibaroudene, H. (2022). Engineering approaches for cardiac organoid formation and their characterization. *Translational Research, 250*, 46-67. doi:https://doi.org/10.1016/j.trsl.2022.08.009

Kim, H., Kamm, R. D., Vunjak-Novakovic, G., & Wu, J. C. (2022). Progress in multicellular human cardiac organoids for clinical applications. *Cell Stem Cell, 29*(4), 503-514. doi:10.1016/j.stem.2022.03.012

Kim, J., Sullivan, G. J., & Park, I.-H. (2021). How well do brain organoids capture your brain? *iScience, 24*(2), 102063. doi:https://doi.org/10.1016/j.isci.2021.102063

Klempíř, O., Krupička, R., Krůšek, J., Dittert, I., Petráková, V., Petrák, V., & Taylor, A. (2020). Application of spike sorting algorithm to neuronal signals originated from boron doped diamond micro-electrode arrays. *Physiol Res, 69*(3), 529-536. doi:10.33549/physiolres.934366

Lee, S. G., Kim, Y. J., Son, M. Y., Oh, M. S., Kim, J., Ryu, B., . . . Chung, H. M. (2022). Generation of human iPSCs derived heart organoids structurally and functionally similar to heart. *Biomaterials, 290*, 121860. doi:10.1016/j.biomaterials.2022.121860

Lewis-Israeli, Y. R., Wasserman, A. H., Gabalski, M. A., Volmert, B. D., Ming, Y., Ball, K. A., . . . Aguirre, A. (2021). Self-assembling human heart organoids for the modeling of cardiac development and congenital heart disease. *Nature Communications, 12*(1), 5142. doi:10.1038/s41467-021-25329-5

Lian, X., Zhang, J., Azarin, S. M., Zhu, K., Hazeltine, L. B., Bao, X., . . . Palecek, S. P. (2013). Directed cardiomyocyte differentiation from human pluripotent stem cells by modulating Wnt/beta-catenin signaling under fully defined conditions. *Nat Protoc, 8*(1), 162-175. doi:10.1038/nprot.2012.150

Patino-Guerrero, A., Ponce Wong, R. D., Kodibagkar, V. D., Zhu, W., Migrino, R. Q., Graudejus, O., & Nikkhah, M. (2023). Development and Characterization of Isogenic Cardiac Organoids from Human-Induced Pluripotent Stem Cells Under Supplement Starvation Regimen. *ACS Biomaterials Science & Engineering, 9*(2), 944-958. doi:10.1021/acsbiomaterials.2c01290

Richards, D. J., Li, Y., Kerr, C. M., Yao, J., Beeson, G. C., Coyle, R. C., . . . Mei, Y. (2020). Human cardiac organoids for the modelling of myocardial infarction and drug cardiotoxicity. *Nature Biomedical Engineering, 4*(4), 446-462. doi:10.1038/s41551-020-0539-4

Sala, L., Ward-van Oostwaard, D., Tertoolen, L. G. J., Mummery, C. L., & Bellin, M. (2017). Electrophysiological Analysis of human Pluripotent Stem Cell-derived Cardiomyocytes (hPSC-CMs) Using Multi-electrode Arrays (MEAs). *J Vis Exp*(123), e55587. doi:10.3791/55587

Santana, L. F., Cheng, E. P., & Lederer, W. J. (2010). How does the shape of the cardiac action potential control calcium signaling and contraction in the heart? *J Mol Cell Cardiol, 49*(6), 901-903. doi:10.1016/j.yjmcc.2010.09.005

Shadrin, I. Y., Allen, B. W., Qian, Y., Jackman, C. P., Carlson, A. L., Juhas, M. E., & Bursac, N. (2017). Cardiopatch platform enables maturation and scale-up of human pluripotent stem cell-derived engineered heart tissues. *Nature Communications, 8*(1), 1825. doi:10.1038/s41467-017-01946-x

Simeonov, S., & Schäffer, T. E. (2019). Ultrafast Imaging of Cardiomyocyte Contractions by Combining Scanning Ion Conductance Microscopy with a Microelectrode Array. *Analytical Chemistry, 91*(15), 9648-9655. doi:10.1021/acs.analchem.9b01092

Spencer, T. M., Blumenstein, R. F., Pryse, K. M., Lee, S.-L., Glaubke, D. A., Carlson, B. E., . . . Genin, G. M. (2017). Fibroblasts Slow Conduction Velocity in a Reconstituted Tissue Model of Fibrotic Cardiomyopathy. *ACS Biomaterials Science & Engineering, 3*(11), 3022-3028. doi:10.1021/acsbiomaterials.6b00576

Tasnim, K., & Liu, J. (2022). Emerging Bioelectronics for Brain Organoid Electrophysiology. *Journal of Molecular Biology, 434*(3), 167165. doi:https://doi.org/10.1016/j.jmb.2021.167165

Tertoolen, L. G. J., Braam, S. R., van Meer, B. J., Passier, R., & Mummery, C. L. (2018). Interpretation of field potentials measured on a multi electrode array in pharmacological toxicity screening on primary and human pluripotent stem cell-derived cardiomyocytes. *Biochemical and Biophysical Research Communications, 497*(4), 1135-1141. doi:https://doi.org/10.1016/j.bbrc.2017.01.151

Varzideh, F., Mahmoudi, E., & Pahlavan, S. (2019). Coculture with noncardiac cells promoted maturation of human stem cell–derived cardiomyocyte microtissues. *Journal of Cellular Biochemistry, 120*(10), 16681-16691. doi:https://doi.org/10.1002/jcb.28926

Veldhuizen, J., Mann, H. F., Karamanova, N., Van Horn, W. D., Migrino, R. Q., Brafman, D., & Nikkhah, M. (2022). Modeling long QT syndrome type 2 on-a-chip via in-depth assessment of isogenic gene-edited 3D cardiac tissues. *Sci Adv, 8*(50), eabq6720. doi:10.1126/sciadv.abq6720

Wells, S. P., Waddell, H. M., Sim, C. B., Lim, S. Y., Bernasochi, G. B., Pavlovic, D., . . . Bell, J. R. (2019). Cardiomyocyte functional screening: interrogating comparative electrophysiology of high-throughput model cell systems. *American Journal of Physiology-Cell Physiology, 317*(6), C1256-C1267. doi:10.1152/ajpcell.00306.2019

CHAPTER 6

CONCLUSIONS AND FUTURE DIRECTIONS

This chapter details the achievements that have been accomplished towards each of the specific aims of this PhD dissertation. It also describes challenges and discusses possible future directions for each aim.

6.1 SIGNIFICANCE

6.1.1 Specific Aim 1

In this aim we described the nanoengineering and biofunctionalization of one-dimensional (1D) gold nanoparticles, namely gold nanoribbons (AuNRs). Additionally, we presented the integration of the AuNRs with isogenic cardiac organoids derived from human induced pluripotent stem cells (hiPSC). We performed a thorough characterization of the synthesized AuNRs, including their size and morphology, and optical properties (surface plasmon resonance). We also described a method for the simple quantification of their mass by the correlation of ICP-MS and spectrophotometry. Notably, we presented for the first time the biofunctionalization of the AuNRs by performing surface molecule exchange through PEGylation, changing CTAB molecules by PEG molecules. We demonstrated that by performing the PEGylation, the cytotoxicity of the AuNRs is significantly reduced, and that the PEGylated AuNRs are suitable for culturing with hiPSC-derived cardiac cells.

We also presented under this aim, the optimized fabrication of isogenic cardiac organoids. To this end we first described our protocol for the differentiation and

characterization of hiPSC-derived cardiomyocytes (hiPSC-CMs) and hiPSC-derived cardiac fibroblasts (hiPSC-CFs). We determined that the optimal conditions for organoid fabrication consisted of 5,000 cells per organoid, seeded for seven days in agarose microwells (800μm depth, 800μm diameter). Remarkably, we presented for the first time the integration of biofunctionalized AuNRs with human isogenic cardiac organoids. In order to evaluate the effect of the AuNRs in the three-dimensional (3D) cardiac microenvironment, four experimental groups were designed:

- Monoculture without AuNRs: 100% hiPSC-CMs, 0μg/ml.
- Monoculture with AuNRs: 100% hiPSC-CMs, 10μg/ml.
- Coculture without AuNRs: 70% hiPSC-CMs, 30% hiPSC-CFs, 0μg/ml.
- Coculture with AuNRs: 70% hiPSC-CMs, 30% hiPSC-CFs, 10μg/ml.

It was found that the AuNRs were successfully integrated in the cardiac organoids, and that the nanoparticles did not cause cytotoxic effects in the cardiac cells. Analysis of the transcriptomic profile showed upregulation of cardiac-relevant genes in the coculture groups. This suggests that a more mature phenotype was caused due to the presence of hiPSC-CF in the cardiac organoids. The presence of AuNRs did not have any negative effect in the formation of cardiac organoids. However, their contribution towards the maturation of the cardiac organoids appears to be negligible at the applied dose.

6.1.2 Specific Aim 2

In this aim we focused on studying the mechanisms for the fabrication of isogenic cardiac organoids under a supplement starvation regimen. To this end, we designed a supplement-free treatment in order to induce metabolic synchronization of hiPSC-CMs.

The supplement starvation regime for the hiPSC-CMs consisted of a 24-hour incubation period with supplement-free media upon the fabrication of the cardiac organoids. We utilized the optimized cell culture conditions from the previous aim to fabricate the cardiac organoids (5,000 cells per organoid, incubated for seven days in the agarose microwells to induce cellular aggregation). We designed four experimental conditions in order to evaluate the effects of the supplement starvation regime along with the coculture with cardiac fibroblasts, as follows:

- B27M: 100% hiPSC-CMs, supplemented media
- B27C: 70% hiPSC-CMs, 30% hiPSC-CFs, supplemented media
- SFM: 100% hiPSC-CMs, supplement-free media
- SFC: 70% hiPSC-CMs, 30% hiPSC-CFs, supplement-free media

We performed extensive mechanistic-, morphological-, and molecular-level evaluations on the cardiac organoids. We found that the coculture organoids (B27C and SFC) presented faster cellular aggregation, denoted by a significantly reduced diameter on day one after seeding, when compared with the monoculture organoids. We also found that the coculture organoids present a significantly rounder morphology. This is indicative of improved tissue compaction. Additionally, our molecular assays showed that the coculture organoids presented a more mature genotype, denoted by the upregulation and relative higher expression of cardiac-relevant genes.

6.1.3 Specific Aim 3

Aim 3 focused on the electrophysiological characterization of isogenic cardiac organoids fabricated under supplement starvation utilizing a microelectrode array (MEA)

platform. We first optimized the surface treatment of the glass MEA platform in order to encourage the contact of the cardiac cells with the electrodes. We seeded monoculture (100% hiPSC-CMs) and coculture (70% hiPSC-CMs, 30% hiPSC-CFs) cardiac organoids on the MEAs and acquired the field potentials (FPs) generated by the spontaneous beating of the cardiac tissues. Spatiotemporal heatmaps were created to facilitate the visualization of the acquired FPs. Relevant features such as signal amplitude, maximums, and minimums were calculated, and presented in spatial heatmaps. These heatmaps were used in combination with phase-contrast images in order to select regions of interest (ROIs). From the selected ROIs we were able to develop an algorithm for the calculation of the conduction velocity (CV) of the cardiac organoids. Interestingly, we found a trend for decreased CV in the coculture organoids, presumably due to the presence of the hiPSC-CFs.

6.1.4 Contributions

The following is a collection of publications in scientific peer-reviewed journals and local and international conferences that have emerged from the work presented in this dissertation.

6.1.4.1. Peer-reviewed journal articles

1. **A. Patino-Guerrero**, H. Esmaeili, R.Q. Migrino, M. Nikkhah, "Nanoengineering of gold nanoribbons and their integration with isogenic hiPSC-derived cardiac organoids", *Submitted to **RSC Advances**, Under Review*, Expected publication: Spring 2023.

2. H. Esmaeili, **A. Patino-Guerrero**, R. Nelson, N. Karamanova, T. M. Fisher, W. Zhu, F. Perreault, R. Q. Migrino, M. Nikkhah, "Mechanistic Assessment of Gold Nanorod-induced Maturation of Human Stem Cell-derived Cardiac Tissues". *Submitted to* ***Biomaterials****. Under Review*. Expected publication: Spring 2023.
3. **A. Patino-Guerrero**, R. Ponce, O. Graudejus, W. Zhu, R.Q. Migrino, M. Nikkhah, "Development and Characterization of Isogenic Cardiac Organoids from Human-Induced Pluripotent Stem Cells Under Supplement Starvation Regimen", ***ACS Biomaterials Science & Engineering*** 9, 2 (2023): 944–958.
4. A.A. Benbuk, H. Esmaeili, S. Liu, **A. Patino-Guerrero**, R.Q. Migrino, M. Nikkhah, J. Blain-Christen, "Passive and Flexible Wireless Electronics Fabricated on Parylene/PDMS Substrate for Stimulation of Human Stem Cell-Derived Cardiomyocytes." ***ACS sensors*** 7.11 (2022): 3287-3297.
5. H. Esmaeili, **A. Patino-Guerrero**, M. Hasany, M. O. Aansari, A. Memic, A. Dolatshahi-Pirouz, M. Nikkhah, "Electroconductive Biomaterials for Cardiac Tissue Engineering", ***Acta Biomaterialia***. 139 (2022): 118-140.
6. **A. Patino-Guerrero**, J. Veldhuizen, W. Zhu, R. Migrino, & M. Nikkhah, "Three-dimensional scaffold-free microtissues engineered for cardiac repair". ***Journal of Materials Chemistry B***, 8.34 (2020): 7571-7590.

6.1.4.2. Conference presentations

1. **A. Patino-Guerrero**, M. Nikkhah, "Microengineering Isogenic Cardiac Organoids from hiPSC-Derived Cells Under Starvation Regime", *BMES Annual Meeting*, San Antonio, TX. (Oct. 2022).

2. **A. Patino-Guerrero**, M. Nikkhah, "Engineering of Isogenic Cardiac Organoids Derived from Human-Induced Pluripotent Stem Cells Under Serum Starvation Regime", *7th ABRC-Flinn Research Conference*, Phoenix, AZ. (Apr 2022).
3. **A. Patino-Guerrero**, M. Nikkhah, "Generation of Isogenic Human Induced Pluripotent Stem Cell-Derived Cardiac Organoids Embedded with Gold Nanoribbons", *AZ Regenerative Medicine Symposium*, Tempe, AZ. (Nov 2021).
4. **A. Patino-Guerrero**, M. Nikkhah, "Integration of Isogenic Human Induced Pluripotent Stem Cell Derived Cardiac Organoids with Gold Nanoribbons for Myocardial Repair". *Fusion 2021*, Tempe, AZ. (Apr 2021). ***Tony Stark award for best technology innovation.**
5. **A. Patino-Guerrero**, R.Q. Migrino, M. Nikkhah, "Development of Gold Nanoribbons-Embedded Isogenic Human Induced Pluripotent Stem Cell Derived Cardiac Organoids for Myocardial Repair", *6th Annual ABRC-Flinn Research Conference*, Phoenix, AZ. (Feb 2021).
6. **A. Patino-Guerrero**, K. Rajwade, F. Perreault, R. Migrino, M. Nikkhah, "Effect of Gold Nanorods in the Formation of Scaffold-free Stem Cell-derived Cardiac Microtissues", *BMES Annual Meeting*, Online. (Oct 2020).
7. **A. Patino-Guerrero**, R. Migrino, M. Nikkhah, "Engineering of Scaffold-free and Electrically Conductive Cardiac Microtissues", *5th Annual ABRC-Flinn Research Conference*, Phoenix, AZ. (Feb 2020).

6.2 PROJECT CHALLENGES

While completing this dissertation, we were presented with a fair amount of challenges. These challenges were resolved to the best of our abilities, and the most relevant are detailed below. Out of all the challenges that we encountered, the most critical was the maintenance and the successful directed differentiation of hiPSCs. For example, stem cells are prone to spontaneous differentiation. In addition, the directed differentiation of CMs is not a trivial process and involves many variables, such as small molecules doses, cell seeding density, and cell confluency, among others. Thus, we first optimized the cell culture conditions to maintain the pluripotency of the hiPSCs, which was corroborated through the monitoring of the morphology and staining for pluripotency biomarkers. Additionally, we were able to adapt and optimize the protocol for the differentiation of the hiPSC-CMs. Moreover, after extensive literature research, we were able to select a hiPSC cell line (IMR90-4, WiCell) that is highly cardiogenic. These optimization steps led to the continuous production of hiPSC-CMs, necessary for the completion of our experiments.

The main challenges specific to Aim 1 were in regards of the gold nanoribbons (AuNRs) synthesis. While the original protocol used for the synthesis of the AuNRs reported nanoparticles of a final size of up to ~38μm (Y. Xu et al., 2015), we required AuNRs with reduced length to not interfere with cell-cell interactions (Dylan J. Richards et al., 2016). Thus, we performed a thorough optimization of the synthesis protocol. By adjusting the incubation time for the growth phase, we were able to control the final size of the AuNRs. The final size of the AuNRs was confirmed and quantified using TEM imaging. Additionally, the centrifugation settings for the purification of the nanoparticles

were also determined by a series of time and speed sweeps. This was necessary due to: 1) the need to stop the growth reaction exactly after 8 hours of incubation, 2) missing centrifugation speed and time settings in the original protocol, and 3) to increase the yield per batch of the AuNRs. Our adaption of the synthesis protocol led to AuNRs with a suitable size for cardiac tissue engineering and with an appropriate concentration for our specific experiments.

During the development of Aim 2, we faced technical challenges to perform the microscopic imaging of the hiPSC-CMs ultrastructures within the cardiac organoids. On the early stages of this part of the project we encounter that our immunohistochemistry (IHC) protocol needed optimization. Thus, to enhance the resulting images required the improvement of our cryopreservation and cryosectioning techniques, as well as optimizing the antibodies concentration utilized in the IHC. Lastly, we opted for utilizing a confocal microscope in order to reduce the background noise of the images and to increase their overall resolution and quality. The combination of this optimized elements allowed us to observe and quantify the characteristic striations of the CMs sarcomeric structures.

Finally, for our Aim 3, the main challenge was related to processing the data acquired from the microelectrode array (MEA) platform. Due to the significant amount of data points collected from each experiment, the processing and visualization of the data was time- and labor-intensive and required high computational power. After receiving input from our collaborators, we were able to create the spatiotemporal heatmaps for the representation of the FPs. Moreover, we decided to focus our efforts on analyzing the data obtained from specific ROIs that were selected with help of the spatiotemporal heatmaps

and phase-contrast images. This allowed the extraction of relevant features from the FPs in an efficient way.

6.3 FUTURE PERSPECTIVES

6.3.1. Optimization for the integration of AuNRs

While we demonstrated that is feasible to integrate PEGylated AuNRs into cardiac organoids, their effect in the functional contractility and transcriptomic profile was negligible. Thus, future work could focus on further elucidate the role of the AuNRs and optimize their integration with cardiac organoids in order to improve their effect. For example, it has been demonstrated that the effect of some nanoparticles is dose-dependent. Therefore, testing different concentrations of the AuNRs can help casting light on their potential benefits for the maturation and performance of the cardiac organoids. Additionally, investigating the mechanisms that lead to the aggregation of the AuNRs can help prevent this phenomenon *in vitro*, supporting a more homogeneous distribution of the nanoparticles within the cardiac organoids. Future evaluation of the effect of the AuNRs can include an expanded gene panel for assessing the transcriptomic profile, as well as evaluation of the cellular ultrastructures and electrophysiology features.

6.3.2. Further investigation of the supplement starvation regimen

One first approach for expanding our research from Chapter 4 could focus on optimizing the supplement starvation regime for the hiPSC-CMs. For example, it has been reported that intermittent and prolonged supplement starvation can lead to the maturation of specific cells and can help with the directed differentiation of CMs. Thus, designing and implementing a more prolonged starvation regime may enhance its effects over the cardiac

organoids. Also, the utilization of more advanced molecular biology tools such as RNA-seq would provide a more comprehensive transcriptomic profile of the organoids. Moreover, this approach could offer insight of the possible modulation of molecular pathways due to the supplement starvation regime and the presence of hiPSC-CFs. Finally, after a more thorough characterization of the cardiac organoids has been completed, we could explore the utilization of these optimized organoids for pharmacological research and cardiac repair.

6.3.3. Extraction of other electrophysiological features from FPs

In the Chapter 5 of this dissertation, we set up an electrophysiology module in our lab that allowed for the acquisition of FPs generated by the spontaneous beating of the isogenic cardiac organoids. We then optimized the seeding and culturing conditions of the cardiac microtissues acquire the spontaneous beating signals utilizing MEAs. To this extend, we have set the basis for the creation of spatiotemporal heatmaps and the selection of ROIs. This has facilitated the visualization and processing of the acquired FPs. Thus, further research on this topic could focus on the extraction of other complex features from the FPs. For example, evaluating the depolarization and repolarization times of the organoids could provide more information regarding their maturation state and cellular composition. Additionally, analysis regarding tissue synchronicity can offer insight regarding cell-cell interactions within the organoids. Future work in relation with this project can also focus on utilizing the tools that were developed in Chapter 6 to test cardiac organoids under varied experimental conditions. For example, the electrophysiological evaluation of organoids decorated with AuNRs. This could help gaining more

understanding on how nanoparticles can regulate and enhance the microenvironment of the cardiac organoids. Further, the extraction of electrophysiological features could elucidate how the integration of nanoparticles modulates cell-cell interactions within the microtissues. Finally, another avenue to pursue under this project would be to perform the electrophysiological evaluation of cardiac organoids under an electrical stimulation regimen. It is accepted that prolonged periods of electrical stimulation can induce hiPSC-CMs maturation. Additionally, we could explore the electrical response of the organoids under electrical stimulation to evaluate features such as FP amplitude, electrical pacing, and tissue synchronicity. All this would provide a more comprehensive characterization of the engineered tissues.

REFERENCES

Ahadian, S., Zhou, Y., Yamada, S., Estili, M., Liang, X., Nakajima, K., . . . Matsue, T. (2016). Graphene induces spontaneous cardiac differentiation in embryoid bodies. *Nanoscale, 8*(13), 7075-7084. doi:10.1039/C5NR07059G

Ahmed, R. E., Anzai, T., Chanthra, N., & Uosaki, H. (2020). A Brief Review of Current Maturation Methods for Human Induced Pluripotent Stem Cells-Derived Cardiomyocytes. *Frontiers in Cell and Developmental Biology, 8*. doi:10.3389/fcell.2020.00178

Alkilany, A. M., & Murphy, C. J. (2010). Toxicity and cellular uptake of gold nanoparticles: what we have learned so far? *Journal of Nanoparticle Research, 12*(7), 2313-2333.

Alkilany, A. M., Nagaria, P. K., Hexel, C. R., Shaw, T. J., Murphy, C. J., & Wyatt, M. D. (2009). Cellular Uptake and Cytotoxicity of Gold Nanorods: Molecular Origin of Cytotoxicity and Surface Effects. *Small, 5*(6), 701-708. doi:https://doi.org/10.1002/smll.200801546

Amendola, V., Pilot, R., Frasconi, M., Maragò, O. M., & Iatì, M. A. (2017). Surface plasmon resonance in gold nanoparticles: a review. *Journal of Physics: Condensed Matter, 29*(20), 203002. doi:10.1088/1361-648X/aa60f3

Amezcua, R., Shirolkar, A., Fraze, C., & Stout, D. A. (2016). Nanomaterials for Cardiac Myocyte Tissue Engineering. *Nanomaterials, 6*(7), 133. Retrieved from https://www.mdpi.com/2079-4991/6/7/133

Annabi, N., Tsang, K., Mithieux, S. M., Nikkhah, M., Ameri, A., Khademhosseini, A., & Weiss, A. S. (2013). Highly elastic micropatterned hydrogel for engineering functional cardiac tissue. *Advanced Functional Materials, 23*(39), 4950-4959.

Apyari, V. V., Dmitrienko, S. G., & Zolotov, Y. A. (2013). Unusual application of common digital devices: Potentialities of Eye-One Pro mini-spectrophotometer – A monitor calibrator for registration of surface plasmon resonance bands of silver and gold nanoparticles in solid matrices. *Sensors and Actuators B: Chemical, 188*, 1109-1115. doi:https://doi.org/10.1016/j.snb.2013.07.097

Arai, K., Murata, D., Verissimo, A. R., Mukae, Y., Itoh, M., Nakamura, A., . . . Nakayama, K. (2018). Fabrication of scaffold-free tubular cardiac constructs using a Bio-3D printer. *PLOS ONE, 13*(12), e0209162. doi:10.1371/journal.pone.0209162

Ashtari, K., Nazari, H., Ko, H., Tebon, P., Akhshik, M., Akbari, M., . . . Soleimani, M. (2019). Electrically conductive nanomaterials for cardiac tissue engineering. *Advanced Drug Delivery Reviews, 144*, 162-179.

Augustine, R., Dan, P., Hasan, A., Khalaf, I. M., Prasad, P., Ghosal, K., . . . Maureira, P. (2021). Stem cell-based approaches in cardiac tissue engineering: controlling the microenvironment for autologous cells. *Biomedicine & Pharmacotherapy, 138*, 111425. doi:https://doi.org/10.1016/j.biopha.2021.111425

Baei, P., Hosseini, M., Baharvand, H., & Pahlavan, S. (2020). Electrically conductive materials for in vitro cardiac microtissue engineering. *Journal of Biomedical Materials Research Part A*.

Ban, K., Bae, S., & Yoon, Y.-s. (2017). Current strategies and challenges for purification of cardiomyocytes derived from human pluripotent stem cells. *Theranostics, 7*(7), 2067.

Bar, A., & Cohen, S. (2020). Inducing Endogenous Cardiac Regeneration: Can Biomaterials Connect the Dots? *Frontiers in Bioengineering and Biotechnology, 8*, 126.

Bargehr, J., Ong, L. P., Colzani, M., Davaapil, H., Hofsteen, P., Bhandari, S., . . . Sampaziotis, F. (2019). Epicardial cells derived from human embryonic stem cells augment cardiomyocyte-driven heart regeneration. *Nature Biotechnology, 37*(8), 895-906.

Barsotti, M. C., Felice, F., Balbarini, A., & Di Stefano, R. (2011). Fibrin as a scaffold for cardiac tissue engineering. *Biotechnology and Applied Biochemistry, 58*(5), 301-310.

Bazhutina, A., Balakina-Vikulova, N. A., Kursanov, A., Solovyova, O., Panfilov, A., & Katsnelson, L. B. (2021). Mathematical modelling of the mechano-electric coupling in the human cardiomyocyte electrically connected with fibroblasts. *Prog Biophys Mol Biol, 159*, 46-57. doi:10.1016/j.pbiomolbio.2020.08.003

Beauchamp, P., Jackson, C. B., Ozhathil, L. C., Agarkova, I., Galindo, C. L., Sawyer, D. B., . . . Zuppinger, C. (2020). 3D Co-culture of hiPSC-Derived Cardiomyocytes With Cardiac Fibroblasts Improves Tissue-Like Features of Cardiac Spheroids. *Frontiers in Molecular Biosciences, 7*. doi:10.3389/fmolb.2020.00014

Beauchamp, P., Moritz, W., Kelm, J. M., Ullrich, N. D., Agarkova, I., Anson, B. D., . . . Zuppinger, C. (2015). Development and Characterization of a Scaffold-Free 3D Spheroid Model of Induced Pluripotent Stem Cell-Derived Human Cardiomyocytes. *Tissue Engineering Part C: Methods, 21*(8), 852-861. doi:10.1089/ten.tec.2014.0376

Bedada, F. B., Wheelwright, M., & Metzger, J. M. (2016). Maturation status of sarcomere structure and function in human iPSC-derived cardiac myocytes. *Biochimica et Biophysica Acta (BBA) - Molecular Cell Research, 1863*(7, Part B), 1829-1838. doi:https://doi.org/10.1016/j.bbamcr.2015.11.005

Behfar, A., Crespo-Diaz, R., Terzic, A., & Gersh, B. J. (2014). Cell therapy for cardiac repair—lessons from clinical trials. *Nature Reviews Cardiology, 11*(4), 232.

Belostotskaya, G., Hendrikx, M., Galagudza, M., & Suchkov, S. (2020). How to Stimulate Myocardial Regeneration in Adult Mammalian Heart: Existing Views and New Approaches. *BioMed Research International, 2020*.

Benam, K. H., Dauth, S., Hassell, B., Herland, A., Jain, A., Jang, K.-J., . . . Ingber, D. E. (2015). Engineered In Vitro Disease Models. *Annual Review of Pathology: Mechanisms of Disease, 10*(1), 195-262. doi:10.1146/annurev-pathol-012414-040418

Benjamin, E. J., Blaha, M. J., Chiuve, S. E., Cushman, M., Das, S. R., Deo, R., . . . Stroke Stat, S. (2017). Heart Disease and Stroke Statistics-2017 Update A Report From the American Heart Association. *Circulation, 135*(10), E146-E603. doi:10.1161/cir.0000000000000485

Bergmann, O., Bhardwaj, R. D., Bernard, S., Zdunek, S., Barnabé-Heider, F., Walsh, S., . . . Frisén, J. (2009). Evidence for Cardiomyocyte Renewal in Humans. *Science, 324*(5923), 98-102. doi:10.1126/science.1164680

Besser, R. R., Ishahak, M., Mayo, V., Carbonero, D., Claure, I., & Agarwal, A. (2018). Engineered Microenvironments for Maturation of Stem Cell Derived Cardiac Myocytes. *Theranostics, 8*(1), 124-140. doi:10.7150/thno.19441

Bhatt, A. S., Ambrosy, A. P., & Velazquez, E. J. (2017). Adverse remodeling and reverse remodeling after myocardial infarction. *Current Cardiology Reports, 19*(8), 71.

Bhute, V. J., Bao, X., Dunn, K. K., Knutson, K. R., McCurry, E. C., Jin, G., . . . Palecek, S. P. (2017). Metabolomics identifies metabolic markers of maturation in human pluripotent stem cell-derived cardiomyocytes. *Theranostics, 7*(7), 2078.

Biendarra-Tiegs, S. M., Clemens, D. J., Secreto, F. J., & Nelson, T. J. (2020). Human Induced Pluripotent Stem Cell-Derived Non-Cardiomyocytes Modulate Cardiac Electrophysiological Maturation Through Connexin 43-Mediated Cell-Cell Interactions. *Stem Cells Dev, 29*(2), 75-89. doi:10.1089/scd.2019.0098

Binah, O., Dolnikov, K., Sadan, O., Shilkrut, M., Zeevi-Levin, N., Amit, M., . . . Itskovitz-Eldor, J. (2007). Functional and developmental properties of human embryonic stem cells-derived cardiomyocytes. *J Electrocardiol, 40*(6 Suppl), S192-196. doi:10.1016/j.jelectrocard.2007.05.035

Braunwald, E. (2013). Heart failure. *JACC Heart Fail, 1*(1), 1-20. doi:10.1016/j.jchf.2012.10.002

Breslin, S., & O'Driscoll, L. (2013). Three-dimensional cell culture: the missing link in drug discovery. *Drug Discovery Today, 18*(5-6), 240-249.

Bretzner, F., Gilbert, F., Baylis, F., & Brownstone, R. M. (2011). Target populations for first-in-human embryonic stem cell research in spinal cord injury. *Cell Stem Cell, 8*(5), 468-475.

Brewer, G. J., & Cotman, C. W. (1989). Survival and growth of hippocampal neurons in defined medium at low density: advantages of a sandwich culture technique or low oxygen. *Brain Research, 494*(1), 65-74. doi:10.1016/0006-8993(89)90144-3

Brewer, G. J., Torricelli, J. R., Evege, E. K., & Price, P. J. (1993). Optimized survival of hippocampal neurons in B27-supplemented Neurobasal, a new serum-free medium combination. *J Neurosci Res, 35*(5), 567-576. doi:10.1002/jnr.490350513

Bridges, D. C., Tovar, K. R., Wu, B., Hansma, P. K., & Kosik, K. S. (2018). MEA Viewer: A high-performance interactive application for visualizing electrophysiological data. *PLOS ONE, 13*(2), e0192477. doi:10.1371/journal.pone.0192477

Brodland, G. W. (2002). The differential interfacial tension hypothesis (DITH): a comprehensive theory for the self-rearrangement of embryonic cells and tissues. *J. Biomech. Eng., 124*(2), 188-197.

Campostrini, G., Meraviglia, V., Giacomelli, E., van Helden, R. W. J., Yiangou, L., Davis, R. P., . . . Mummery, C. L. (2021). Generation, functional analysis and applications of isogenic three-dimensional self-aggregating cardiac microtissues from human pluripotent stem cells. *Nat Protoc, 16*(4), 2213-2256. doi:10.1038/s41596-021-00497-2

Cantwell, C. D., Roney, C. H., Ng, F. S., Siggers, J. H., Sherwin, S. J., & Peters, N. S. (2015). Techniques for automated local activation time annotation and conduction velocity estimation in cardiac mapping. *Computers in Biology and Medicine, 65*, 229-242. doi:https://doi.org/10.1016/j.compbiomed.2015.04.027

Carmeliet, E. (2019). Conduction in cardiac tissue. Historical reflections. *Physiological Reports, 7*(1), e13860. doi:https://doi.org/10.14814/phy2.13860

Cha, J. M., Park, H., Shin, E. K., Sung, J. H., Kim, O., Jung, W., . . . Kim, J. (2017). A novel cylindrical microwell featuring inverted-pyramidal opening for efficient cell spheroid formation without cell loss. *Biofabrication, 9*(3), 035006.

Chang, D., Shimizu, T., Haraguchi, Y., Gao, S., Sakaguchi, K., Umezu, M., . . . Okano, T. (2015). Time course of cell sheet adhesion to porcine heart tissue after transplantation. *PLOS ONE, 10*(10).

Chen, S. L., Fang, W. W., Ye, F., Liu, Y. H., Qian, J., Shan, S. J., . . . Sun, J. P. (2004). Effect on left ventricular function of intracoronary transplantation of autologous bone marrow mesenchymal stem cell in patients with acute myocardial infarction. *Am J Cardiol, 94*(1), 92-95. doi:10.1016/j.amjcard.2004.03.034

Chen, W., Bian, W., Zhou, Y., & Zhang, J. (2021). Cardiac Fibroblasts and Myocardial Regeneration. *Frontiers in Bioengineering and Biotechnology, 9*. doi:10.3389/fbioe.2021.599928

Chimene, D., Alge, D. L., & Gaharwar, A. K. (2015). Two-dimensional nanomaterials for biomedical applications: Emerging trends and future prospects. *Advanced Materials, 27*(45), 7261-7284.

Cho, S., Discher, D. E., Leong, K. W., Vunjak-Novakovic, G., & Wu, J. C. (2022). Challenges and opportunities for the next generation of cardiovascular tissue engineering. *Nature Methods, 19*(9), 1064-1071. doi:10.1038/s41592-022-01591-3

Cho, S., Lee, C., Skylar-Scott, M. A., Heilshorn, S. C., & Wu, J. C. (2021). Reconstructing the heart using iPSCs: Engineering strategies and applications. *Journal of Molecular and Cellular Cardiology, 157*, 56-65. doi:https://doi.org/10.1016/j.yjmcc.2021.04.006

Choi, J. S., Lee, H. J., Rajaraman, S., & Kim, D. H. (2021). Recent advances in three-dimensional microelectrode array technologies for in vitro and in vivo cardiac and neuronal interfaces. *Biosens Bioelectron, 171*, 112687. doi:10.1016/j.bios.2020.112687

Chong, J. J., Yang, X., Don, C. W., Minami, E., Liu, Y.-W., Weyers, J. J., . . . Palpant, N. J. (2014). Human embryonic-stem-cell-derived cardiomyocytes regenerate non-human primate hearts. *Nature, 510*(7504), 273-277.

Chowdhury, R. A., Tzortzis, K. N., Dupont, E., Selvadurai, S., Perbellini, F., Cantwell, C. D., . . . Peters, N. S. (2018). Concurrent micro- to macro-cardiac electrophysiology in myocyte cultures and human heart slices. *Scientific Reports, 8*(1), 6947. doi:10.1038/s41598-018-25170-9

Chun, Y. W., Balikov, D. A., Feaster, T. K., Williams, C. H., Sheng, C. C., Lee, J.-B., . . . Ess, K. C. (2015). Combinatorial polymer matrices enhance in vitro maturation of human induced pluripotent stem cell-derived cardiomyocytes. *Biomaterials, 67*, 52-64.

Chung, W. G., Kim, E., Song, H., Lee, J., Lee, S., Lim, K., . . . Park, J.-U. (2022). Recent Advances in Electrophysiological Recording Platforms for Brain and Heart Organoids. *Advanced NanoBiomed Research, 2*(12), 2200081. doi:https://doi.org/10.1002/anbr.202200081

Cleutjens, J. P., & Creemers, E. E. (2002). Integration of concepts: cardiac extracellular matrix remodeling after myocardial infarction. *Journal of Cardiac Failure, 8*(6), S344-S348.

Colliva, A., Braga, L., Giacca, M., & Zacchigna, S. (2020). Endothelial cell–cardiomyocyte crosstalk in heart development and disease. *The Journal of Physiology, 598*(14), 2923-2939. doi:https://doi.org/10.1113/JP276758

Connor, E. E., Mwamuka, J., Gole, A., Murphy, C. J., & Wyatt, M. D. (2005). Gold Nanoparticles Are Taken Up by Human Cells but Do Not Cause Acute Cytotoxicity. *Small, 1*(3), 325-327. doi:https://doi.org/10.1002/smll.200400093

Correia, C., Koshkin, A., Duarte, P., Hu, D., Carido, M., Sebastião, M. J., . . . Teixeira, A. P. (2018). 3D aggregate culture improves metabolic maturation of human pluripotent stem cell derived cardiomyocytes. *Biotechnology and Bioengineering, 115*(3), 630-644.

Correia, C., Koshkin, A., Duarte, P., Hu, D., Teixeira, A., Domian, I., . . . Alves, P. M. (2017). Distinct carbon sources affect structural and functional maturation of cardiomyocytes derived from human pluripotent stem cells. *Sci Rep, 7*(1), 8590. doi:10.1038/s41598-017-08713-4

Cutts, J., Nikkhah, M., & Brafman, D. A. (2015). Biomaterial approaches for stem cell-based myocardial tissue engineering: supplementary issue: stem cell biology. *Biomarker insights, 10*, BMI. S20313.

Daghero, H., Doffe, F., Varela, B., Yozzi, V., Verdes, J. M., Crispo, M., . . . Pagotto, R. (2022). Jejunum-derived NF-κB reporter organoids as 3D models for the study of TNF-alpha-induced inflammation. *Scientific Reports, 12*(1), 14425. doi:10.1038/s41598-022-18556-3

Dahlmann, J., Kensah, G., Kempf, H., Skvorc, D., Gawol, A., Elliott, D. A., . . . Gruh, I. (2013). The use of agarose microwells for scalable embryoid body formation and cardiac differentiation of human and murine pluripotent stem cells. *Biomaterials, 34*(10), 2463-2471.

Daseke, M. J., Tenkorang, M. A. A., Chalise, U., Konfrst, S. R., & Lindsey, M. L. (2020). Cardiac fibroblast activation during myocardial infarction wound healing: Fibroblast polarization after MI. *Matrix Biology, 91-92*, 109-116. doi:https://doi.org/10.1016/j.matbio.2020.03.010

Davies, J. A. (2018). Chapter 1 - Organoids and mini-organs: Introduction, history, and potential. In J. A. Davies & M. L. Lawrence (Eds.), *Organoids and Mini-Organs* (pp. 3-23): Academic Press.

De Angelis, E., Pecoraro, M., Rusciano, M. R., Ciccarelli, M., & Popolo, A. (2019). Cross-Talk between Neurohormonal Pathways and the Immune System in Heart Failure: A Review of the Literature. *Int J Mol Sci, 20*(7). doi:10.3390/ijms20071698

Desroches, B. R., Zhang, P., Choi, B.-R., King, M. E., Maldonado, A. E., Li, W., . . . Hartmann, K. M. (2012). Functional scaffold-free 3-D cardiac microtissues: a novel

model for the investigation of heart cells. *American Journal of Physiology-Heart and Circulatory Physiology, 302*(10), H2031-H2042.

Di Costanzo, E., Giacomello, A., Messina, E., Natalini, R., Pontrelli, G., Rossi, F., . . . Twarogowska, M. (2018). A discrete in continuous mathematical model of cardiac progenitor cells formation and growth as spheroid clusters (Cardiospheres). *Mathematical Medicine and Biology: a Journal of the IMA, 35*(1), 121-144.

Dias, T. P., Pinto, S. N., Santos, J. I., Fernandes, T. G., Fernandes, F., Diogo, M. M., . . . Cabral, J. M. (2018). Biophysical study of human induced Pluripotent Stem Cell-Derived cardiomyocyte structural maturation during long-term culture. *Biochemical and Biophysical Research Communications, 499*(3), 611-617.

Didier, C. M., Kundu, A., DeRoo, D., & Rajaraman, S. (2020). Development of in vitro 2D and 3D microelectrode arrays and their role in advancing biomedical research. *Journal of Micromechanics and Microengineering, 30*(10), 103001. doi:10.1088/1361-6439/ab8e91

Dolatshahi-Pirouz, A., Nikkhah, M., Kolind, K., Dokmeci, M. R., & Khademhosseini, A. (2011). Micro- and Nanoengineering Approaches to Control Stem Cell-Biomaterial Interactions. *Journal of Functional Biomaterials, 2*(3), 88-106. doi:10.3390/jfb2030088

Doyle, M. J., Lohr, J. L., Chapman, C. S., Koyano-Nakagawa, N., Garry, M. G., & Garry, D. J. (2015). Human Induced Pluripotent Stem Cell-Derived Cardiomyocytes as a Model for Heart Development and Congenital Heart Disease. *Stem Cell Rev Rep, 11*(5), 710-727. doi:10.1007/s12015-015-9596-6

Dykman, L., & Khlebtsov, N. (2012). Gold nanoparticles in biomedical applications: recent advances and perspectives. *Chemical Society Reviews, 41*(6), 2256-2282.

Emmert, M. Y., Wolint, P., Wickboldt, N., Gemayel, G., Weber, B., Brokopp, C. E., . . . Jaconi, M. E. (2013). Human stem cell-based three-dimensional microtissues for advanced cardiac cell therapies. *Biomaterials, 34*(27), 6339-6354.

Emmert, M. Y., Wolint, P., Winklhofer, S., Stolzmann, P., Cesarovic, N., Fleischmann, T., . . . Scherman, J. (2013). Transcatheter based electromechanical mapping guided intramyocardial transplantation and in vivo tracking of human stem cell based three dimensional microtissues in the porcine heart. *Biomaterials, 34*(10), 2428-2441.

Esmaeili, H., Patino-Guerrero, A., Hasany, M., Ansari, M. O., Memic, A., Dolatshahi-Pirouz, A., & Nikkhah, M. (2022). Electroconductive biomaterials for cardiac tissue engineering. *Acta Biomater, 139*, 118-140. doi:10.1016/j.actbio.2021.08.031

Fan, C., Tang, Y., Zhao, M., Lou, X., Pretorius, D., Menasche, P., . . . Zhang, J. (2020). CHIR99021 and fibroblast growth factor 1 enhance the regenerative potency of

human cardiac muscle patch after myocardial infarction in mice. *J Mol Cell Cardiol, 141*, 1-10. doi:10.1016/j.yjmcc.2020.03.003

Fan, D., Takawale, A., Lee, J., & Kassiri, Z. (2012). Cardiac fibroblasts, fibrosis and extracellular matrix remodeling in heart disease. *Fibrogenesis Tissue Repair, 5*(1), 15. doi:10.1186/1755-1536-5-15

Fennema, E., Rivron, N., Rouwkema, J., van Blitterswijk, C., & de Boer, J. (2013). Spheroid culture as a tool for creating 3D complex tissues. *Trends in Biotechnology, 31*(2), 108-115. doi:https://doi.org/10.1016/j.tibtech.2012.12.003

Feric, N. T., & Radisic, M. (2016). Strategies and Challenges to Myocardial Replacement Therapy. *Stem Cells Translational Medicine, 5*(4), 410-416. doi:10.5966/sctm.2015-0288

Fozzard, H. A., & Gibbons, W. R. (1973). Action potential and contraction of heart muscle. *The American Journal of Cardiology, 31*(2), 182-192. doi:https://doi.org/10.1016/0002-9149(73)91031-X

Frens, G. (1973). Controlled nucleation for the regulation of the particle size in monodisperse gold suspensions. *Nature Physical Science, 241*(105), 20-22.

Frey, O., Misun, P. M., Fluri, D. A., Hengstler, J. G., & Hierlemann, A. (2014). Reconfigurable microfluidic hanging drop network for multi-tissue interaction and analysis. *Nature Communications, 5*(1), 1-11.

Frisch, S. M., & Screaton, R. A. (2001). Anoikis mechanisms. *Current Opinion in Cell Biology, 13*(5), 555-562. doi:https://doi.org/10.1016/S0955-0674(00)00251-9

Gerbin, K. A., Yang, X., Murry, C. E., & Coulombe, K. L. (2015). Enhanced electrical integration of engineered human myocardium via intramyocardial versus epicardial delivery in infarcted rat hearts. *PLOS ONE, 10*(7).

Ghiroldi, A., Piccoli, M., Cirillo, F., Monasky, M. M., Ciconte, G., Pappone, C., & Anastasia, L. (2018). Cell-based therapies for cardiac regeneration: A comprehensive review of past and ongoing strategies. *International Journal of Molecular Sciences, 19*(10), 3194.

Giacomelli, E., Bellin, M., Sala, L., Van Meer, B. J., Tertoolen, L. G., Orlova, V. V., & Mummery, C. L. (2017). Three-dimensional cardiac microtissues composed of cardiomyocytes and endothelial cells co-differentiated from human pluripotent stem cells. *Development, 144*(6), 1008-1017.

Giacomelli, E., Meraviglia, V., Campostrini, G., Cochrane, A., Cao, X., van Helden, R. W., . . . Davis, R. P. (2020). Human-iPSC-Derived Cardiac Stromal Cells Enhance

Maturation in 3D Cardiac Microtissues and Reveal Non-cardiomyocyte Contributions to Heart Disease. *Cell Stem Cell*.

Goldfracht, I., Efraim, Y., Shinnawi, R., Kovalev, E., Huber, I., Gepstein, A., . . . Gepstein, L. (2019). Engineered heart tissue models from hiPSC-derived cardiomyocytes and cardiac ECM for disease modeling and drug testing applications. *Acta Biomaterialia, 92*, 145-159. doi:https://doi.org/10.1016/j.actbio.2019.05.016

Golpanian, S., Wolf, A., Hatzistergos, K. E., & Hare, J. M. (2016). Rebuilding the damaged heart: mesenchymal stem cells, cell-based therapy, and engineered heart tissue. *Physiological Reviews, 96*(3), 1127-1168.

Gomez-Garcia, M. J., Quesnel, E., Al-Attar, R., Laskary, A. R., & Laflamme, M. A. (2021). Maturation of human pluripotent stem cell derived cardiomyocytes in vitro and in vivo. *Semin Cell Dev Biol, 118*, 163-171. doi:10.1016/j.semcdb.2021.05.022

Gori, T., Lelieveld, J., & Münzel, T. (2020). Perspective: cardiovascular disease and the Covid-19 pandemic. *Basic Research in Cardiology, 115*(3), 32. doi:10.1007/s00395-020-0792-4

Griffith, C. K., Miller, C., Sainson, R. C., Calvert, J. W., Jeon, N. L., Hughes, C. C., & George, S. C. (2005). Diffusion limits of an in vitro thick prevascularized tissue. *Tissue Engineering, 11*(1-2), 257-266.

Halbert, S., Bruderer, R., & Lin, T. (1971). In vitro organization of dissociated rat cardiac cells into beating three-dimensional structures. *The Journal of Experimental Medicine, 133*(4), 677-695.

Hall, C., Gehmlich, K., Denning, C., & Pavlovic, D. (2021). Complex Relationship Between Cardiac Fibroblasts and Cardiomyocytes in Health and Disease. *J Am Heart Assoc, 10*(5), e019338. doi:10.1161/JAHA.120.019338

Hartman, M. E., Dai, D.-F., & Laflamme, M. A. (2016). Human pluripotent stem cells: Prospects and challenges as a source of cardiomyocytes for in vitro modeling and cell-based cardiac repair. *Advanced Drug Delivery Reviews, 96*, 3-17. doi:https://doi.org/10.1016/j.addr.2015.05.004

He, J.-Q., Ma, Y., Lee, Y., Thomson, J. A., & Kamp, T. J. (2003). Human Embryonic Stem Cells Develop Into Multiple Types of Cardiac Myocytes. *Circulation Research, 93*(1), 32-39. doi:10.1161/01.RES.0000080317.92718.99

Hirt, M. N., Hansen, A., & Eschenhagen, T. (2014). Cardiac tissue engineering: state of the art. *Circulation Research, 114*(2), 354-367.

Hoang, P., Wang, J., Conklin, B. R., Healy, K. E., & Ma, Z. (2018). Generation of spatial-patterned early-developing cardiac organoids using human pluripotent stem cells. *Nature protocols, 13*(4), 723.

Holgate, S. T. (2010). Exposure, uptake, distribution and toxicity of nanomaterials in humans. *Journal of Biomedical Nanotechnology, 6*(1), 1-19.

Holzwarth, J. M., & Ma, P. X. (2011). 3D nanofibrous scaffolds for tissue engineering. *Journal of Materials Chemistry, 21*(28), 10243-10251. doi:10.1039/C1JM10522A

Hong, X., Tan, C., Chen, J., Xu, Z., & Zhang, H. (2015). Synthesis, properties and applications of one- and two-dimensional gold nanostructures. *Nano Research, 8*(1), 40-55. doi:10.1007/s12274-014-0636-3

Huang, J., Jiang, Y., Ren, Y., Liu, Y., Wu, X., Li, Z., & Ren, J. (2020). Biomaterials and biosensors in intestinal organoid culture, a progress review. *Journal of Biomedical Materials Research Part A, 108*(7), 1501-1508. doi:10.1002/jbm.a.36921

Huh, D., Torisawa, Y.-s., Hamilton, G. A., Kim, H. J., & Ingber, D. E. (2012). Microengineered physiological biomimicry: Organs-on-Chips. *Lab on a Chip, 12*(12), 2156-2164. doi:10.1039/C2LC40089H

Inamdar, A. A., & Inamdar, A. C. (2016). Heart failure: diagnosis, management and utilization. *Journal of Clinical Medicine, 5*(7), 62.

Iseoka, H., Miyagawa, S., Fukushima, S., Saito, A., Masuda, S., Yajima, S., . . . Sawa, Y. (2017). Pivotal Role of Non-cardiomyocytes in Electromechanical and Therapeutic Potential of Induced Pluripotent Stem Cell-Derived Engineered Cardiac Tissue. *Tissue Engineering Part A, 24*(3-4), 287-300. doi:10.1089/ten.tea.2016.0535

Jackson, S. L., Tong, X., King, R. J., Loustalot, F., Hong, Y., & Ritchey, M. D. (2018). National Burden of Heart Failure Events in the United States, 2006 to 2014. *Circ Heart Fail, 11*(12), e004873. doi:10.1161/CIRCHEARTFAILURE.117.004873

Jacot, J. G., Martin, J. C., & Hunt, D. L. (2010). Mechanobiology of cardiomyocyte development. *Journal of Biomechanics, 43*(1), 93-98.

Jawad, H., Ali, N. N., Lyon, A. R., Chen, Q. Z., Harding, S. E., & Boccaccini, A. R. (2007). Myocardial tissue engineering: a review. *Journal of Tissue Engineering and Regenerative Medicine, 1*(5), 327-342. doi:10.1002/term.46

Jeong, E., Choi, S., & Cho, S.-W. (2023). Recent Advances in Brain Organoid Technology for Human Brain Research. *ACS Applied Materials & Interfaces, 15*(1), 200-219. doi:10.1021/acsami.2c17467

Jiang, Y., Park, P., Hong, S. M., & Ban, K. (2018). Maturation of Cardiomyocytes Derived from Human Pluripotent Stem Cells: Current Strategies and Limitations. *Molecules and cells, 41*(7), 613-621. doi:10.14348/molcells.2018.0143

Joddar, B., Natividad-Diaz, S. L., Padilla, A. E., Esparza, A. A., Ramirez, S. P., Chambers, D. R., & Ibaroudene, H. (2022). Engineering approaches for cardiac organoid formation and their characterization. *Translational Research, 250*, 46-67. doi:https://doi.org/10.1016/j.trsl.2022.08.009

Kamakura, T., Makiyama, T., Sasaki, K., Yoshida, Y., Wuriyanghai, Y., Chen, J., . . . Horie, M. (2013). Ultrastructural maturation of human-induced pluripotent stem cell-derived cardiomyocytes in a long-term culture. *Circulation Journal, 77*(5), 1307-1314.

Kang, S.-M., Kim, D., Lee, J.-H., Takayama, S., & Park, J. Y. (2021). Engineered Microsystems for Spheroid and Organoid Studies. *Advanced Healthcare Materials, 10*(2), 2001284. doi:https://doi.org/10.1002/adhm.202001284

Kankala, R. K., Zhu, K., Sun, X.-N., Liu, C.-G., Wang, S.-B., & Chen, A.-Z. (2018). Cardiac tissue engineering on the nanoscale. *ACS Biomaterials Science & Engineering, 4*(3), 800-818.

Karperien, L., Navaei, A., Godau, B., Dolatshahi-Pirouz, A., Akbari, M., & Nikkhah, M. (2019). Nanoengineered biomaterials for cardiac regeneration. In *Nanoengineered Biomaterials for Regenerative Medicine* (pp. 95-124): Elsevier.

Kawai, Y., Tohyama, S., Arai, K., Tamura, T., Soma, Y., Fukuda, K., . . . Kobayashi, E. (2022). Scaffold-Free Tubular Engineered Heart Tissue From Human Induced Pluripotent Stem Cells Using Bio-3D Printing Technology in vivo. *Frontiers in Cardiovascular Medicine, 8*. doi:10.3389/fcvm.2021.806215

Kawamura, A., Miyagawa, S., Fukushima, S., Kawamura, T., Kashiyama, N., Ito, E., . . . Hatazawa, J. (2016). Teratocarcinomas arising from allogeneic induced pluripotent stem cell-derived cardiac tissue constructs provoked host immune rejection in mice. *Scientific Reports, 6*, 19464.

Kehat, I., Kenyagin-Karsenti, D., Snir, M., Segev, H., Amit, M., Gepstein, A., . . . Gepstein, L. (2001). Human embryonic stem cells can differentiate into myocytes with structural and functional properties of cardiomyocytes. *The Journal of Clinical Investigation, 108*(3), 407-414.

Kermanizadeh, A., Balharry, D., Wallin, H., Loft, S., & Møller, P. (2015). Nanomaterial translocation–the biokinetics, tissue accumulation, toxicity and fate of materials in secondary organs–a review. *Critical Reviews in Toxicology, 45*(10), 837-872.

Kerr, C. M., Richards, D., Menick, D. R., Deleon-Pennell, K. Y., & Mei, Y. (2021). Multicellular Human Cardiac Organoids Transcriptomically Model Distinct Tissue-Level Features of Adult Myocardium. *Int J Mol Sci, 22*(16). doi:10.3390/ijms22168482

Keung, W., Boheler, K. R., & Li, R. A. (2014). Developmental cues for the maturation of metabolic, electrophysiological and calcium handling properties of human pluripotent stem cell-derived cardiomyocytes. *Stem Cell Research & Therapy, 5*(1), 17.

Khammanit, R., Chantakru, S., Kitiyanant, Y., & Saikhun, J. (2008). Effect of serum starvation and chemical inhibitors on cell cycle synchronization of canine dermal fibroblasts. *Theriogenology, 70*(1), 27-34. doi:10.1016/j.theriogenology.2008.02.015

Khan, M. A., Hashim, M. J., Mustafa, H., Baniyas, M. Y., Al Suwaidi, S. K. B. M., AlKatheeri, R., . . . Al Darmaki, R. S. (2020). Global epidemiology of ischemic heart disease: results from the global burden of disease study. *Cureus, 12*(7).

Kharaziha, M., Memic, A., Akbari, M., Brafman, D. A., & Nikkhah, M. (2016). Nano-Enabled Approaches for Stem Cell-Based Cardiac Tissue Engineering. *Advanced Healthcare Materials, 5*(13), 1533-1553. doi:https://doi.org/10.1002/adhm.201600088

Kharaziha, M., Nikkhah, M., Shin, S.-R., Annabi, N., Masoumi, N., Gaharwar, A. K., . . . Khademhosseini, A. (2013). PGS: Gelatin nanofibrous scaffolds with tunable mechanical and structural properties for engineering cardiac tissues. *Biomaterials, 34*(27), 6355-6366.

Kharaziha, M., Shin, S. R., Nikkhah, M., Topkaya, S. N., Masoumi, N., Annabi, N., . . . Khademhosseini, A. (2014). Tough and flexible CNT–polymeric hybrid scaffolds for engineering cardiac constructs. *Biomaterials, 35*(26), 7346-7354.

Khlebtsov, N., & Dykman, L. (2011). Biodistribution and toxicity of engineered gold nanoparticles: a review of in vitro and in vivo studies. *Chemical Society Reviews, 40*(3), 1647-1671.

Kholia, S., Ranghino, A., Garnieri, P., Lopatina, T., Deregibus, M. C., Rispoli, P., . . . Camussi, G. (2016). Extracellular vesicles as new players in angiogenesis. *Vascular Pharmacology, 86*, 64-70.

Kim, H., Kamm, R. D., Vunjak-Novakovic, G., & Wu, J. C. (2022). Progress in multicellular human cardiac organoids for clinical applications. *Cell Stem Cell, 29*(4), 503-514. doi:10.1016/j.stem.2022.03.012

Kim, J., Sullivan, G. J., & Park, I.-H. (2021). How well do brain organoids capture your brain? *iScience*, *24*(2), 102063. doi:https://doi.org/10.1016/j.isci.2021.102063

Kim, T. Y., Kofron, C. M., King, M. E., Markes, A. R., Okundaye, A. O., Qu, Z., . . . Choi, B.-R. (2018). Directed fusion of cardiac spheroids into larger heterocellular microtissues enables investigation of cardiac action potential propagation via cardiac fibroblasts. *PloS one*, *13*(5).

Kitsara, M., Agbulut, O., Kontziampasis, D., Chen, Y., & Menasché, P. (2017). Fibers for hearts: a critical review on electrospinning for cardiac tissue engineering. *Acta Biomaterialia*, *48*, 20-40.

Klempíř, O., Krupička, R., Krůšek, J., Dittert, I., Petráková, V., Petrák, V., & Taylor, A. (2020). Application of spike sorting algorithm to neuronal signals originated from boron doped diamond micro-electrode arrays. *Physiol Res*, *69*(3), 529-536. doi:10.33549/physiolres.934366

Klotz, S., Foronjy, R. F., Dickstein, M. L., Gu, A., Garrelds, I. M., Jan Danser, A., . . . Burkhoff, D. (2005). Mechanical unloading during left ventricular assist device support increases left ventricular collagen cross-linking and myocardial stiffness. *Circulation*, *112*(3), 364-374.

Kopanja, L., Kralj, S., Zunic, D., Loncar, B., & Tadic, M. (2016). Core–shell superparamagnetic iron oxide nanoparticle (SPION) clusters: TEM micrograph analysis, particle design and shape analysis. *Ceramics International*, *42*(9), 10976-10984. doi:https://doi.org/10.1016/j.ceramint.2016.03.235

Kowalski, W. J., Yuan, F., Nakane, T., Masumoto, H., Dwenger, M., Ye, F., . . . Keller, B. B. (2017). Quantification of cardiomyocyte alignment from three-dimensional (3D) confocal microscopy of engineered tissue. *Microscopy and Microanalysis*, *23*(4), 826-842.

Kurtz, A. (2008). Mesenchymal stem cell delivery routes and fate. *International Journal of Stem Cells*, *1*(1), 1.

Kussauer, S., David, R., & Lemcke, H. (2019). hiPSCs Derived Cardiac Cells for Drug and Toxicity Screening and Disease Modeling: What Micro- Electrode-Array Analyses Can Tell Us. *Cells*, *8*(11). doi:10.3390/cells8111331

Laflamme, M. A., Chen, K. Y., Naumova, A. V., Muskheli, V., Fugate, J. A., Dupras, S. K., . . . Police, S. (2007). Cardiomyocytes derived from human embryonic stem cells in pro-survival factors enhance function of infarcted rat hearts. *Nature Biotechnology*, *25*(9), 1015-1024.

Laflamme, M. A., & Murry, C. E. (2005). Regenerating the heart. *Nature Biotechnology, 23*(7), 845-856.

Laflamme, M. A., & Murry, C. E. (2011). Heart regeneration. *Nature, 473*(7347), 326-335. doi:10.1038/nature10147

Lee, D. J., Cavasin, M. A., Rocker, A. J., Soranno, D. E., Meng, X., Shandas, R., & Park, D. (2019). An injectable sulfonated reversible thermal gel for therapeutic angiogenesis to protect cardiac function after a myocardial infarction. *Journal of Biological Engineering, 13*(1), 6.

Lee, R. H., Kim, B., Choi, I., Kim, H., Choi, H. S., Suh, K., . . . Jung, J. S. (2004). Characterization and expression analysis of mesenchymal stem cells from human bone marrow and adipose tissue. *Cellular Physiology and Biochemistry, 14*(4-6), 311-324.

Lee, S. G., Kim, Y. J., Son, M. Y., Oh, M. S., Kim, J., Ryu, B., . . . Chung, H. M. (2022). Generation of human iPSCs derived heart organoids structurally and functionally similar to heart. *Biomaterials, 290*, 121860. doi:10.1016/j.biomaterials.2022.121860

Lee, W. Y., Chang, Y. H., Yeh, Y. C., Chen, C. H., Lin, K. M., Huang, C. C., . . . Sung, H. W. (2009). The use of injectable spherically symmetric cell aggregates self-assembled in a thermo-responsive hydrogel for enhanced cell transplantation. *Biomaterials, 30*(29), 5505-5513. doi:10.1016/j.biomaterials.2009.07.006

Lee, W. Y., Wei, H. J., Lin, W. W., Yeh, Y. C., Hwang, S. M., Wang, J. J., . . . Sung, H. W. (2011). Enhancement of cell retention and functional benefits in myocardial infarction using human amniotic-fluid stem-cell bodies enriched with endogenous ECM. *Biomaterials, 32*(24), 5558-5567. doi:10.1016/j.biomaterials.2011.04.031

Lewis-Israeli, Y. R., Wasserman, A. H., Gabalski, M. A., Volmert, B. D., Ming, Y., Ball, K. A., . . . Aguirre, A. (2021). Self-assembling human heart organoids for the modeling of cardiac development and congenital heart disease. *Nature Communications, 12*(1), 5142. doi:10.1038/s41467-021-25329-5

Li, J., Hua, Y., Miyagawa, S., Zhang, J., Li, L., Liu, L., & Sawa, Y. (2020). hiPSC-Derived Cardiac Tissue for Disease Modeling and Drug Discovery. *International Journal of Molecular Sciences, 21*(23). doi:10.3390/ijms21238893

Li, Q., Huang, C., Liu, L., Hu, R., & Qu, J. (2018). Effect of Surface Coating of Gold Nanoparticles on Cytotoxicity and Cell Cycle Progression. *Nanomaterials, 8*(12). doi:10.3390/nano8121063

Li, Z., & Guan, J. (2011). Hydrogels for cardiac tissue engineering. *Polymers, 3*(2), 740-761.

Lian, X., Zhang, J., Azarin, S. M., Zhu, K., Hazeltine, L. B., Bao, X., . . . Palecek, S. P. (2013). Directed cardiomyocyte differentiation from human pluripotent stem cells by modulating Wnt/beta-catenin signaling under fully defined conditions. *Nat Protoc, 8*(1), 162-175. doi:10.1038/nprot.2012.150

Liaw, N. Y., & Zimmermann, W.-H. (2016). Mechanical stimulation in the engineering of heart muscle. *Advanced Drug Delivery Reviews, 96*, 156-160.

Liu, Y.-W., Chen, B., Yang, X., Fugate, J. A., Kalucki, F. A., Futakuchi-Tsuchida, A., . . . Baldessari, A. (2018). Human embryonic stem cell–derived cardiomyocytes restore function in infarcted hearts of non-human primates. *Nature Biotechnology, 36*(7), 597-605.

Liu, Y., Zhang, Y., Mei, T., Cao, H., Hu, Y., Jia, W., . . . Liu, Z. (2022). hESCs-Derived Early Vascular Cell Spheroids for Cardiac Tissue Vascular Engineering and Myocardial Infarction Treatment. *Advanced Science, 9*(9), 2104299. doi:https://doi.org/10.1002/advs.202104299

Lopaschuk, G. D., & Jaswal, J. S. (2010). Energy metabolic phenotype of the cardiomyocyte during development, differentiation, and postnatal maturation. *Journal of cardiovascular pharmacology, 56*(2), 130-140.

Lopez-Chaves, C., Soto-Alvaredo, J., Montes-Bayon, M., Bettmer, J., Llopis, J., & Sanchez-Gonzalez, C. (2018). Gold nanoparticles: Distribution, bioaccumulation and toxicity. In vitro and in vivo studies. *Nanomedicine: Nanotechnology, Biology and Medicine, 14*(1), 1-12. doi:https://doi.org/10.1016/j.nano.2017.08.011

Lundy, S. D., Zhu, W.-Z., Regnier, M., & Laflamme, M. A. (2013). Structural and functional maturation of cardiomyocytes derived from human pluripotent stem cells. *Stem Cells and Development, 22*(14), 1991-2002.

Lux, M., Andrée, B., Horvath, T., Nosko, A., Manikowski, D., Hilfiker-Kleiner, D., . . . Hilfiker, A. (2016). In vitro maturation of large-scale cardiac patches based on a perfusable starter matrix by cyclic mechanical stimulation. *Acta Biomaterialia, 30*, 177-187.

Ma, Z., Wang, J., Loskill, P., Huebsch, N., Koo, S., Svedlund, F. L., . . . Conklin, B. R. (2015). Self-organizing human cardiac microchambers mediated by geometric confinement. *Nature Communications, 6*(1), 1-10.

Makkar, R. R., Smith, R. R., Cheng, K., Malliaras, K., Thomson, L. E., Berman, D., . . . Johnston, P. V. (2012). Intracoronary cardiosphere-derived cells for heart

regeneration after myocardial infarction (CADUCEUS): a prospective, randomised phase 1 trial. *The Lancet, 379*(9819), 895-904.

Mallapaty, S. (2020). Revealed: two men in China were first to receive pioneering stem-cell treatment for heart-disease. *Nature*.

Maron, B. (1983). Myocardial disorganisation in hypertrophic cardiomyopathy. Another point of view. *British Heart Journal, 50*(1), 1.

Marsano, A., Maidhof, R., Wan, L. Q., Wang, Y., Gao, J., Tandon, N., & Vunjak-Novakovic, G. (2010). Scaffold stiffness affects the contractile function of three-dimensional engineered cardiac constructs. *Biotechnology Progress, 26*(5), 1382-1390.

Martin, T. G., & Kirk, J. A. (2020). Under construction: The dynamic assembly, maintenance, and degradation of the cardiac sarcomere. *J Mol Cell Cardiol, 148*, 89-102. doi:10.1016/j.yjmcc.2020.08.018

Masuda, S., & Shimizu, T. (2016). Three-dimensional cardiac tissue fabrication based on cell sheet technology. *Advanced Drug Delivery Reviews, 96*, 103-109.

Masumoto, H., Ikuno, T., Takeda, M., Fukushima, H., Marui, A., Katayama, S., . . . Sakata, R. (2014). Human iPS cell-engineered cardiac tissue sheets with cardiomyocytes and vascular cells for cardiac regeneration. *Scientific Reports, 4*, 6716.

Mathur, A., Ma, Z., Loskill, P., Jeeawoody, S., & Healy, K. E. (2016). In vitro cardiac tissue models: current status and future prospects. *Advanced Drug Delivery Reviews, 96*, 203-213.

Matthys, O. B., Hookway, T. A., & McDevitt, T. C. (2016). Design principles for engineering of tissues from human pluripotent stem cells. *Current Stem Cell Reports, 2*(1), 43-51.

Maxeiner, H., Krehbiehl, N., Müller, A., Woitasky, N., Akintürk, H., Müller, M., . . . Wenzel, S. (2010). New insights into paracrine mechanisms of human cardiac progenitor cells. *European Journal of Heart Failure, 12*(7), 730-737. doi:10.1093/eurjhf/hfq063

Mc Namara, K., Alzubaidi, H., & Jackson, J. K. (2019). Cardiovascular disease as a leading cause of death: how are pharmacists getting involved? *Integrated Pharmacy Research and Practice, 8*, 1-11. doi:10.2147/IPRP.S133088

McMurtrey, R. J. (2016). Analytic models of oxygen and nutrient diffusion, metabolism dynamics, and architecture optimization in three-dimensional tissue constructs with applications and insights in cerebral organoids. *Tissue Engineering Part C: Methods, 22*(3), 221-249.

Mehrali, M., Thakur, A., Pennisi, C. P., Talebian, S., Arpanaei, A., Nikkhah, M., & Dolatshahi-Pirouz, A. (2017). Nanoreinforced hydrogels for tissue engineering: Biomaterials that are compatible with load-bearing and electroactive tissues. *Advanced Materials, 29*(8), 1603612.

Miyagi, Y., Chiu, L. L., Cimini, M., Weisel, R. D., Radisic, M., & Li, R.-K. (2011). Biodegradable collagen patch with covalently immobilized VEGF for myocardial repair. *Biomaterials, 32*(5), 1280-1290.

Mueller, X. M. (2004). Drug immunosuppression therapy for adult heart transplantation. Part 1: immune response to allograft and mechanism of action of immunosuppressants. *The Annals of Thoracic Surgery, 77*(1), 354-362.

Murphy, C. J., Gole, A. M., Stone, J. W., Sisco, P. N., Alkilany, A. M., Goldsmith, E. C., & Baxter, S. C. (2008). Gold Nanoparticles in Biology: Beyond Toxicity to Cellular Imaging. *Accounts of Chemical Research, 41*(12), 1721-1730. doi:10.1021/ar800035u

Nabel, E. G., & Braunwald, E. (2012). A tale of coronary artery disease and myocardial infarction. *N Engl J Med, 366*(1), 54-63. doi:10.1056/NEJMra1112570

Nagaraju, S., Truong, D., Mouneimne, G., & Nikkhah, M. (2018). Microfluidic tumor–vascular model to study breast cancer cell invasion and intravasation. *Advanced Healthcare Materials, 7*(9), 1701257.

Nagase, K., Yamato, M., Kanazawa, H., & Okano, T. (2018). Poly (N-isopropylacrylamide)-based thermoresponsive surfaces provide new types of biomedical applications. *Biomaterials, 153*, 27-48.

Napiwocki, B. N., Lang, D., Stempien, A., Zhang, J., Vaidyanathan, R., Makielski, J. C., . . . Crone, W. C. (2021). Aligned human cardiac syncytium for in vitro analysis of electrical, structural, and mechanical readouts. *Biotechnology and Bioengineering, 118*(1), 442-452. doi:https://doi.org/10.1002/bit.27582

Napolitano, A. P., Dean, D. M., Man, A. J., Youssef, J., Ho, D. N., Rago, A. P., . . . Morgan, J. R. (2007). Scaffold-free three-dimensional cell culture utilizing micromolded nonadhesive hydrogels. *Biotechniques, 43*(4), 494-500.

Navaei, A., Eliato, K. R., Ros, R., Migrino, R. Q., Willis, B. C., & Nikkhah, M. (2019). The influence of electrically conductive and non-conductive nanocomposite scaffolds on the maturation and excitability of engineered cardiac tissues. *Biomaterials Science, 7*(2), 585-595.

Navaei, A., Moore, N., Sullivan, R. T., Truong, D., Migrino, R. Q., & Nikkhah, M. (2017). Electrically conductive hydrogel-based micro-topographies for the development of organized cardiac tissues. *RSC advances, 7*(6), 3302-3312.

Navaei, A., Rahmani Eliato, K., Ros, R., Migrino, R. Q., Willis, B. C., & Nikkhah, M. (2019). The influence of electrically conductive and non-conductive nanocomposite scaffolds on the maturation and excitability of engineered cardiac tissues. *Biomater Sci, 7*(2), 585-595. doi:10.1039/c8bm01050a

Navaei, A., Saini, H., Christenson, W., Sullivan, R. T., Ros, R., & Nikkhah, M. (2016). Gold nanorod-incorporated gelatin-based conductive hydrogels for engineering cardiac tissue constructs. *Acta Biomater, 41*, 133-146. doi:10.1016/j.actbio.2016.05.027

Navaei, A., Truong, D., Heffernan, J., Cutts, J., Brafman, D., Sirianni, R. W., . . . Nikkhah, M. (2016). PNIPAAm-based biohybrid injectable hydrogel for cardiac tissue engineering. *Acta Biomaterialia, 32*, 10-23.

Neto, A., Correia, C., Oliveira, M., Rial-Hermida, M., Alvarez-Lorenzo, C., Reis, R., & Mano, J. (2015). A novel hanging spherical drop system for the generation of cellular spheroids and high throughput combinatorial drug screening. *Biomaterials Science, 3*(4), 581-585.

Nguyen, A. H., Marsh, P., Schmiess-Heine, L., Burke, P. J., Lee, A., Lee, J., & Cao, H. (2019). Cardiac tissue engineering: state-of-the-art methods and outlook. *Journal of Biological Engineering, 13*(1), 57. doi:10.1186/s13036-019-0185-0

Nguyen, D. C., Hookway, T. A., Wu, Q., Jha, R., Preininger, M. K., Chen, X., . . . Maher, K. (2014). Microscale generation of cardiospheres promotes robust enrichment of cardiomyocytes derived from human pluripotent stem cells. *Stem Cell Reports, 3*(2), 260-268.

Nie, F.-Q., Xu, Z.-K., Huang, X.-J., Ye, P., & Wu, J. (2003). Acrylonitrile-based copolymer membranes containing reactive groups: surface modification by the immobilization of poly (ethylene glycol) for improving antifouling property and biocompatibility. *Langmuir, 19*(23), 9889-9895.

Niebruegge, S., Bauwens, C. L., Peerani, R., Thavandiran, N., Masse, S., Sevaptisidis, E., . . . Kumacheva, E. (2009). Generation of human embryonic stem cell-derived mesoderm and cardiac cells using size-specified aggregates in an oxygen-controlled bioreactor. *Biotechnology and Bioengineering, 102*(2), 493-507.

Nikkhah, M., Akbari, M., Paul, A., Memic, A., Dolatshahi-Pirouz, A., & Khademhosseini, A. (2016). Gelatin-Based Biomaterials For Tissue Engineering And Stem Cell Bioengineering. *Biomaterials from Nature for Advanced Devices and Therapies*, 37-62. doi:https://doi.org/10.1002/9781119126218.ch3

Nikkhah, M., Edalat, F., Manoucheri, S., & Khademhosseini, A. (2012). Engineering microscale topographies to control the cell–substrate interface. *Biomaterials, 33*(21), 5230-5246.

Noguchi, R., Nakayama, K., Itoh, M., Kamohara, K., Furukawa, K., Oyama, J.-i., . . . Morita, S. (2016). Development of a three-dimensional pre-vascularized scaffold-free contractile cardiac patch for treating heart disease. *The Journal of Heart and Lung Transplantation, 35*(1), 137-145.

Nugraha, B., Buono, M. F., von Boehmer, L., Hoerstrup, S. P., & Emmert, M. Y. (2019). Human Cardiac Organoids for Disease Modeling. *Clin Pharmacol Ther, 105*(1), 79-85. doi:10.1002/cpt.1286

Nunes, S. S., Miklas, J. W., Liu, J., Aschar-Sobbi, R., Xiao, Y., Zhang, B., . . . Hsieh, A. (2013). Biowire: a platform for maturation of human pluripotent stem cell–derived cardiomyocytes. *Nature Methods, 10*(8), 781.

Ogasawara, T., Okano, S., Ichimura, H., Kadota, S., Tanaka, Y., Minami, I., . . . Shiba, Y. (2017). Impact of extracellular matrix on engraftment and maturation of pluripotent stem cell-derived cardiomyocytes in a rat myocardial infarct model. *Sci Rep, 7*(1), 8630. doi:10.1038/s41598-017-09217-x

Oltolina, F., Zamperone, A., Colangelo, D., Gregoletto, L., Reano, S., Pietronave, S., . . . Diena, M. (2015). Human cardiac progenitor spheroids exhibit enhanced engraftment potential. *PLOS ONE, 10*(9).

Ong, C. S., Fukunishi, T., Zhang, H., Huang, C. Y., Nashed, A., Blazeski, A., . . . Tung, L. (2017). Biomaterial-free three-dimensional bioprinting of cardiac tissue using human induced pluripotent stem cell derived cardiomyocytes. *Scientific Reports, 7*(1), 1-11.

Pagano, F., Picchio, V., Chimenti, I., Sordano, A., De Falco, E., Peruzzi, M., . . . Sciarretta, S. (2019). On the Road to Regeneration:“Tools” and “Routes” Towards Efficient Cardiac Cell Therapy for Ischemic Cardiomyopathy. *Current Cardiology Reports, 21*(11), 133.

Pal, A., Smith, C. I., Palade, J., Nagaraju, S., Alarcon-Benedetto, B. A., Kilbourne, J., . . . Nikkhah, M. (2020). Poly (N-isopropylacrylamide)-based dual-crosslinking biohybrid injectable hydrogels for vascularization. *Acta Biomaterialia, 107*, 138-151.

Pal, A., Vernon, B. L., & Nikkhah, M. (2018). Therapeutic neovascularization promoted by injectable hydrogels. *Bioactive Materials, 3*(4), 389-400.

Park, J., Kim, Y. S., Ryu, S., Kang, W. S., Park, S., Han, J., . . . Kim, B.-S. (2015a). Graphene Potentiates the Myocardial Repair Efficacy of Mesenchymal Stem Cells by Stimulating the Expression of Angiogenic Growth Factors and Gap Junction Protein. *Advanced Functional Materials, 25*(17), 2590-2600. doi:https://doi.org/10.1002/adfm.201500365

Park, J., Kim, Y. S., Ryu, S., Kang, W. S., Park, S., Han, J., . . . Kim, B. S. (2015b). Graphene potentiates the myocardial repair efficacy of mesenchymal stem cells by stimulating the expression of angiogenic growth factors and gap junction protein. *Advanced Functional Materials, 25*(17), 2590-2600.

Pasqualini, F. S., Sheehy, S. P., Agarwal, A., Aratyn-Schaus, Y., & Parker, K. K. (2015). Structural phenotyping of stem cell-derived cardiomyocytes. *Stem Cell Reports, 4*(3), 340-347. doi:10.1016/j.stemcr.2015.01.020

Patino-Guerrero, A., Ponce Wong, R. D., Kodibagkar, V. D., Zhu, W., Migrino, R. Q., Graudejus, O., & Nikkhah, M. (2023). Development and Characterization of Isogenic Cardiac Organoids from Human-Induced Pluripotent Stem Cells Under Supplement Starvation Regimen. *ACS Biomaterials Science & Engineering, 9*(2), 944-958. doi:10.1021/acsbiomaterials.2c01290

Patino-Guerrero, A., Veldhuizen, J., Zhu, W., Migrino, R. Q., & Nikkhah, M. (2020). Three-dimensional scaffold-free microtissues engineered for cardiac repair. *J Mater Chem B, 8*(34), 7571-7590. doi:10.1039/d0tb01528h

Paul, A., Hasan, A., Kindi, H. A., Gaharwar, A. K., Rao, V. T., Nikkhah, M., . . . Shum-Tim, D. (2014). Injectable graphene oxide/hydrogel-based angiogenic gene delivery system for vasculogenesis and cardiac repair. *ACS Nano, 8*(8), 8050-8062.

Pedde, R. D., Mirani, B., Navaei, A., Styan, T., Wong, S., Mehrali, M., . . . Dolatshahi-Pirouz, A. (2017). Emerging biofabrication strategies for engineering complex tissue constructs. *Advanced Materials, 29*(19), 1606061.

Perin, E. C., & López, J. (2006). Methods of stem cell delivery in cardiac diseases. *Nature Clinical Practice Cardiovascular Medicine, 3*(1), S110-S113.

Phelan, M. A., Gianforcaro, A. L., Gerstenhaber, J. A., & Lelkes, P. I. (2019). An Air Bubble-Isolating Rotating Wall Vessel Bioreactor for Improved Spheroid/Organoid Formation. *Tissue Engineering Part C: Methods, 25*(8), 479-488. doi:10.1089/ten.tec.2019.0088

Pinto, A. R., Ilinykh, A., Ivey, M. J., Kuwabara, J. T., D'Antoni, M. L., Debuque, R., . . . Tallquist, M. D. (2016). Revisiting Cardiac Cellular Composition. *Circ Res, 118*(3), 400-409. doi:10.1161/CIRCRESAHA.115.307778

Pitaktong, I., Lui, C., Lowenthal, J., Mattson, G., Jung, W.-H., Bai, Y., . . . Gerecht, S. (2020). Early Vascular Cells Improve Microvascularization Within 3D Cardiac Spheroids. *Tissue Engineering Part C: Methods, 26*(2), 80-90.

Polonchuk, L., Chabria, M., Badi, L., Hoflack, J.-C., Figtree, G., Davies, M. J., & Gentile, C. (2017). Cardiac spheroids as promising in vitro models to study the human heart microenvironment. *Scientific Reports, 7*(1), 1-12.

Pomeroy, J. E., Helfer, A., & Bursac, N. (2019). Biomaterializing the promise of cardiac tissue engineering. *Biotechnology Advances*.

Prabhu, S. D., & Frangogiannis, N. G. (2016). The Biological Basis for Cardiac Repair After Myocardial Infarction. *Circulation Research, 119*(1), 91-112. doi:doi:10.1161/CIRCRESAHA.116.303577

Radisic, M., Deen, W., Langer, R., & Vunjak-Novakovic, G. (2005). Mathematical model of oxygen distribution in engineered cardiac tissue with parallel channel array perfused with culture medium containing oxygen carriers. *American Journal of Physiology-Heart and Circulatory Physiology, 288*(3), H1278-H1289.

Radisic, M., Park, H., Gerecht, S., Cannizzaro, C., Langer, R., & Vunjak-Novakovic, G. (2007). Biomimetic approach to cardiac tissue engineering. *Philosophical transactions of the Royal Society of London. Series B, Biological sciences, 362*(1484), 1357-1368. doi:10.1098/rstb.2007.2121

Rajabi-Zeleti, S., Jalili-Firoozinezhad, S., Azarnia, M., Khayyatan, F., Vahdat, S., Nikeghbalian, S., . . . Aghdami, N. (2014). The behavior of cardiac progenitor cells on macroporous pericardium-derived scaffolds. *Biomaterials, 35*(3), 970-982.

Rambanapasi, C., Zeevaart, J. R., Buntting, H., Bester, C., Kotze, D., Hayeshi, R., & Grobler, A. (2016). Bioaccumulation and Subchronic Toxicity of 14 nm Gold Nanoparticles in Rats. *Molecules, 21*(6). doi:10.3390/molecules21060763

Ravenscroft, S. M., Pointon, A., Williams, A. W., Cross, M. J., & Sidaway, J. E. (2016). Cardiac Non-myocyte Cells Show Enhanced Pharmacological Function Suggestive of Contractile Maturity in Stem Cell Derived Cardiomyocyte Microtissues. *Toxicological Sciences, 152*(1), 99-112. doi:10.1093/toxsci/kfw069

Ravi, M., Paramesh, V., Kaviya, S., Anuradha, E., & Solomon, F. P. (2015). 3D cell culture systems: advantages and applications. *Journal of Cellular Physiology, 230*(1), 16-26.

Rezai, N., Corbel, S. Y., Dabiri, D., Kerjner, A., Rossi, F. M., McManus, B. M., & Podor, T. J. (2005). Bone marrow-derived recipient cells in murine transplanted hearts:

potential roles and the effect of immunosuppression. *Laboratory Investigation, 85*(8), 982-991.

Ribeiro, M. C., Tertoolen, L. G., Guadix, J. A., Bellin, M., Kosmidis, G., D'Aniello, C., . . . Feinberg, A. W. (2015). Functional maturation of human pluripotent stem cell derived cardiomyocytes in vitro–correlation between contraction force and electrophysiology. *Biomaterials, 51*, 138-150.

Richards, D. J., Coyle, R. C., Tan, Y., Jia, J., Wong, K., Toomer, K., . . . Mei, Y. (2017). Inspiration from heart development: Biomimetic development of functional human cardiac organoids. *Biomaterials, 142*, 112-123.

Richards, D. J., Li, Y., Kerr, C. M., Yao, J., Beeson, G. C., Coyle, R. C., . . . Mei, Y. (2020). Human cardiac organoids for the modelling of myocardial infarction and drug cardiotoxicity. *Nature Biomedical Engineering, 4*(4), 446-462. doi:10.1038/s41551-020-0539-4

Richards, D. J., Tan, Y., Coyle, R., Li, Y., Xu, R., Yeung, N., . . . Mei, Y. (2016). Nanowires and Electrical Stimulation Synergistically Improve Functions of hiPSC Cardiac Spheroids. *Nano Letters, 16*(7), 4670-4678. doi:10.1021/acs.nanolett.6b02093

Robertson, C., Tran, D. D., & George, S. C. (2013). Concise review: maturation phases of human pluripotent stem cell-derived cardiomyocytes. *Stem Cells, 31*(5), 829-837. doi:10.1002/stem.1331

Roche, C. D., Brereton, R. J. L., Ashton, A. W., Jackson, C., & Gentile, C. (2020). Current challenges in three-dimensional bioprinting heart tissues for cardiac surgery. *Eur J Cardiothorac Surg, 58*(3), 500-510. doi:10.1093/ejcts/ezaa093

Rodriguez, A., Elabd, C., Amri, E., Ailhaud, G., & Dani, C. (2005). The human adipose tissue is a source of multipotent stem cells. *Biochimie, 87*(1), 125-128.

Ronaldson-Bouchard, K., Ma, S. P., Yeager, K., Chen, T., Song, L., Sirabella, D., . . . Vunjak-Novakovic, G. (2018). Advanced maturation of human cardiac tissue grown from pluripotent stem cells. *Nature, 556*(7700), 239-243.

Roth, G. A., Mensah, G. A., Johnson, C. O., Addolorato, G., Ammirati, E., Baddour, L. M., . . . Fuster, V. (2020). Global Burden of Cardiovascular Diseases and Risk Factors, 1990–2019: Update From the GBD 2019 Study. *Journal of the American College of Cardiology, 76*(25), 2982-3021. doi:https://doi.org/10.1016/j.jacc.2020.11.010

Rouwkema, J., Koopman, B. F., Blitterswijk, C. A. V., Dhert, W. J., & Malda, J. (2009). Supply of nutrients to cells in engineered tissues. *Biotechnology and Genetic Engineering Reviews, 26*(1), 163-178.

Rungarunlert, S., Klincumhom, N., Bock, I., Nemes, C., Techakumphu, M., Pirity, M. K., & Dinnyes, A. (2011). Enhanced cardiac differentiation of mouse embryonic stem cells by use of the slow-turning, lateral vessel (STLV) bioreactor. *Biotechnology Letters, 33*(8), 1565-1573.

Rupert, C. E., Kim, T. Y., Choi, B.-R., & Coulombe, K. L. K. (2020). Human Cardiac Fibroblast Number and Activation State Modulate Electromechanical Function of hiPSC-Cardiomyocytes in Engineered Myocardium. *Stem Cells International, 2020*, 9363809. doi:10.1155/2020/9363809

Sadayappan, S., & de Tombe, P. P. (2012). Cardiac myosin binding protein-C: redefining its structure and function. *Biophys Rev, 4*(2), 93-106. doi:10.1007/s12551-012-0067-x

Saini, H., Navaei, A., Van Putten, A., & Nikkhah, M. (2015). 3D Cardiac Microtissues Encapsulated with the Co-Culture of Cardiomyocytes and Cardiac Fibroblasts. *Advanced healthcare materials, 4*(13), 1961-1971. doi:10.1002/adhm.201500331

Saini, H., Sam, F. S., Kharaziha, M., & Nikkhah, M. (2018). 8 Micropatterning. *Cell and Material Interface: Advances in Tissue Engineering, Biosensor, Implant, and Imaging Technologies*, 187.

Sakaguchi, K., Shimizu, T., & Okano, T. (2015). Construction of three-dimensional vascularized cardiac tissue with cell sheet engineering. *Journal of Controlled Release, 205*, 83-88. doi:https://doi.org/10.1016/j.jconrel.2014.12.016

Sakalem, M. E., De Sibio, M. T., da Costa, F. A. d. S., & de Oliveira, M. (2021). Historical evolution of spheroids and organoids, and possibilities of use in life sciences and medicine. *Biotechnology Journal*, *16*(5), 2000463. doi:https://doi.org/10.1002/biot.202000463

Sala, L., Ward-van Oostwaard, D., Tertoolen, L. G. J., Mummery, C. L., & Bellin, M. (2017). Electrophysiological Analysis of human Pluripotent Stem Cell-derived Cardiomyocytes (hPSC-CMs) Using Multi-electrode Arrays (MEAs). *J Vis Exp*(123), e55587. doi:10.3791/55587

Santana, L. F., Cheng, E. P., & Lederer, W. J. (2010). How does the shape of the cardiac action potential control calcium signaling and contraction in the heart? *J Mol Cell Cardiol, 49*(6), 901-903. doi:10.1016/j.yjmcc.2010.09.005

Santos-Martinez, M. J., Rahme, K., Corbalan, J. J., Faulkner, C., Holmes, J. D., Tajber, L., . . . Radomski, M. W. (2014). Pegylation Increases Platelet Biocompatibility of Gold Nanoparticles. *Journal of Biomedical Nanotechnology, 10*(6), 1004-1015. doi:10.1166/jbn.2014.1813

Savarese, G., & Lund, L. H. (2017). Global public health burden of heart failure. *Cardiac failure review, 3*(1), 7.

Schwartz, S. D., Hubschman, J.-P., Heilwell, G., Franco-Cardenas, V., Pan, C. K., Ostrick, R. M., . . . Lanza, R. (2012). Embryonic stem cell trials for macular degeneration: a preliminary report. *The Lancet, 379*(9817), 713-720.

Scuderi, G. J., & Butcher, J. (2017). Naturally Engineered Maturation of Cardiomyocytes. *Frontiers in Cell and Developmental Biology, 5*(50). doi:10.3389/fcell.2017.00050

Segers, V. F., & Lee, R. T. (2008). Stem-cell therapy for cardiac disease. *Nature, 451*(7181), 937-942.

Sekiya, S., Shimizu, T., Yamato, M., Kikuchi, A., & Okano, T. (2006). Bioengineered cardiac cell sheet grafts have intrinsic angiogenic potential. *Biochemical and Biophysical Research Communications, 341*(2), 573-582.

Shadrin, I. Y., Allen, B. W., Qian, Y., Jackman, C. P., Carlson, A. L., Juhas, M. E., & Bursac, N. (2017). Cardiopatch platform enables maturation and scale-up of human pluripotent stem cell-derived engineered heart tissues. *Nature Communications, 8*(1), 1825. doi:10.1038/s41467-017-01946-x

Shafei, A. E. S., Ali, M. A., Ghanem, H. G., Shehata, A. I., Abdelgawad, A. A., Handal, H. R., . . . El-Shal, A. S. (2017). Mesenchymal stem cell therapy: A promising cell-based therapy for treatment of myocardial infarction. *The journal of Gene Medicine, 19*(12), e2995.

Shapira-Schweitzer, K., & Seliktar, D. (2007). Matrix stiffness affects spontaneous contraction of cardiomyocytes cultured within a PEGylated fibrinogen biomaterial. *Acta Biomaterialia, 3*(1), 33-41.

Shapira, A., Feiner, R., & Dvir, T. (2016). Composite biomaterial scaffolds for cardiac tissue engineering. *International Materials Reviews, 61*(1), 1-19.

Shard, A. G., Wright, L., & Minelli, C. (2018). Robust and accurate measurements of gold nanoparticle concentrations using UV-visible spectrophotometry. *Biointerphases, 13*(6), 061002. doi:10.1116/1.5054780

Shettigar, R. R., Misra, N. M., & Patel, K. (2018). Cationic surfactant (CTAB) a multipurpose additive in polymer-based drilling fluids. *Journal of Petroleum Exploration and Production Technology, 8*(2), 597-606. doi:10.1007/s13202-017-0357-8

Shi, L., Zhang, J., Zhao, M., Tang, S., Cheng, X., Zhang, W., . . . Wang, Q. (2021). Effects of polyethylene glycol on the surface of nanoparticles for targeted drug delivery. *Nanoscale, 13*(24), 10748-10764. doi:10.1039/D1NR02065J

Shimizu, T., Yamato, M., Isoi, Y., Akutsu, T., Setomaru, T., Abe, K., . . . Okano, T. (2002). Fabrication of pulsatile cardiac tissue grafts using a novel 3-dimensional cell sheet manipulation technique and temperature-responsive cell culture surfaces. *Circulation Research, 90*(3), e40-e48.

Shin, S. R., Jung, S. M., Zalabany, M., Kim, K., Zorlutuna, P., Kim, S. b., . . . Kong, J. (2013). Carbon-nanotube-embedded hydrogel sheets for engineering cardiac constructs and bioactuators. *ACS Nano, 7*(3), 2369-2380.

Shin, S. R., Zihlmann, C., Akbari, M., Assawes, P., Cheung, L., Zhang, K., . . . Wan, K. t. (2016). Reduced graphene oxide-gelMA hybrid hydrogels as scaffolds for cardiac tissue engineering. *Small, 12*(27), 3677-3689.

Shukla, R., Bansal, V., Chaudhary, M., Basu, A., Bhonde, R. R., & Sastry, M. (2005). Biocompatibility of gold nanoparticles and their endocytotic fate inside the cellular compartment: a microscopic overview. *Langmuir, 21*(23), 10644-10654.

Simeonov, S., & Schäffer, T. E. (2019). Ultrafast Imaging of Cardiomyocyte Contractions by Combining Scanning Ion Conductance Microscopy with a Microelectrode Array. *Analytical Chemistry, 91*(15), 9648-9655. doi:10.1021/acs.analchem.9b01092

Slotvitsky, M. M., Tsvelaya, V. A., Podgurskaya, A. D., & Agladze, K. I. (2020). Formation of an electrical coupling between differentiating cardiomyocytes. *Scientific Reports, 10*(1), 7774. doi:10.1038/s41598-020-64581-5

Snir, M., Kehat, I., Gepstein, A., Coleman, R., Itskovitz-Eldor, J., Livne, E., & Gepstein, L. (2003). Assessment of the ultrastructural and proliferative properties of human embryonic stem cell-derived cardiomyocytes. *Am J Physiol Heart Circ Physiol, 285*(6), H2355-2363. doi:10.1152/ajpheart.00020.2003

Souders, C. A., Bowers, S. L., & Baudino, T. A. (2009). Cardiac fibroblast: the renaissance cell. *Circ Res, 105*(12), 1164-1176. doi:10.1161/CIRCRESAHA.109.209809

Spencer, T. M., Blumenstein, R. F., Pryse, K. M., Lee, S.-L., Glaubke, D. A., Carlson, B. E., . . . Genin, G. M. (2017). Fibroblasts Slow Conduction Velocity in a Reconstituted Tissue Model of Fibrotic Cardiomyopathy. *ACS Biomaterials Science & Engineering, 3*(11), 3022-3028. doi:10.1021/acsbiomaterials.6b00576

Sreejit, P., & Verma, R. (2013). Natural ECM as biomaterial for scaffold based cardiac regeneration using adult bone marrow derived stem cells. *Stem Cell Reviews and Reports, 9*(2), 158-171.

Stella Stoter, A. M., Hirt, M. N., Stenzig, J., & Weinberger, F. (2020). Assessment of Cardiotoxicity With Stem Cell-based Strategies. *Clin Ther, 42*(10), 1892-1910. doi:10.1016/j.clinthera.2020.08.012

Sun, L., Huang, C., Gong, T., & Zhou, S. (2010). A biocompatible approach to surface modification: biodegradable polymer functionalized super-paramagnetic iron oxide nanoparticles. *Materials Science and Engineering: C, 30*(4), 583-589.

Sun, Q., Zhang, Z., & Sun, Z. (2014). The potential and challenges of using stem cells for cardiovascular repair and regeneration. *Genes & Diseases, 1*(1), 113-119.

Sundnes, J., Lines, G. T., Cai, X., Nielsen, B. F., Mardal, K.-A., & Tveito, A. (2007). *Computing the electrical activity in the heart* (Vol. 1): Springer Science & Business Media.

Taddei, M. L., Giannoni, E., Fiaschi, T., & Chiarugi, P. (2012). Anoikis: an emerging hallmark in health and diseases. *J Pathol, 226*(2), 380-393. doi:10.1002/path.3000

Takada, T., Sasaki, D., Matsuura, K., Miura, K., Sakamoto, S., Goto, H., . . . Hagiwara, N. (2022). Aligned human induced pluripotent stem cell-derived cardiac tissue improves contractile properties through promoting unidirectional and synchronous cardiomyocyte contraction. *Biomaterials, 281*, 121351. doi:10.1016/j.biomaterials.2021.121351

Takahashi, K., Tanabe, K., Ohnuki, M., Narita, M., Ichisaka, T., Tomoda, K., & Yamanaka, S. (2007). Induction of pluripotent stem cells from adult human fibroblasts by defined factors. *Cell, 131*(5), 861-872.

Tan, Y., Richards, D., Coyle, R. C., Yao, J., Xu, R., Gou, W., . . . Mei, Y. (2017). Cell number per spheroid and electrical conductivity of nanowires influence the function of silicon nanowired human cardiac spheroids. *Acta biomaterialia, 51*, 495-504.

Tan, Y., Richards, D., Xu, R., Stewart-Clark, S., Mani, S. K., Borg, T. K., . . . Mei, Y. (2015). Silicon nanowire-induced maturation of cardiomyocytes derived from human induced pluripotent stem cells. *Nano Letters, 15*(5), 2765-2772.

Tasnim, K., & Liu, J. (2022). Emerging Bioelectronics for Brain Organoid Electrophysiology. *Journal of Molecular Biology, 434*(3), 167165. doi:https://doi.org/10.1016/j.jmb.2021.167165

Tertoolen, L. G. J., Braam, S. R., van Meer, B. J., Passier, R., & Mummery, C. L. (2018). Interpretation of field potentials measured on a multi electrode array in pharmacological toxicity screening on primary and human pluripotent stem cell-

derived cardiomyocytes. *Biochemical and Biophysical Research Communications, 497*(4), 1135-1141. doi:https://doi.org/10.1016/j.bbrc.2017.01.151

Thomson, K. S., Korte, F. S., Giachelli, C. M., Ratner, B. D., Regnier, M., & Scatena, M. (2013). Prevascularized microtemplated fibrin scaffolds for cardiac tissue engineering applications. *Tissue Engineering Part A, 19*(7-8), 967-977.

Thygesen, K., Alpert, J. S., & White, H. D. (2007). Universal Definition of Myocardial Infarction. *Circulation, 116*(22), 2634-2653. doi:doi:10.1161/CIRCULATIONAHA.107.187397

Tirziu, D., Giordano, F. J., & Simons, M. (2010). Cell communications in the heart. *Circulation, 122*(9), 928-937. doi:10.1161/CIRCULATIONAHA.108.847731

Tonsho, M., Michel, S., Ahmed, Z., Alessandrini, A., & Madsen, J. C. (2014). Heart transplantation: challenges facing the field. *Cold Spring Harbor Perspectives in Medicine, 4*(5), a015636.

Torella, D., Ellison, G. M., Méndez-Ferrer, S., Ibanez, B., & Nadal-Ginard, B. (2006). Resident human cardiac stem cells: role in cardiac cellular homeostasis and potential for myocardial regeneration. *Nature Clinical Practice Cardiovascular Medicine, 3*(1), S8-S13.

Truong, D., Fiorelli, R., Barrientos, E. S., Melendez, E. L., Sanai, N., Mehta, S., & Nikkhah, M. (2019). A three-dimensional (3D) organotypic microfluidic model for glioma stem cells–Vascular interactions. *Biomaterials, 198*, 63-77.

Truong, D. D., Kratz, A., Park, J. G., Barrientos, E. S., Saini, H., Nguyen, T., . . . Nikkhah, M. (2019). A human organotypic microfluidic tumor model permits investigation of the interplay between patient-derived fibroblasts and breast cancer cells. *Cancer Research, 79*(12), 3139-3151.

Ulmer, B. M., Stoehr, A., Schulze, M. L., Patel, S., Gucek, M., Mannhardt, I., . . . Hansen, A. (2018). Contractile work contributes to maturation of energy metabolism in hiPSC-derived cardiomyocytes. *Stem Cell Reports, 10*(3), 834-847.

Valdoz, J. C., Johnson, B. C., Jacobs, D. J., Franks, N. A., Dodson, E. L., Sanders, C., . . . Van Ry, P. M. (2021). The ECM: To Scaffold, or Not to Scaffold, That Is the Question. *Int J Mol Sci, 22*(23). doi:10.3390/ijms222312690

van Spreeuwel, A., Bax, N., Bastiaens, A., Foolen, J., Loerakker, S., Borochin, M., . . . Bouten, C. (2014). The influence of matrix (an) isotropy on cardiomyocyte contraction in engineered cardiac microtissues. *Integrative Biology, 6*(4), 422-429.

Varzideh, F., Mahmoudi, E., & Pahlavan, S. (2019). Coculture with noncardiac cells promoted maturation of human stem cell–derived cardiomyocyte microtissues.

Journal of Cellular Biochemistry, 120(10), 16681-16691. doi:https://doi.org/10.1002/jcb.28926

Vasquez, C., Benamer, N., & Morley, G. E. (2011). The cardiac fibroblast: functional and electrophysiological considerations in healthy and diseased hearts. *Journal of cardiovascular pharmacology, 57*(4), 380-388. doi:10.1097/FJC.0b013e31820cda19

Veerman, C. C., Kosmidis, G., Mummery, C. L., Casini, S., Verkerk, A. O., & Bellin, M. (2015). Immaturity of human stem-cell-derived cardiomyocytes in culture: fatal flaw or soluble problem? *Stem Cells Dev, 24*(9), 1035-1052. doi:10.1089/scd.2014.0533

Velasco, V., Shariati, S. A., & Esfandyarpour, R. (2020). Microtechnology-based methods for organoid models. *Microsystems & Nanoengineering, 6*(1), 76. doi:10.1038/s41378-020-00185-3

Veldhuizen, J., Chavan, R., Moghadas, B., Park, J. G., Kodibagkar, V. D., Migrino, R. Q., & Nikkhah, M. (2022). Cardiac ischemia on-a-chip to investigate cellular and molecular response of myocardial tissue under hypoxia. *Biomaterials, 281*, 121336. doi:10.1016/j.biomaterials.2021.121336

Veldhuizen, J., Cutts, J., Brafman, D. A., Migrino, R. Q., & Nikkhah, M. (2020). Engineering anisotropic human stem cell-derived three-dimensional cardiac tissue on-a-chip. *Biomaterials, 256*, 120195. doi:https://doi.org/10.1016/j.biomaterials.2020.120195

Veldhuizen, J., Mann, H. F., Karamanova, N., Van Horn, W. D., Migrino, R. Q., Brafman, D., & Nikkhah, M. (2022). Modeling long QT syndrome type 2 on-a-chip via in-depth assessment of isogenic gene-edited 3D cardiac tissues. *Science Advances, 8*(50), eabq6720. doi:10.1126/sciadv.abq6720

Veldhuizen, J., Migrino, R. Q., & Nikkhah, M. (2019). Three-dimensional microengineered models of human cardiac diseases. *Journal of biological engineering, 13*(1), 29.

Virag, J. I., & Murry, C. E. (2003). Myofibroblast and endothelial cell proliferation during murine myocardial infarct repair. *The American Journal of Pathology, 163*(6), 2433-2440.

Virani, S. S., Alonso, A., Benjamin, E. J., Bittencourt, M. S., Callaway, C. W., Carson, A. P., . . . Delling, F. N. (2020). Heart disease and stroke statistics—2020 update: a report from the American Heart Association. *Circulation*, E139-E596.

Voges, H. K., Mills, R. J., Elliott, D. A., Parton, R. G., Porrello, E. R., & Hudson, J. E. (2017). Development of a human cardiac organoid injury model reveals innate regenerative potential. *Development, 144*(6), 1118-1127.

Volarevic, V., Markovic, B. S., Gazdic, M., Volarevic, A., Jovicic, N., Arsenijevic, N., . . . Stojkovic, M. (2018). Ethical and safety issues of stem cell-based therapy. *International Journal of Medical Sciences, 15*(1), 36.

Vrandečić, N. S., Erceg, M., Jakić, M., & Klarić, I. (2010). Kinetic analysis of thermal degradation of poly(ethylene glycol) and poly(ethylene oxide)s of different molecular weight. *Thermochimica Acta, 498*(1), 71-80. doi:https://doi.org/10.1016/j.tca.2009.10.005

Wang, L., Huang, G., Sha, B., Wang, S., Han, Y., Wu, J., . . . Xu, F. (2014). Engineering three-dimensional cardiac microtissues for potential drug screening applications. *Current Medicinal Chemistry, 21*(22), 2497-2509.

Wang, L., Jiang, X., Ji, Y., Bai, R., Zhao, Y., Wu, X., & Chen, C. (2013). Surface chemistry of gold nanorods: origin of cell membrane damage and cytotoxicity. *Nanoscale, 5*(18), 8384-8391. doi:10.1039/C3NR01626A

Wang, X., Xi, W.-c., & Wang, F. (2014). The beneficial effects of intracoronary autologous bone marrow stem cell transfer as an adjunct to percutaneous coronary intervention in patients with acute myocardial infarction. *Biotechnology Letters, 36*(11), 2163-2168.

Wanjare, M., & Huang, N. F. (2017). Regulation of the microenvironment for cardiac tissue engineering. *Regenerative Medicine, 12*(2), 187-201. doi:10.2217/rme-2016-0132

Wells, S. P., Waddell, H. M., Sim, C. B., Lim, S. Y., Bernasochi, G. B., Pavlovic, D., . . . Bell, J. R. (2019). Cardiomyocyte functional screening: interrogating comparative electrophysiology of high-throughput model cell systems. *American Journal of Physiology-Cell Physiology, 317*(6), C1256-C1267. doi:10.1152/ajpcell.00306.2019

Willets, K. A., & Van Duyne, R. P. (2007). Localized surface plasmon resonance spectroscopy and sensing. *Annual review of physical chemistry, 58*(1), 267-297.

Williams, C., Budina, E., Stoppel, W. L., Sullivan, K. E., Emani, S., Emani, S. M., & Black III, L. D. (2015). Cardiac extracellular matrix–fibrin hybrid scaffolds with tunable properties for cardiovascular tissue engineering. *Acta Biomaterialia, 14*, 84-95.

Woodcock, E. A., & Matkovich, S. J. (2005). Cardiomyocytes structure, function and associated pathologies. *Int J Biochem Cell Biol, 37*(9), 1746-1751. doi:10.1016/j.biocel.2005.04.011

Wu, Y., & Guo, L. (2018). Enhancement of Intercellular Electrical Synchronization by Conductive Materials in Cardiac Tissue Engineering. *IEEE Transactions on Biomedical Engineering, 65*(2), 264-272. doi:10.1109/TBME.2017.2764000

Xu, M., Zhu, J., Wang, F., Xiong, Y., Wu, Y., Wang, Q., . . . Liu, S. (2016). Improved in vitro and in vivo biocompatibility of graphene oxide through surface modification: poly (acrylic acid)-functionalization is superior to PEGylation. *ACS Nano, 10*(3), 3267-3281.

Xu, Y., Wang, X., Chen, L., Zhao, Y., He, L., Yang, P., . . . Zhang, Q. (2015). High-yield synthesis of gold nanoribbons by using binary surfactants. *Journal of Materials Chemistry C, 3*(7), 1447-1451. doi:10.1039/C4TC02603A

Yan, Y., Bejoy, J., Xia, J., Griffin, K., Guan, J., & Li, Y. (2019). Cell population balance of cardiovascular spheroids derived from human induced pluripotent stem cells. *Scientific Reports, 9*(1), 1-12.

Yang, J., Ding, N., Zhao, D., Yu, Y., Shao, C., Ni, X., . . . Hu, S. (2021). Intermittent Starvation Promotes Maturation of Human Embryonic Stem Cell-Derived Cardiomyocytes. *Front Cell Dev Biol, 9*, 687769. doi:10.3389/fcell.2021.687769

Yang, J., Yamato, M., Kohno, C., Nishimoto, A., Sekine, H., Fukai, F., & Okano, T. (2005). Cell sheet engineering: recreating tissues without biodegradable scaffolds. *Biomaterials, 26*(33), 6415-6422.

Yang, X., Pabon, L., & Murry, C. E. (2014). Engineering Adolescence. *Circulation Research, 114*(3), 511-523. doi:doi:10.1161/CIRCRESAHA.114.300558

Yu, D., Wang, X., & Ye, L. (2021). Cardiac Tissue Engineering for the Treatment of Myocardial Infarction. *Journal of Cardiovascular Development and Disease, 8*(11). doi:10.3390/jcdd8110153

Yu, J., Vodyanik, M. A., Smuga-Otto, K., Antosiewicz-Bourget, J., Frane, J. L., Tian, S., . . . Stewart, R. (2007). Induced pluripotent stem cell lines derived from human somatic cells. *Science, 318*(5858), 1917-1920.

Zacharias, D. G., Nelson, T. J., Mueller, P. S., & Hook, C. C. (2011). *The science and ethics of induced pluripotency: what will become of embryonic stem cells?* Paper presented at the Mayo Clinic Proceedings.

Zhang, D., Shadrin, I. Y., Lam, J., Xian, H.-Q., Snodgrass, H. R., & Bursac, N. (2013). Tissue-engineered cardiac patch for advanced functional maturation of human ESC-derived cardiomyocytes. *Biomaterials, 34*(23), 5813-5820.

Zhang, H. Z., Kim, M. H., Lim, J. H., & Bae, H.-R. (2013). Time-dependent expression patterns of cardiac aquaporins following myocardial infarction. *Journal of Korean Medical Science, 28*(3), 402-408.

Zhang, J., Tao, R., Campbell, K. F., Carvalho, J. L., Ruiz, E. C., Kim, G. C., . . . Kamp, T. J. (2019). Functional cardiac fibroblasts derived from human pluripotent stem cells via second heart field progenitors. *Nat Commun, 10*(1), 2238. doi:10.1038/s41467-019-09831-5

Zhang, J., Wilson, G. F., Soerens, A. G., Koonce, C. H., Yu, J., Palecek, S. P., . . . Kamp, T. J. (2009). Functional cardiomyocytes derived from human induced pluripotent stem cells. *Circulation Research, 104*(4), e30-e41.

Zhang, J., Zhu, W., Radisic, M., & Vunjak-Novakovic, G. (2018). Can we engineer a human cardiac patch for therapy? *Circulation Research, 123*(2), 244-265.

Zhang, Z., & Lin, M. (2014). Fast loading of PEG–SH on CTAB-protected gold nanorods. *RSC Advances, 4*(34), 17760-17767. doi:10.1039/C3RA48061E

Zhao, C., Xu, X., Ferhan, A. R., Chiang, N., Jackman, J. A., Yang, Q., . . . Weiss, P. S. (2020). Scalable Fabrication of Quasi-One-Dimensional Gold Nanoribbons for Plasmonic Sensing. *Nano Letters, 20*(3), 1747-1754. doi:10.1021/acs.nanolett.9b04963

Zhao, S., Xu, Z., Wang, H., Reese, B. E., Gushchina, L. V., Jiang, M., . . . Shen, R. (2016). Bioengineering of injectable encapsulated aggregates of pluripotent stem cells for therapy of myocardial infarction. *Nature Communications, 7*(1), 1-12.

Ziaeian, B., & Fonarow, G. C. (2016). Epidemiology and aetiology of heart failure. *Nature Reviews Cardiology, 13*(6), 368-378.

Zong, X., Bien, H., Chung, C.-Y., Yin, L., Fang, D., Hsiao, B. S., . . . Entcheva, E. (2005). Electrospun fine-textured scaffolds for heart tissue constructs. *Biomaterials, 26*(26), 5330-5338.

Zorlutuna, P., Annabi, N., Camci-Unal, G., Nikkhah, M., Cha, J. M., Nichol, J. W., . . . Khademhosseini, A. (2012). Microfabricated biomaterials for engineering 3D tissues. *Advanced Materials, 24*(14), 1782-1804.

Zuppinger, C. (2019). 3D Cardiac Cell Culture: A Critical Review of Current Technologies and Applications. *Frontiers in Cardiovascular Medicine, 6*(87). doi:10.3389/fcvm.2019.00087

APPENDIX A

SUPPLEMENTARY INFORMATION FOR CHAPTER 3

The following files and figures are available as part of the supporting information:

Figures

- Figure A1. Diameter track of cardiac organoids
- Figure A2. Cardiac organoids after harvesting

Videos

Supplementary videos are readable using media players in Windows operating system.

- Video A1. Cardiac organoids after harvesting (Mono-culture, 0µg/ml)
- Video A2. Cardiac organoids after harvesting (Mono-culture, 0µg/ml)
- Video A3. Cardiac organoids after harvesting (Mono-culture, 0µg/ml)
- Video A4. Cardiac organoids after harvesting (Mono-culture, 0µg/ml)

Tables

- Table A1. Table of resources
- Table A2. qRT-PCR Primer sequences

A)

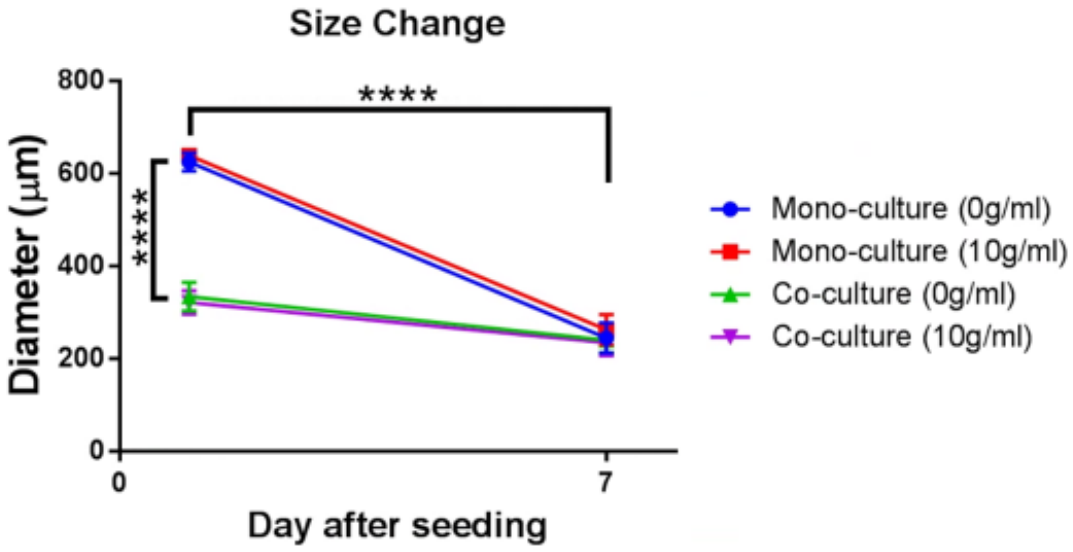

B)

		Mono-culture		Co-culture	
		0 μg/ml	10μg/ml	0 μg/ml	10μg/ml
Day 1	Mean (μm)	624.062	638.090	333.667	321.129
	Std Dev (μm)	34.513	26.240	53.569	43.885
Day 7	Mean (μm)	244.642	262.296	239.559	234.593
	Std Dev (μm)	56.569	56.429	46.300	49.232

Figure A1. Diameter track of cardiac organoids. A) Size (diameter) change of the four experimental groups on day 1 and day 7 after seeding in the agarose microwells (****: p-value <0.0001). B) Reported final sizes (mean and standard deviation) of the cardiac organoids.

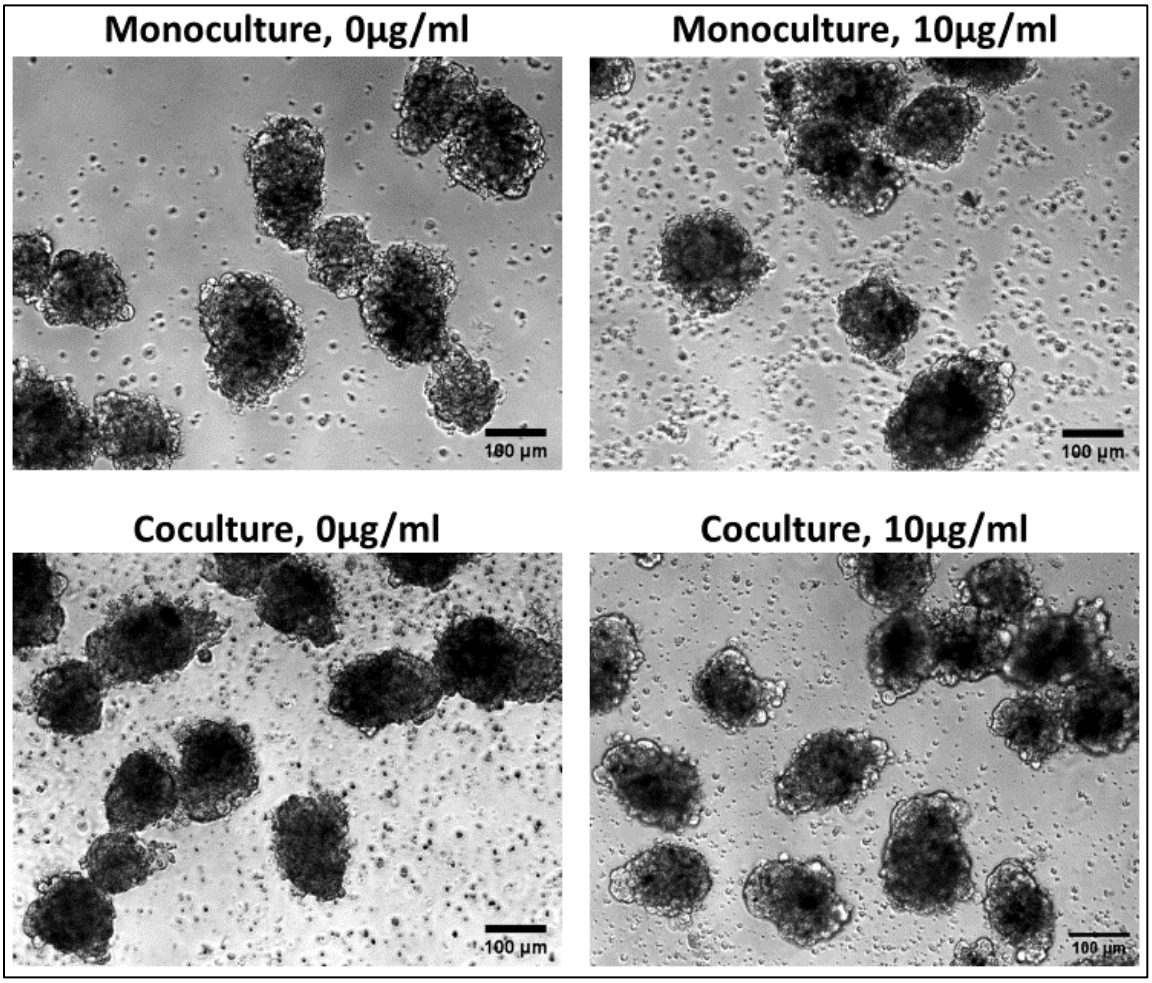

Figure A2. Cardiac organoids after harvesting. Representative phase-contrast images of the cardiac organoids after being harvested from the agarose microwells.

Table A1. Table of resources

Table of resources			
Human stem cell culture			
Reagent or resource	**Working concentration**	**Source**	**Identifier**
mTeSR-1	N/A	Stem Cell Technologies	85850
hESC-Matrigel	N/A	Corning	354277
EDTA	0.5mM	Corning	46-034-Cl
DPBS	1x	Gibco	21600-069
Fetal Bovine Serum	N/A	Gibco	10437-028
DMSO	N/A	Sigma Aldrich	276855
Differentiation of hiPSC-derived cardiomyocytes			
Reagent or Resource	**Concentration**	**Source**	**Identifier**
RPMI 1640	N/A	Corning	10-040-CVR
B27 Minus insulin Supplement	2% (v/v)	Gibco	A18956-02
Penicillin-Streptomycin (10,000 U/mL)	1% (v/v)	Gibco	15-140-122
EZSolution CHIR99021	6-9 µM	BioVision	1748-5
IWP2	5mM	Sigma Aldrich	I05365MG
B27 Supplement	2% (v/v)	Gibco	17504-001
RPMI 1640, glucose-free	N/A	Corning	10-043-CV
Sodium lactate	4mM	Sigma Aldrich	L4263-100ML
TrypLE Express	N/A	Gibco	12-604-021
Differentiation of hiPSC-derived cardiac fibroblasts			
Reagent or Resource	**Concentration**	**Source**	**Identifier**
DMEM, high glucose	N/A	Gibco	11965-092
Human serum albumin	500µg/ml	Sigma Aldrich	A9511
Linoleic acid	0.6µM		
Lecithin	0.6µg/ml		
β-fibroblast growth factor	70ng/µl	Sigma Aldrich	SRP6159-10UG
Trypsin-EDTA (0.5%)	1x	Gibco	15400054
Fibroblast Growth Media-3	N/A	PromoCell	C-23130
Gold nanoribbons syntesis			
Reagent or Resource	**Concentration**	**Source**	**Identifier**
CTAB	0.1M	VWR	97062-432
Gold(III) chloride trihydrate (HAuCl)	0.01M	Sigma Aldrich	254169-500MG
Sodium borohydrate	0.01M	Sigma Aldrich	452882
L-Ascorbic acid	0.1M	Sigma Aldrich	A0278
Sodium oleate (NaOL)	N/A	Fisher scientific	O005725G
Gold nanoribbons PEGylation			
Reagent or Resource	**Concentration**	**Source**	**Identifier**
Polyethylene glycol (mPEG-SH) [MW: 5000]	2mM	Laysan Bio	
Ethanol	20%	VWR	470301-070
Tris-HCl	50mM	VWR	97061-260
DPBS	1x	Gibco	21600-069
Agarose microwells			
Reagent or Resource	**Concentration**	**Source**	**Identifier**
Silicon molds	N/A	Microtissues	24-35
Agarose	2%	VWR	0710-25G
Cardiac organoid cryosectioning			
Reagent or Resource	**Concentration**	**Source**	**Identifier**
Glycine	100mM	Sigma Aldrich	G8898-500G
Tween-20	0.05% (v/v)	Sigma Aldrich	P2287-100ML
Sucrose	15% and 30%	Alfa Aesar	A15583
OCT compound	N/A	Tissue-Tek	4583
qRT-PCR			
Reagent or Resource	**Concentration**	**Source**	**Identifier**
RNA Microprep kit	N/A	Zymo	R1050
iScript™ Reverse Transcription Supermix	N/A	BioRad	1708841
iTaq Universal SYBR Green Supermix	N/A	BioRad	1725121
Cardiac organoid imaging			
Reagent or Resource	**Concentration**	**Source**	**Identifier**
Viability assay kit	N/A	Biotium	30002-T
Click-iT Plus TUNEL assay kit	N/A	Invitrogen	C10619

Table A2. qRT-PCR Primer sequences

Gene	Sequence Sense	Sequence	Reference
ACTN2	Forward	GGCACCCAGATTGAGAACAT	https://doi.org/10.1016/j.biomaterials.2020.120195
	Reverse	CCTGAATAGCAAAGCGAAGG	
GJA1	Forward	TACCAAACAGCAGCGGAGTT	https://doi.org/10.1016/j.biomaterials.2020.120195
	Reverse	TGGGCACCACTCTTTTGCTT	
MYH6	Forward	TCCTGCGGCCCAGATTCTTC	https://doi.org/10.1016/j.biomaterials.2020.120195
	Reverse	TCTTCCTTGTCATCGGGCAC	
MYH7	Forward	CACAGCCATGGGAGATTCGG	https://doi.org/10.1016/j.biomaterials.2020.120195
	Reverse	CACAGCCATGGGAGATTCGG	
TNNT2	Forward	GACAGAGCGGAAAAGTGGGA	https://doi.org/10.1016/j.biomaterials.2020.120195
	Reverse	CTCCTTGGCCTTCTCCCTCA	
TNNI3	Forward	CCTGCGGAGAGTGAGGATCT	https://doi.org/10.1016/j.biomaterials.2020.120195
	Reverse	CCGGTTTTCCTTCTCGGTGT	
RYR2	Forward	AGCCAGTGTCATCCACCAAC	https://doi.org/10.1016/j.biomaterials.2020.120195
	Reverse	ACTGATCACAGGTGGCTGAA	
18s	Forward	GTAACCCGTTGAACCCCATT	https://doi.org/10.1016/j.biomaterials.2020.120195
	Reverse	CCATCCAATCGGTAGTAGCG	

APPENDIX B

SUPPLEMENTARY INFORMATION FOR CHAPTER 4

The following files and figures are available as part of the supporting information:

Figures:

- Figure B1. Immunostaining for hiPSCs (Nanog, Sox2) and hiPSC-CFs.
- Figure B2. Phase-contrast images of hiPSC-CMs and cardiac organoids.
- Figure B3. TUNEL assay of sectioned cardiac organoids.

Tables:

- Table B1. Table of resources
- Table B2. qRT-PCR primer sequences

Videos:

Supplementary videos are readable using media players in Windows operating system.

- Video B1. hiPSC-CMs monolayer D-1 (Before supplement starvation)
- Video B2. hiPSC-CMs monolayer D0 (Supplemented media)
- Video B3. hiPSC-CMs monolayer D0 (Supplement-free media)
- Video B4. B27M: Representative cardiac organoid D7
- Video B5. B27C: Representative cardiac organoid D7
- Video B6. SFM: Representative cardiac organoid D7
- Video B7. SFC: Representative cardiac organoid D7
- Video B8. SFM cardiac organoids seeded on MEAs
- Video B9. SFC cardiac organoids seeded on MEAs
- Video B10. SFM FPs amplitude heatmap (0.5x speed)
- Video B11. SFC FPs amplitude heatmap (0.5x speed)

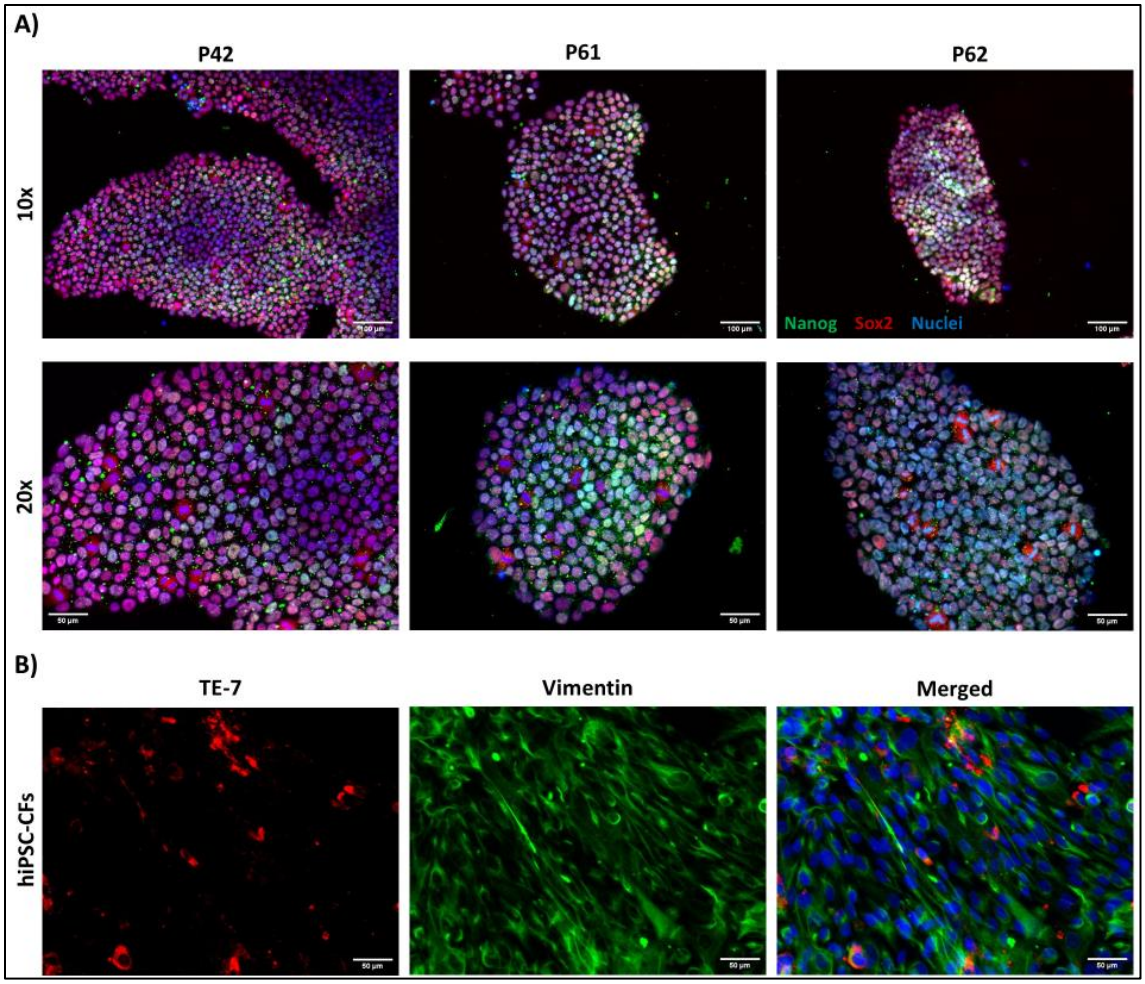

Figure B1. Immunocytochemistry for the characterization of hiPSC pluripotency and hiPSC-CFs. A) Staining of hiPSC monolayers of different passages is shown to demonstrate that the pluripotent state of the hiPSCs is maintained in cell culture. Top row: 10x magnification. Bottom row: 20x magnification. (Green: Nanog; Red: Sox2; Blue: Nuclei) (Scale bars: 100µm). B) Staining of hiPSC-CFs monolayers (Red: fibroblast marker (TE-7); Green: vimentin; Blue: Nuclei) (Scale bars: 50µm).

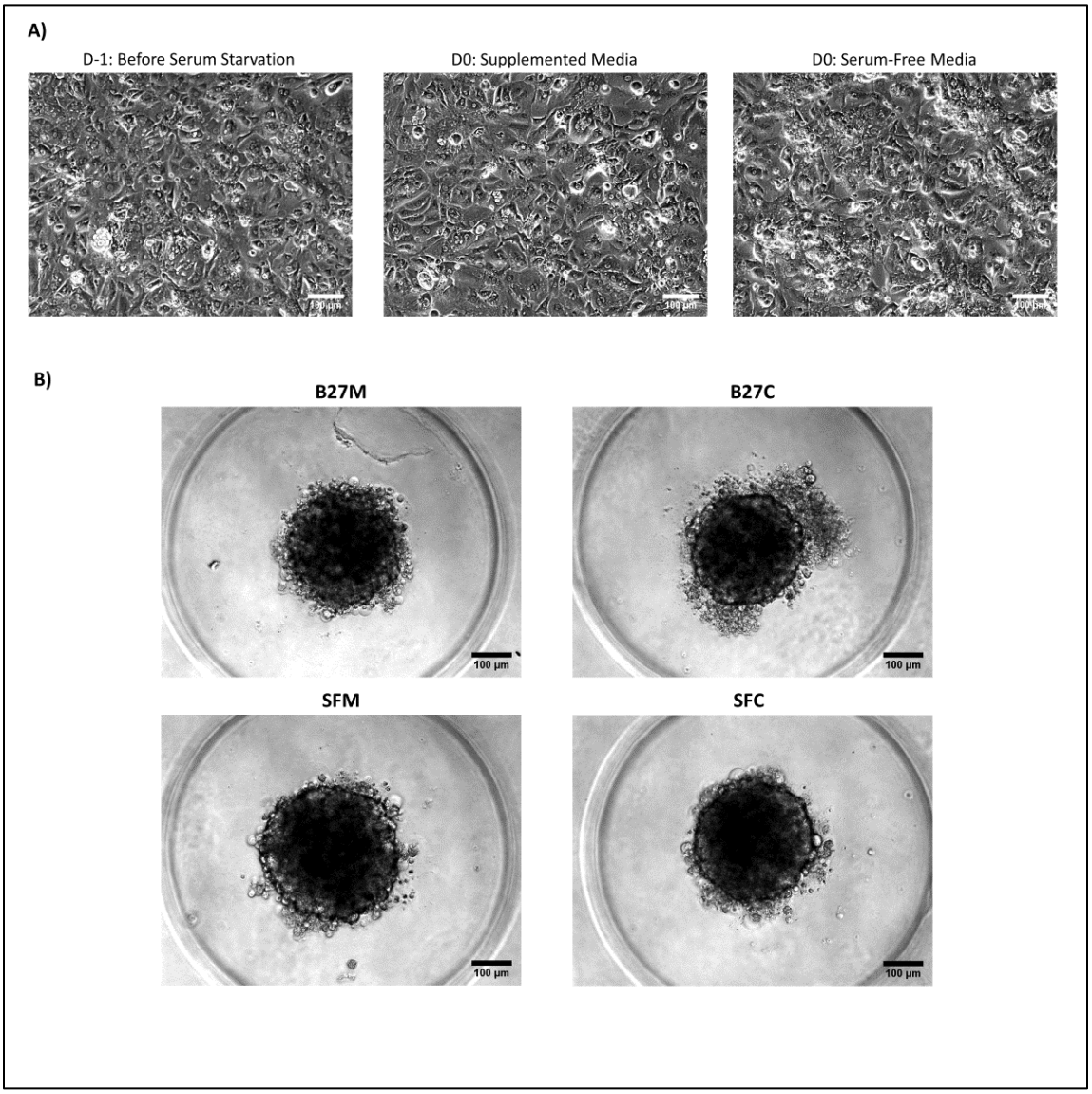

Figure B2. Phase-contrast images of hiPSC-CMs and cardiac organoids: A) Cardiomyocytes on 2D culture, before and after the serum starvation. B) Isogenic cardiac organoids in agarose microwells on D7 after seeding.

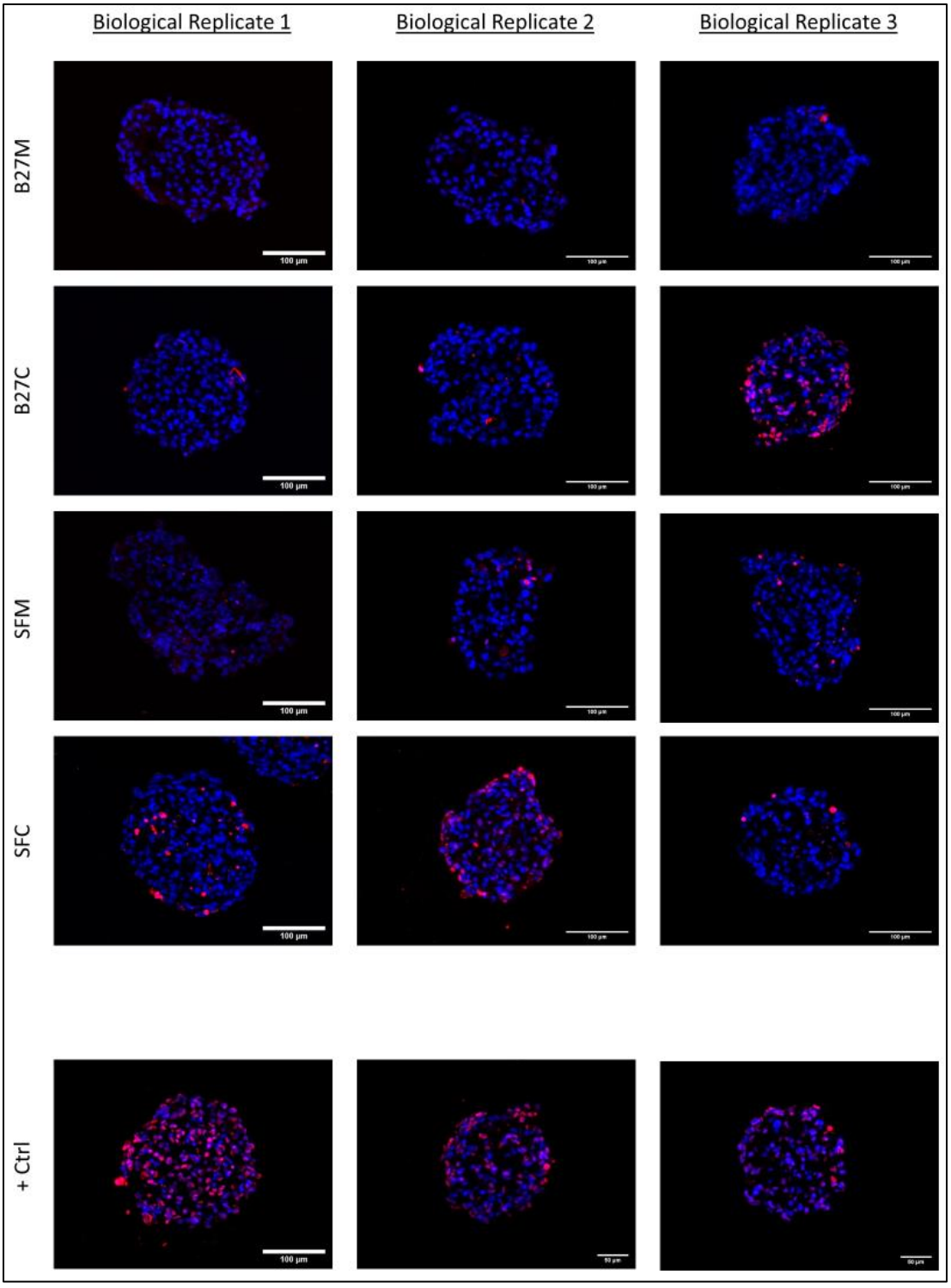

Figure B3. TUNEL assay of sectioned cardiac organoids. Three biological replicates for TUNEL assay, showing no significant cell death. The positive control was performed by treating a sample with DNAse I prior the TUNEL assay staining.

Table B1. Table of resources

Table of resources			
Human Stem Cell culture			
Reagent or Resource	**Concentration**	**Source**	**Identifier**
mTeSR-1	N/A	Stem Cell Technologies	85850
hESC-Matrigel	N/A	Corning	354277
EDTA	0.5mM	Corning	46-034-Cl
DPBS	1x	Gibco	21600-069
Fetal Bovine Serum	N/A	Gibco	10437-028
DMSO	N/A	Sigma Aldrich	276855
Differentiation of hiPSC-derived cardiomyocytes			
Reagent or Resource	**Concentration**	**Source**	**Identifier**
RPMI 1640	N/A	Corning	10-040-CVR
B27 Minus Insulin Supplement	2% (v/v)	Gibco	A18956-02
Penicillin-Streptomycin (10,000 U/mL)	1% (v/v)	Gibco	15-140-122
EZSolution CHIR99021	6-9 µM	BioVision	1748-5
IWP2	5mM	Sigma Aldrich	I05365MG
B27 Supplement	2% (v/v)	Gibco	17504-001
RPMI 1640, glucose-free	N/A	Corning	10-043-CV
Sodium lactate	4mM	Sigma Aldrich	L4263-100ML
TrypLE Express	N/A	Gibco	12-604-021
Differentiation of hiPSC-derived cardiomyocytes			
Reagent or Resource	**Concentration**	**Source**	**Identifier**
DMEM, high glucose	N/A	Gibco	11965-092
β-fibroblast growth factor	70ng/µl	Sigma Aldrich	SRP6159-10UG
Trypsin-EDTA (0.5%)	1x	Gibco	15400054
Fibroblast Growth Media-3	N/A	PromoCell	C-23130
Supplement Starvation regime for hiPSC-CMs			
Reagent or Resource	**Concentration**	**Source**	**Identifier**
DMEM	N/A		11965-092
Sodium pyruvate	100mg/l	Sigma Aldrich	P5280-25G
Agarose microwells			
Reagent or Resource	**Concentration**	**Source**	**Identifier**
Silicon molds	N/A	Microtissues	24-35
Agarose	2%	VWR	0710-25G

Cardiac organoid cryosectioning			
Reagent or Resource	**Concentration**	**Source**	**Identifier**
Glycine	100mM	Sigma Aldrich	G8898-500G
Tween-20	0.05% (v/v)	Sigma Aldrich	P2287-100ML
Sucrose	15% and 30%	Alfa Aesar	A15583
OCT compound	N/A	Tissue-Tek	4583
Immunohistochemistry			
Reagent or Resource	**Concentration**	**Source**	**Identifier**
Paraformaldehide	4%	ThermoScientific	61899-AK
Triton X-100	0.2% (v/)	Sigma Aldrich	T8787-100ML
Bovine serum albumin (radioimmunoassay grade)	0.1% (w/v)	Sigma Aldrich	A9647-100G
Tween-20	0.05%(v/v)	Sigma Aldrich	P2287-100ML
Sodium azide	0.02% (w/v)	Sigma Aldrich	S2002-25G
Goat Serum	10%	ImmunoReagents	10152-212
Vectashield Plus Antifade Mounting Medium	N/A	Vector	H-1900-10
Click-iT Plus TUNEL Assay for In Situ Apoptosis Detection, Alexa Fluor 594 dye	N/A	Invitrogen	C10618
Antibodies			
Sarcomeric Alpha Actinin (Mouse)	1:100	Thermo Fisher	MA1-22863
Connexin 43 (Rabbit)	1:125	Abcam	ab11370
Vimentin (Rabbit)	1:100	Cell Signaling	D24H3
TE-7 (Mouse)	1:100	EMD Millipore	CBL271
Sox2	1:200	Cell Signaling	D6D9
Nanog	1:200	Abcam	ab62734
Alexa Fluor 488 goat anti-mouse	1:500	Invitrogen	A11001
Alexa Fluor 594 goat anti-rabbit	1:500	Invitrogen	A11012
4’,6-diamidino-1-phenylindole (DAPI)	1:1000	Tocris Bioscience	57-485-0
qRT-PCR			
Reagent or Resource	**Concentration**	**Source**	**Identifier**
RNA Microprep kit	N/A	Zymo	R1050
iScript™ Reverse Transcription Supermix	N/A	BioRad	1708841
iTaq Universal SYBR Green Supermix	N/A	BioRad	1725121

Table B2. qPCR Primer Sequences

Gene	Sequence Sense	Sequence	Reference
ACTN2	Forward	GGCACCCAGATTGAGAACAT	https://doi.org/10.1016/j.biomaterials.2020.120195
	Reverse	CCTGAATAGCAAAGCGAAGG	
GJA1	Forward	TACCAAACAGCAGCGGAGTT	https://doi.org/10.1016/j.biomaterials.2020.120195
	Reverse	TGGGCACCACTCTTTTGCTT	
MYH6	Forward	TCCTGCGGCCCAGATTCTTC	https://doi.org/10.1016/j.biomaterials.2020.120195
	Reverse	TCTTCCTTGTCATCGGGCAC	
MYH7	Forward	CACAGCCATGGGAGATTCGG	https://doi.org/10.1016/j.biomaterials.2020.120195
	Reverse	CACAGCCATGGGAGATTCGG	
TNNT2	Forward	GACAGAGCGGAAAAGTGGGA	https://doi.org/10.1016/j.biomaterials.2020.120195
	Reverse	CTCCTTGGCCTTCTCCCTCA	
TNNI3	Forward	CCTGCGGAGAGTGAGGATCT	https://doi.org/10.1016/j.biomaterials.2020.120195
	Reverse	CCGGTTTTCCTTCTCGGTGT	
MLC2V	Forward	GGCGCCAACTCCAACGTGTT	https://doi.org/10.1016/j.biomaterials.2020.120195
	Reverse	ACGTTCACTCGCCCAAGGGC	
MLC2A	Forward	GAGGACAAGGTCAACACCCT	https://doi.org/10.1016/j.biomaterials.2013.04.026
	Reverse	CGCACCTTCTTCTCTTGCTC	
SERCA (ATP2A2)	Forward	CATCAAGCACACTGATCCCGT	https://doi.org/10.1016/j.biomaterials.2020.120195
	Reverse	CCACTCCCATAGCTTTCCCAG	
CASQ2	Forward	GTTGCCCGGGACAATACTGA	https://doi.org/10.1016/j.biomaterials.2020.120195
	Reverse	CTGTGACATTCACCACCCCA	
RYR2	Forward	AGCCAGTGTCATCCACCAAC	https://doi.org/10.1016/j.biomaterials.2020.120195
	Reverse	ACTGATCACAGGTGGCTGAA	
S100A1	Forward	AGACCCTCATCAACGTGTTC	NCBI Primer blast
	Reverse	CACAAGCACCACATACTCCT	
18s	Forward	GTAACCCGTTGAACCCCATT	https://doi.org/10.1016/j.biomaterials.2020.120195
	Reverse	CCATCCAATCGGTAGTAGCG	

APPENDIX C

SUPPLEMENTARY INFORMATION FOR CHAPTER 5

CODE C1

```
% % Creation of Amplitude heatmaps for FPs acquired with the glass
% MEAs/INTAN interphase
%
% This code serves to process the FPs from the 60 channels
corresponding
% to the 60 electrodes of the MEAs, recorded at a sampling rate of 30
kHz.
% This code creates heatmaps for displaying the peak-to-peak amplitude,
and
% the minimum and maximum values recorded for each of the electrodes.
%
% INPUT: Recorded FPs in a .txt file. This file must have the recording
% timepoints in the first column. The columns 2-61 must correspond to
the
% recorded amplitudes of each of the MEAs channels
%
% OUTPUT: The output of this code is in the form of 3 MATLAB figures
% that represent the spatial arrangement of the MEAs.
% The figures correspond to the peak-to-peak amplitude, and the minimum
% and maximum recorded values for each of the electrodes.
%
%
% A custom colorscale was created in order to facilitate the
%visualization of the displayed heatmaps. This custom colorscale is
%included as an appendix.
%


%% CODE INPUT

clear all
close all

%Reading data from txt file %%

x_SFM='SFM_1_-_0to20sec.txt';
data_SFM= importdata(x_SFM);
time=data_SFM(:,1);
data_SFM=data_SFM(:,2:61);

%% Signal peak-to-peak and min and man calculation

for a=1:60
    M1_SFM(a)=rms(data_SFM(:,a));
    M2_SFM(a)=peak2peak(data_SFM(:,a));
    M3_SFM(a)=min (data_SFM(:,a));
```

```
    M4_SFM(a)=max(data_SFM(:,a));
end
L=size(time);

%% Electrode-channel spatial correlation
% This matrix correlates the channel# (1-60) with its spatial
localization in the
% electrode grid. This correlation was obtained from the MEAs
manufacturer.

C=[...
    47,1;     48,2;    46,3;    45,4;    38,5;    37,6;    28,7;
36,8;    27,9;    17,10;...
    26,11;    16,12;   35,13;   25,14;   15,15;   14,16;   24,17;
34,18;   13,19;   23,20;...
    12,21;    22,22;   33,23;   21,24;   32,25;   31,26;   44,27;
43,28;   41,29;   42,30;...
    52,31;    51,32;   53,33;   54,34;   61,35;   62,36;   71,37;
63,38;   72,39;   82,40;...
    73,41;    83,42;   64,43;   74,44;   84,45;   85,46;   75,47;
65,48;   86,49;   76,50;...
    87,51;    77,52;   66,53;   78,54;   67,55;   68,56;   55,57;
56,58;   58,59;   57,60];


%% Index reassign matrix

for j=1:60

      a=C(j,1);
      b=C(j,2);

      Mrms_SFM(a)=M1_SFM(b);
      Mp2p_SFM(a)=M2_SFM(b);
      Mmin_SFM(a)=M3_SFM(b);
      Mmax_SFM(a)=M4_SFM(b);

end

Mrms_SFM(88)=0;
Mp2p_SFM(88)=0;
Mmin_SFM(88)=0;
Mmax_SFM(88)=0;

%% Electrode mapping matrix
x=10:10:80;
y=1:8;
[X1,Y1] = meshgrid(x,y);
R=X1+Y1;
```

```
%Zeroing grid Matrix

for i=1:40
    for j=1:40
        M1(i,j)=0;
    end
end

rms_grid_SFM=M1;
p2p_grid_SFM=M1;
min_grid_SFM=M1;
max_grid_SFM=M1;

e=38;
k=8;

for i=1:8
    d=3;
    for j=1:8
        rms_grid_SFM(e,d)=Mrms_SFM(R(i,j));
        p2p_grid_SFM(e,d)=Mp2p_SFM(R(i,j));
        min_grid_SFM(e,d)=Mmin_SFM(R(i,j));
        max_grid_SFM(e,d)=Mmax_SFM(R(i,j));
        d=d+5;
    end
    e=e-5;
    k=k-1;
end


%% Heatmap plotting

load CustomJet

figure
    imagesc(p2p_grid_SFM)
    axis ('tight')
    title('\fontsize{18}Peak-to-peak Amplitude Map')
    colorbar
    colormap (CustomJet);
    grid on
    clim([0 10413])

    ax=gca;
    ax.GridColor=[0 0 0];
    ax.Layer = 'top';
    ax.GridAlpha=1;
```

```
    ax.XTickLabel=[];
    ax.YTickLabel=[];


figure
    imagesc(min_grid_SFM)
    title('\fontsize{18}Minimum Amplitude Value')
    axis ('tight')
    colorbar
    colormap (flipud(CustomJet));
    grid on
    clim([-4024.4 0])

    ax=gca;
    ax.GridColor=[0 0 0];
    ax.Layer = 'top';
    ax.GridAlpha=1;
    ax.XTickLabel=[];
    ax.YTickLabel=[];


figure
    imagesc(max_grid_SFM)
    title('\fontsize{18}Maximum Amplitude Value')
    axis ('tight')
    colorbar
    colormap (CustomJet);
    grid on
    clim([0 6389] )

    ax=gca;
    ax.GridColor=[0 0 0];
    ax.Layer = 'top';
    ax.GridAlpha=1;
    ax.XTickLabel=[];
    ax.YTickLabel=[];
```

CODE C2

```
% % Creation of amplitude heatmap videos for FPs acquired with the glass
% MEAs/INTAN interphase
%
```

```
% This code serves to process the FPs from the 60 channels corresponding
% to the 60 electrodes of the MEAs, recorded at a sampling rate of 30 kHz.
% This code creates real-time heatmap videos for displaying the recorded
amplitude of
% each of the MEAs electrodes.
%
% INPUT: Recorded FPs in a .txt file. This file must have the recording
% timepoints in the first column. The columns 2-61 must correspond to the
% recorded amplitudes of each of the MEAs channels
%
% OUTPUT: The output of this code is in the form of a MP4 video that
% represents the spatial arrangement of the MEAs and the recorded amplitude
% in µV for each of the MEAs electrodes.
%
%

clear all
close all

%%CODE INPUT

% Read data from txt file %%

x_B27C='SFC_1_-_0to20sec.txt';
data= importdata(x_B27C);
time=data(:,1);
data=data(:,2:61);
L=size(time);

%% Electrode correlation matrix%%
%This matrix correlates the channel# (1-60) with its spatial localization in
the
% electrode grid. This correlation was obtained from the MEAs manufacturer.

C=[...
    47,1;     48,2;    46,3;    45,4;    38,5;    37,6;    28,7;    36,8;
27,9;    17,10;...
    26,11;    16,12;   35,13;   25,14;   15,15;   14,16;   24,17;   34,18;
13,19;   23,20;...
    12,21;    22,22;   33,23;   21,24;   32,25;   31,26;   44,27;   43,28;
41,29;   42,30;...
    52,31;    51,32;   53,33;   54,34;   61,35;   62,36;   71,37;   63,38;
72,39;   82,40;...
    73,41;    83,42;   64,43;   74,44;   84,45;   85,46;   75,47;   65,48;
86,49;   76,50;...
    87,51;    77,52;   66,53;   78,54;   67,55;   68,56;   55,57;   56,58;
58,59;   57,60];

%% Index reassign matrix%%

for j=1:60
       a=C(j,1);
       b=C(j,2);
```

```
      M(:,a)= data(:,b);
end

M(:,88)=zeros(L);

%% 3D Matrix %%
% Electrode mapping matrix
x=10:10:80;
y=1:8;
[X1,Y1] = meshgrid(x,y);
R=X1+Y1;

% Zeroing grid Matrix
for i=1:40
    for j=1:40
        M1(i,j)=0;
    end
end

e=38;
k=8;

for i=1:8
    d=3;
    for j=1:8
        M1(e,d,:)=M(:,R(i,j));
        d=d+5;
    end
    e=e-5;
    k=k-1;
end

a=1;

for m=1:501:501000 %for final video @ 60fps
    M2(:,:,a)= M1(:,:,m);
    a=a+1;
end

zmin=min(min(min(M2)));
zmax=max(max(max(M2)));
z1=zmin+abs(zmin);
z2=zmax+abs(zmin);

z2_surf=abs(z2);


%%     Plot each frame of the video
for n=1:1000

    M2(:,:,n)=M2(:,:,n)+abs(zmin);

    surf(M2(:,:,n),'FaceColor','interp', 'EdgeColor','interp');
        clim([0 8.5233e+03])
```

```
        axis([0 40 0 40 z1 z2])
        colormap ("colorcube");
        view ([-30, 15])
        hold on

        ax=gca;
        ax.GridColor=[0 0 0];
        ax.Layer = 'top';
        ax.GridAlpha=1;
        ax.XTickLabel=[];
        ax.YTickLabel=[];

        imagesc(M2(:,:,n),'AlphaData',0.85);
        clim([0 8.5233e+03])
        colormap ("colorcube");
        colorbar
        title ('\fontsize{18}SFM')

        ax=gca;
        ax.GridColor=[0 0 0];
        ax.Layer = 'top';
        ax.GridAlpha=1;
        ax.XTickLabel=[];
        ax.YTickLabel=[];
        view ([-30, 15])

    moviePlot(n)=getframe(gcf);

    hold off

end

%% Create video

myVideo=VideoWriter('N1_SFC_shade2_1x_40x40colorcube_normal2SFC','MPEG-4');

myVideo.FrameRate= 60; % Real time video
% myVideo.FrameRate= 30; % Time=0.5x
% myVideo.FrameRate= 15; % Time=0.25x

open (myVideo);
writeVideo(myVideo, moviePlot);
close (myVideo);
```

APPENDIX D

COPYRIGHT PERMISSIONS

Three-dimensional scaffold-free microtissues engineered for cardiac repair

A. Patino-Guerrero, J. Veldhuizen, W. Zhu, R. Q. Migrino and M. Nikkhah, *J. Mater. Chem. B*, 2020, **8**, 7571 **DOI:** 10.1039/D0TB01528H

To request permission to reproduce material from this article, please go to the Copyright Clearance Center request page.

If you are **an author contributing to an RSC publication, you do not need to request permission** provided correct acknowledgement is given.

If you are **the author of this article, you do not need to request permission to reproduce figures and diagrams** provided correct acknowledgement is given. If you want to reproduce the whole article in a third-party publication (excluding your thesis/dissertation for which permission is not required) please go to the Copyright Clearance Center request page.

Read more about how to correctly acknowledge RSC content.

ACS Publications
Most Trusted. Most Cited. Most Read.

Development and Characterization of Isogenic Cardiac Organoids from Human-Induced Pluripotent Stem Cells Under Supplement Starvation Regimen

Author: Alejandra Patino-Guerrero, Ruben D. Ponce Wong, Vikram D. Kodibagkar, et al
Publication: ACS Biomaterials Science & Engineering
Publisher: American Chemical Society
Date: Feb 1, 2023

PERMISSION/LICENSE IS GRANTED FOR YOUR ORDER AT NO CHARGE

This type of permission/license, instead of the standard Terms and Conditions, is sent to you because no fee is being charged for your order. Please note the following:

- Permission is granted for your request in both print and electronic formats, and translations.
- If figures and/or tables were requested, they may be adapted or used in part.
- Please print this page for your records and send a copy of it to your publisher/graduate school.
- Appropriate credit for the requested material should be given as follows: "Reprinted (adapted) with permission from {COMPLETE REFERENCE CITATION}. Copyright {YEAR} American Chemical Society." Insert appropriate information in place of the capitalized words.
- One-time permission is granted only for the use specified in your RightsLink request. No additional uses are granted (such as derivative works or other editions). For any uses, please submit a new request.

If credit is given to another source for the material you requested from RightsLink, permission must be obtained from that source.

BACK CLOSE WINDOW

APPENDIX E

PERMISSION TO USE CO-AUTHORED MATERIAL

Permissions from the co-authors of "**Three-dimensional scaffold-free microtissues engineered for cardiac repair**"

Permission to Use Co-Authored Material

I hereby grant permission for the utilization of the manuscript titled: "**Three-dimensional scaffold-free microtissues engineered for cardiac repair**", published in *Journal of Materials Chemistry B, 8(34), 7571-7590.*

The cited manuscript will be used as part of the Dissertation titled "**Development and Characterization of Isogenic Cardiac Organoids Derived from Human Pluripotent Stem Cells**", which will be presented to the Arizona State University Graduate College by Alejandra Patino-Guerrero in partial fulfillment of the requirements for the degree of Doctor of Philosophy.

Permission is hereby grated by (Printed name): Jaimeson Veldhuizen

Signature: 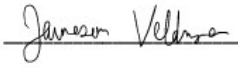

Date: 03/31/2023

Permission to Use Co-Authored Material

I hereby grant permission for the utilization of the manuscript titled: "**Three-dimensional scaffold-free microtissues engineered for cardiac repair**", published in *Journal of Materials Chemistry B, 8(34), 7571-7590*.

The cited manuscript will be used as part of the Dissertation titled "**Development and Characterization of Isogenic Cardiac Organoids Derived from Human Pluripotent Stem Cells**", which will be presented to the Arizona State University Graduate College by Alejandra Patino-Guerrero in partial fulfillment of the requirements for the degree of Doctor of Philosophy.

Permission is hereby grated by (Printed name): Wuqiang Zhu

Signature: Wuqiang Zhu

Date: March 30, 2023

Permission to Use Co-Authored Material

I hereby grant permission for the utilization of the manuscript titled: "**Three-dimensional scaffold-free microtissues engineered for cardiac repair**", published in *Journal of Materials Chemistry B, 8(34), 7571-7590.*

The cited manuscript will be used as part of the Dissertation titled "**Development and Characterization of Isogenic Cardiac Organoids Derived from Human Pluripotent Stem Cells**", which will be presented to the Arizona State University Graduate College by Alejandra Patino-Guerrero in partial fulfillment of the requirements for the degree of Doctor of Philosophy.

Permission is hereby grated by (Printed name): _____

Signature: _____ RAYMOND Q. MIGRINO 200761 Digitally signed by RAYMOND Q. MIGRINO 200761 Date: 2023.04.03 09:57:27 -07'00'

Date: _____

Permission to Use Co-Authored Material

I hereby grant permission for the utilization of the manuscript titled: "**Three-dimensional scaffold-free microtissues engineered for cardiac repair**", published in *Journal of Materials Chemistry B, 8(34), 7571-7590*.

The cited manuscript will be used as part of the Dissertation titled "**Development and Characterization of Isogenic Cardiac Organoids Derived from Human Pluripotent Stem Cells**", which will be presented to the Arizona State University Graduate College by Alejandra Patino-Guerrero in partial fulfillment of the requirements for the degree of Doctor of Philosophy.

Permission is hereby grated by (Printed name): Mehdi Nikkhah

Signature: 

Date: 3/31/2023

Permissions from the co-authors of "**Development and Characterization of Isogenic Cardiac Organoids from Human-Induced Pluripotent Stem Cells Under Supplement Starvation Regimen**"

Permission to Use Co-Authored Material

I hereby grant permission for the utilization of the manuscript titled: "**Development and Characterization of Isogenic Cardiac Organoids from Human-Induced Pluripotent Stem Cells Under Supplement Starvation Regimen**", published in *ACS Biomaterials Science & Engineering 9, 2 (2023): 944–958*.

The cited manuscript will be used as part of the Dissertation titled "**Development and Characterization of Isogenic Cardiac Organoids Derived from Human Pluripotent Stem Cells**", which will be presented to the Arizona State University Graduate College by Alejandra Patino-Guerrero in partial fulfillment of the requirements for the degree of Doctor of Philosophy.

Permission is hereby grated by (Printed name): Ruben D. Ponce Wong

Signature: 

Date: 03/30/2023

Permission to Use Co-Authored Material

I hereby grant permission for the utilization of the manuscript titled: "**Development and Characterization of Isogenic Cardiac Organoids from Human-Induced Pluripotent Stem Cells Under Supplement Starvation Regimen**", published in *ACS Biomaterials Science & Engineering 9, 2 (2023): 944–958*.

The cited manuscript will be used as part of the Dissertation titled "**Development and Characterization of Isogenic Cardiac Organoids Derived from Human Pluripotent Stem Cells**", which will be presented to the Arizona State University Graduate College by Alejandra Patino-Guerrero in partial fulfillment of the requirements for the degree of Doctor of Philosophy.

Permission is hereby grated by (Printed name): Vikram D Kodibagkar

Signature: Vikram Kodibagkar

Date: 3/31/23

Permission to Use Co-Authored Material

I hereby grant permission for the utilization of the manuscript titled: "**Development and Characterization of Isogenic Cardiac Organoids from Human-Induced Pluripotent Stem Cells Under Supplement Starvation Regimen**", published in *ACS Biomaterials Science & Engineering 9, 2 (2023): 944–958*.

The cited manuscript will be used as part of the Dissertation titled "**Development and Characterization of Isogenic Cardiac Organoids Derived from Human Pluripotent Stem Cells**", which will be presented to the Arizona State University Graduate College by Alejandra Patino-Guerrero in partial fulfillment of the requirements for the degree of Doctor of Philosophy.

Permission is hereby grated by (Printed name): Wuqiang Zhu

Signature: Wuqiang zhu

Date: March 30, 2023

Permission to Use Co-Authored Material

I hereby grant permission for the utilization of the manuscript titled: "**Development and Characterization of Isogenic Cardiac Organoids from Human-Induced Pluripotent Stem Cells Under Supplement Starvation Regimen**", published in *ACS Biomaterials Science & Engineering 9, 2 (2023): 944–958*.

The cited manuscript will be used as part of the Dissertation titled "**Development and Characterization of Isogenic Cardiac Organoids Derived from Human Pluripotent Stem Cells**", which will be presented to the Arizona State University Graduate College by Alejandra Patino-Guerrero in partial fulfillment of the requirements for the degree of Doctor of Philosophy.

Permission is hereby grated by (Printed name): _____

Signature: RAYMOND Q. MIGRINO 200761 Digitally signed by RAYMOND Q. MIGRINO 200761 Date: 2023.04.03 09:58:23 -07'00'

Date: _____

Permission to Use Co-Authored Material

I hereby grant permission for the utilization of the manuscript titled: "**Development and Characterization of Isogenic Cardiac Organoids from Human-Induced Pluripotent Stem Cells Under Supplement Starvation Regimen**", published in *ACS Biomaterials Science & Engineering 9, 2 (2023): 944–958*.

The cited manuscript will be used as part of the Dissertation titled "**Development and Characterization of Isogenic Cardiac Organoids Derived from Human Pluripotent Stem Cells**", which will be presented to the Arizona State University Graduate College by Alejandra Patino-Guerrero in partial fulfillment of the requirements for the degree of Doctor of Philosophy.

Permission is hereby grated by (Printed name): Oliver Graudejus

Signature: _____

Date: 3-30-2023

Permission to Use Co-Authored Material

I hereby grant permission for the utilization of the manuscript titled: "**Development and Characterization of Isogenic Cardiac Organoids from Human-Induced Pluripotent Stem Cells Under Supplement Starvation Regimen**", published in *ACS Biomaterials Science & Engineering 9, 2 (2023): 944–958*.

The cited manuscript will be used as part of the Dissertation titled "**Development and Characterization of Isogenic Cardiac Organoids Derived from Human Pluripotent Stem Cells**", which will be presented to the Arizona State University Graduate College by Alejandra Patino-Guerrero in partial fulfillment of the requirements for the degree of Doctor of Philosophy.

Permission is hereby grated by (Printed name): Mehdi Nikkhah

Signature: _____

Date: 3/31/2023